MINE DESIGN AND SLOPE STABILITY ANALYSIS FOR CARBONATITE DEPOSITS UNDER HIGH-STRESS CONDITIONS IN GREAT RIFT VALLEY AREA, AFRICA

ダイソン, モーゼス

MINE DESIGN AND SLOPE STABILITY ANALYSIS FOR CARBONATITE DEPOSITS UNDER HIGH-STRESS CONDITIONS IN GREAT RIFT VALLEY AREA, AFRICA

DEPARTMENT OF EARTH RESOURCES ENGINEERING

GRADUATE SCHOOL OF ENGINEERING

KYUSHU UNIVERSITY

Dyson MOSES

FEBRUARY, 2022

MINE DESIGN AND SLOPE STABILITY ANALYSIS FOR CARBONATITE DEPOSITS UNDER HIGH-STRESS CONDITIONS IN GREAT RIFT VALLEY AREA, AFRICA

DOCTORAL THESIS

SUBMITTED TO THE GRADUATE SCHOOL OF ENGINEERING

DEPARTMENT OF EARTH RESOURCES ENGINEERING

ROCK ENGINEERING AND MINING MACHINERY LABORATORY

KYUSHU UNIVERSITY

AS A PARTIAL FULFILLMENT OF THE REQUIREMENTS FOR THE DEGREE OF

DOCTOR OF ENGINEERING

BY

DYSON MOSES

SUPERVISED BY

PROF. DR. HIDEKI SHIMADA

DEPARTMENT OF EARTH RESOURCES ENGINEERING

GRADUATE SCHOOL OF ENGINEERING

KYUSHU UNIVERSITY

FUKUOKA, JAPAN

FEBRUARY, 2022

ABSTRACT

Rare earth elements (REE) are presently in explosive demand due to their application in high-tech devices such as computer memory, rechargeable batteries, autocalytic converters, super magnets, and mobile phones. But the economically exploitable REEs tend to occur in limited geological environments and carbonatites are highly potential hosts of REE, hence they are a specially targeted rock mass. Malawi, Africa is among the few countries endowed with exceptional carbonatite intrusions and among the intrusions existent, Songwe Hill has proven economical for mine development. Since the deposit at the site is near the surface, open-pit mining (OPM) has been proposed for the development of the deposit. However, OPM is beleaguered with stability problems culminating in failures due to principally poor designs that overlook some integral components. One overly overlooked aspect as a mining bottleneck is *in situ* stress, which has only been considered in underground mining based on the premises that the stress environment in OPM is dilationary other than confining and that failures are gravity-driven. Nevertheless, stress regimes, particularly in tectonically active regions like the East African Rift Valley system, can inevitably play a key role in the failure process on excavations. On the other hand, despite carbonatites being competent rock mass, they are characterized by in situ damage due to brecciation and have multi-faceted angular blocks generated by fractures and discontinuity sets. The failure mechanisms in such hard rocks entail initiation and progression of failure along the existing weakness planes, even in intact states. In order to develop an optimal mine design in such carbonatite deposit under high-stress conditions in Great Rift Valley area, an integrated approach entailing rock mass characterization, kinematic and numerical methods was applied for design guideline. The main contents of the research can be summarized as follows:

Chapter 1: Introduces the significance of REE, their production and consumption disequilibrium, and the geological environments of occurrence. The emplacement of the carbonatite complex, which is a host of REE, is also discussed. The carbonatite complexes are basically intruded into the country rock through an exceptional magmatic activity with an alkaline rich magma. The later stages of the Songwe carbonatite emplacement is uniquely featured with carbonatite transition from a magmatic to a hydrothermal regime where expelled fluids lead to fenitization, fluorite and Mn-Fe veining disseminated throughout the rock mass. The chapter also gives the background of the research, research objectives and methods.

Chapter 2: The chapter is dedicated to evaluating the geological and geotechnical conditions of the carbonatite rock mass. A field survey revealed distinctive features that the carbonatite complex is characterized by in situ rock damage due to brecciation, which is a result of hydro-fracturing involving high-pressure fluids due to high tectonic forces trending along pre-existing plane of weakness, and has high discontinuity frequency per unit area occurring parallel to the horizontal stress direction. To understand the rock quality in relation to mining, qualitative and quantitative rock mass classification systems, namely Geological Strength Index (GSI) and Rock Mass Rating (RMR) respectively, were applied to describe the rock mass. Based on the evaluation, carbonatites can be described as competent with RMR class II rating 60-74, and GSI value range of 55-69. In spite of the competency, they tend to have multi-faceted angular blocks generated by discontinuity sets, which pose a potential for structural controlled instabilities.

Chapter 3: Gives a discourse on the potential modes of slope failure in the discontinuity dominated carbonatite rock mass as revealed in chapter 2, performed using the kinematic approach. The kinematic checks were executed using Dips V 6.0 software designed to analyze features related to engineering analysis of rock structures. The outcome of the analysis indicate that the carbonatite rock masses have high potential of planar slope instability at steeper angles, for the case of Songwe at 45°. Since carbonatites occur in tectonically active regions, the high horizontal stresses acting parallel to discontinuity planes intersecting the orientation of the slope faces could act as a catalyst to failures. In order to minimize the risk of failure, slope angle optimization to a gentler angle can be adopted as a counter-measure. For the case study area, the risk of failure was observed to be high in the south and east sections of the pit, hence slope angle optimization to 40° was suggested, which could reduce the risk of failure to high safety. Meanwhile, relatively steep angles in the opposite sections are implementable at safety viz. 43° in the north and 42° in the west sections.

Chapter 4: Presents analyses of stability conditions and deformation behavior of pit slopes under structurally complex and prevailing high-stress conditions in Great Rift Valley area in order to come up with ultimate optimal design guidelines for rare carbonatite deposits. This was achieved by numerical methods carried out with finite difference method and finite element method codes using FLAC^{3D} V 5.0 and Phase^{2} V 7.0 software respectively. The analyses were performed in elasto-plastic state with Mohr-Coulomb constitutive model and failure criterion.

Due to the competency of the rock mass, analysis shows that overall slopes can be developed at steep angles of 45-50° at a shallow depth of ≤ 250 m, but caution has to be taken at greater depth and when discontinuities are predominant. With regards to in situ stress, a qualitative evaluation of the stability state through shear strain analysis reveals that the pit wall stability conditions could be compromized under high-stress regimes such that non-uniformity of stress state leads to the development of a secondary potential failure surface (PFS) in addition to the primary circular PFS which has been the sole engineering concern in slope stability analyses. Furthermore, the displacement values, at the state of stress equilibrium (k=1), were found to be almost four times lower than at k=2.5 and two times lower when k=0.5. This demonstrates that non-uniform high-stresses could indeed adversely affect pit wall performance. To test the criticality of the risk to failure, the strain criterion to failure, which is a ratio of the maximum deformation and the height of excavation, was applied and the shear strain rate indicates that the rock mass slopes may not be significantly endangered, a phenomenon accredited to its competence. For instance, the maximum possible strain rate of 0.04%, which is below the lower bound strain at collapse of 0.1% was recorded in the study case. In terms of in situ rock damage, the existence of breccia in the competent rock mass has the capability to reduce the stability performance of the pit wall and the enormity of the impact increases at gentle dipping angle in close range to the slope toe. However, as the initial position of breccia moves away from the pit wall, the stability performance increases at gentle dipping angle namely 30° and 40°. On the contrary, at the dipping angle of 50° the performance of slope reduces, and at steeper angle >50°, the impact becomes negligible. Thus, for OPM design in brecciated rock masses, the ratio of at least 1:5 between the breccia distance from slope toe and pit depth is proposed to counter its impact. If breccia is close to the pit limit, a deliberate effort must be made to mine out or truncate it.

Chapter 5: Covers the aspect of mining economics. The objective is to give a forecast of the project performance in order to know the value of investing in the REE mining venture. The assessment is based on economic performance indicators namely; Net Present Value (NPV), Internal Rate of Return (IRR), and profitability index (PI). The results show that steeper slope angles have higher prospects of profit due to low stripping ratio than gentle angles but their safety is unreliable. This requires the mining trade off between resource recovery and safety.

For the case study project, the indicators at a discounted rate of 10% indicate that the deposit can be developed at a profit with NPV, IRR and PI at US$658.54 million, 33%, and 2.6 respectively but at the slope angle that gives a fair equilibrium on recovery and safety, NPV is around U$$580 million, IRR at 32%, and PI at 2.3. On a different note, sensitivity analysis shows that mineral price volatility is very sensitive on project performance, hence at the core of the decision to mine the REE or not.

Chapter 6: Gives the mine excavation plan and design. Basically, final slope design has to seriously consider equilibrating the fulcrum of mining profits and safety. In carbonatite deposits it has shown that overall slopes can be developed at steep angles at shallow depth in order to yield high returns. But, since the contact zones of carbonatites and fenite may be fractured and also the existence of dicontinuities and brecciation coupled with high tectonic stresses, the ultimate slope design at greater depth ought to be at the optimal gentle angle. In the case of Songwe Mine, considering the topography and the mineralization extent, the extraction sequencing is suggested to commence from the sloping face of the hill where ore hosting rock is exposed to the surface to shorten payback period and then create subsequent push backs in a top-down approach targeting an OSA of 40° in high RL section, which at preliminary stage guarantees a high geotechnical safety assurance and good returns though requirement for stripping is fairly high.

Chapter 7: This chapter concludes the findings of this research.

ACKNOWLEDGEMENTS

I would like to express my sincere gratitude to my supervisor; Prof. Dr. Hideki Shimada and co-supervisor Assoc. Prof. Dr. Takashi Sasaoka for their superb supervision, kind support, excellent guidance, thoughtful insight and professional skepticism that helped me to refine my work. I further acknowledge and appreciate the examination committee members; Prof. Dr. Kiyonubu Kasama and Prof. Dr. Akira Imai, who critically evaluated my work and gave constructive comments.

I also extend my special thanks to Asst. Prof. Dr. Akihiro Hamanaka and Dr. Sugeng Wahyudi for the contributions, support and guidance in a number of ways during my research work. Many thanks goes to all my colleagues in the Rock Engineering and Mining Machinery Laboratory for co-knowledge creation and sharing spirit, support and motivation.

I am highly grateful to JICA under the KIZUNA program for all the financial assistance rendered throughout the study period. This work was impossible without your generous scholarship provisions.

I am also indebted to extend my thanks to Mkango Resources Company through the president Mr. Alexander Lemon and the Chief Executive Officer Mr. Will Dawes for allowing me to conduct my research on their mining project. Most importantly, I express my appreciation to the company for selflessly providing basic key data set required in the research study.

Ultimately, I owe my kind thanks to all my family members for their moral support, understanding and endurance during my study period. I reckon they can finally afford a smile and say it was worthy a sacrifice. Above all, to GOD be the glory.

Fukuoka, February, 2022

Dyson MOSES

TABLE OF CONTENTS

LIST OF FIGURES

LIST OF TABLES

1 INTRODUCTION

Rare earth elements (REE), which are a group of seventeen chemical elements in the periodic table, have been at the center of explosive demand over the last few decades. The demand for the REE is due to the expansion in the applications of REE and their alloys in various high technological devices such as computer memory, rechargeable batteries, autocalytic converters, super magnets, mobile phones, superconductors, LED lighting, fluorescent materials, solar panels and magnetic resonance imaging (MRI) agents. Since the metals are being consumed at an unprecedentedly high rate for a variety of applications, they have been described as "The Vitamins of Modern Industry" (Balaram , 2019). More recently, the rise in demand for REE is particularly for energy efficient gadgets (green technology) which are faster, lighter, smaller and more efficient. Table 1.1 summarizes the wide range applications of REE in the modern technological industry.

Table 1.1 REE utilization in the world today in different areas

Area	Applications
Electronics	Television screens, computers, cell phones, silicon chips, monitor displays, long-life rechargeable batteries, camera lenses, light emitting diodes (LEDs), compact fluorescent lamps (CFLs), baggage scanners, marine propulsion systems
Manufacturing	High strength magnets, metal alloys, stress gauges, ceramic pigments, colorants in glassware, chemical oxidizing agent, polishing powders, plastics creation, automotive catalytic converters
Medical Science	Portable X-ray machines, X-ray tubes, magnetic resonance imagery (MRI) contrast agents, nuclear medicine imaging, cancer treatment applications, and for genetic screening tests, medical and dental lasers
Technology	Lasers, optical glass, fiber optics, masers, radar detection devices, nuclear fuel rods, mercury-vapor lamps, highly reflective glass, computer memory, high temperature superconductors
Renewable Energy	Hybrid automobiles, wind turbines, next generation rechargeable batteries, biofuel catalysts

1.1 Rare Earth Elements Production and Utilization Conundrum

Despite being found in a wide range of minerals, including silicates, carbonates like carbonatite, oxides and phosphates, the economically exploitable REEs tend to occur in limited geological environments because they do not fit into most mineral structures (Balaram, 2019; Simandl & Paradis, 2018). Hence, the occurrence of the REE in limited environments has triggered an imbalance in production and utilization with trade war being the inevitable eventuality. Generally, China has predominated the REE production since 1994 seconded by the United States of America (USA) (Figure 1.1). However, USA ceased production of REE between 2003 and 2011 and they relied on imports from China and other REE producing nations. The demand for these strategic minerals is apparently high in USA with many technological advances sprouting. Since supply and demand normally determine the market price of the commodity, the dominance of China had put them in the pore position to monopolize the REE market. In 2010, China, boasting of the dominance of more than 95% of global REE production, imposed a reduction in export quotas by 40% a decision which oversaw the dysprosium price increase hundred times higher in 2011 than the plateau price phase in 2002/2003 (Renner & Wellmer, 2020; Charalampides et al., 2015).

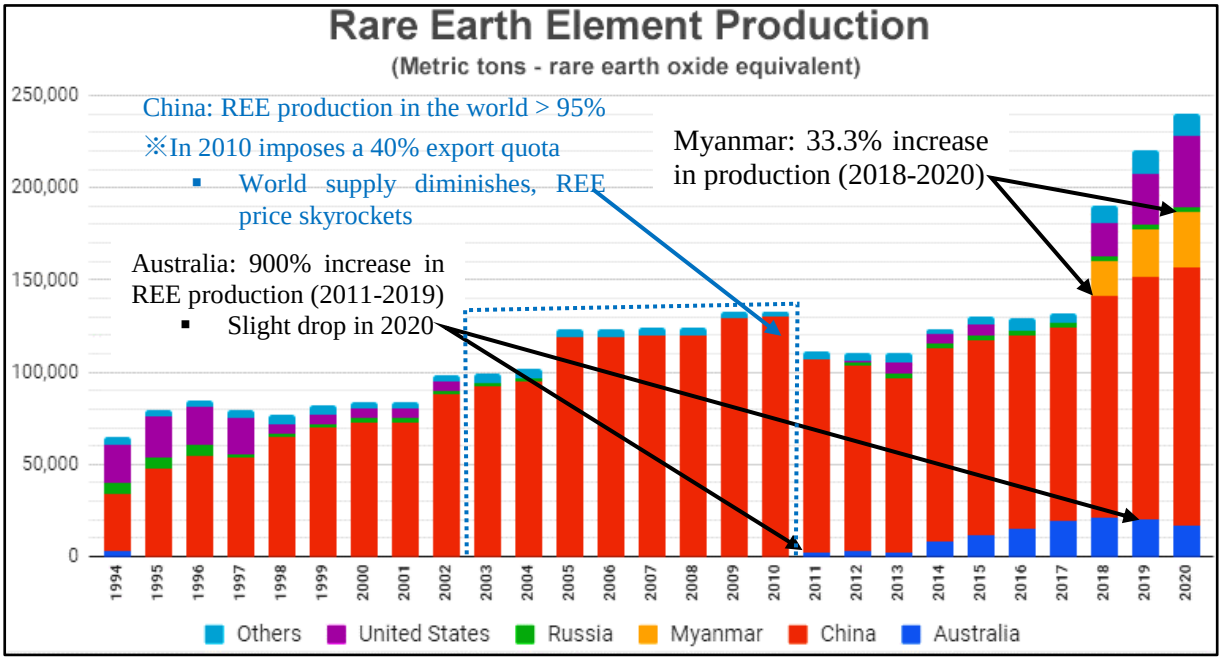

Figure 1.1 REE production trends by countries (King, 2020)

The development prompted the World Trade Organization (WTO) to intervene since there were concerns that inadequate access to supplies in resources scarce countries and inappropriate exploitation in resource-rich regions could escalate trade conflict. From this background, as supplies shrunk, prices kept increasing and mining companies perceived high prices as an opportunity and commenced to develop new sources of supply in various countries. In 2014, Australia increased their REE production after entering into the frame in 2011. By 2019 the production in Australia increased by 900% before slightly dropping in 2020 apparently due to COVID-19. Another new face in REE production is Myanmar. The country's REE production was first recorded in 2018 with an initial production of 30,000 tonnes, and the production has increase by 33.3% as of 2020. Meanwhile, the bar of production for the label of other countries has taken an increasing trend since 2015. Decades of exploration for REE mineral occurrences has demonstrated that carbonatites are highly potential hosts of REE, hence they are special target rock mass. Malawi is among the few countries that have the potential for exploitable mineralization of REE in the carbonatite complex. The country has a number of carbonatite complexes within the intrusive Chilwa alkaline province (CAP) of Malawi which have been extensively studied and documented, resulting in excellent memoirs such as Chilwa Island, Tundulu, Kangankunde, and Songwe Hill carbonatite (see Figure 1.2). However, the Songwe Hill carbonatite has by far been described to have "high potentiality for a carbonatite hosted REE deposit".

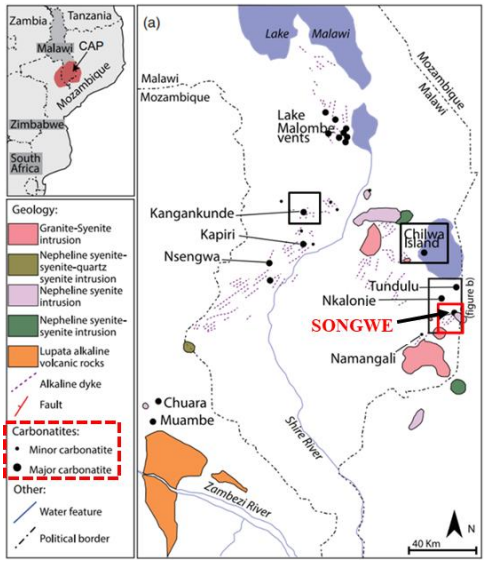

Figure 1.2 Map showing the distribution of carbonatite intrusions in the Chilwa Alkaline Province of Malawi (modified after Broom-Fendley et al., 2021)

1.2 Carbonatite Complex Tectonic Setting

Carbonatite complexes get emplaced in different tectonic settings. The most prominent settings are the continental cratonic and non-cratonic settings (see Figure 1.3). In these settings, the emplacement is into the Archean and Proterozoic rocks, or in Phanerozoic rocks that are underlain by Precambrian basement (Simandl et al., 2018; Woolley & Church, 2005). The intrusions of carbonatites tend to be closely associated with the extensional tectonic settings like the East African Rift System (EARS) where the Songwe Hill and the Ol Doinyo Lengai carbonatite complexes are located. The strong affinity of carbonatite complexes to rifting settings implies intense magmatic activity where the intrusions are related to large igneous provinces such as the Malawi Chilwa Alkaline Province (CAP). Carbonatites have also been identified in oceanic regions namely; the Canary Islands, the Cape Verde Islands, and the Kerguelen Islands situated in the African continent. Thus, it is considered that these islands are underlain by remnants of continental lithosphere stranded during drifting of the African plate (Woolley & Church, 2005). Generally, based on the work of Simandl & Paradis (2018), few carbonatites and alkaline-carbonatite complexes are favourable hosts of metallic and industrial mineral deposits. In the publication by the authors, statistics indicate that roughly 6% of the 527 reported carbonatites and alkaline carbonatite complexes host active mines of which 3% hold historic mines and 11% contain established mineral resources.

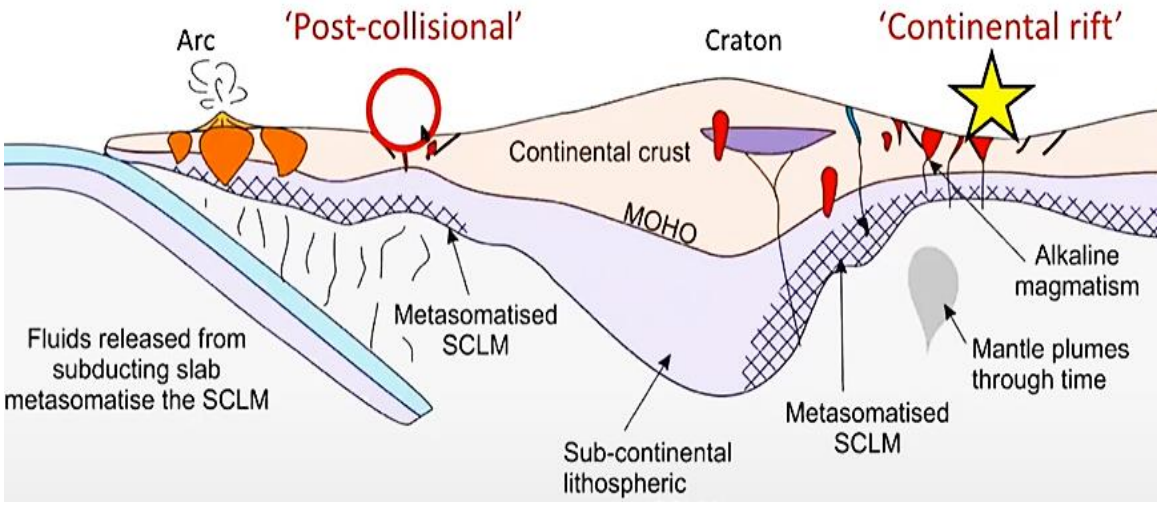

Figure 1.3 Tectonic setting of carbonatites and carbonatite complexes (Goodenough, et al., 2016)

1.3 Rare Earth Elements Mineralization in Carbonatites

Carbonatites are defined as igneous rocks containing more than 50% modal primary carbonates and less than 20 wt. % SiO_2 (Simandl & Paradis, 2018; Woolley & Church, 2005; Xu et al.,2015). Carbonatites of magmatic origin are associated with the magmatism of carbonate-bearing rocks in alkaline rock complexes. The categorization of these rocks is based on the predominating carbonate minerals. In this regard, the carbonatites are pitched into "calcite carbonatite", dolomite carbonatite" and "ferro-carbonatite" (See Figure 1.4). In a scenario where more than one carbonate minerals coexist, the nomenclature of the carbonatite is achieved by naming the carbonate minerals in the order of increasing modal concentrations. For instance, a 'calcite-dolomite carbonatite' consists predominantly of dolomite.

The classification based on wt. % ratios divide carbonatites into: (i) calico-carbonatites when the ratio of CaO/ (CaO + MgO + FeO + Fe^2O_3+ MnO) is greater than 0.8, (ii) magnesio-carbonatite with [MgO > (FeO+Fe^2O_3+MnO)] and ferro-carbonatite when [MgO < (FeO+ Fe^2O_3 + MnO)] (refer to Figure 1.4). Studies by Simandl et al. (2018), Petibon et al. (1998), and Peterson (1990) have described a 'natrocarbonatite' as a special variety of carbonatite consisting mainly of Na–K–Ca carbonates, such as nyerereite [(Na, K) 2Ca $(CO_3)_2$] and gregoryite [(Na, K, Ca) 2–x (CO_3)], known from Ol Doinyo Lengai volcano (Tanzania). Carbonatites are of great economic interest because they mostly contain anomalous concentrates of REE. Apart from being a rich source of REEs, carbonatites can also be a host of economic mineral elements like; phosphorous, niobium, tantalum, copper, fluorite titanium, zirconium, and industrial minerals like apatite, barite, and vermiculite.

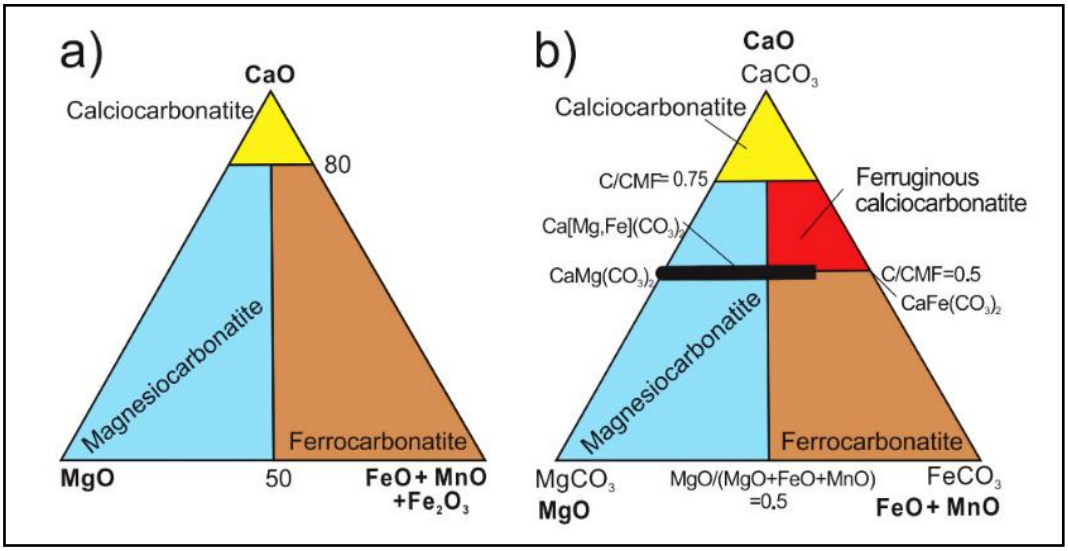

Figure 1.4 Carbonatite classifications according to (a) IUGS based on wt. % (Le Maitre 2002) and (b) Gittins and Harmer (1997) based on molar proportions (Simandl & Paradis, 2018)

1.4 Mineralization Theories

The origin and formation of carbonatite intrusions have been extensively debated and new theories are still being proposed based on the uniqueness of the compositions. Currently, three main hypotheses are applied to explain the origin and the process of emplacement. The carbonatite melts are argued to be derived from the following processes: (i) immiscible separation of parental carbonatite silicate magmas at crustal or mantle pressures, (ii) crystal fractionation of parental carbonate silicate magmas such as olivine melilites, and (iii) low degree partial melting of carbonated mantle peridotite less than 70km depth (Simandl & Paradis, 2018). Nevertheless, irrespective of the mode of formation, most researchers concur that alkalis (Sodium (Na) and Potassium (K)) play pivotal roles in the genesis of calcite and dolomite carbonates as well as ferro-carbonatite intrusions. In other carbonatite complexes like the Malawi Kangamkunde and Songwe Hill, late-stage events involving hydrothermal fluid have been observed. The hydrothermal interactions with the pre-existing carbonatites culminate into the formation of Strontium (Sr-), Bastinesite (Ba-), and REE-bearing carbonatite (Ngwenya , 1994; Wall & Mariano, 1996). In some cases, the interactions involve pre-existing carbonatites with groundwater enriched in hematite, calcite, or dolomite. From the metasomatic events that develop later, it can be concluded that not all carbonatites are associated with alkali silicate rocks because in some cases typical volcanic minerals are absent.

This is a typical scenario in China which happens to be the predominating REE producing country with most of the deposits being of secondary hydrothermal origin in sedimentary rock types. Xu et al. (2015) have extensively discussed the hydrothermal deposits that exist in China drawing attention to new theories.

1.5 Models of Alkaline Carbonatite Complexes

Carbonatite complexes across the globe have different morphologies and geometries. The model of emplacement sets unique characterization of the rock masses. By far, three models of carbonatite morphologies attempt to generalize the emplacement and features of the complexes. However, critical models examination demonstrates that none of the models depicts all of the possible rock associations that have been encountered in alkaline-carbonatite complexes, which brings in a question of universal applicability. Despite this fact, regardless of the model adopted, the intrusions are sub-volcanic rocks that form radial dykes, cone sheets, and ring dikes with examples cited in the work of Simandl & Paradis (2018). The authors demonstrated that in different carbonatite complexes, the dike and cone sheets have been recognized to comprise of nephelinites, alkaline-rich mafic rocks, melilitolites, phonolites, trachytes, lamprophyrites, ijolites, and carbonates.

Among the models is the classic carbonatite model proposed by Garson and Smith (1958) which is based largely on field observations (Mitchell, 2005). In this model, the carbonatites are not associated with extrusive or intrusive silicate rocks except fenites due to the fact of non-exposure of the deeper parts of the parent plutonic complex. The second model is the Le Bas (1987) model, which nicely depicts age relationships of lithological units and fenitization-type overprints (Swinden & Hall, 2012). The other model propounded by Sage and Watkison (1991) shows a limited number of lithologies relative to the other models. However, the model displays the relationship between the volcanic edifice and crater facies with erosional levels that currently correspond to the level of exposure depicted by carbonatite in southwest Quebec and Ontario in Canada (Simandl & Paradis, 2018). It should be highlighted that the adoption of the model to describe the morphology of the carbonatite complex relies on the tectonic setting.

The field relationships that can be drawn from the Songwe Hill demonstrate that the Songwe carbonatite intruded and fenitized the edges of the adjacent Mauze nepheline syenite, but the radiometric ages of Songwe intrusion (132.9 ± 6.7 Ma) and Mauze intrusion (134.6 ± 4.4 Ma) are barely distinguishable though the former can be described as relatively younger to the later. The primary evidence that cements the emplacement sequence is the equigranular texture of the fenite, incorporating large rectangular pseudomorphs of feldspar which is texturally evocative of the neighbouring nepheline syenite (Broom-Fendley et al., 2017). Nevertheless, the indistinguishable emplacement ages of the two intrusions provides circumstantial evidence of a genetic connection signifying direct emplacement of the carbonatite making it unique to the conventional emplacement theories of carbonatites discussed in preceding sections. In terms of chemical evolution, studies by Ngwenya (1994) and Broom-Fendley et al. (2017) discussed that Songwe is characterized by Fe-rich carbonatites, which are more enriched in Light Rare Earth Elements (LREE) and SrO, and the calcite carbonatite comprising relatively coarse grained apatite, zircon and calcite, which represent a cumulate developed from a lower level of the intrusion.

The later stages of Songwe carbonatite complex emplacement, is featured with carbonatites transition from a magmatic to a hydrothermal regime where expelled fluids lead to fenitization, fluorite and Mn-Fe mineralization manifested in veins disseminated throughout the host carbonatite and formation of cavities which were identified during the drilling phases. Another notable exceptional feature of the Songwe carbonatite is the late apatite phase that forms anhedral stringers and cross cuts many carbonate phases, which has not been previously documented in other carbonatites. The confirmation of this phenomenon is based on the strong correlation between P_2O_5 and the Heavy Rare Earth Elements (HREE) apparently controlled by the uptake of the HREE in late-stage apatite phase (Broom-Fendley et al., 2017). Thus, a critical review of Songwe Hill carbonatite shows that the complex partially conforms to the model represented by the Les Bas (1987) modified as represented in Figure 1.5

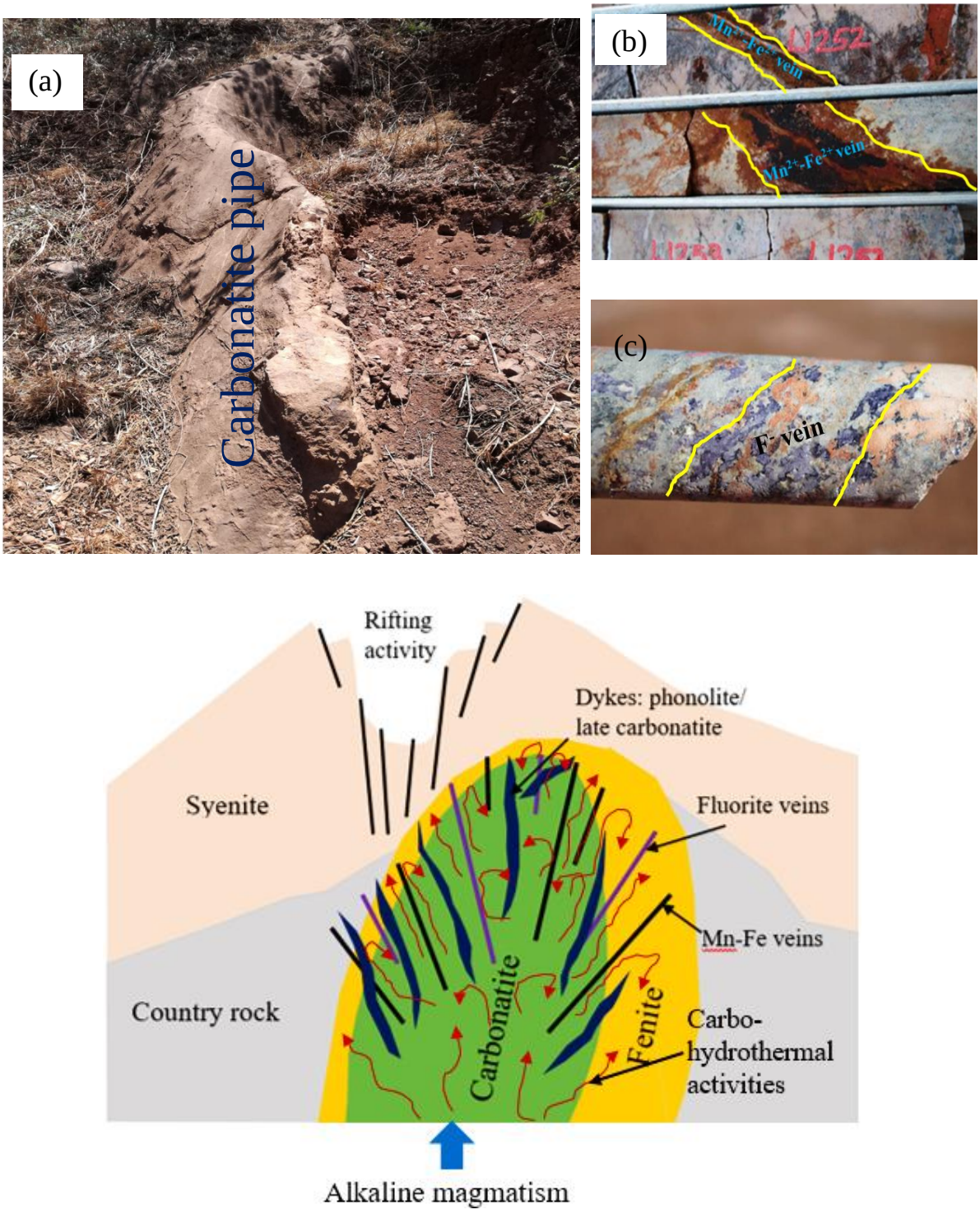

(d) Songwe carbonatite complex representation

Figure 1.5 A simplified Songwe carbonatite emplacement model: (a) late stage carbonatite pipe, (b) Mn-Fe vein in core samples, (c) Flourite vein in core samples, and (d) intrusion model

1.6 Songwe Project Research Background

The discovery of the Songwe Hill carbonatite, which is a potential host of REE, dates back to the 1930s. The Geological Survey of Malawi (GSD) documented eleven occurrences of carbonatites among them; Songwe Hill and Tundulu, which were investigated by Dixey et al. (1937) who ultimately described the Songwe Hill occurrence as a volcanic vent consisting of limestone, feldspar rock, and agglomerate. Carbonatite exploration was stepped up in the 1950s with Garson's study. The study provided a comprehensive account of the carbonatites including a detailed discussion of Songwe Hill with a geological map indicating a volcanic vent filled with feldspathic breccia and agglomerate and intruded by sheets of carbonatite (Garson & Smith, 1965). In the early 1980s, GSD requested for technical assistance from the Japanese government for further exploration of Songwe Hill. In response to the Malawian government, the Japanese government through Japan International Cooperation Agency (JICA) and Metals Mining Agency (MMAJ) conducted a mineral exploration program in the CAP from 1986 to 1988. After the first phase of the programme, which consisted of geological and geochemical surveys, and a drilling program, it was determined that the Songwe Hill had "high potentiality" for a carbonatite REE deposit (see Figure 1.6).

Corollary to the first phase results, two more phases were conducted. The second phase involved 11 diamond drill holes summing up to 558m and was defined by a number of mineralized zones. The third phase in 1988, which was designed to refine the delineation of the extent and grade of the mineralized zone on the northern side of Songwe Hill, involved 8 drill holes totalling 401.2m with a maximum vertical drill hole depth of 55m (Swinden & Hall, 2012). The assays of phase 2 and 3 drill holes were done at 5m lengths for seven key REE elements. The results revealed the occurrence of REE comprising lanthanum, cerium, neodymium, samarium, europium, terbium, dysprosium, ytterbium and yttrium as well as strontium, niobium, and thorium. The principal REE-bearing minerals identified using thin section, X-ray Fluorescence (XRF) and Electron Microprobe Analysis (EMPA) analysis included synchysite, bastnäsite, strontianite, monazite, pyrochlore, and apatite (Witley et al., 2019). In 2009 Mkango Resources Company, encouraged by the initial work and results realized by MMAJ, obtained an exploration license for a detailed exploration. The outcome of the exploration project has preliminarily demonstrated that the Songwe deposit could be mineable at a profit.

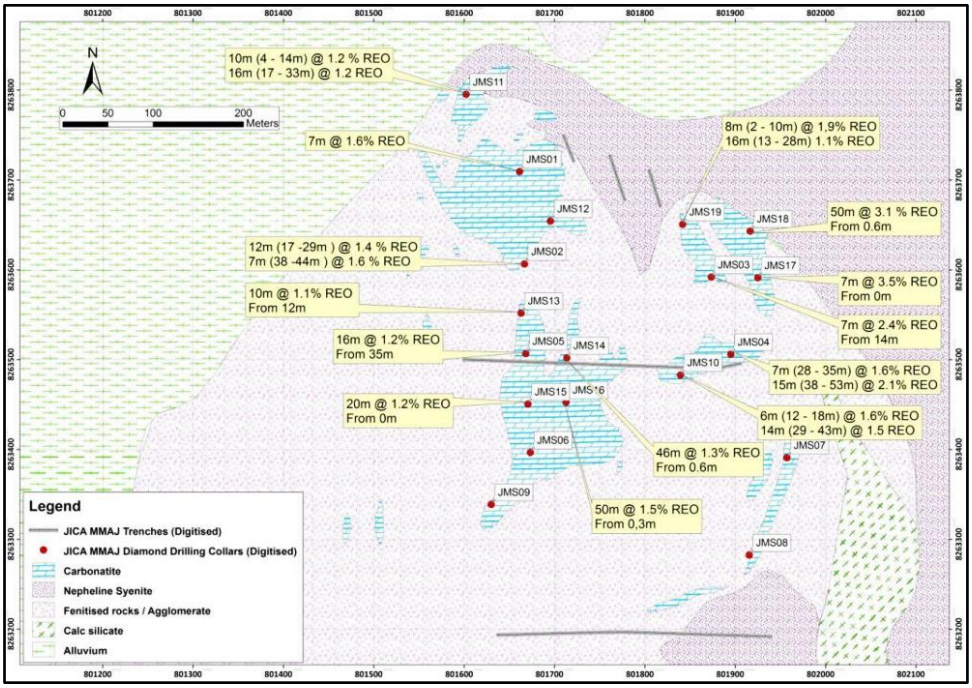

Figure 1.6 Assay results of the drilling program by GSD and MMAJ (Swinden & Hall, 2012)

1.7 Exploitation of REE and Challenges in Active Tectonic Settings

The statistics presented by Simandl & Paradis (2018) indicate that carbonatites have remarkable potential, and a newly discovered alkaline-carbonatite complex has a 9 out of 100 prospect of hosting a mine. Regardless of the odds, most of the active mines in carbonatite complexes tend to adopt open-pit mining (OPM) methods due to the morphology of the ore deposits. Examples of the active carbonatite mines producing REE and other mineral elements include; Bayan Obo in Mongolia, Maoniuping in China, Mountain Pass in the USA, Mount Weld in Australia, Lovozero in Russia, St-Honore in Canada, Araxa in Brazil, Copper producing carbonatite mine at Parabora in South Africa and Fluorite producing carbonatite mine at Mate Prato in Brazil, Okorusu in Namibia and Amba Dongar in India (Simandl & Paradis, 2018). The aforementioned mines are all OPM, a phenomenon that reflects the mineralization style of the deposits in carbonatite complexes. Open-pit mining is generally touted as a cost-effective mining method allowing a high grade of mechanization and large production volumes and where feasible extract mineral deposits of a very low grade which could not be mined economically using underground methods (Sjoberg, 1996).

As the demand for mineral resources increases to cater for the world's booming population, surface mining operations are expanding and getting deeper. However, slope instability is a major challenge to open-pit mining operations. The instability of the slopes is governed by many factors including the slope structure, stress state, rock mass strength, shock loading, and hydraulic conditions. The resultant to perturbations on slopes could be devastating leading to loss of production, damage to equipment, injury to personnel and most solemn of all, loss of life. Thus, Zaruba and Mencl (1982) stress that it is of primary significance to recognize the conditions that cause slopes to become unstable and the factors that trigger the movement in order to solve slope stability problems.

However, failure mechanisms in hard rock slopes are much more complex since progressive failure in hard rock slopes involves initiation and progression of failure along existing weakness planes, and even in intact rock. As mentioned previously, the carbonatite complexes tend to be situated in active tectonic settings implying possible high-stress conditions. Furthermore, most emplacements form central or inclined breccia zones, ring dykes, cone sheets, and joints. Chen et al. (2019) note that the interaction of structures and tectonic stresses bring a series of safety problems to the slope when the stress equilibrium state is disrupted in the mining process culminating into the unloading of the slope due to unbalanced stress. Cases of mines developed in high in situ stress regimes have been documented although the stresses have not been accounted for failures that occurred.

1.8 Case Review

Over the past decades, slope failures in mines have been documented and mechanisms discussed. Generally, failures have been ascribed to rock mass conditions, slope geometry, structural and geological conditions, and rainfall with no recognition of in situ stress regimes even in active tectonic regions. The Bingham Canyon Mine is one of the mines located in an active intrusive tectonic setting. The late Palaeozoic rocks at the mine are documented to have been structurally thrust faulted over the Precambrian craton during the cretaceous orogeny. The rocks were later intruded and altered by granitic rocks in the Tertiary period. Thus, the rock mass is very fractured with both minor and large fault structures. The copper and molybdenum deposits tend to be dispersed in the intruded stock and adjoining carbonatite sedimentary skarn.

A study by Sjoberg (1996) revealed that the stress state in the mine was characterized by horizontal stresses being greater than the vertical stress with k >1.2. The Bingham Canyon Mine, which dates back to the 1960s and is currently the deepest OPM at 850m, has by far experienced large-scale failures involving up to 2 metric tonnes of material as shown in Figure 1.7. However, despite the fact that the stress regime is high, the failures were squarely attributed to a combined effect of pre-existing discontinuities and excessive water pressure leading to plane shear failure and rotational shear failure respectively (Sjorberg, 1999; Sjoberg, 1996).

Figure 1.7 A huge failure at Bingham Canyon copper mine in Utah, United States (Parra et al., 2018)

At Buzhaoba Mine in China, failure occurred and it was accredited to tectonic stress as a dominating factor (Chen, et al., 2019). According to the analysis, the principal stress direction that was theorized and simulated at 123º caused the instability. As the excavation progressed to a deeper horizon, the cumulative effects of stress were exhibited through rock mass deformation and instability along the direction of the principal stress as shown in Figure 1.8.

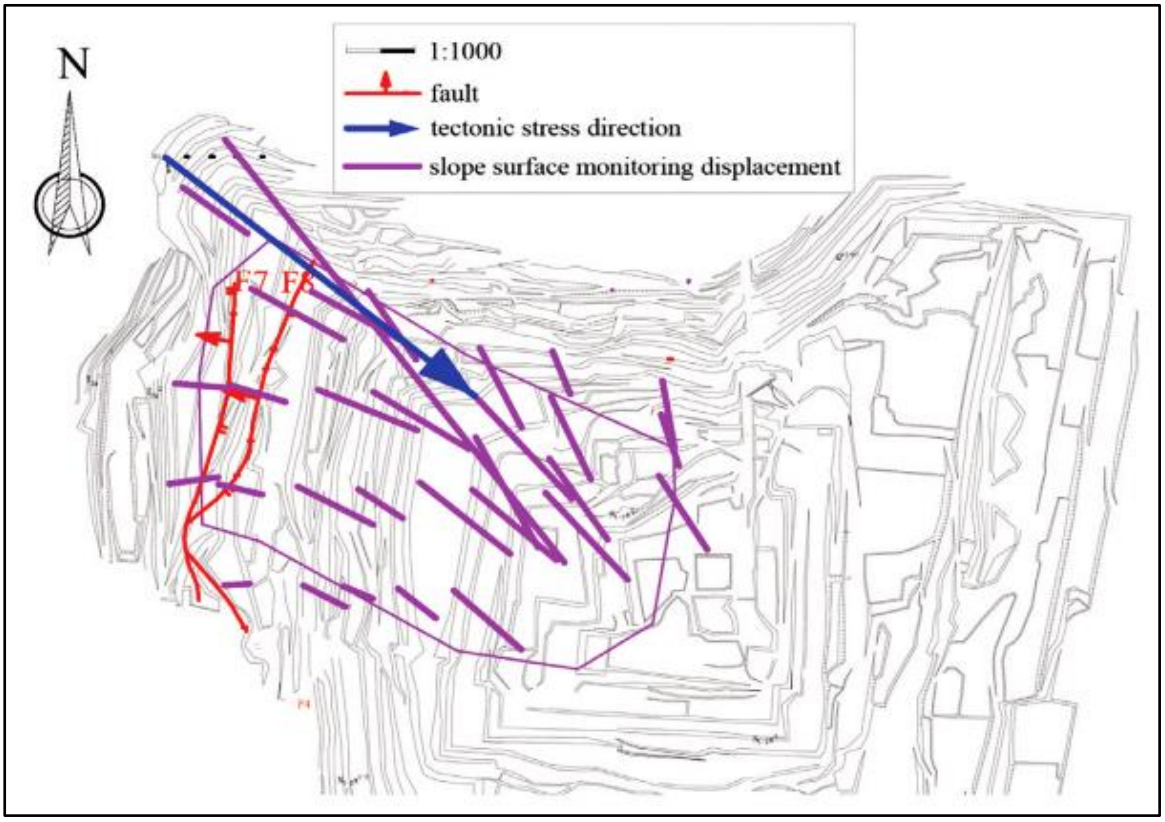

Figure 1.8 Displacement vectors and the direction of tectonic stress in the Buzhaoba Open-pit Mine, China (Chen et al., 2019)

In South Africa, the Sandsloot Open-pit Mine is a typical example of an active tectonic environment that encountered instability (see Figure 1.9). The geology of Sandsloot is characterized by the Bushveld igneous complex which is a resultant of igneous activity leading to the emplacement of a mafic phase (the Rustenburg Layered Suite) followed by an acidic phase (the Bushveld Granophyre and the Lebowa Granite Suite) (Bye & Bell, 2001). The authors further demonstrated that the tectonism at the mine is characterized by three major joint sets, which relate to the emplacement of the Potgietersrus Limb, and the minor joints around the Sandsloot Mine are postulated to have formed by randomized contraction jointing on the cooling of the Bushveld intrusive phase. Without any reference to in situ stress among governing factors, Bye & Bell (2001) accredited the principal cause of the slope instability at the mine to the steep dipping and persistent joints.

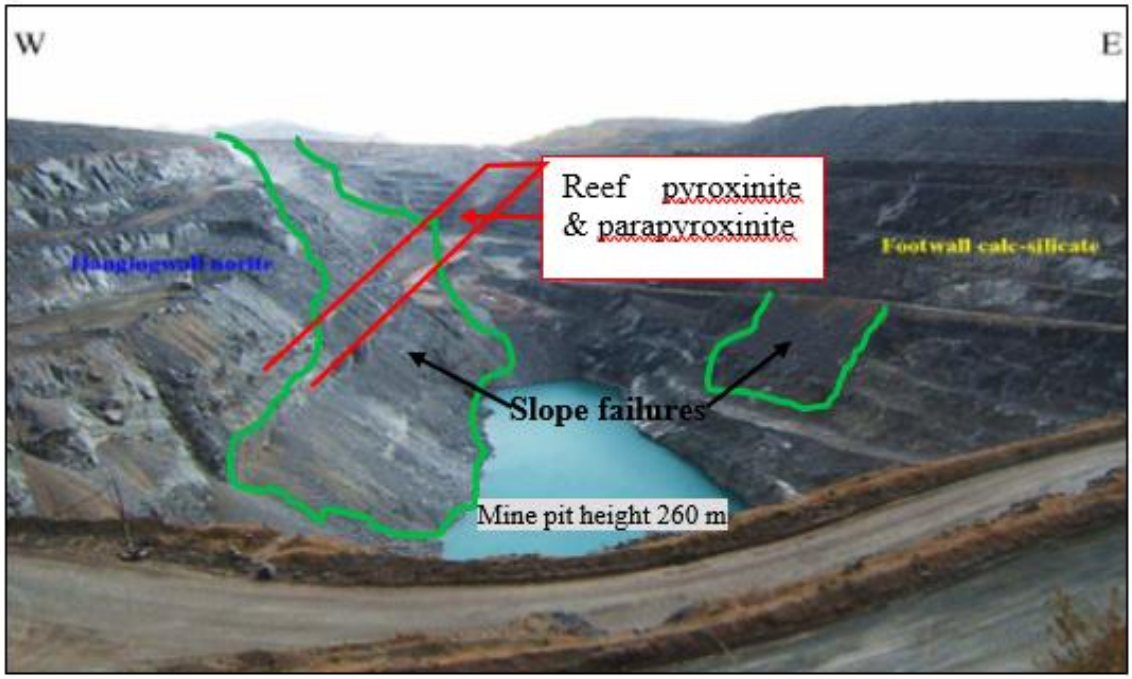

Figure 1.9 Slope failures at Sandsloot Open-pit (Little , 2019)

1.9 Problem Statement

Considering that the deposit at Songwe is near to the surface, open-pit mining has been proposed for the extraction of the REE mineral resources. As aforementioned, the OPM has a number of advantages when exploiting shallow lying and even low-grade deposits. Nevertheless, the mining method is beleaguered by stability challenges resulting in failure of slopes due to partly poor designs that overlook some integral components. To substantiate the assertion, Llano-Serna et al. (2016) quantify that roughly, two open-pit failures occur worldwide annually. For instance, in 2016, a slope failure at Katanga Open-pit Mine in the Democratic Republic of Congo (DRC) registered seven fatalities and in 2015 the Thabazimbi Mine in South Africa was closed affecting 360 contractors and 800 employees following a massive slope failure (Epiga, 2017). The instability leading to failure of slopes is caused by downward movements of material due to gravity as shear stresses exceed the shear strength. Currently, there is no standard classification system for mine slope designs and it is regarded as uncertain if a universal system is conceivable (Sullivan, 2013).

The planned REE mine at Songwe might not be immuned to slope instabilities given the fact that it lies within the East African Rift-valley System (EARS) which is an active intraplate tectonic setting with potentially high-stress fields. Furthermore, failure mechanisms in hard rock slopes involving high-stress regimes are much more complex since progressive failure in hard rock slopes involves initiation and progression of failure along existing weakness planes, and even in intact state. Meanwhile, consideration of in situ stress as a mining bottleneck has only been considered in underground mining based on the premises that the stress environment in OPM is dilationary other than confining and that failures are gravity-driven. This statement may be inadequate and needs to be questioned for the design of large slopes. Stresses inevitably play a key role in the failure process on excavations. Thus, it is crucial to comprehend the deformational response of the rock mass, especially carbonatite complexes, in open-pit as a function of stress fields and geological complexity if carbonatites. In that respect, the aim of the study is to develop mine design guideline for carbonatite deposits under prevailing high-stress conditions in Great Rift Valley setting.

1.9.1 Specific Objectives

To achieve the overarching aim of the study, the following specific objectives were pursued;

a. Characterizing the rock mass to understand its quality and key structural features
b. Assessing potential structural controlled failure modes
c. Developing and evaluating stability conditions of pit walls of the conceptual designs under different conditions
d. Performing preliminary mining economics in relation to the conceptual designs

1.10 Research Methodology

In this research work an integrated approach entailing rock mass characterization, kinematic and numerical methods was adopted. The study was built around three principal facets: field survey, laboratory experimental work, and numerical modelling as shown in Figure 1.10. Fieldwork was carried out to validate the available geological and structural information in the study area and collect fresh rock and/or core samples for experimental studies in the laboratory. Data collected from the field survey include: geological and structural data, and geotechnical data; RQD and discontinuities metadata.

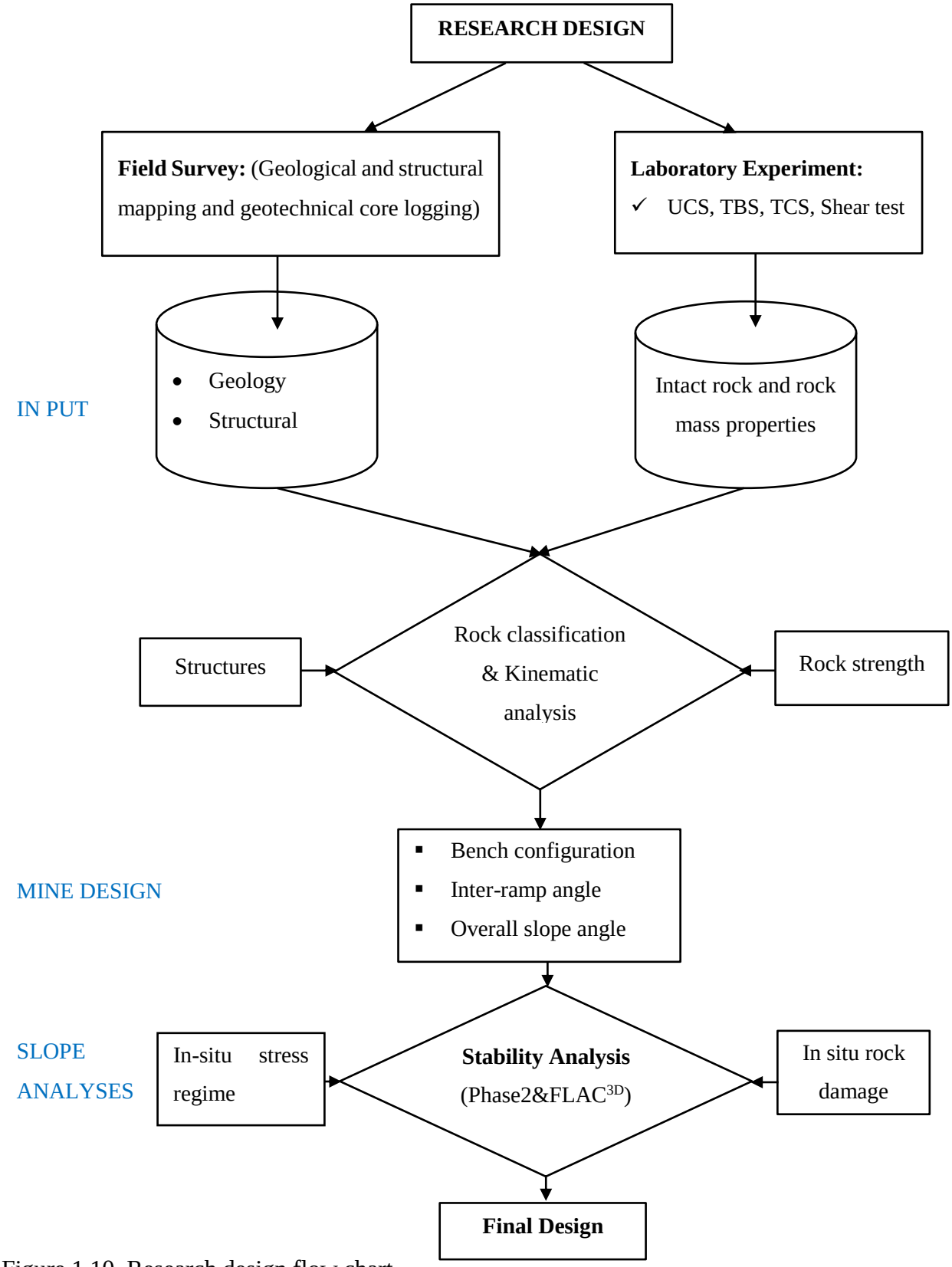

Figure 1.10. Research design flow chart

In the laboratory, rock strength tests were carried out using rock and/or core samples collected during the field survey. The tests conducted included: Uniaxial compressive strength (UCS), tensile Brazilian strength (TBS), triaxial compressive strength (TCS), and shear strength tests. With the data from the field survey and laboratory experiments, we evaluated the rock mass quality by applying the rock mass characterization techniques. Prior to computer modelling, kinematic analysis was conducted using Dips v 6.0 software used to graphically examine potential modes of instability that could occur in the rock mass with respect to attributes of the discontinuities. Ultimately, computer modelling was done to represent the mechanical response of rock mass to external and internal stresses. Numerical modelling was achieved by applying finite difference code using FLAC^{3D} V 5.0 and finite element code using Phase^{2} v 7.0 software. From the results obtained conclusions were drawn leading to the recommendations on optimal design for the development of carbonatite deposits

1.11 References

Balaram, V. (2019). Rare Earth Elements: A review of Applications, Occurrence, Exploration, Analysis, Recycling, and Environmental Impact. *Geoscience Frontiers*, 1285-1303. doi:10.1016/j.gsf.2018.12.005

Broom-Fendley, S., Brady, A. E., Horstwood, M. S., Woolley, A. R., Mtegha, J., Wall, F., & Gunn, G. (2017). Geology, Geochemistry and Geochronology of the Songwe Hill Carbonatite, Malawi. *Journal of African Earth Sciences* (134), 10-23.

Broom-Fendley, S., Elliott, H. A., Beard, C. D., Wall, F., Armitage, P. E., Brady, A. E., Dawes, W. (2021). Enrichment of Heavy REE and Th in Carbonatite-derived Fenite Breccia. *Geological Magazine*, 1-17. doi:https://doi.org/10.1017/S0016756821000601

Charalampides, G., Vatalis, K. I., Apostoplos, B., & Ploutarch-Nikolas, B. (2015). Rare Earth Elements: Industrial Applications and Economic Dependency of Europe. *Procedia Economics and Finance, 24*, 126 – 135. Doi: 10.1016/S2212-5671(15)00630-9

Chen, S., Lai, G. T., Han, L., & Tovele, G. S. (2019). Effects of Tectonic Stresses and Structural Planes on Slope Deformation and Stability at the Buzhaoba Open Pit Mine, China. *Sains Malaysiana*, *48*(2), 317–324. Doi: 10.17576/jsm-2019-4802-07

Epiga, S. N. (2017). *Planning and Design of a Stable Slope for an Open Pit Hard Rock Mine.* Johannesburg: Technology in Extraction Metallurgy.

Garson, M. S., & Smith, C. W. (1965). *Carbonatite and Agglomeratic Vents in the Western Shire Valley.* Zomba: Geological Survey Department.

Goodenough, K. M., Schilling, J., Jonsson, E., Kalvig, P., Charles, N., Tuduri, J., . . . Keulen, N. (2016). Europe's rare earth element resource potential: An overview of REE metallogenetic provinces and their geodynamic setting. *Ore Geology Reviews, 72*(1), 838-856. doi:https://doi.org/10.1016/j.oregeorev.2015.09.019

King, H. M. (2020, 4 28). *REE - Rare Earth Elements and their Uses*. Retrieved from geology.com: https://geology.com/articles/rare-earth-elements/

Little , M. J. (2019). Slope Monitoring Strategy at Sandsloot Open Pit Operation. *The South African Institute of Mining and Metallurgy* (s. 210-230). Cape Town: The South African Institute of Mining and Metallurgy.

Mitchell, R. H. (2005). Carbonatites and Carbonatites and Carbonatites. *The Canadian Mineralogist, 43*, 2049-2068.

Ngwenya, B. I. (1994). Hydrothermal Rare Earth Mineralization in Carbonatites of the Tundulu Complex, Malawi: Processes at the Fluid/rock Interface. *Geochimica et Cosmochimica Acta, 58*(9), 2061-2072. Doi: 10.1016/0016-7037(94)90285-2

Peterson, T. D. (1990). Petrology and Genesis of Natrocarbonatite. *Mineralogy and Petrology, 105*(2), 1432-0967. doi:http://dx.doi.org/10.1007/BF00678981

Petibon, C. M., Kjarsgaard, B. A., Jenner, G. A., & Jackson, S. E. (1998). Phase Relationships of a Silicate-bearing Natrocarbonatite from Oldoinyo Lengai at 20 and 100 MPa. *Journal of Petrology, 39*(11-12), 2137–2151. doi:https://doi.org/10.1093/petroj/39.11-12.2137

Renner, S., & Wellmer, F. W. (2020). Volatility Drivers on the Metal Market and Exposure of Producing Countries. *Mineral Economics, 33*, 311–340.

Simandl, G. J., & Paradis, S. (2018). Carbonatites: Related Ore Deposits, Resources, Footprint, and Exploration Methods. *Applied Earth Science, 127:4, 123-152, 127*(4), 123-152. doi: 10.1080/25726838.2018.1516935

Sjoberg, J. (1996). *Large Scale Slope Stability in Open Pit Mining.* Sweden: Division of Rock Mechanics; Lulea University of Technology.

Sullivan, T. D. (2013). Pit Slope Design and Risk – A View of the Current State of the Art. *The South African Institute of Mining and Metallurgy*, 51-80.

Swinden, S., & Hall, M. (2012). *NI 43-101 Technical Report and Mineral Resource Estimate for the Songwe Hill Rare Earth Element (REE) Project, Phalombe District, Republic of Malawi.* Pretoria, South Africa: The MSA Group.

Wall, F., & Mariano, A. N. (1996). Rare Earth Minerals in Carbonatites: A Discussion Centered on the Kangankunde Carbonatite, Malawi. In A. P. Jones, F. Wall, & C. T. Williams, *Chemistry, Origin and Ore Deposits* (pp. 193-225). U.K: Chapman & Hall, London.

Witley, J. C., Swinden, S., Trusler, G., & Dempers, N. (2019). *Songwe Hill Rare Earth Elements (REE) Project, Phalombe District, Malawi.* South Africa: MSA Group.

Woolley, A. R., & Church, A. A. (2005). Extrusive Carbonatites: A brief review. *Lithos, 85*, 1-14. doi:10.1016/j.lithos.2005.03.018

Xu, C., Wang, L., Song, W., & Wu, M. (2015). Carbonatites in China: A Review for Genesis and Mineralization. *Geoscience Frontiers, 1*, 105-114. doi:10.1016/j.gsf.2010.09.001

2 GEOLOGY AND GEOTECHNICAL FEATURES OF SONGWE HILL

2.1 Location

Songwe Hill is situated in Phalombe district South-eastern region of Malawi. The area is approximately 70km from the old capital Zomba and about 90km from the commercial city of Blantyre (Figure 2.1). On international boulders, Malawi shares boundaries with Tanzania to the north, Zambia to the west and Mozambique surrounds the country from east to west. The study area of Songwe Hill is adjacent to Mozambique separated by the syenitic intrusion of Mauze Mountain. Access to the area is mainly by secondary gravel and dirt roads after branching off the Migowi trading nearly 12km to Songwe campsite.

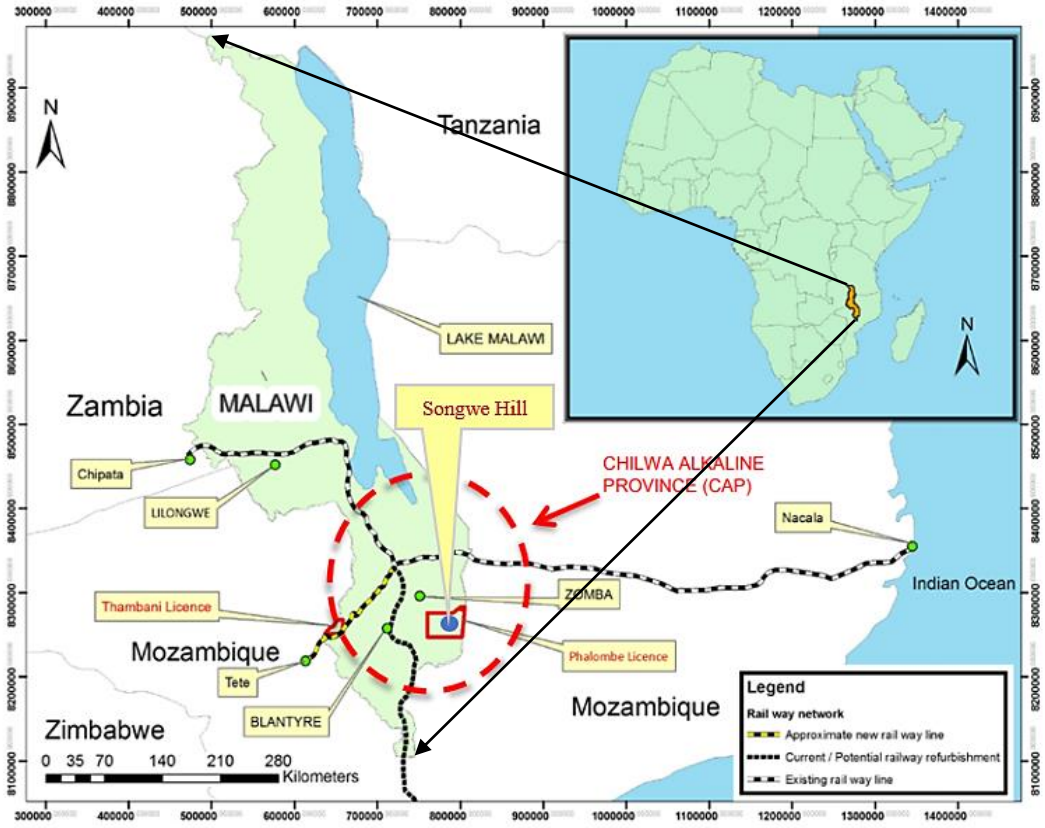

Figure 2.1. Map of Malawi showing project licensed area

2.2 Tectonic Setting

The study area lies within the Malawi Rift System (MRS) which is part of the EARS that, apart from volcanic activities, is experiencing fairly high seismicity (Figure 2.2). Ebinger has described the EARS as a natural laboratory for studies of active continental extension (Wadge et al., 2016). The EARS is an intra-continental ridge system, which consists of an axial rift and prelude of oceanic opening. The system shows up at the surface as a series of several thousand kilometers long aligned successions of adjacent individual tectonic basins (rift valleys), separated from each other by relative shoals and generally bordered by uplifted shoulders. The basins are controlled by faults and form a subsiding graben or trough, approximately one hundred kilometers long, a few tens kilometers in width, empty or filled with sediments and/or volcanic rocks (Chorowicz, 2005). As seen from Figure 2.2, the MRS is part of the western branch of the EARS and covers the Malawi Lake Basin, and extends south of Malawi into neighbouring Mozambique.

In relation to tectonism, the understanding of the in situ stress fields is crucial in mining. As articulated by Heidbach et al. (2018), the crustal in situ stress field is not only key for the understanding of geodynamic processes such as global plate tectonics and earthquakes, but it is also essential for the management of geo-reservoirs, mining activities, and underground storage sites for energy and waste. Heidbach, et al. (2018) adds that from the in situ stress state the distance to a given failure criterion for any point in the subsurface can be derived and this distance is critical as it indicates the stress changes that are required for reactivation of a pre-existing fault or creation of a new fracture due to induced or natural processes. Wadge et al. (2016) highlighted that, in rift zones, the horizontal stress is much more variable (Figure 2.3) and the differential value may be several tens of MPas, which is ascribed to the abrupt changes in the material properties (e.g., Young's modulus) of different lithologies. Depending on the faulting mechanism, the horizontal stress may be predominant or not. For instance, in a normal faulting regime, the vertical stress component is greater than the two horizontal stress components and lower in other faulting regimes.

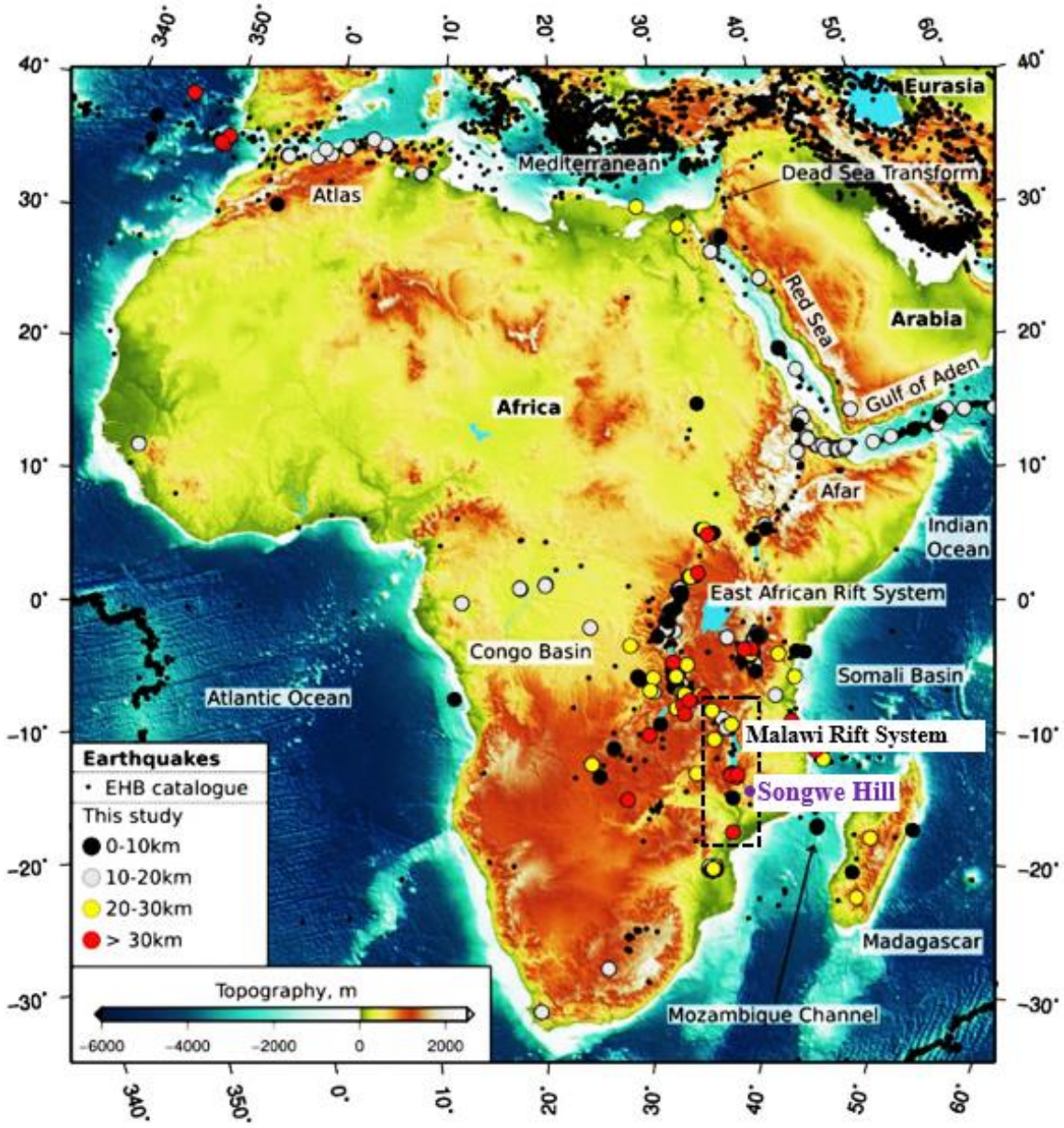

Figure 2.2 Tectonic and seismic activity along the EARS (Craig et al., 2011)

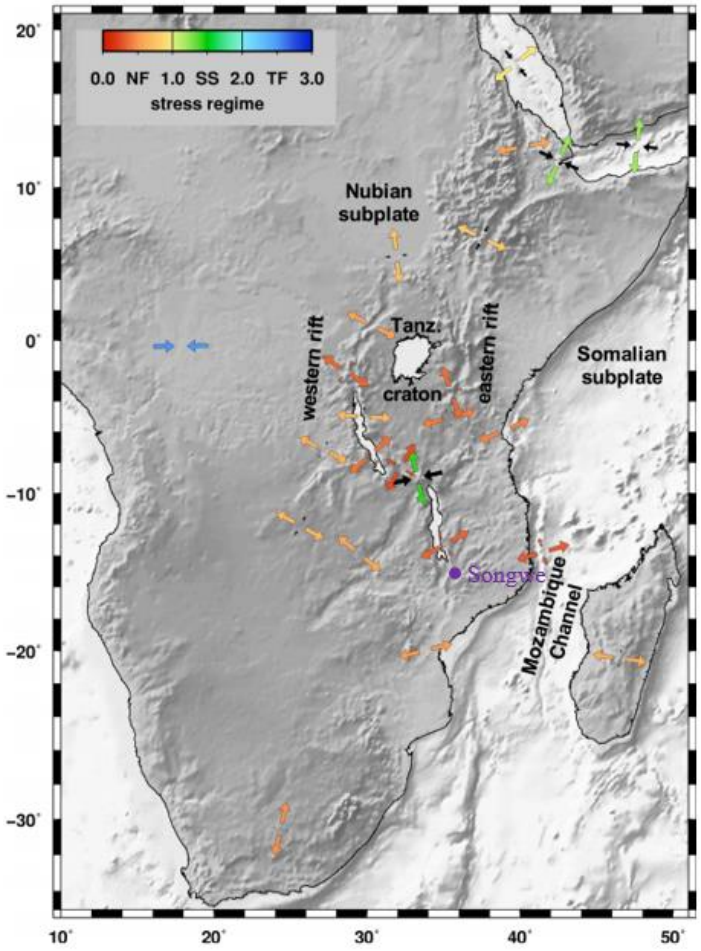

Figure 2.3 Vectors for the orientations of horizontal principal stress (Chorowicz, 2005)

2.3 Geological Setting

2.3.1 General Geology

The geology in Malawi is generally predominated by igneous and metamorphic rock masses. These crystalline rocks are of Precambrian to Lower Palaeozoic age which are referred to as the Malawi Basement Complex (Figure 2.4). Over time, the Basement rocks have undergone a prolonged structural and metamorphic history. At various localities, the Precambrian to early Palaeozoic basement complex is overlain by a sequence of Permo-Carboniferous to Lower Jurassic sedimentary rocks of the Karoo super-group and superficial Tertiary to recent Karoo sediments (Carter and Bennet, 1973).

The post-Basement Complex development of the country was dominated by epeirogenic movements, faulting, and the formation of the Malawi Rift Valley which is part of the East African Rift System (EARS). Songwe Hill forms part of the young alkaline volcanic activity that extensively intruded into the Malawi southern region basement rocks. The emplacement of the alkaline intrusions occurred during the Late Jurassic – Early Cretaceous period which affected an area approximately 300-400 km in diameter in the south of Malawi and in Mozambique (Broom-fendley et al., 2017). The entire southern region that was affected by this episode of alkaline volcanism in Malawi is called the Chilwa Alkaline Province (CAP) as shown in Figure 2.4.

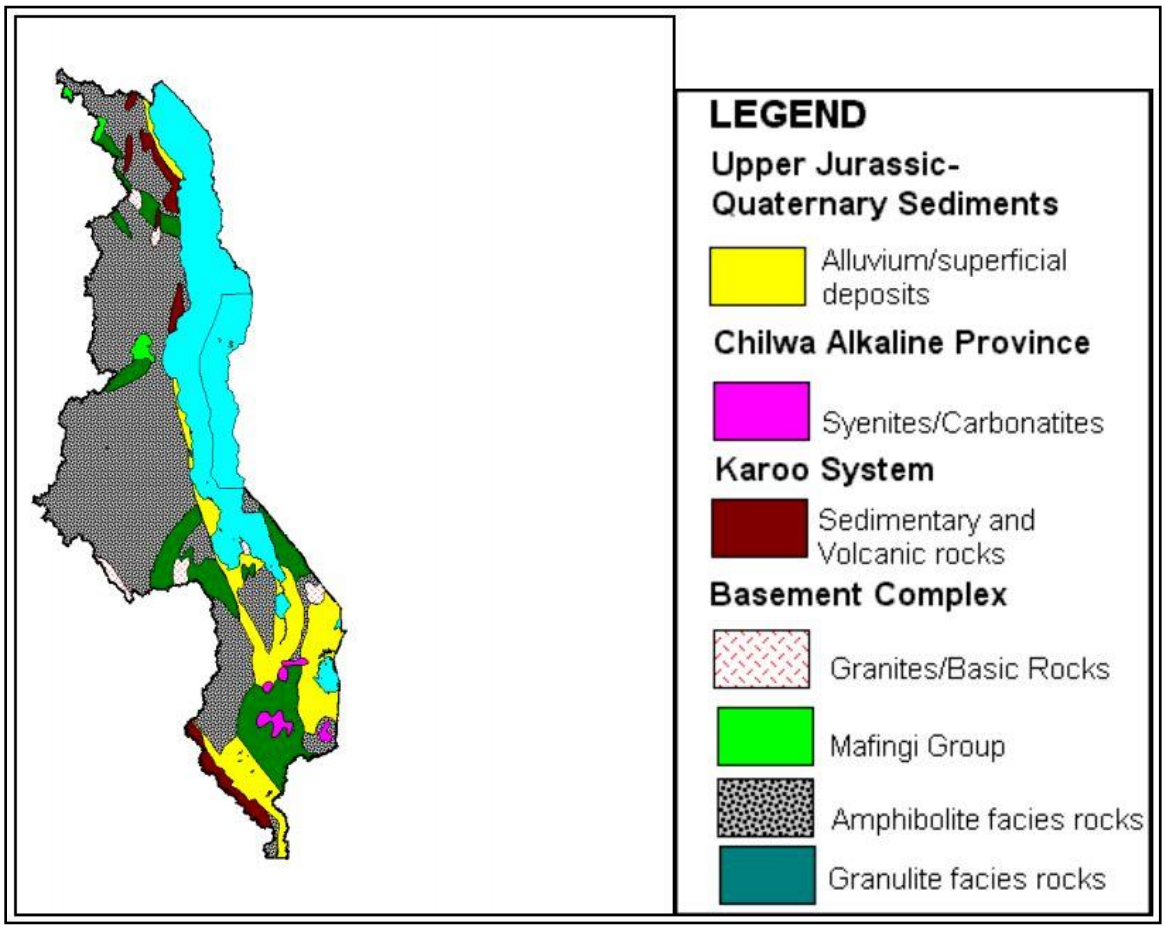

Figure 2.4 General geology of Malawi after (Land, 2009)

2.3.2 Chilwa Alkaline Rocks

The alkaline intrusion of the CAP range in age from 98 Ma to 137 Ma, making it the oldest igneous province associated with the eastern branch of the East African Rift (Witley et al., 2019). The largest alkaline intrusions of the CAP; Mulanje Mountain and Zomba Plateaux consist of peralkaline granite and quartz-bearing syenite. A considerable number of intrusions are composed of syenites, nepheline syenites, ijolite, nephelinite, carbonatite, and small phonolite plugs and breccia vents. Carbonatites are widely emplaced throughout the CAP. There are seventeen carbonatite intrusions that have been documented in southern Malawi and adjoining Mozambique at the junction of the north-south-trending fault system of the East African Rift and east-west-trending fault system of the Zambezi Rift (Witley et al., 2019). Songwe Hill is a large carbonatitic vent (Figure 2.5) within the Province alongside three other substantial carbonatite complexes: Chilwa Island, Kangamkunde and Tundulu. Many smaller intrusions of carbonatite occur throughout the Province.

The aforementioned four large carbonatite complexes have metasomatized aureoles characterized by the presence of fenites. The fenites are a by-product of the cooling and crystallization of carbonatitic and alkaline melts ejected in multiple phases through the fenitization process. The fenitization process involves the removal of silica from the protolith and is marked by an increase in alkaline content ($Na_2O + K_2O$) irrespective of silica content or mobility (Simandl and Paradis, 2018). Elliott, et al. (2018) reviewed 17 carbonatite complexes globally in an attempt to classify fenites, and applying the whole-rock ratio of Na to K, they categorized fenites as sodic, intermediate or potassic. For the Songwe carbonatite complex, the field observations, logging data, and chemical analysis conducted reveal that the rock mass is intimately associated with potassic fenite which reflects that the fenitization was predominated by potassium metasomatism consisting mainly of K-feldspar other than sodium metasomatism.

2.3.3 Local Geology

The surface geological mapping and drill cores at Songwe Hill show that the principal geological units of the carbonatite complex include: carbonatite, fenite, and breccia (Figure 2.6).

Minor geological units consist of veins of apatite and fluorite-rick rock and phonolite and dolerite dykes. These alkaline intrusive bodies got emplaced into the basement granulite and gneiss with a cross-cutting relationship. Broom-Fendley et al. (2017) presented new petrographic and geochemical observations following their thin sections analyses, which revealed the occurrence of a number of accessory minerals.

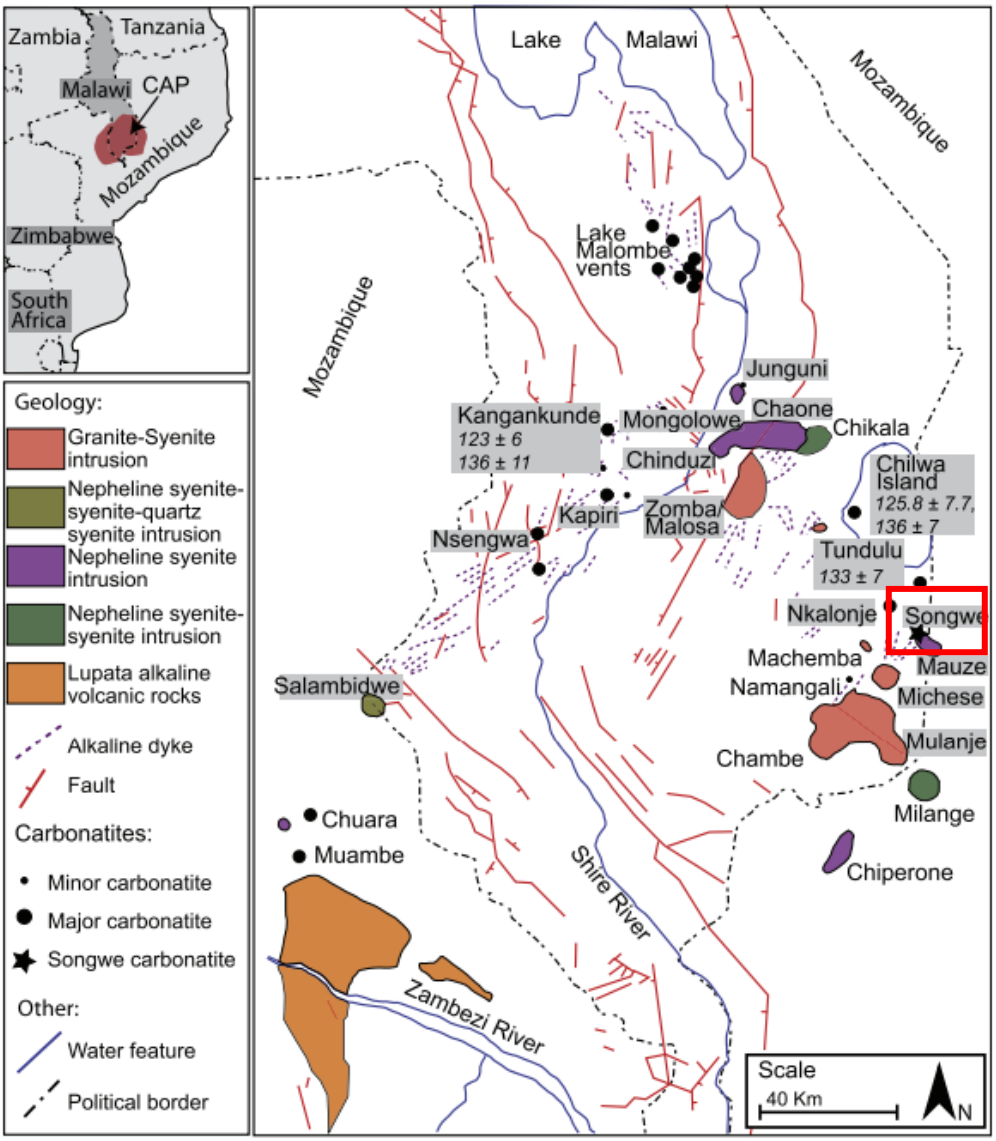

Figure 2.5 Map of the Chilwa Alkaline Province after (Broom-Fendley et al., 2017)

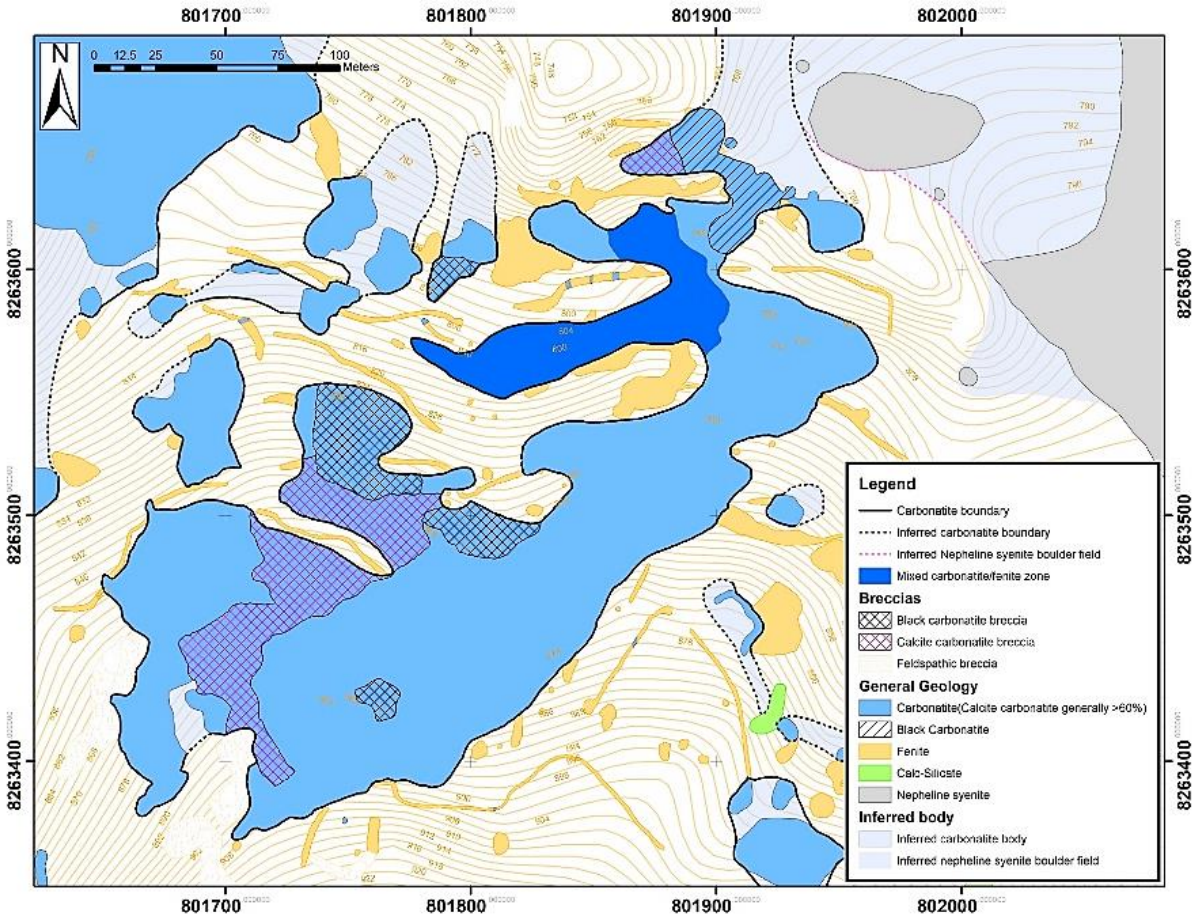

Figure 2.6 Geology of Songwe Hill

2.3.3.1 Carbonatite

The carbonatite at Songwe Hill is best exposed on the north and north-eastern facing slopes with a relatively smaller extent along the north-western slope. There are essentially three REE mineralized carbonatites namely: coarse-grained calcite carbonatite (sovite); fine-grained carbonatite (alvikite); and Fe-rich ferroan calcite carbonatite (Figure 2.7). Mkango Resources Company adopted the shorthand C1, C2, and C3 respectively to distinguish the different types of carbonatite. The shorthand is based on the carbonatite nomenclature with respect to carbonate mineralogy (e.g. calcite carbonatite, dolomite carbonatite, and ankerite carbonatite) and chemically they are classified as; Calcio-carbonatite (C1), Magnesio-carbonatite (C2), and Ferro-carbonatite (C3).

The lithological logging has demonstrated that C1 is rare at Songwe as it just occurs as a rounded clast in other carbonatite types. Thin section results by Broom-Fendley et al. (2017) discovered a composition of medium-grained anhedral calcite (90 vol %), minor anhedral ankerite (5 vol %) and assemblage of ovoid apatite, subhedral zircon, euhedral pyrite, anhedral pyrochlore, and anhedral K-feldspar. On the contrary, C2 is ubiquitous and largely comprises of fine-grained calcite with minor interstitial ankerite. However, in some samples, xenocrysts of zircon, pyrochlore, pyrite and K-feldspar are present and are rounded and altered to varying degrees. Additionally, localized assemblages of euhedral synchysite-(Ce), baryte, and anhedral strontianite are disseminated throughout the C2 carbonatite. The C3, as identified in logged core samples, occurs as veins in calcite carbonatite, breccia clasts and as discreet masses. Fe-and Mn-rich carbonatite and Fe- and Mn oxides with apatite and minor amounts of alkali (K-) feldspar dominate the Fe-rich carbonatite. The occurrence of C3 is abundant at the center of the intrusion.

The groundmass of C3 includes bands of pale apatite-bearing layers and LREE-flourcarbonate-bearing layers suggesting multi-phase intrusions. Minor hematite (4 vol %) and zircon (1 vol %) were also identified in the groundmass (Broom-fendley et al., 2017). In some cases, carbonatite is mingled with fenite breccia. The carbonatite-rich breccias tend to have an abundance of light grey, fine-grained calcite carbonatite clasts with subordinate fenite clasts (Elliott, et al., 2018). Dependent on the proportions of carbonatite and fenite fragments, the calcite carbonatite breccia could be light grey or orange-red in color respectively. When the breccias are predominated by feldspars, which sometimes could be fenitized, the groundmass tends to be fine-grained carbonatite rich with an abundance of iron and manganese oxides and occasionally pyrochlore. According to the field observations made by the researcher, the carbonatite breccias have angular to sub-angular carbonatite fragments in a fine-grained grey carbonatite rich to feldspathic groundmass. From the core logs, the fluorite and sulphides occur as disseminations, patches and veins. The presence of sulphides, though as trace elements, calls for a critical consideration in the extraction and treatment of the tailings to prevent possible acid mine drainage

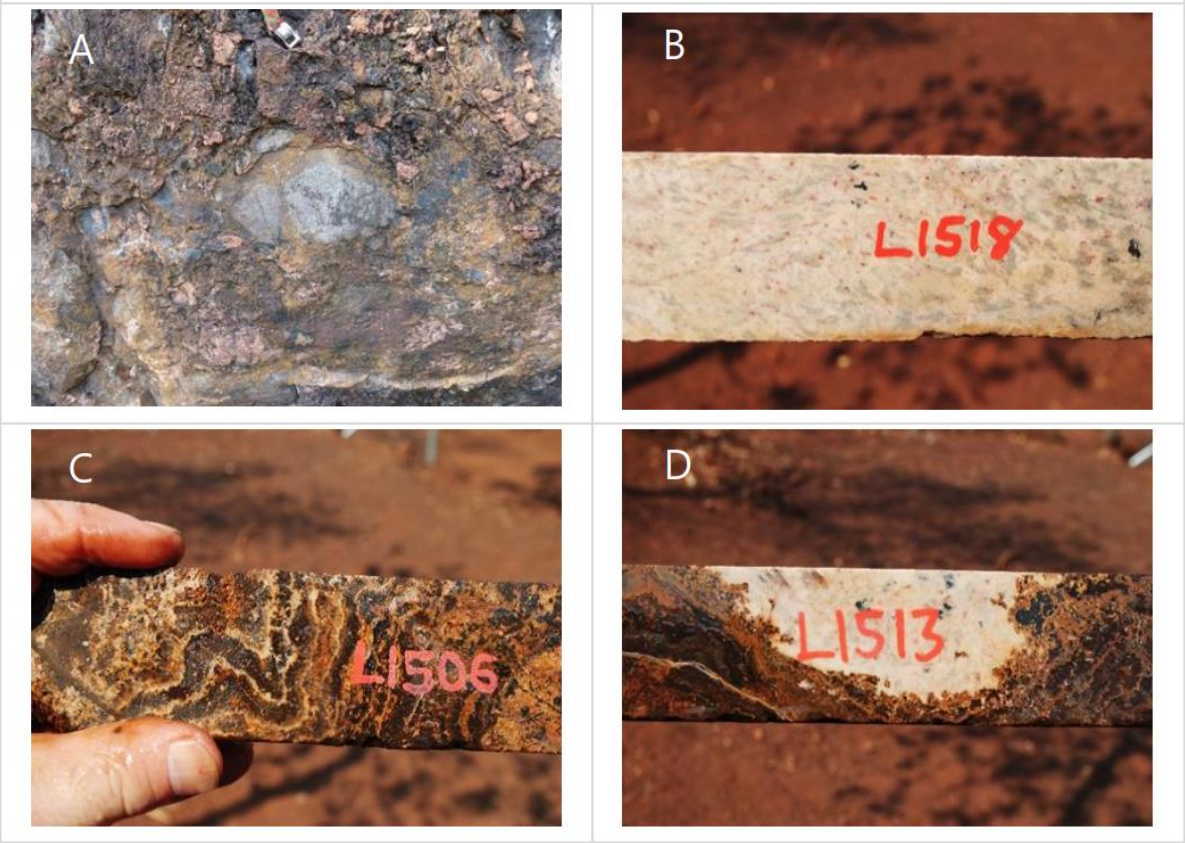

Figure 2.7. Principal carbonatite lithologies in the Songwe complex: A - a coarse C1 calcite carbonatite in fenite breccia; B – white fine-grained C2 calcite carbonatite; C – laminated and veined black to orange C3 carbonatite and D – an enclaved C2 carbonatite.

2.3.3.2 Fenite

Fenites at Songwe Hill tend to surround the carbonatite intrusion. Large blocks of fenite show evidence of being in situ and inferred as fractured blocks from the margins, or the roof of the carbonatite. Concerning the texture, the fenites exhibit a coarse-grained equigranular igneous texture (see Figure 2.8a), strongly signifying an igneous protolith. It is postulated that the major carbonatite intrusion did not crop out to the surface since the fenite is continuous with only rare carbonatite veinlets.

2.3.3.3 Late Stage Intrusions

The carbonatite complex at Songwe Hill is uniquely predominated by veins and dykes which cross-cut the main lithologies. The black Mn-Fe veins are one of the late intrusions which is abundant throughout the complex (see Figure 2.8b). Broom-Fendley et al. (2017), found that the veins range in size from less than 1 cm to several meters exhibiting a wide range of Mn-Fe ratios, and are mineralized with synchesite (Ce) and apatite. However, the veins are typically unmineralized when they occur in pure Fe oxide. The rocks consist of carbonatite rhombs and Fe- and Mn oxides characterized by limonitization. The Songwe Hill complex is also cross-cut by late apatite-Fluorite veins which are visible in both outcrop and drill hole core (Figure 2.8c). Garson & Smith (1965) first identified apatite-fluorite rocks in boulders approximately half a mile northeast of Songwe Hill and the finding was confirmed in the drill cores logged by Mkango Resources Company.

The composition of the veins is largely fluorite, apatite, calcite/ferroan-calcite, quartz and barite with accessories that include xenotime, zircon, rutile/anatase, Mn-oxides, hematite, and synchesite/parasite (Broom-Fendley et al., 2017). The crystal structure of fluorite is sub-anhedral and typically occurs in elongate stringer and in discrete patches which vary in size from 20-200μm while apatite is subhedral and clumps together in veins made of equigranular crystals measuring 150-200μm in size. The other late intrusions are silicate dykes mainly phonolitic in composition. Surface mapping of the area revealed the aphanitic or porphyritic textured dyke cross-cutting the carbonatite complex (Figure 2.8d). The dykes show a range of alterations from minimal modification to extensive alteration and fenitization. In porphyritic textured phonolite dykes, the xenoliths are generally sub-rounded to sub-angular nepheline syenites which are relatively unaltered.

(a) Fenite breccia with Mn-Fe veining

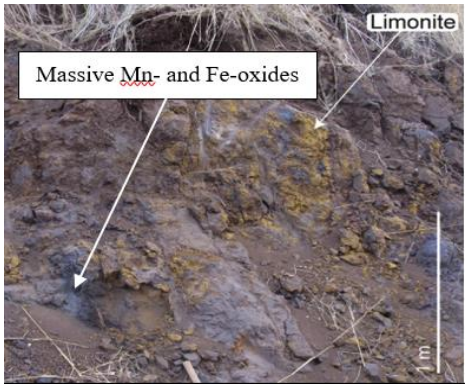

(b) Mn-Fe vein with limonite alterations

(c) Fluorite-apatite veins in fluorocarbonate

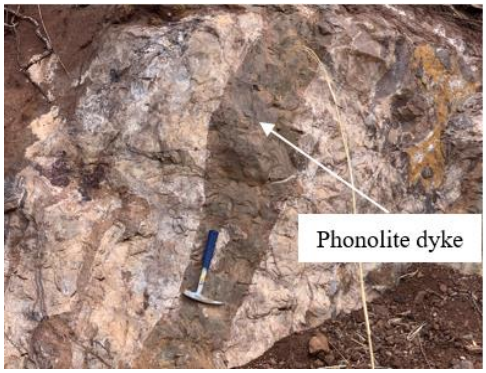

(d) Phonolite dyke cross-cutting carbonatite

Figure 2.8. Fenite and late stage intrusions that predominate the carbonatite complex

2.3.3.4 Structural Features of Songwe

As previously mentioned, Songwe Hill lies within the active tectonic environment of the MRS which is part of the main EARS. Thus, faulting and development of joints is not an uncommon phenomenon but the structural disruptions at the site are not reflected on a macro scale except for a mappable fault at the foot of the Hill as shown in Figure 2.9. Witley et al. (2019) attempted to present subtle evidence of structural deformation which they argued to be reflected in sharp lithological breaks across the area. They concluded that the lithological breaks corresponded to the faults interpreted from the ground magnetic. However, it must be admitted that the fault traces were considered as an approximation, given that the resolution of the magnetic image was low at the scale of the geological map.

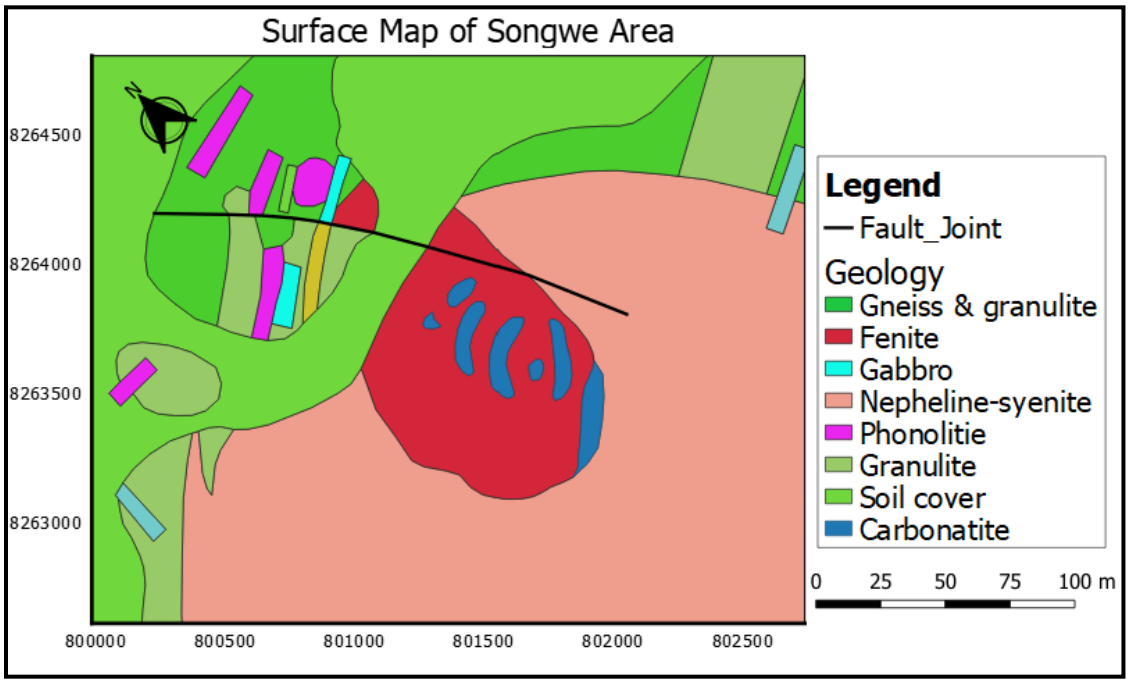

Figure 2.9. Geological map with structural features

2.4 Mineralization

The Songwe Hill carbonatite has been enriched in REE at the time when it was intruded and the redistribution and enhancement were reportedly due to the late-stage hydrothermal and carbo-hydrothermal activity. Meanwhile, the assay results published in Mkango Resources' technical report indicate that the REEs are mainly hosted in synchesite and apatite. The mineralization at the carbonatite complex occurs in all the geological domains with the highest grades and consistent mineralization in the carbonatites. Mineral Resource Estimate (MRE) from drill core samples show that the lithologies mixed with fenite locally carry high enough grade over significant widths worthy including in the mineral resources but mineralization is inconsistent throughout their full extent. Witley et al. (2019) also highlight that fenites locally contain economically interesting concentrations of REE but seldom over economic widths.

During intrusion period, the carbonatite underwent fractionation in the subsurface as evidenced by the cumulate C1 carbonatites that occur as fragments. Later, fluid exsolution from the C2 carbonatite metasomatized the surrounding silicate rocks producing fenites which got incorporated in carbonatite by stopping or in explosion breccias related to continued fluid over-pressuring of the magma chamber (Witley et al., 2019). Fundamentally, the carbonatite system evolved, and an extensive and intense hydro-carbothermal phase developed, culminating into widespread re-distribution of mobile elements in the system.

2.5 Rock Mass Characterization

In order to comprehend the general characteristic behavior and rock conditions of the carbonatite complexes, rock mass classification was performed using the Songwe Hill carbonatite complex. There are a number of classification systems that can be selected with respect to the intended purpose of application. The schemes of rock classification are generally categorized as qualitative and quantitative based on the mode of characterization. Qualitative (descriptive) schemes include Geological Strength Index (GSI) and Rock Load while Q, Rock Mass Rating (RMR), Rock Structure Rating (RSR), and Rock Quality Designation (RQD) systems are quantitative (Abbas & Konietzky, 2017). The selection of the method to be used in a study is very much dependent on the application significance. In this work, GSI was opted in the characterization of the rock mass owing to its extensive applicability, especially in rock slope analysis. GSI system, introduced by Hoek in 1994, is a widely accepted scheme for describing the rock mass reliably fast and simple. The method is a result of a combination of observations of the rock mass conditions (Terzaghi's descriptions) with the relationships developed from the extensive experience gained using the RMR-system. The relationship drawn between rock mass structure and rock discontinuity conditions is used to estimate an average GSI value for a rock mass as shown in Figure 2.10. This classification system is defined by the generalized Hoek-Brown (H-B) failure criterion for jointed rock masses as

$$\sigma_1' = \sigma_3' + \sigma_{ci}\left(m_b\frac{\sigma_3'}{\sigma_{ci}} + s\right)^a \qquad (2.1)$$

Where σ_1' and σ_3' are the maximum and minimum effective stresses at failure,

m_b is the value of the H-B constant for the rock mass,

s and *a* are constants, which rely on the rock mass characteristics, and

σ_{ci} is the uniaxial compressive strength of the intact rock pieces.

In making an estimate of the strength and deformability of jointed rock masses, the H-B criterion takes into account three properties which include:

1. The uniaxial compressive strength (σ_{ci}) of the intact rock elements,
2. The value of the H-B constant (m_i) for these intact rock elements, and
3. The value of the GSI for the rock mass

Once the GSI value has been either estimated or computed, the parametric constants that describe the rock mass strength characteristics are calculated as follows:

$$m_b = m_i exp\left(\frac{GSI - 100}{28}\right) \qquad (2.2)$$

$$s = exp\left(\frac{GSI - 100}{9 - 3D}\right) \qquad (2.3)$$

and

$$a = \frac{1}{2} + \frac{1}{6}\left(e^{-GSI/15} - e^{-20/3}\right) \qquad (2.4)$$

where *D* is the degree of disturbance in the rock mass

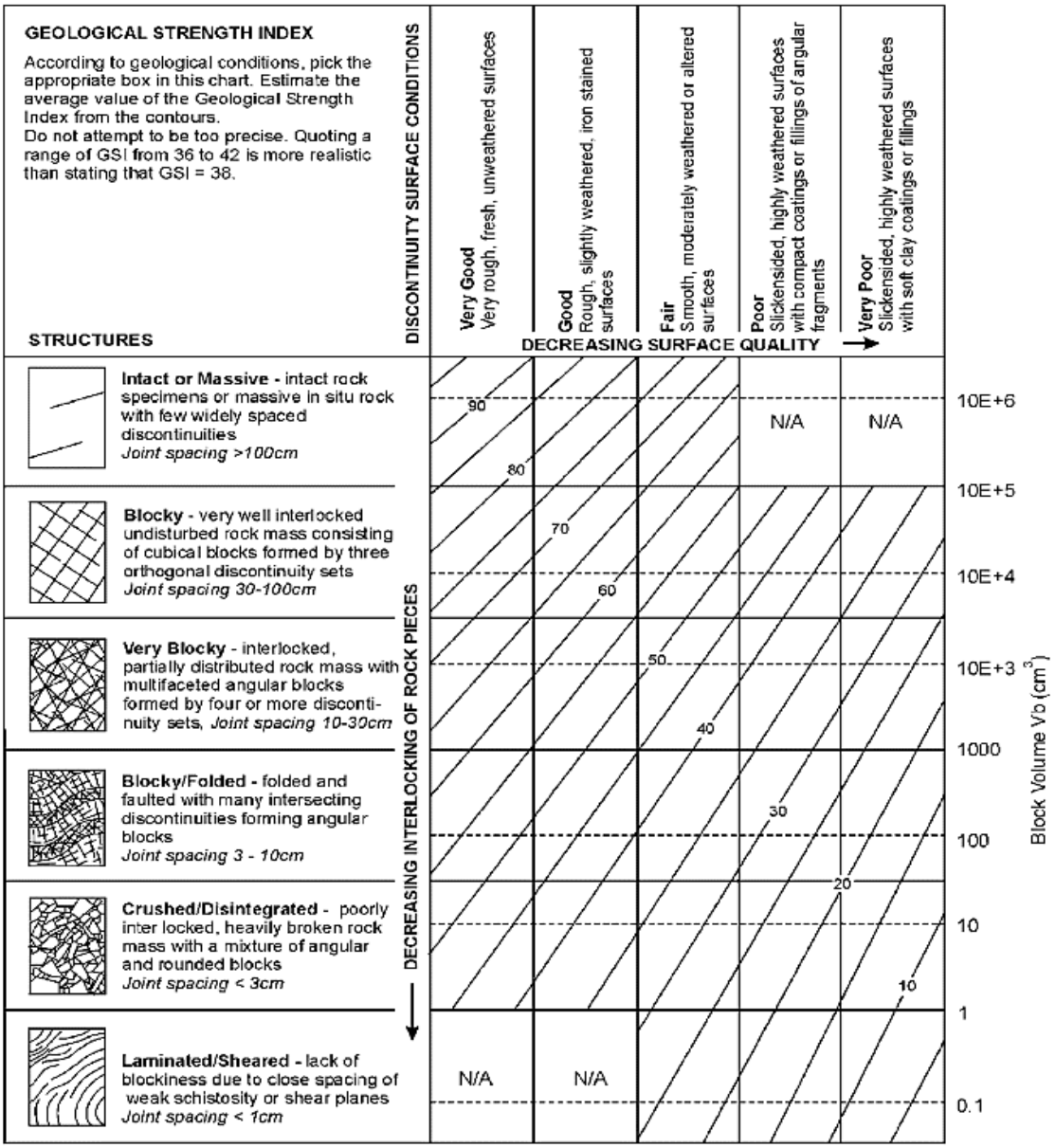

Figure 2.10 Estimate of GSI based on visual inspection of geological conditions (Hoek,et al., 2013)

However, Marinos et al. (2005) highlight that GSI ought to be ideally assigned from the field observation of the rock mass by aptly experienced engineering geological personnel. This is because the system relies on the qualitative assessment of the structure and surface conditions of the rock mass, and assigns a numerical value based on the assessment.

The qualitative description in arriving at a characterization value has been criticized to be prone to subjectivity. Another limitation of the direct application of GSI value to rock mass when dealing with pit slopes is that at the time of open-pit slope design, exposure of critical rock mass units is often limited, or unavailable. Mostly, information on rock mass conditions may be accessible only from the drill core, from which GSI cannot be directly assigned (Thomas, Ayemin, & Neilsen, 2015). To circumvent these constraints, empirical relationships have been developed between GSI and a number of rock mass classification schemes. Among a plethora of quantitative schemes, the RMR system was preferred to characterize the rock mass because of its easiness and versatility in engineering practices involving; tunnels, mines, slopes, and foundations. In addition, the scheme has withstood the test of time with a high universal acceptance on account of its varied applications amounting to over 351 case histories (Bieniawski, 1989). The RMR system as applied in slope analysis makes use of the five basic parameters to characterize a rock mass. The parameters include: UCS of rock material, RQD, discontinuity spacing, condition of discontinuity surface, and groundwater conditions. RQD is derived as a percentage of the sum of intact core pieces longer than 10cm divided by the total length of the core run (see Equation 2.5). The RMR method can be presented statistically as in Equation 2.6:

$$RQD = \frac{\sum L_{IR} \geq 100mm}{L_T} \times 100\% \qquad (2.5)$$

where, L_{IR} is the length of intact rock pieces and L_T is the total core run length

$$RMR = \sum_{i=1}^{5} R_{P_i} \qquad (2.6)$$

where R_{P_i} is the rating of each of the five parameters

To get a representative RMR value and interpretation of the rock mass, a set of guidelines were adhered to as presented in Table 2.1. In carrying out rock mass characterization, surface observations, geotechnical log sheets of drilled core and core sample laboratory experimental results were used. Geotechnical log sheets provided information on RQD, joint spacing, and joint conditions carefully recorded from the diamond drill core.

The data was logged at a regular interval of a 3 meter run, as such an average value was computed to characterize the rock on each drill hole. The persistence of joints was determined through scan line mapping of rock cuts created when making drill pads. Commonly, the length of the majority of the joints was ≥ 3 meters. To determine the UCS values, laboratory tests were run on representative samples collected from drill holes. The samples were prepared according to International Society of Rock Mechanics (ISRM) standards.

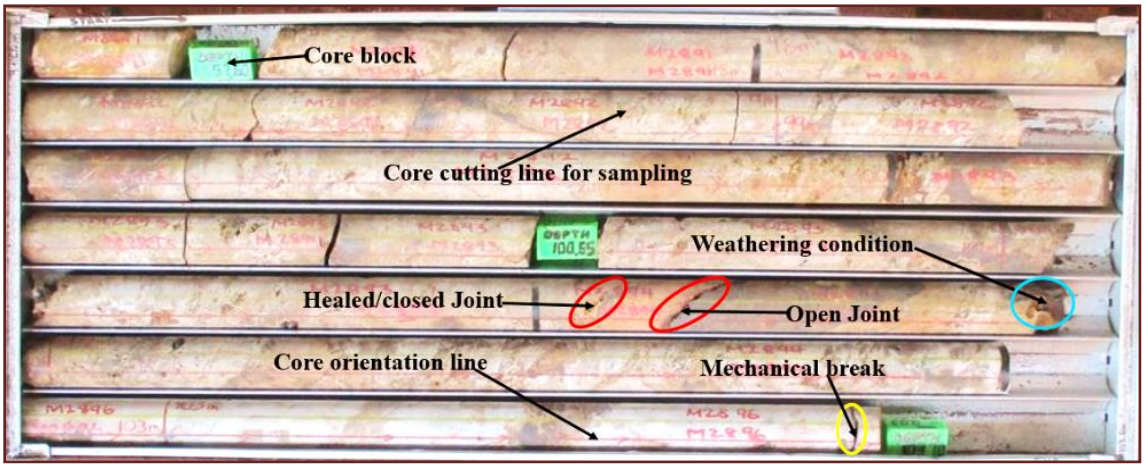

Figure 2.11 A sample tray of diamond drill core

The quality rating of the parameters for the carbonatite rock mass is presented in Table 2.2. The rating for each parameter was averaged from geotechnical drill holes' data to get general representative values, and the averaged sum of the values were fitted in Table 2.1 of RMR guideline for description. From the rating results, carbonatite rock masses can be described as a good rock with a classification of "II" (Table 2.3). For Songwe carbonatite, the RMR rating was found to be 62. To derive the GSI value, the computed RMR value was mathematically reworked based on the relationship formula by Singh & Goel (2011) given as;

$$GSI = RMR - 5 \qquad (2.7)$$

From the mathematical correlation of GSI and RMR, the GSI value of the Songwe carbonatite complex is evaluated to be 57.

The qualitative interpretation of the rock mass based on computed GSI value implies that the carbonatite rock mass is a good rock with a structure of multi-faceted angular blocks generated by three or more joint sets with a surface quality of being rough, slightly weathered and iron-stained surface (refer to Figure 2.10). The description is quite in agreement with the quantitative RMR interpretation of the rock mass characterization.

Table 2.1 Guidelines for rock mass classification system and ratings

Parameter	**Range of Values**						
UCS (MPa)	> 250	100-250	50-100	25-50	5-25	1-5	1
Rating	15	12	7	4	2	1	0
RQD (%)	90-100	75-90	50-75	25-50	< 25		
Rating	20	17	13	8	5		
Joint spacing (J_s) (m)	> 2	0.6-2	0.2-0. 6	0.06-0.2	< 0.06		
Rating	20	15	10	8	5		
Discontinuity length (J_l)(m)	< 1	1-3	3-10	10-20	> 20		
Rating	6	4	2	1	0		
Joint separation (J_s)(mm)	None	< 0.1	0.1-1.0	1-5	> 5		
Rating	6	5	4	1	0		
Joint roughness (J_r)(mm)	Very rough	Rough	Slightly rough	Smooth	Slickensided		
Rating	6	5	3	1	0		
Infilling (J_I) (mm)	None	Hard < 5	Hard > 5	Soft < 5	Soft		
Rating	6	4	2	2	> 5		
Joint weathering (J_w)	Unweathered	Slightly weathered	Moderately weathered	Highly weathered	Decomposed		
Rating	6	5	3	1	0		
Groundwater (Gw) (inflow per 10m)	Dry	Damp	Wet	Dripping	Flowing		
Rating	15	10	7	4	0		

Table 2.2 Rock mass characterization of Songwe carbonatite complex

Hole ID	UCS	RQD	J_s	Condition of Discontinuities (J_c)					GW	RMR
				J_l	J_s	J_r	J_l	J_w		
PX038	7	13	10	4	1	3	2	3	15	**58**
PX045	4	13	10	4	4	5	4	3	15	**62**
PX051	4	8	8	4	1	3	0	1	15	**44**
PX055	12	13	10	4	1	3	2	5	15	**65**
PX057	7	17	15	4	4	5	4	3	15	**74**
PX058	7	17	15	4	4	5	4	3	15	**74**
PX059	7	17	10	4	1	5	2	3	15	**64**
PX063	7	17	10	4	1	5	2	3	15	**64**
PX070	4	13	10	4	1	5	2	3	15	**57**
PX077	7	17	10	4	4	5	2	3	15	**67**
PX087	7	13	10	4	1	3	2	5	15	**60**
PX089	7	13	10	4	1	3	2	5	15	**60**
PX093	7	13	10	4	1	5	2	3	15	**60**
Average	7	14	11	4	2	4	2	3	15	**62**

Table 2.3 Rock mass quality classes of RMR classification system

Rock mass description	Very good	Good	Fair	Poor	Very poor
Ranking	100-81	80-61	60-41	40-21	< 20
Class	I	II	III	IV	V

2.6 Summary

Since all rock masses have inherent complex characteristics of the field conditions, this chapter was dedicated to evaluating the geological and geotechnical conditions of the carbonatite rock mass based on the Songwe Hill carbonatite complex as a representative case. The distinctive features observed from field survey shows that the carbonatite complex is characterized by in situ rock damage due to brecciation, which is a result of hydro-fracturing involving high-pressure fluids and tectonic forces along pre-existing plane of weakness, and has high fracture frequency per unit area indicative of high tectonic stress regime.

Furthermore, the rock mass is pervasively altered through fenitization causing rock transition cavities and fractures between the carbonatite and fenite. To understand the rock quality in relation to mining, both qualitative and quantitative rock mass classification systems, viz. GSI and RMR respectively, were applied to characterize the rock mass. Based on the evaluation, the magmatic carbonatite rock masses can be described as competent, but, in spite of the competency, they tend to have multi-faceted angular blocks generated by three or more discontinuity sets though most of the joints are filled with calcite infill. Thus, for OPM development in such rock masses, possible structural controlled failures need to be carefully evaluated.

2.7 References

Abbas, S. M., & Konietzky, H. (2017). *Rock Mass Classification Systems*. Gustav-Zeuner-Straße: TU Bergakademie Freiberg. Germany: Geotechnical Institute.

Bieniawski, Z. T. (1989). *Engineering Rock Mass Classification*: A Complete Manual for Engineers and Geologists in Mining, Civil and Petroleum Engineering. Toronto, Canada: John Wiley and Sons.

Broom-Fendley, S., Brady, A. E., Horstwood, M. S., Woolley, A. R., Mtegha, J., Wall, F., .Gunn, G. (2017). Geology, Geochemistry And Geochronology of the Songwe Hill Carbonatite, Malawi. *Journal of African Earth Sciences* (134), 10-23.

Carter, G. S., & Bennet, J. D. (1973). *The Geology and Mineral Resources of Malawi* (Revised Ed.). Zomba: Malawi Government Printer.

Chorowicz, J. (2005). The East African Rift System. *Journal of African Earth Sciences*, 43, 379-410.

Craig, T. J., Jackson, J. A., Priestley, K., & McKenzie, D. (2011). Earthquake Distribution Patterns in Africa: Their Relationship to Variations in Lithospheric and Geological Structure, and their Rheological Implications. *Geophysical Journal International*, 185, 403–434. doi:10.1111/j.1365-246X.2011.04950.x

Elliott, H. A., Wall, F., Chakhmouradian, A. R., Siegfried, P. R., Dahlgren, S., Weatherley, S., Deady, E. (2018). Fenites associated with carbonatite complexes: A review. *Ore Geology Reviews*, 38-59. doi:https://doi.org/10.1016/j.oregeorev.2017.12.003

Garson, M. S., & Smith, C. W. (1965). *Carbonatite and Agglomeratic Vents in the Western Shire Valley. Zomba*: Geological Survey Department.

Heidbach, O., Rajabi, M., Cui, X., Fuchs, K., Müller, B., Reinecker, J., Zoback, M. (2018). The World Stress Map Database Release 2016: Crustal Stress Pattern Across Scales. *Tectonophysics*, 744, 484–498. Doi.org/10.1016/j.tecto.2018.07.007

Llano-Serna, M. A., Williams, D. J., & Ruest, M. R. (2016). Analysis of Kennecott Utah Copper's Bingham Canyon Mine Pit Wall Slides. *Tailings and Mine Waste* (pp. 787-794). Colorado, USA: The MPM applied to the mining industry.

Marinos, V., Marinos, P., & Hoek, E. (2005). The Geological Strength Index: Applications and Limitations. *Bull Eng Geol Environ*, 64, 55–65. Doi:10.1007/s10064-004-0270-5

Singh, B., & Goel, K. R. (2011). Engineering rock mass classification: tunneling, foundations, and landslides. Oxford, UK: Butterworth-Heinemann

Simandl , G. J., & Paradis, S. (2018). Carbonatites: Related Ore Deposits, Resources, Footprint, and Exploration Methods. *Applied Earth Science*, 127(4), 123-152. doi:10.1080/25726838.2018.1516935

Wadge, G., Biggs, J., Lloyd, R., & Kendall, J. M. (2016). Historical Volcanism and the State of Stress in the East African Rift System. *Front. Earth Sci*, 4(86), 1-24. doi:https://doi.org/10.3389/feart.2016.00086

Witley, J. C., Swinden, S., Trusler, G., & Dempers, N. (2019). Songwe Hill Rare Earth Elements (REE) Project, Phalombe District, Malawi. South Africa: MSA Group.

3 KINEMATIC ANALYSIS OF SLOPE STABILITY

3.1 Introduction

Geological structures in OPM are significantly critical when evaluating a slope in an active mine or at a potential mine developmental site. Major geological structures like bedding planes, faults, cleavages, fractures and joints may greatly affect the stability of OPM. Problems with discontinuities in rock slopes have led to several detrimental slope failures over the years and have grown to be of considerable concern to mining and geotechnical engineers as discussed by Chen et al. (2019), Smith & Arnhardt (2016), Al Mandalawi et al. (2016), Kıncal (2014) and Barnett (2003). Hence, prior to deterministic analyses of the stability of slope using either limit equilibrium or numerical methods, it is important to establish potential instability modes on an excavation. In geotechnical engineering, kinematic analysis has been extensively applied to pre-determine the discontinuity-controlled stability condition of rock slopes in different instability modes, namely planar, wedge, and toppling type of failures (Aksoy & Ercanoglu, 2009). The Kinematic checks as applied in slope stability, examine potential modes of slope failure in rock mass with respect to an existing or proposed slope geometry. The approach is purely geometric since the prediction of failure modes is based on the interactions of the structures. The requirements to conduct kinematic analysis are a combination of discontinuity and slope face orientation together with friction angle.

The general practice in kinematic analyses involves an assessment based on plotting all measured discontinuity planes on a stereographic projection net and evaluating the position (dip and dip orientation) of particular planes represented as the poles at the centers of the concentration zones. This evaluation with respect to the slope angle and the friction angle (ϕ) of the discontinuity plane(s) in concern is extensively discussed in Hoek & Bray (2005) and Kliche (1999) among many authors. Meanwhile, Aksoy & Ercanoglu (2009) adapted the kinematic analyses to the logic of geographic information system (GIS) in the way to compare the intersections, orientations and dips of the discontinuity planes, with the slope geometry from Digital Elevation Model (DEM).

In another development, Shen et al. (2012) integrated the GIS and the numerical simulation for slope stability analysis. Furthermore, with the advances in computer technologies Aksoy & Ercanoglu (2009) and Nelson et al. (2007) produced a computer program that applied fuzzy logic models from various combined data bases for stability analysis. Basically, in the former technique, the kinematic checks have different approaches in the stereographic representation like the Markland test and friction cone approach. Ideally, the Markland test is a very critical tool for identifying the discontinuities that could lead to planar, wedge or toppling failure type in rock mass and eliminating other discontinuities from consideration (Kliche, 1999). The test is as well reliably crucial for conducting a sector analysis of a mine high wall or road cut given the fact that each different alignment of the high wall or road cut can be analyzed independently. However, in this study, the friction cone method, which combines elements of kinematics and kinetics (motion and tectonic forces), is applied to perform the analysis at Songwe Hill mine site to provide the guidelines of mining planning and development in carbonatite rock mass.

3.2 Failure Modes

Generally, possible failures in rock slope analysis are: planar failure, wedge failure, and toppling failure. The conditions under which the failures occur have been expounded by several authors (Hoek & Bray, 2005; Kliche, 1999; Goodman, 1989). As presented in Figure 3.1, in planar failure, the rock mass slides on a single surface making it easier to conduct a 2-dimensional analysis which is useful for demonstrating the sensitivity of the slopes to changes in shear strength, groundwater and applied forces. On the other hand, wedge failure takes place when a rock mass slides on two intersecting planes in which case the blocks are presumed to be tetrahedron defined by the two intersecting planes, the slope face and the upper slope surface. In the case of toppling, the possibility is only when a set of well-developed or through-going discontinuities dip steeply into the slope. The failure process in toppling is such that long, thin columns of rock formed by the steeply dipping discontinuities may rotate about a pivot point located at the lowest corner of the block (Kliche, 1999). Another failure mode, which is characteristic of landslides and not covered herein, is circular failure. The circular failure occurs from a process of localization of deformation.

Unlike other failure modes, it is difficult to generalize circular failure because there is no specific shape of the failure surface and the associated failure mechanisms are not easily predictable.

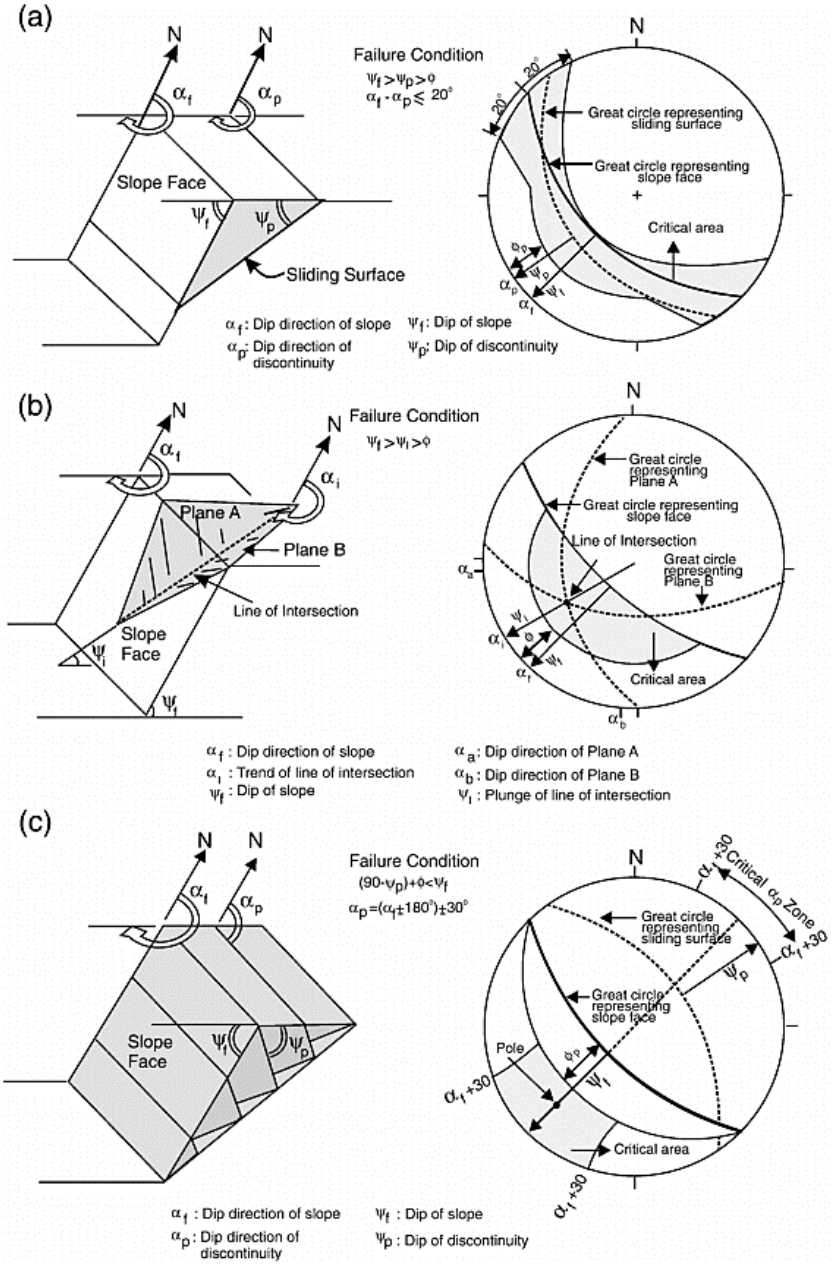

Figure 3.1 Slope failure modes and the kinematic conditions for discontinuity-controlled rock slope instabilities: (a). planar failure; (b). wedge failure and (c). toppling failure (Aksoy & Ercanoglu, 2009)

3.3 Methodology

The approach to kinematic analysis is summarized in Figure 3.3. The input data for the study was obtained from field investigation and laboratory experiments. To perform the kinematic analysis, Dips 6.0 software (Rocscience, 2019), was used in plotting the discontinuities based on the dip and dip direction of the joints. Dips 6.0 is an application designed to analyze features related to engineering analysis of rock structures. The program permits the analysis and visualization of structural data employing similar techniques applied in manual stereographic projections. The parametric setting of the analysis entailed friction angle set at 35° based on shear strength test results. This value is represented by a plane circle termed friction cone in the stereonet determined by counting the great circles of the stereonet from outside inwards. The overall pit slope face was first set at the steep possible angle of 45° for deep surface mines (Saadoun et al., 2018; Stacey et al., 2003; Sjorberg, 1999) and the direction was varied with respect to the slope face as 360°/ 0°, 90°, 180°, and 270°. The slope angle (α) of the slope face is represented by curved plane in the stereonet. Lastly, dip of the discontinuities (β) and dip directions are represented by vector points since the number of joints is high. The analysis was carried out in a pole vector mode and discontinuities from drill hole logging were assumed continuous and through-going since there is no excavated surface to ascertain continuity.

The procedures of the probabilistic kinematic analysis involved; determining the orientation of discontinuities collected from the rock mass, establishing the dip direction of the discontinuities, determining the dip angle range of the critical slip surface and figuring out the possible ultimate slope angle of the planned open-pit mine. The values of structural dip and dip direction were determined using a geotechnical goniometer during the logging process and by a campus in field mapping. The core, shown in Figure 3.2, from which the data was collected was oriented in order to have in situ measurements of directional properties of the discontinuities. The dips of discontinuities were divided in a 10°interval and the dip direction were categorized in a 45° interval with respect to the structural dip. From the geotechnical core logs, joints were overly predominant discontinuities established followed by fault traces and fault gorges.

(a) (b)

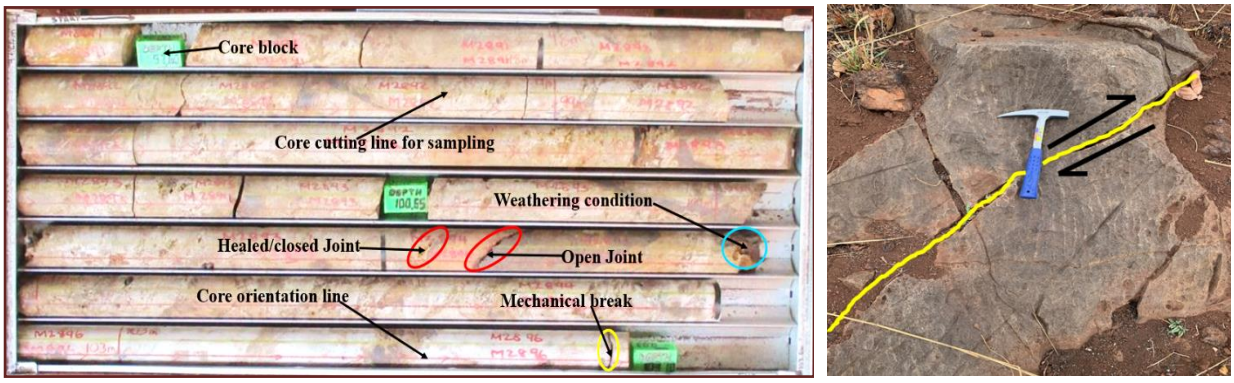

Figure 3.2 Input data for kinematic analysis: a) geotechnical logging of structures from drill core, b) joint trace from surface mapping

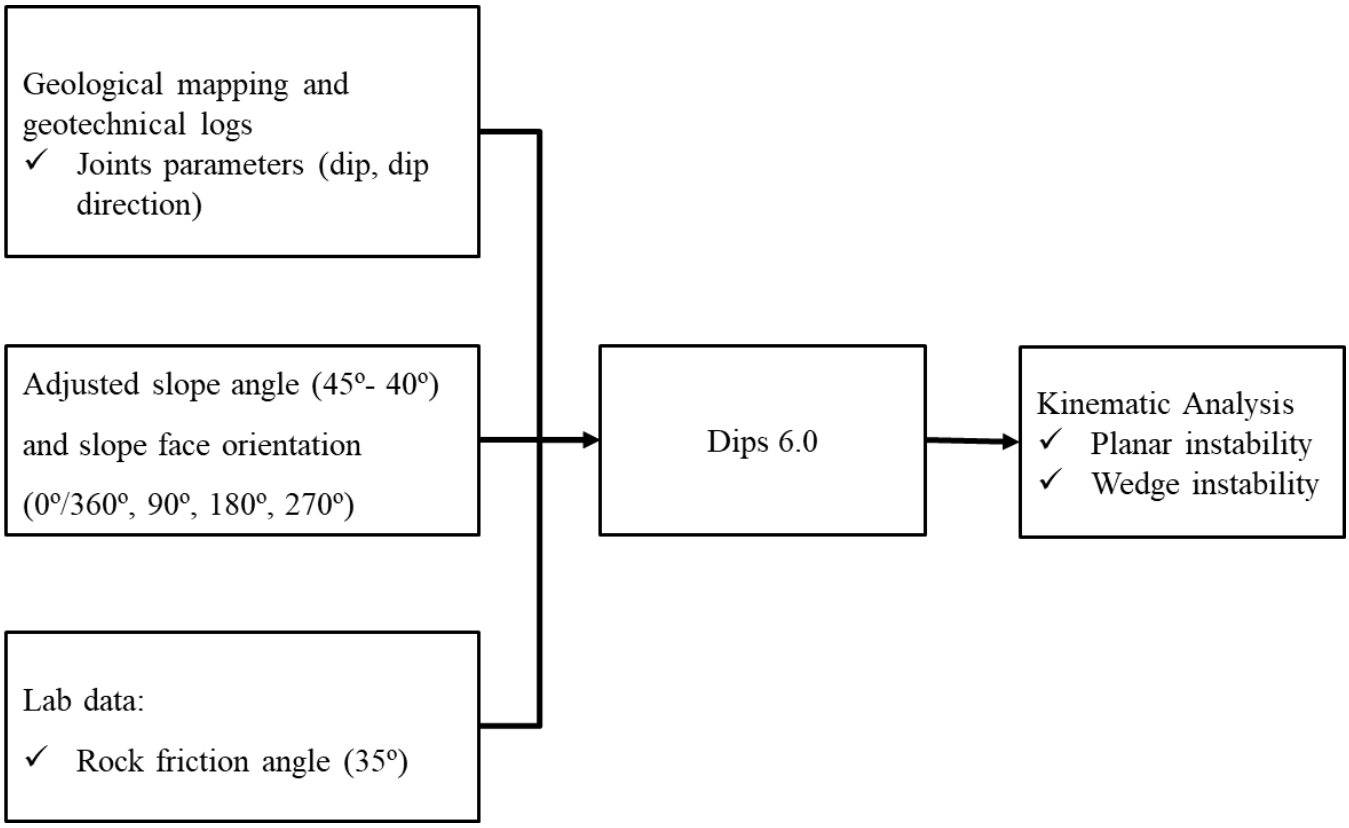

Figure 3.3 Procedure for kinematic analysis

3.4 Results and Discussion

3.4.1 Discontinuity Distribution

The distribution of the discontinuities, as presented in the density radar chart in Figure 3.4, show that majority of the discontinuities dip into the north facing slope section. Statistically, 23% of the discontinuities have a dip direction of ≤ 45°, 13% dip to 45-90° direction, 12% have 270-315° orientation, 11% dip in the 90-135°, 135-180° and 315-359° direction and 9% dip in the 180-225° direction. Thus, in general, 35% of the joints dip Northwards, 23% Eastwards, 22% Westwards and 20% Southwards. Apparently more discontinuities appear to orientate parallel to the direction of the minimum principal stress in the S-N direction.

3.4.2 Planar Failure Analysis

In planar instability, the rock mass slides on a single plane since only one surface is involved. Ideally, for planar failure to occur, the joint plane has to dip downward in almost the same direction as the slope face at a less steep angle. Where the joint plane is exposed in the slope face, the plane is regarded to "daylight", a condition conducive for rock mass sliding. Hoek & Bray (2005), Kliche (1999) and Goodman (1989) summarily proposed that the following conditions must be fulfilled for planar sliding to occur on a discrete plane

i. The plane on which sliding occurs must strike parallel or nearly parallel (within approximately ≥ 20 degrees) to the slope face.

ii. The failure plane must "daylight" in the slope face. This implies that the dip of the slope face must be steeper than the apparent dip of the failure plane

iii. The dip of the failure plane must be greater than the angle of friction of this plane.

The above conditions can be related symbolically as

$$\alpha > \beta > \varphi$$

where: α = dip of the slope face, β = dip of the discontinuity, and φ = angle of friction for the rock mass

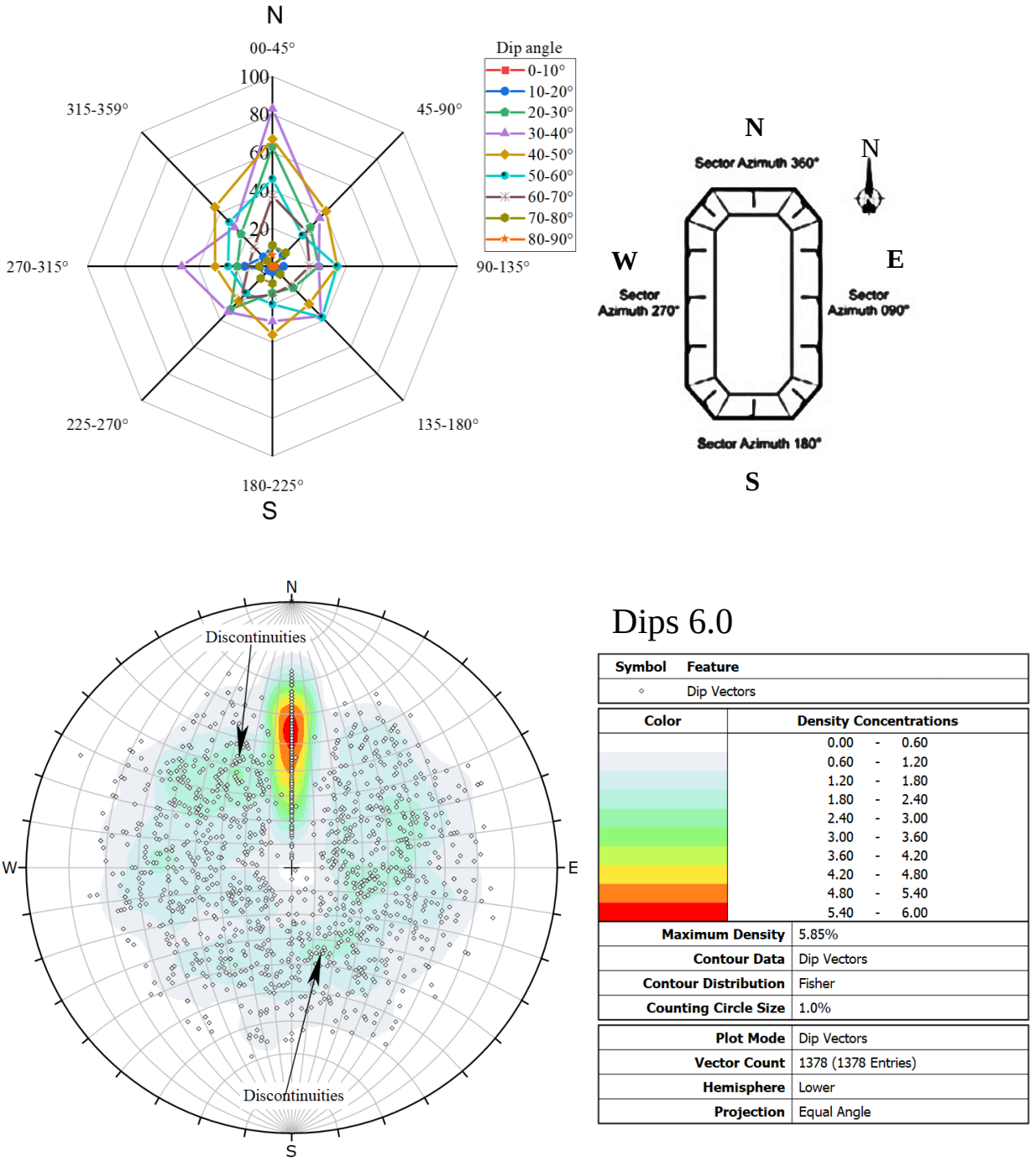

Figure 3.4 Discontinuity distribution based on their attributes

Planar instability analysis was performed for Songwe Mine to assess potentiality of planar failure. The slope performance against discontinuities is benchmarked using probability of failure (PoF), which is defined as the likelihood of the failure occurring on an excavated section. The performed analysis shows that the risk of planar failure is relatively high in the south section facing northern side of the mine. The kinematic analysis indicates that out of a total of 1378 discontinuities, 83 discontinuities in the south section would potentially be critical in influencing planar slope failure of the mine pit (Figure 3.5). This represents 18% PoF for a sectional north dipping discontinuities and a crude probability of 6% with respect to all the plotted discontinuities. In the east and west facing sections of the planned pit, the risk of failure is relatively low with 53 and 51 joint planes plotting in the critical zone of potential failure in the western and eastern section respectively (Figure 3.6;Figure 3.7). Statistically, the PoF for the slopes is at 17% and 16% when considering the discontinuities in the respective sections. However, the crude PoF is at 4% in the western section and 3.7% in the eastern section. The section with the lowest risk of failure is the south facing section, which has 36 discontinuity planes plotting in the critical zone of potential failure (Figure 3.8). This represents a 13% sectional PoF and a crude probability of 2.6%. Thus, the sectional overall probability of planar failure of the entire mine is 16% which is relatively high against the acceptable stability criteria empirically determined (Obregon & Mitri, 2019; Adams, 2015; Read & Stacey, 2009).

Being in a tectonically active region, the potential high horizontal stresses could act as a catalyst to planar failures rendering the mine vulnerable. To minimize the potential risk of planar failure identified in the analysis, slope angle optimization would be crucial. In that regards, a number of analyzes were performed to evaluate the optimal design against potentially critical discontinuities that may dip in and daylight in the slope face. The runs executed include 43°, 41°, and 40° overall slope angles, and the results of the analyses are presented in Figure 3.9 to Figure 3.20. In mining, exploitation of ore in OPM involves relating slope angle design to a pair of contradiction between resource recovery and safety. Fundamentally, the heightening and steepening of excavation bench slopes may affect the intersection points with day-lighting discontinuities in excavated face compromising the security of the overall slope. Thus, slope angle optimization aids in striking a balance between safety and mining economic profits.

Based on the current analysis, an optimized slope angle could be adopted within an acceptable angle between 40°and 45° with emphasis on safety at this preliminary stage of the mine development.

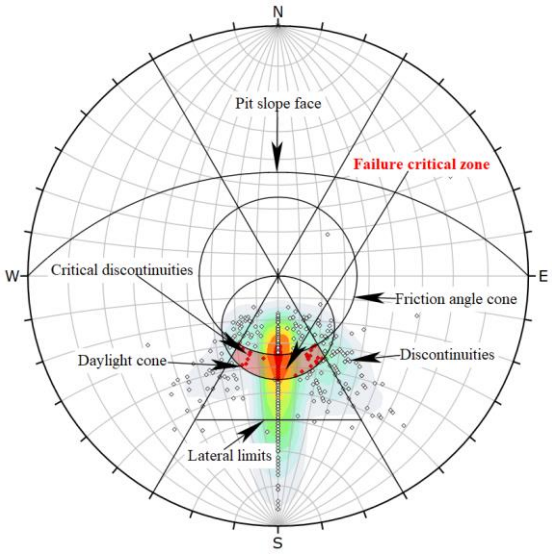

Symbol	Feature
◦	Pole Vectors
◆	Critical Vectors

Color	Density Concentrations
	0.00 - 1.90
	1.90 - 3.80
	3.80 - 5.70
	5.70 - 7.60
	7.60 - 9.50
	9.50 - 11.40
	11.40 - 13.30
	13.30 - 15.20
	15.20 - 17.10
	17.10 - 19.00

Maximum Density	18.09%
Contour Data	Pole Vectors
Contour Distribution	Fisher
Counting Circle Size	1.0%

Kinematic Analysis	Planar Sliding
Slope Dip	45
Slope Dip Direction	0/360
Friction Angle	35°
Lateral Limits	30°

	Critical	Total	%
Planar Sliding (All)	83	461	18.00%

Figure 3.5 Planar slope stability condition of the southern section at an angle of 45°

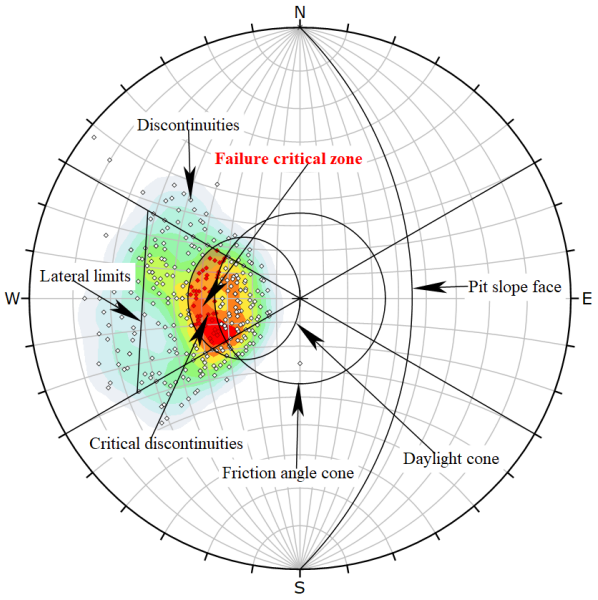

Symbol	Feature
◦	Pole Vectors
◆	Critical Vectors

Color	Density Concentrations
	0.00 - 1.10
	1.10 - 2.20
	2.20 - 3.30
	3.30 - 4.40
	4.40 - 5.50
	5.50 - 6.60
	6.60 - 7.70
	7.70 - 8.80
	8.80 - 9.90
	9.90 - 11.00

Maximum Density	10.76%
Contour Data	Pole Vectors
Contour Distribution	Fisher
Counting Circle Size	1.0%

Kinematic Analysis	Planar Sliding
Slope Dip	45
Slope Dip Direction	90
Friction Angle	35°
Lateral Limits	30°

	Critical	Total	%
Planar Sliding (All)	53	320	16.56%

Figure 3.6 Planar slope stability condition of the western section at an angle of 45°

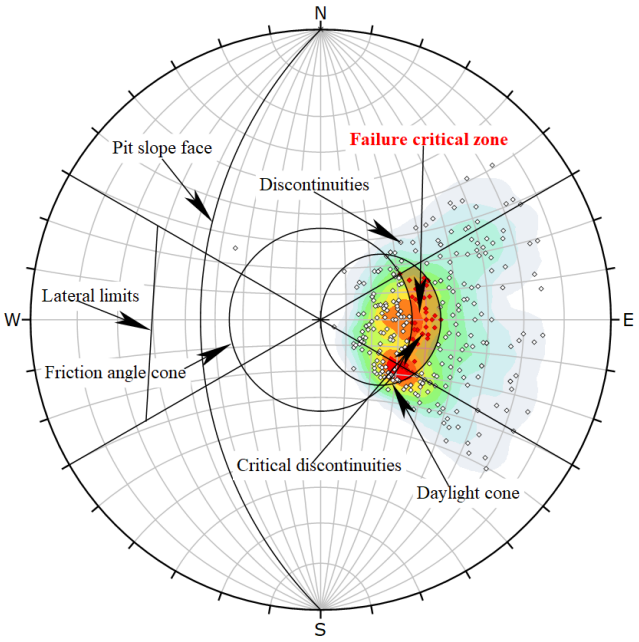

Symbol	Feature
◦	Pole Vectors
◆	Critical Vectors

Color	Density Concentrations
	0.00 - 1.20
	1.20 - 2.40
	2.40 - 3.60
	3.60 - 4.80
	4.80 - 6.00
	6.00 - 7.20
	7.20 - 8.40
	8.40 - 9.60
	9.60 - 10.80
	10.80 - 12.00

Maximum Density	11.67%
Contour Data	Pole Vectors
Contour Distribution	Fisher
Counting Circle Size	1.0%

Kinematic Analysis	Planar Sliding
Slope Dip	45
Slope Dip Direction	270
Friction Angle	35°
Lateral Limits	30°

	Critical	Total	%
Planar Sliding (All)	51	317	16.09%

Figure 3.7 Planar slope stability condition in the eastern section at an angle of 45°

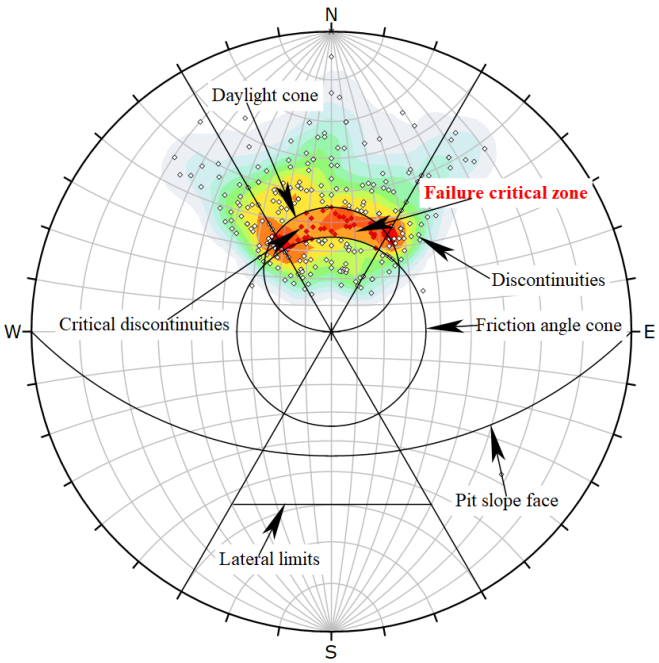

Symbol	Feature
◦	Pole Vectors
◆	Critical Vectors

Color	Density Concentrations
	0.00 - 1.00
	1.00 - 2.00
	2.00 - 3.00
	3.00 - 4.00
	4.00 - 5.00
	5.00 - 6.00
	6.00 - 7.00
	7.00 - 8.00
	8.00 - 9.00
	9.00 - 10.00

Maximum Density	9.78%
Contour Data	Pole Vectors
Contour Distribution	Fisher
Counting Circle Size	1.0%

Kinematic Analysis	Planar Sliding
Slope Dip	45
Slope Dip Direction	180
Friction Angle	35°
Lateral Limits	30°

	Critical	Total	%
Planar Sliding (All)	36	268	13.43%

Figure 3.8 Planar slope stability condition in the northern section at an angle of 45°

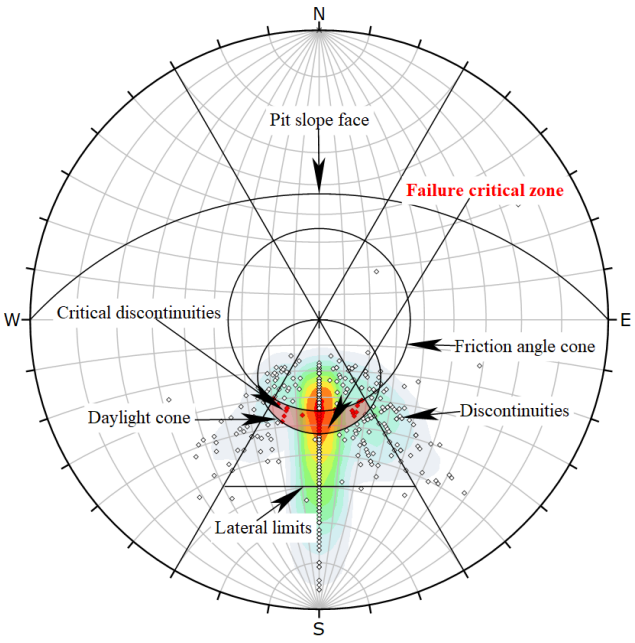

Symbol	Feature
◇	Pole Vectors
◆	Critical Vectors

Color	Density Concentrations
	0.00 - 1.90
	1.90 - 3.80
	3.80 - 5.70
	5.70 - 7.60
	7.60 - 9.50
	9.50 - 11.40
	11.40 - 13.30
	13.30 - 15.20
	15.20 - 17.10
	17.10 - 19.00

Maximum Density	18.09%
Contour Data	Pole Vectors
Contour Distribution	Fisher
Counting Circle Size	1.0%

Kinematic Analysis	Planar Sliding
Slope Dip	43
Slope Dip Direction	0/360
Friction Angle	35°
Lateral Limits	30°

	Critical	Total	%
Planar Sliding (All)	62	461	13.45%

Figure 3.9 Planar slope stability condition of the southern section at an angle of 43°

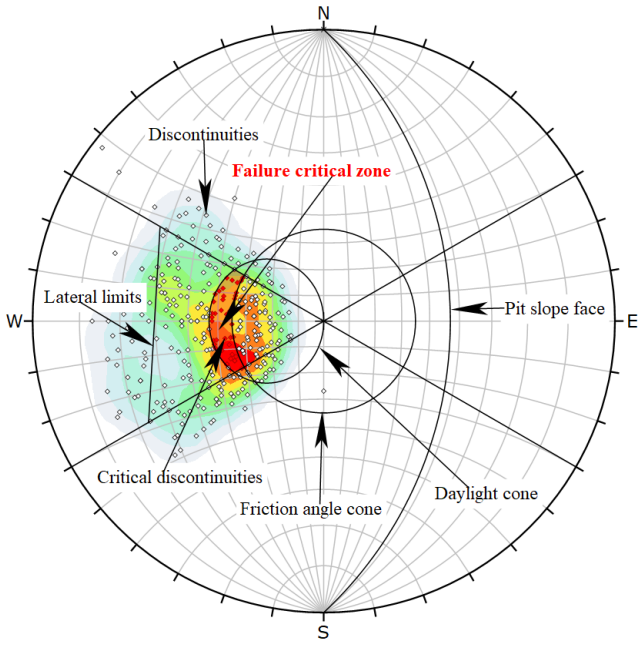

Symbol	Feature
◇	Pole Vectors
◆	Critical Vectors

Color	Density Concentrations
	0.00 - 1.10
	1.10 - 2.20
	2.20 - 3.30
	3.30 - 4.40
	4.40 - 5.50
	5.50 - 6.60
	6.60 - 7.70
	7.70 - 8.80
	8.80 - 9.90
	9.90 - 11.00

Maximum Density	10.76%
Contour Data	Pole Vectors
Contour Distribution	Fisher
Counting Circle Size	1.0%

Kinematic Analysis	Planar Sliding
Slope Dip	43
Slope Dip Direction	90
Friction Angle	35°
Lateral Limits	30°

	Critical	Total	%
Planar Sliding (All)	42	320	13.13%

Figure 3.10 Planar slope stability condition of the western section at an angle of 43°

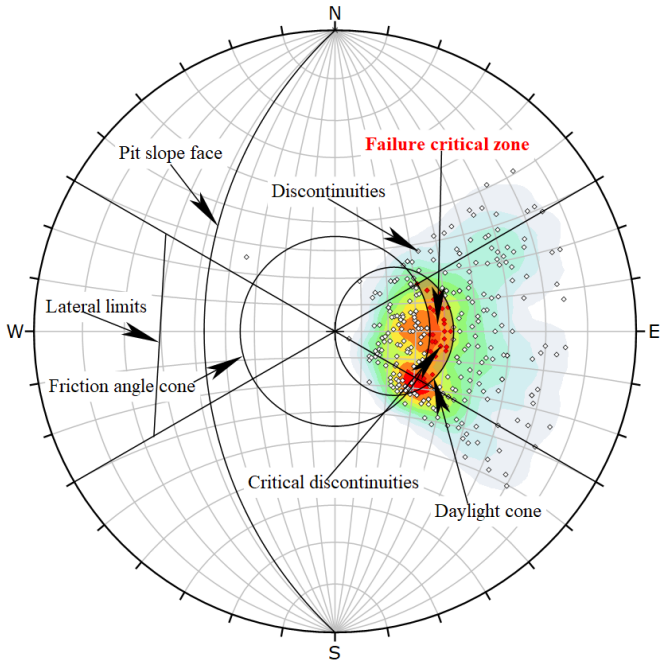

Symbol	Feature
◇	Pole Vectors
◆	Critical Vectors

Color	Density Concentrations
	0.00 - 1.20
	1.20 - 2.40
	2.40 - 3.60
	3.60 - 4.80
	4.80 - 6.00
	6.00 - 7.20
	7.20 - 8.40
	8.40 - 9.60
	9.60 - 10.80
	10.80 - 12.00

Maximum Density	11.67%
Contour Data	Pole Vectors
Contour Distribution	Fisher
Counting Circle Size	1.0%

Kinematic Analysis	Planar Sliding
Slope Dip	43
Slope Dip Direction	270
Friction Angle	35°
Lateral Limits	30°

	Critical	Total	%
Planar Sliding (All)	43	317	13.56%

Figure 3.11 Planar slope stability condition in the eastern section at an angle of 43°

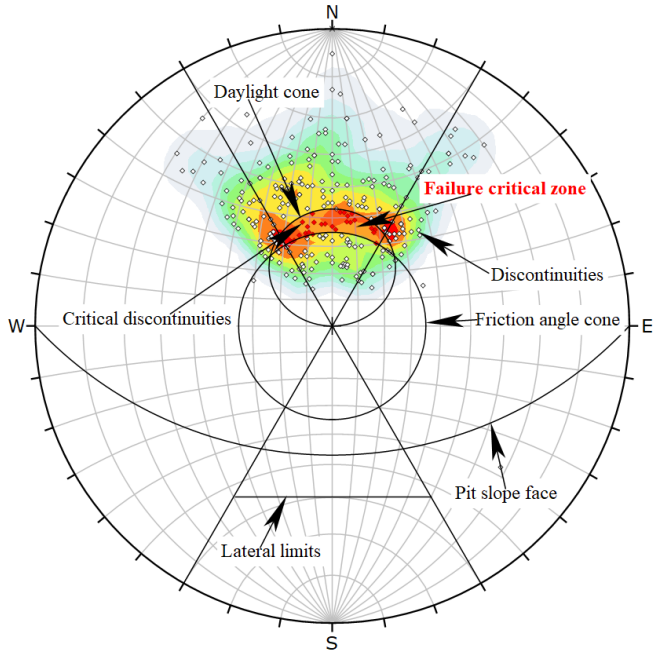

Symbol	Feature
◇	Pole Vectors
◆	Critical Vectors

Color	Density Concentrations
	0.00 - 1.00
	1.00 - 2.00
	2.00 - 3.00
	3.00 - 4.00
	4.00 - 5.00
	5.00 - 6.00
	6.00 - 7.00
	7.00 - 8.00
	8.00 - 9.00
	9.00 - 10.00

Maximum Density	9.78%
Contour Data	Pole Vectors
Contour Distribution	Fisher
Counting Circle Size	1.0%

Kinematic Analysis	Planar Sliding
Slope Dip	43
Slope Dip Direction	180
Friction Angle	35°
Lateral Limits	30°

	Critical	Total	%
Planar Sliding (All)	27	268	10.07%

Figure 3.12 Planar slope stability condition in the northern section at an angle of 43°

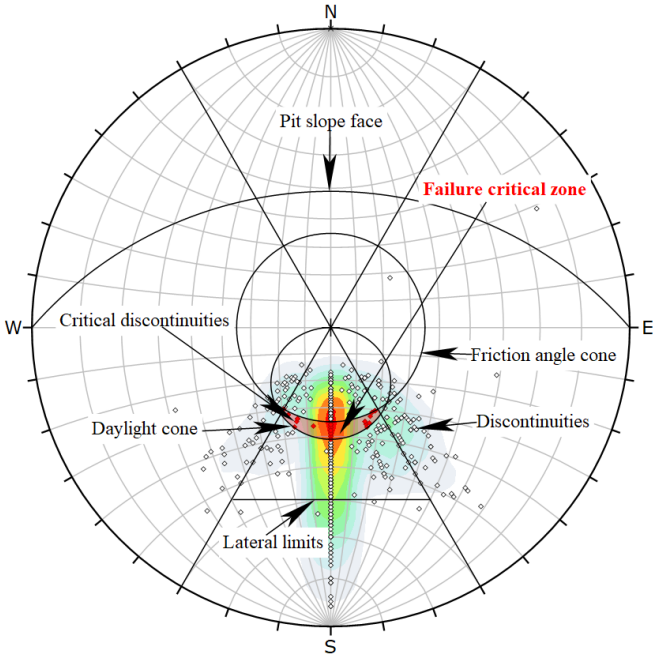

Symbol	Feature
◦	Pole Vectors
◆	Critical Vectors

Color	Density Concentrations
	0.00 - 1.90
	1.90 - 3.80
	3.80 - 5.70
	5.70 - 7.60
	7.60 - 9.50
	9.50 - 11.40
	11.40 - 13.30
	13.30 - 15.20
	15.20 - 17.10
	17.10 - 19.00

Maximum Density	18.09%
Contour Data	Pole Vectors
Contour Distribution	Fisher
Counting Circle Size	1.0%

Kinematic Analysis	Planar Sliding
Slope Dip	41
Slope Dip Direction	0/360
Friction Angle	35°
Lateral Limits	30°

	Critical	Total	%
Planar Sliding (All)	52	461	11.28%

Figure 3.13 Planar slope stability condition of the southern section at an angle of 41°

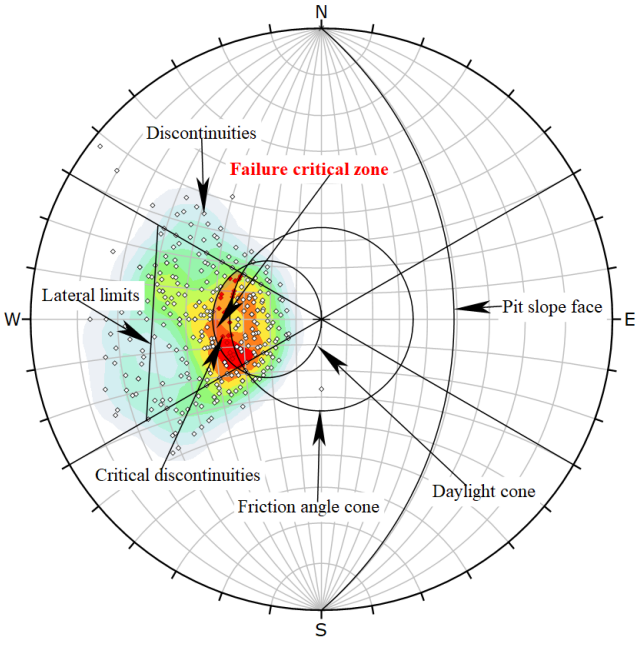

Symbol	Feature
◦	Pole Vectors
◆	Critical Vectors

Color	Density Concentrations
	0.00 - 1.10
	1.10 - 2.20
	2.20 - 3.30
	3.30 - 4.40
	4.40 - 5.50
	5.50 - 6.60
	6.60 - 7.70
	7.70 - 8.80
	8.80 - 9.90
	9.90 - 11.00

Maximum Density	10.76%
Contour Data	Pole Vectors
Contour Distribution	Fisher
Counting Circle Size	1.0%

Kinematic Analysis	Planar Sliding
Slope Dip	41
Slope Dip Direction	90
Friction Angle	35°
Lateral Limits	30°

	Critical	Total	%
Planar Sliding (All)	23	320	7.19%

Figure 3.14 Planar slope stability condition of the western section at an angle of 41°

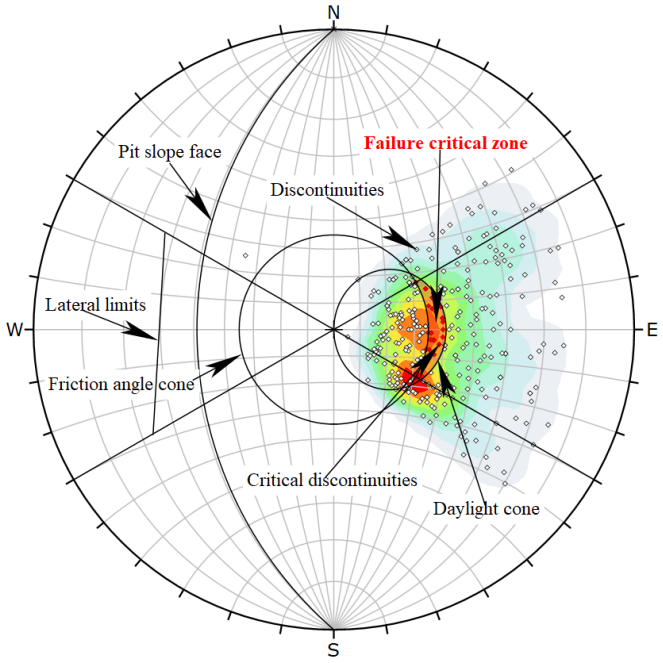

Symbol	Feature
◦	Pole Vectors
◆	Critical Vectors

Color	Density Concentrations
	0.00 - 1.20
	1.20 - 2.40
	2.40 - 3.60
	3.60 - 4.80
	4.80 - 6.00
	6.00 - 7.20
	7.20 - 8.40
	8.40 - 9.60
	9.60 - 10.80
	10.80 - 12.00

Maximum Density	11.67%
Contour Data	Pole Vectors
Contour Distribution	Fisher
Counting Circle Size	1.0%

Kinematic Analysis	Planar Sliding
Slope Dip	41
Slope Dip Direction	270
Friction Angle	35°
Lateral Limits	30°

	Critical	Total	%
Planar Sliding (All)	34	317	10.73%

Figure 3.15 Planar slope stability condition in the eastern section at an angle of 41°

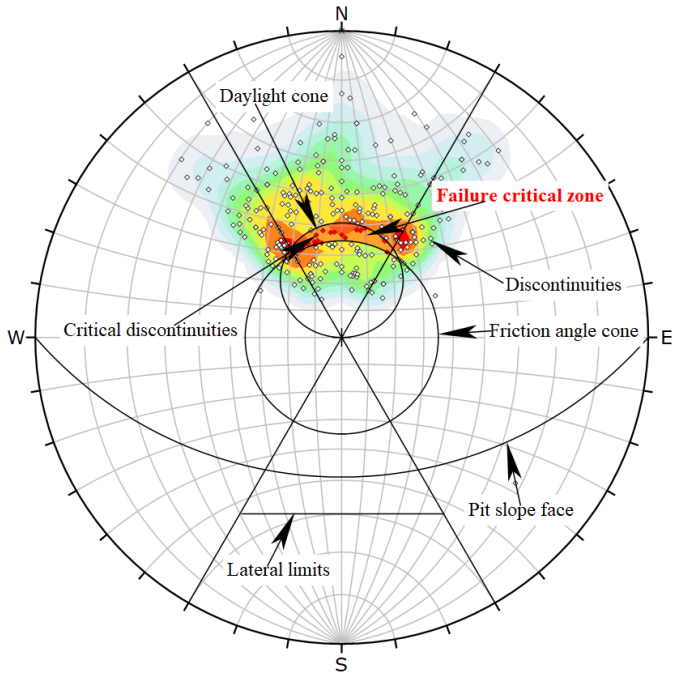

Symbol	Feature
◦	Pole Vectors
◆	Critical Vectors

Color	Density Concentrations
	0.00 - 1.00
	1.00 - 2.00
	2.00 - 3.00
	3.00 - 4.00
	4.00 - 5.00
	5.00 - 6.00
	6.00 - 7.00
	7.00 - 8.00
	8.00 - 9.00
	9.00 - 10.00

Maximum Density	9.78%
Contour Data	Pole Vectors
Contour Distribution	Fisher
Counting Circle Size	1.0%

Kinematic Analysis	Planar Sliding
Slope Dip	41
Slope Dip Direction	180
Friction Angle	35°
Lateral Limits	30°

	Critical	Total	%
Planar Sliding (All)	18	268	6.72%

Figure 3.16 Planar slope stability condition in the northern section at an angle of 41°

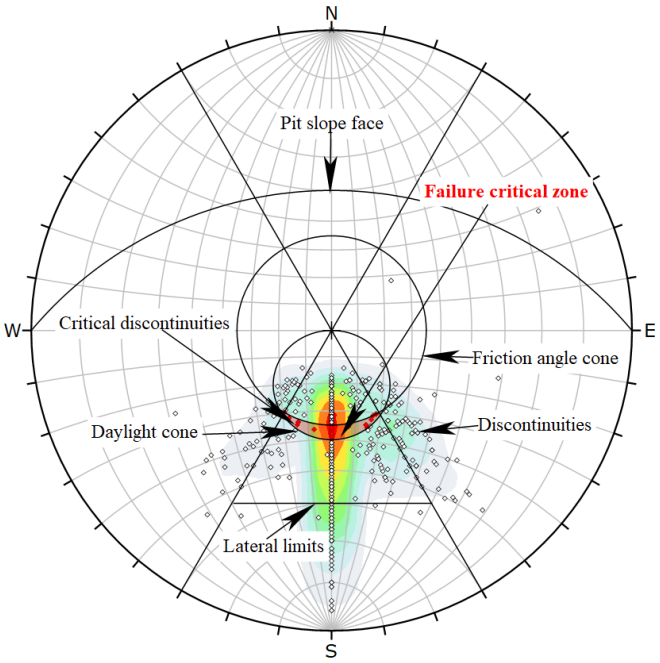

Symbol	Feature
◇	Pole Vectors
◆	Critical Vectors

Color	Density Concentrations
	0.00 - 1.90
	1.90 - 3.80
	3.80 - 5.70
	5.70 - 7.60
	7.60 - 9.50
	9.50 - 11.40
	11.40 - 13.30
	13.30 - 15.20
	15.20 - 17.10
	17.10 - 19.00

Maximum Density	18.09%
Contour Data	Pole Vectors
Contour Distribution	Fisher
Counting Circle Size	1.0%

Kinematic Analysis	Planar Sliding
Slope Dip	40
Slope Dip Direction	0/360
Friction Angle	35°
Lateral Limits	30°

	Critical	Total	%
Planar Sliding (All)	45	461	9.76%

Figure 3.17 Planar slope stability condition of the southern section at an angle of 40°

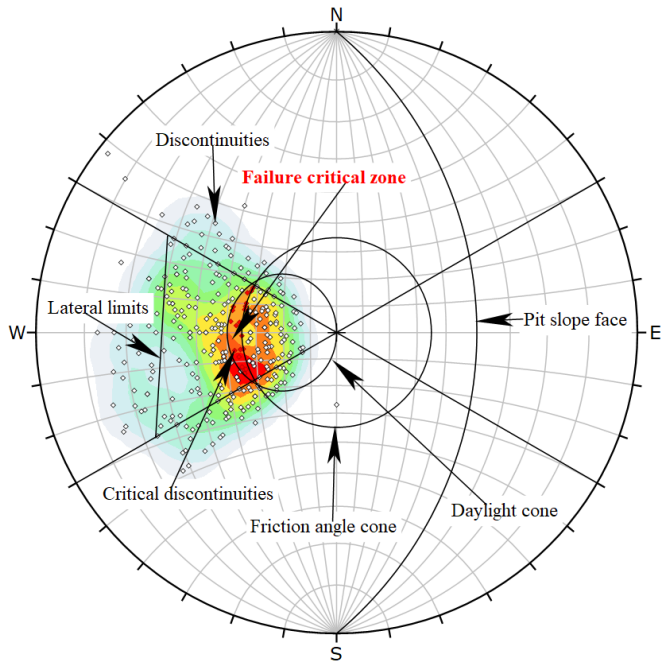

Symbol	Feature
◇	Pole Vectors
◆	Critical Vectors

Color	Density Concentrations
	0.00 - 1.10
	1.10 - 2.20
	2.20 - 3.30
	3.30 - 4.40
	4.40 - 5.50
	5.50 - 6.60
	6.60 - 7.70
	7.70 - 8.80
	8.80 - 9.90
	9.90 - 11.00

Maximum Density	10.76%
Contour Data	Pole Vectors
Contour Distribution	Fisher
Counting Circle Size	1.0%

Kinematic Analysis	Planar Sliding
Slope Dip	40
Slope Dip Direction	90
Friction Angle	35°
Lateral Limits	30°

	Critical	Total	%
Planar Sliding (All)	21	320	6.56%

Figure 3.18 Planar slope stability condition of the western section at an angle of 40°

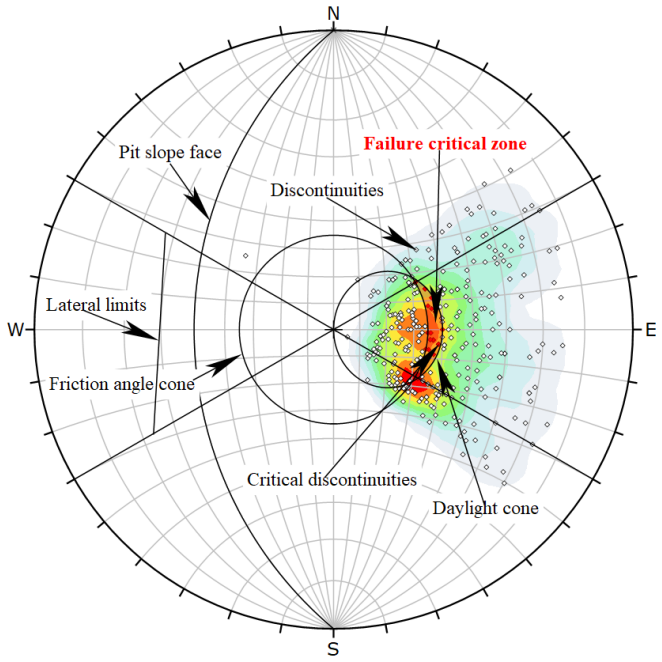

Symbol	Feature
◦	Pole Vectors
◆	Critical Vectors

Color	Density Concentrations
	0.00 - 1.20
	1.20 - 2.40
	2.40 - 3.60
	3.60 - 4.80
	4.80 - 6.00
	6.00 - 7.20
	7.20 - 8.40
	8.40 - 9.60
	9.60 - 10.80
	10.80 - 12.00

Maximum Density	11.67%
Contour Data	Pole Vectors
Contour Distribution	Fisher
Counting Circle Size	1.0%

Kinematic Analysis	Planar Sliding
Slope Dip	40
Slope Dip Direction	270
Friction Angle	35°
Lateral Limits	30°

	Critical	Total	%
Planar Sliding (All)	25	317	7.89%

Figure 3.19 Planar slope stability condition in the eastern section at an angle of 40°

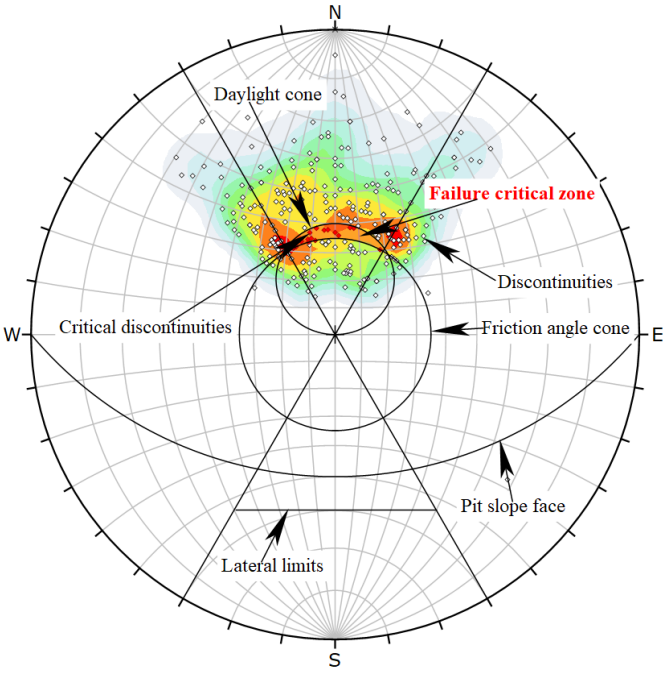

Symbol	Feature
◦	Pole Vectors
◆	Critical Vectors

Color	Density Concentrations
	0.00 - 1.00
	1.00 - 2.00
	2.00 - 3.00
	3.00 - 4.00
	4.00 - 5.00
	5.00 - 6.00
	6.00 - 7.00
	7.00 - 8.00
	8.00 - 9.00
	9.00 - 10.00

Maximum Density	9.78%
Contour Data	Pole Vectors
Contour Distribution	Fisher
Counting Circle Size	1.0%

Kinematic Analysis	Planar Sliding
Slope Dip	40
Slope Dip Direction	180
Friction Angle	35°
Lateral Limits	30°

	Critical	Total	%
Planar Sliding (All)	16	268	5.97%

Figure 3.20 Planar slope stability condition in the northern section at an angle of 40°

After running a series of analyzes, a conservative slope angle of 40° is suggested for consideration. The gentle overall slope angle (OSA) demonstrates that the sectional risk of potential planar failure could be reduced by over 35%, 59%, 46% and 35% in the north, east, south and west facing slopes respectively. This represents an overall 44% reduction of planar failure risk for the entire mine. The mean sectional probability at this OSA is 7% (Figure 3.21) which falls in the optimal value range in the acceptable criteria of slope stability (Obregon & Mitri, 2019; Read & Stacey, 2009). However, sectional pit optimization can as well be considered especially for the north and west sections at slope angles of 43° and 42° respectively. The proposed OSA could be adjusted as more geotechnical information is collected during operationalization but the current conservative excavating slope is meant to evade unnecessary risk taking at an early stage. For instance, Venetia Mine in South Africa was designed at a steepened slope angle of 51° during the initial feasibility study but due to failures experienced during operations, which were predominantly planar failures, the pit slope angle was reduced to 37° and 44° respective of the domains (Barnett, 2003). Although, this represented an enormous increase in the stripping ratio for the mine, but it was extremely necessary step if unacceptable risks were to be circumvented.

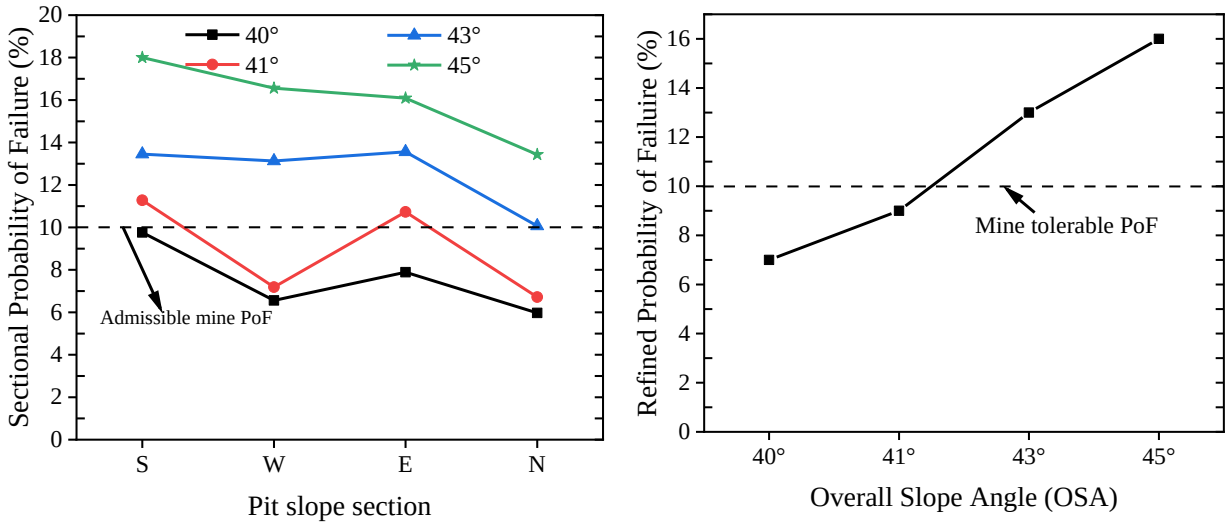

(a) Mine sectional PoF (b) Averaged refined overall mine PoF

Figure 3.21. Probability of potential planar failure

3.4.3 Wedge Failure

Wedge failure can only occur on two intersecting planes of the joints. In this case, the failure block is assumed to be a tetrahedron, the sides of which are defined by the two intersecting planes, the slope face, and the upper slope surface (Kliche, 1999). Generally, the trend of the intersection line that satisfies wedge failure must be orientated within 90°of the dip and the plunge of the intersection line must "daylight" in the slope face (Figure 3.1), implying that the dip of the slope face has to be greater than the plunge of the intersection line (Goodman, 1989; Hoek E. &., 2005; Wyllie & Mah, 2004). However, not all intersecting planes that meet the criteria for possible kinematic failure do actually fail (see Figure 3.22; Figure 3.23). Discontinuities with a low degree of continuity (i.e., those with high percentage of attachments across the planes) may exhibit higher strength in the form of cohesion and, probably, higher friction angle than discontinuities with high continuity (Kliche, 1999). Normally, intersecting major discontinuities such as faults, shear zones, open joints pose a huge risk of wedge type of failure. On the contrary, intersecting minor discontinuities present a low risk of failure.

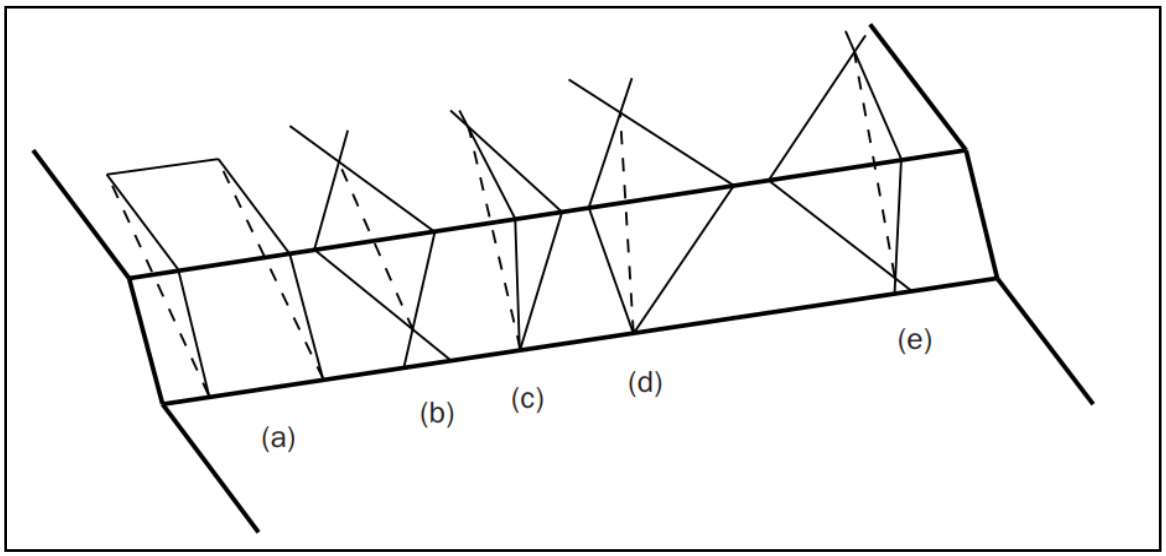

Figure 3.22 Wedges that can fail if strength is overcome (Kliche, 1999)

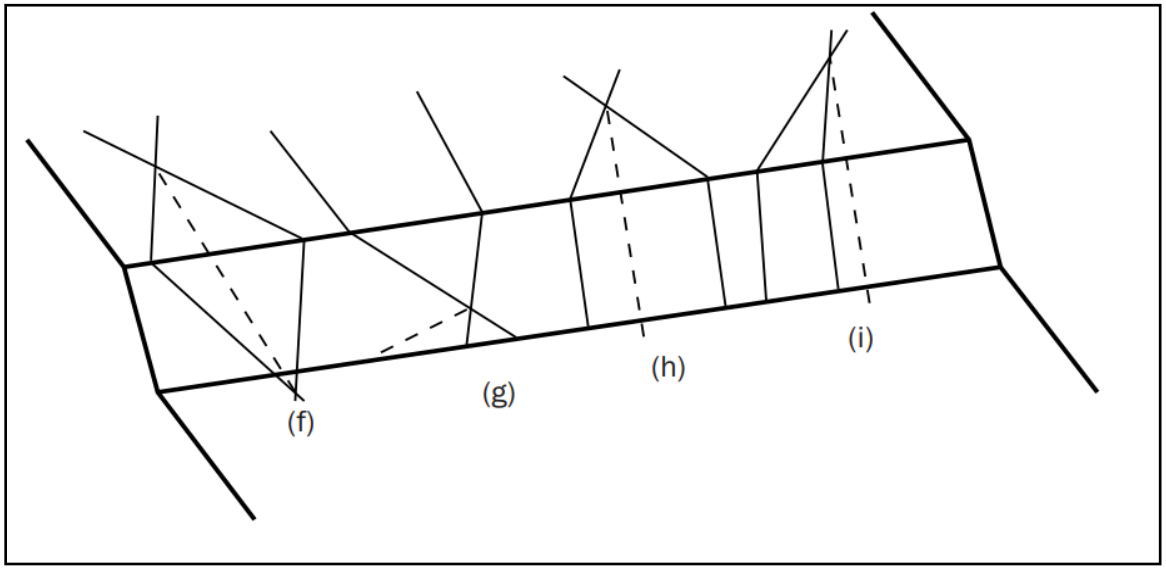

Figure 3.23 Wedges that cannot fail (Kliche, 1999)

In this kinematic analysis, all sections of the planned open-pit registered no critical intersections in the potential failure zones both in the primary and secondary zone (Figure 3.24; Figure 3.25; Figure 3.26; Figure 3.27). Within the primary critical zone, any intersection plotted could directly satisfy the frictional and kinematic conditions for wedge failure. On the contrary, the intersection in the secondary critical zone would be such that the sliding would occur on a joint plane with a dip greater than the friction angle and the other joint acting as a release plane for wedge failure. Since no critical intersections plotted in the critical zones of potential failure, wedge failure could preliminarily be an unlikely phenomenon unless artificial propagation of joint planes under active mining operations due to blasting effect or other intrinsic mechanisms.

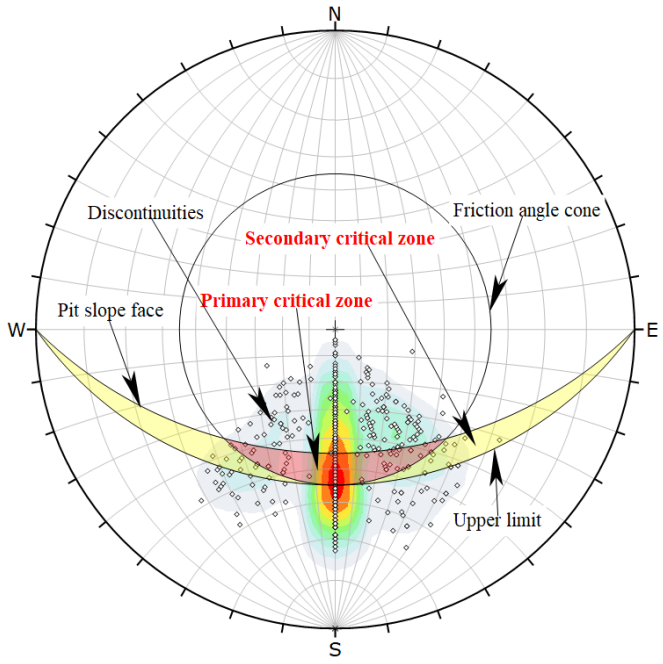

Symbol	Feature
◇	Dip Vectors
▫	Critical Intersection

Color	Density Concentrations
	0.00 - 0.60
	0.60 - 1.20
	1.20 - 1.80
	1.80 - 2.40
	2.40 - 3.00
	3.00 - 3.60
	3.60 - 4.20
	4.20 - 4.80
	4.80 - 5.40
	5.40 - 6.00

Maximum Density	18.09%
Contour Data	Dip Vectors
Contour Distribution	Fisher
Counting Circle Size	1.0%

Kinematic Analysis	Wedge Sliding
Slope Dip	45
Slope Dip Direction	0/360
Friction Angle	35°

	Critical	Total	%
Wedge Sliding	0	461	0%

Figure 3.24 Wedge slope stability condition in the southern section at an angle of 45°

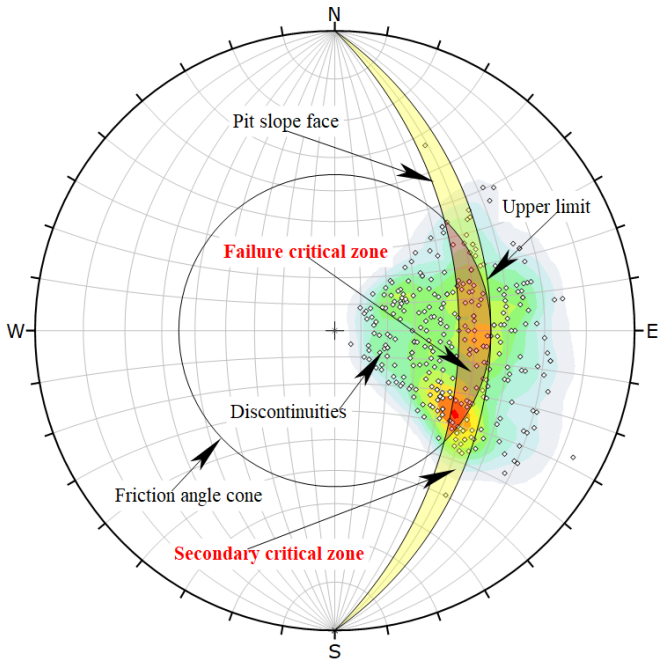

Symbol	Feature
◇	Dip Vectors
▫	Critical Intersection

Color	Density Concentrations
	0.00 - 0.60
	0.60 - 1.20
	1.20 - 1.80
	1.80 - 2.40
	2.40 - 3.00
	3.00 - 3.60
	3.60 - 4.20
	4.20 - 4.80
	4.80 - 5.40
	5.40 - 6.00

Maximum Density	11.67%
Contour Data	Dip Vectors
Contour Distribution	Fisher
Counting Circle Size	1.0%

Kinematic Analysis	Wedge Sliding
Slope Dip	45
Slope Dip Direction	270
Friction Angle	35°

	Critical	Total	%
Wedge Sliding	0	317	0%

Figure 3.25 Wedge slope stability condition in the eastern section at an angle of 45°

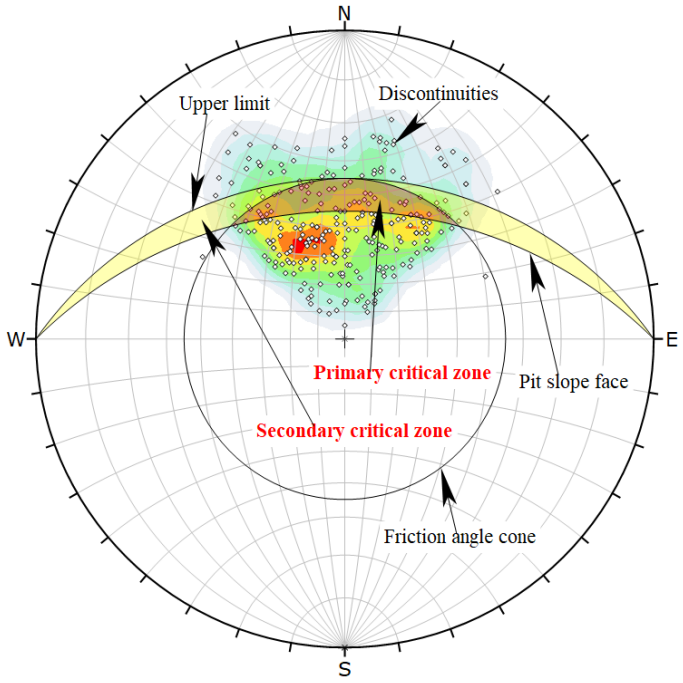

Symbol	Feature
◇	Dip Vectors
▫	Critical Intersection

Color	Density Concentrations
	0.00 - 0.60
	0.60 - 1.20
	1.20 - 1.80
	1.80 - 2.40
	2.40 - 3.00
	3.00 - 3.60
	3.60 - 4.20
	4.20 - 4.80
	4.80 - 5.40
	5.40 - 6.00

Maximum Density	9.78%
Contour Data	Dip Vectors
Contour Distribution	Fisher
Counting Circle Size	1.0%

Kinematic Analysis	Wedge Sliding
Slope Dip	45
Slope Dip Direction	180
Friction Angle	35°

	Critical	Total	%
Wedge Sliding	0	268	0%

Figure 3.26 Wedge slope stability condition in the northern section at an angle of 45°

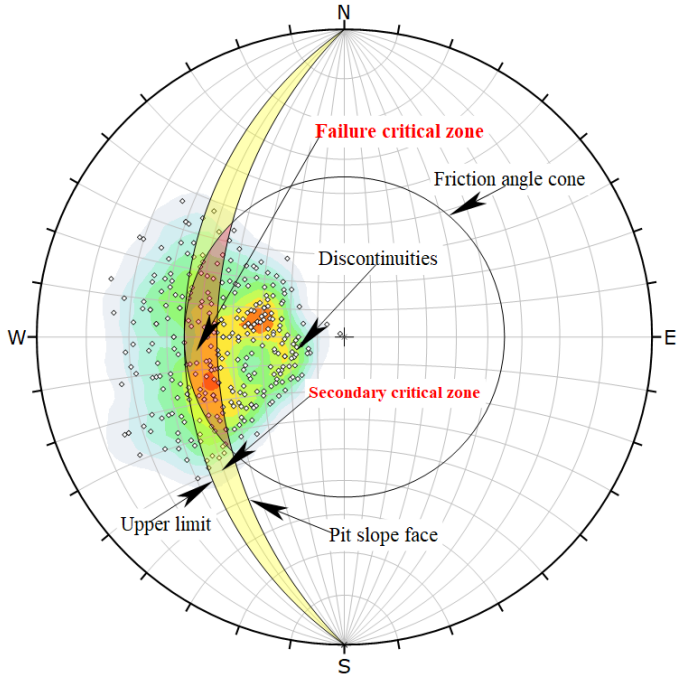

Symbol	Feature
◇	Dip Vectors
▫	Critical Intersection

Color	Density Concentrations
	0.00 - 0.60
	0.60 - 1.20
	1.20 - 1.80
	1.80 - 2.40
	2.40 - 3.00
	3.00 - 3.60
	3.60 - 4.20
	4.20 - 4.80
	4.80 - 5.40
	5.40 - 6.00

Maximum Density	10.76%
Contour Data	Dip Vectors
Contour Distribution	Fisher
Counting Circle Size	1.0%

Kinematic Analysis	Wedge Sliding
Slope Dip	45
Slope Dip Direction	90
Friction Angle	35°

	Critical	Total	%
Wedge Sliding	0	320	0%

Figure 3.27 Wedge slope stability condition in the western section at an angle of 45°

3.5 Mine Design Considerations

Since, the stability of rock slopes in jointed, fractured, bedded or faulted rock is influenced principally by the existence of these structural discontinuities, they have to be carefully considered in mine design. In general, the critical factors are the dip and orientation of the discontinuities relative to the orientation and face angle of the slope and the effective angle of friction along the discontinuities. Besides, these aspects, it is reckoned that the topography and the tectonic stress direction especially in rifting regions can play a critical role. For instance, the topographic setting of the Songwe Mine gives rise to a pit with a high reduced level (RL) in the south section (SS) and low RL in the north section (NS) as shown in Figure 3.28

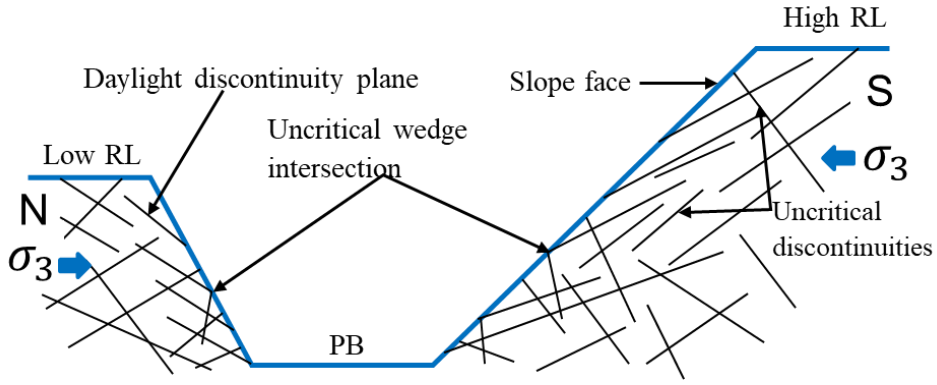

(a) Topographic setting and discontinuity distribution

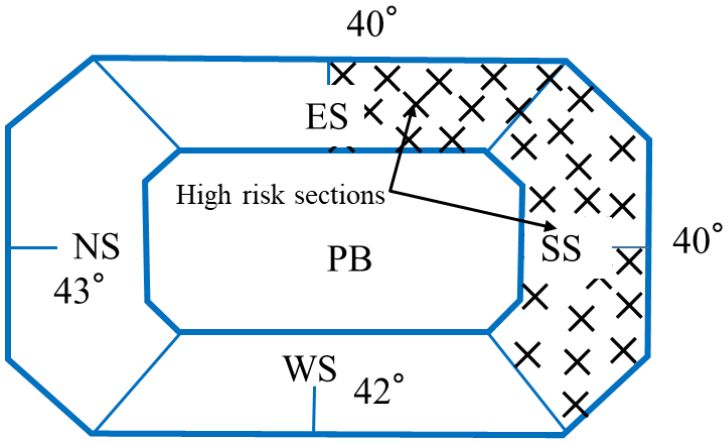

(b) Mine design plan

Figure 3.28 Discontinuities distribution and mine design

Considering the aforementioned aspects, deliberate attempts must be undertaken to minimize the risk, particularly in the south and east sections where the potential for planar failure is high. Excavating from low RL in the north section moving towards high RL in the south section could be dangerous since the orientation and the exposure of the discontinuities may not be fully understood. The best approach to minimize the risk of failure, particularly in the south and east sections, is to adopt a gentler slope angle in a top-down approach. From the statistical results of probability of failure, a slope angle of 40° has a more reliable geotechnical safety but considering economic aspects an optimized angle of 41° can be implemented and monitored as excavation progresses. Meanwhile, steeper angles in the north and west sections can be adopted. While the steepening of rock slopes is exciting to reduce stripping it must be carefully done because more discontinuities can day-lighting into the slope face compromising the performance of the slope. Thus, to avoid any excessive risk taking at mine development stage slope angles of 43° in the north and 42° it the west sections are implementable with safety assurance.

3.6 Summary

The stability of rock slopes in jointed, fractured, bedded or faulted rock is influenced principally by the existence of these structural discontinuities. The critical factors are the dip and orientation of the discontinuities relative to the orientation and face angle of the slope and the effective angle of friction along the discontinuities. To investigate the potential of structural controlled slope failure modes and stability condition of the pit slope a kinematic approach was employed using Dips v 6.0. The outcome of the analysis revealed a considerable potential of planar slope instability at steeper angles, for the case of Songwe at 45°. Since carbonatites occur in tectonically active region, the high horizontal stresses acting parallel to discontinuity planes intersecting the orientation of the slope faces could act as a catalyst to failures. In order to minimize the risk of potential planar failure, slope angle optimization to a gentler angle is proposed as a counter-measure. For the case study area, the risk of failure was observed to be high in the south and east sections of the pit, hence slope angle optimization to 40° was suggested, which could reduce the risk of potential planar failure to safety by over 44%. Meanwhile, steeper angles in the opposite sections are implementable at safety viz. 43° in the north and 42° it the west sections.

On the other hand, wedge failure has been found to be an improbable phenomenon in the rifting region because principally the discontinuities align parallel to the direction of the tectonic stresses. In the Songwe case, critical intersection that necessitates the failure mode could not be encountered in the zone of potential failure this far, hence no likelihood of wedge failure occurrence. However, follow up studies need to be carried out when pit walls get exposed using data from scan line surface mapping to acquire the finer geotechnical details of the major discontinuities (like persistence, aperture) and update the current findings.

3.7 References

Adams, B. M. (2015). *Slope Stability Acceptance Criteria for Opencast Mine Design*. New Zealand: Golder Associates (NZ) Limited.

Aksoy, H., & Ercanoglu, M. (2009). Fuzzified Kinematic Analysis of Discontinuity-Controlled Rock Slope Instabilities. *Engineering Geology*, 89, 206–219. doi:https://doi.org/10.1016/j.enggeo.2006.10.007

Al Mandalawi, M., You, G., Dowling, K., & Dahlhaus, P. (2016). Kinematic Assessment of Slopes at Handlebar Hill Open Cut Mine. *Int. J. of GEOMATE,* 1575-1583.

Barnett, W. P. (2003). Geological control on slope failure mechanisms in the open-pit at the Venetia Mine. *Geological Society of South Africa*, 149-164. doi:https://doi.org/10.2113/106.2-3.149

Chen, S., Lai, G. T., Han, L., & Tovele, G. S. (2019). Effects of Tectonic Stresses and Structural Planes on Slope Deformation and Stability at the Buzhaoba Open Pit Mine, *China. Sains Malaysiana,* 48(2), 317–324. Doi: 10.17576/jsm-2019-4802-07

Goodman, R. E. (1989). *Introduction to Rock Mechanics* (2nd Ed.). Canada: John Wiley and Sons.

Hoek, E. &. (2005). *Rock Slope Engineering* (4th Ed.). New York, USA: The Institute of Mining and Metallurgy.

Kıncal, C. (2014). Application of two new stereographic projection techniques to slope stability problems. *International Journal of Rock Mechanics & Mining Sciences* (66), 136–150.

Kliche, C. A. (1999). *Rock Slope Stability*. Littleton, USA: Society for Mining, Metallurgy, and Exploration, Inc.

Nelson, E. P., Connors, K. A., & Sua´rez, C. S. (2007). GIS-Based Slope Stability Analysis, Chuquicamata Open Pit Copper Mine, Chile. *Natural Resources Research*, 171-189. Doi: 10.1007/s11053-007-9044-7

Obregon, C., & Mitri, H. (2019). Probabilistic Approach for Open Pit Bench Slope Stability Analysis – A mine case study. *International Journal of Mining Science and Technology*, 29, 629–640.

Read, J., & Stacey, P. (2009). *Guidelines for Open Pit Slope Design*. Australia: SCIRO Publishing.

Rocscience. (2019). rocscience.com. Retrieved 12 12, 2019, from https://www.rocscience.com/help/dips/dips/Kinematic_Analysis_Overview.htm

Saadoun, A., Hafsaoui, A., & Fredj, M. (2018). Landslide Study of Lands in Quarrys: Case Chouf Amar - M'sila, Algeria. D. N. Singh, & A. Galaa içinde, *Contemporary Issues in Geoenvironmental Engineering, Sustainable Civil Infrastructures* (s. 15-28). Netherlands: Springer International Publishing. doi:10.1007/978-3-319-61612-4_3

Shen, H., Klapperich, H., Abbas, S. M., & Ibrahim, A. (2012). Slope stability analysis based on the integration of GIS and numerical simulation. *Automation in Construction, 26*, 46-53. doi:10.1016/j.autcon.2012.04.016

Sjorberg, J. (1999). *Analysis of Large Scale Rock Slopes (Ph.D. Thesis).* Lulea: Lulea University of Technology.

Smith, J. V., & Arnhardt, C. (2016). A New Assessment Method for Structural-Control Failure Mechanisms in Rock Slopes — Case Examples. *AIMS Geosciences, 2* (3), 214-230.

Stacey, T. R., Xianbin, Y., Armstrong, R., & Keyter, G. J. (2003). New Slope Stability Considerations for Deep Open Pit Mines. *The South African Institute of Mining and Metallurgy*, 373-390.

Wyllie, D. C., & Mah, C. W. (2004). *Rock Slope Engineering* (4th Ed.). New York: Taylor & Francis Group.

4 NUMERICAL MODELLING AND ANALYSIS

4.1 Introduction

Having established the potential failure modes and the probability of occurrence, it is crucial to deterministically evaluate the stability performance of the pit slopes. This is because the occurrence of slope failures in unstable mine slopes may affect the mining operations due to fatality, machinery damage and make the recovery of ore uneconomical if the mine was in active operation (Read & Stacey, 2009; Sjoberg, 1996). One major challenge in designing in rock masses is that naturally, as presented in Figure 4.1, rock masses are discontinuous, inhomogeneous, anisotropic, and non-elastic (DIANE) (Hudson & Harrison, 2005). Hence, computer-based mathematical representation of the rock mass can be cumbersome due to its inherent complex characteristics of the field conditions. For decades, most slope stability analyses have been performed using Limit Equilibrium Methods (LEM). The underlying concept of the LEM is that the rock masses behave as a rigid material and that the shear strength is mobilized at the same time along the entire failure surface (Brideau et al., 2009). Based on this assumption LEM can only be adequate for analyzing simple failure modes and small-scale analyses.

However, demand for mineral resources has been increasing to cater for the world's growing population and surface mining operations are expanding and getting deeper. This trend requires modelling that covers complex conditions found in rock masses like nonlinear stress-strain behavior, anisotropy, and changes in geometry. Thus, the development of numerical codes over the last decades has revolutionized rock mass modelling thereby superseding the traditional methods. Currently, there are numerous methods that have been developed in an effort to represent the characteristics and behavior of rock masses. Regardless of the method applied, parameters like material properties, intact rock discontinuities, boundary conditions, hydrogeological regime, and permeability are considered in evaluating the stability of the excavations (see Figure 4.1). Numerical modelling has now been described as a valuable tool to enhance the understanding of the response of rock masses to excavation (Hart, 2003).

In general, numerical models discretize the material into finite elements with the appropriate constitutive laws for the corresponding materials. This enables the studying of a number of complex aspects of the stability of a rock slope with respect to stress and deformation response. This is one of the advantages of numerical modelling over LEM since numerical models can represent failure mechanisms and monitor progressive changes as failure occurs. Additionally, in numerical models, no assumption is made regarding failure surface since failure develops naturally where stresses overcome the available strength (Jing, 2003; Sjorberg, 1999). Thus, the objective of this chapter is to analyse stability conditions and deformation behavior of pit slopes using numerical methods under prevailing high-stress conditions in Great Rift Valley area in order to come up with an ultimate optimal design. The procedure involved conducting a series of stability analyses to the recommended and reliable acceptance level of performance.

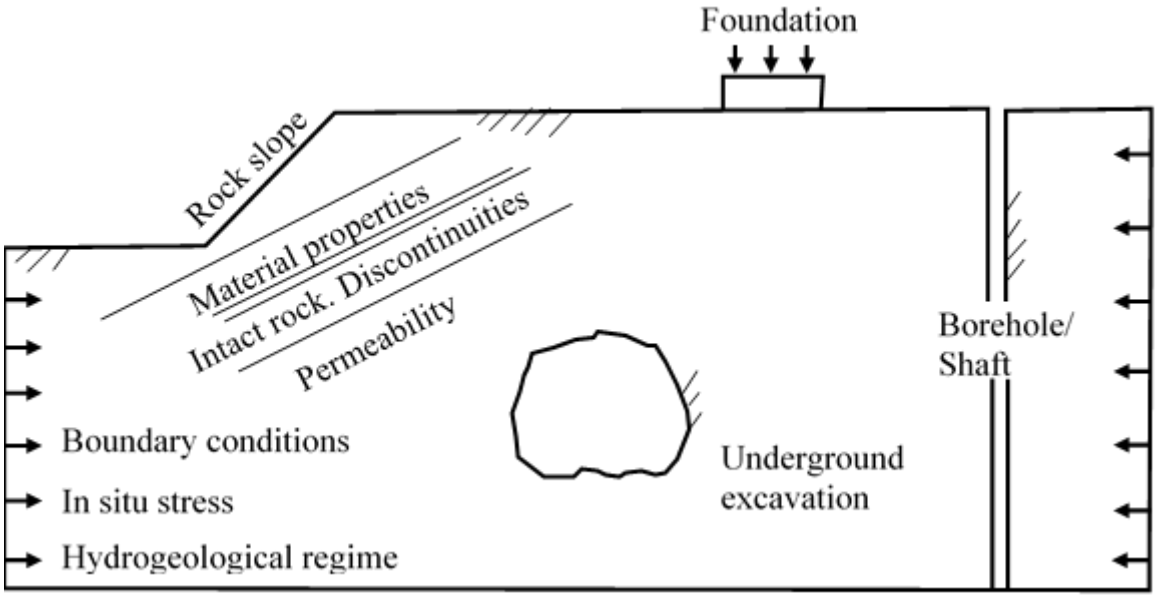

Figure 4.1 Considerations in approaching rock engineering problems

4.2 Selection of Numerical Methods in Rock Mechanics

The application of numerical methods relies on among other things; the scale and complexity of the problem, the fracture system geometry, and the relative scale of the problem (Jing, 2003).

The most commonly applied numerical methods in slope stability analysis are divided into three categories:

1) Continuum methods; the finite difference method (FDM), the finite element method (FEM), and the boundary element method (BEM).

2) Discontinuum methods; the discrete element method (DEM), discrete fracture network (DFN) methods.

3) Hybrid continuum/discrete methods.

The different codes for numerical methods and conventional methods are summarized in Figure 4.2. The verdict to choose a numerical method of continuum or discontinuum rests on various problem-specific factors, and primarily on the problem scale and fracture system geometry. Jing & Hudson (2002) highlighted that the continuum approach can be applied if only a small number of fractures are existent and if fracture aperture and complete block detachment are not momentous factors. On the other hand, the discrete approach is most suitable for moderately fractured rock masses where the number of fractures is too large for the continuum-with-fracture-elements approach, or where large-scale displacements of individual blocks are possible. Nevertheless, it has been shown that there are no absolute advantages of one method over another. To cover for some of the disadvantages of each approach, efforts have been made in code development by combined continuum-discrete models, termed hybrid models. However, in this study numerical method of continuum is applied in simulating the rock slope stability using both FDM and FEM codes.

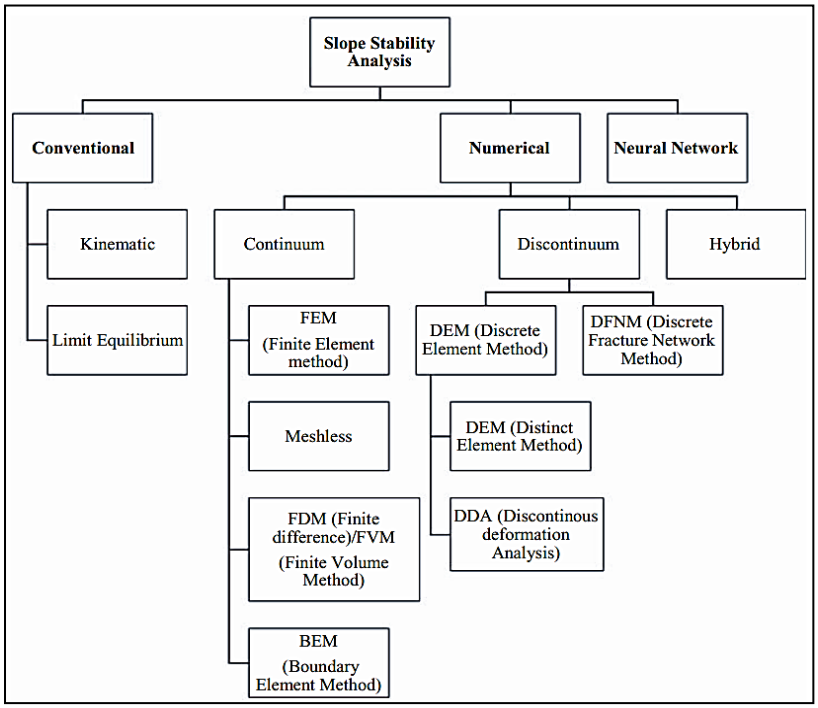

Figure 4.2 A list of available methods for slope stability analysis

4.3 Pit Configuration

Open-pit Mines change considerably in size, shape, and depth with respect to the characteristics of the ore deposit. The topography; mountains or valley floors, is also a significant determinant of OPM dimensions. Regardless of the deposit attributes and topography, fundamental aspects of geometry and planning considerations for OPM tend to resemble. Generally, ore deposit is exploited from top-down in series of horizontal layers having a uniform thickness. Mining operations commence with the removal of the top bench and after a sufficient floor area has been exposed, excavation of the subsequent layer follows. The benches are characterized by bench height (H_B), crest, bench width (W_B), bench face angle (BFA), and toe (see Figure 4.3). The bench face angles can significantly change depending on the rock mass characteristic. In most hard rock pits, the BFA varies from about 55◦ to 80◦ (Hustrulid et al., 2013; Read & Stacey, 2009). The mining process is repeated until the bottom bench elevation is attained and the ultimate pit outline accomplished. Access to the different benches is achieved by a road constructed on the ramps of the stack benches as presented in Figure 4.4.

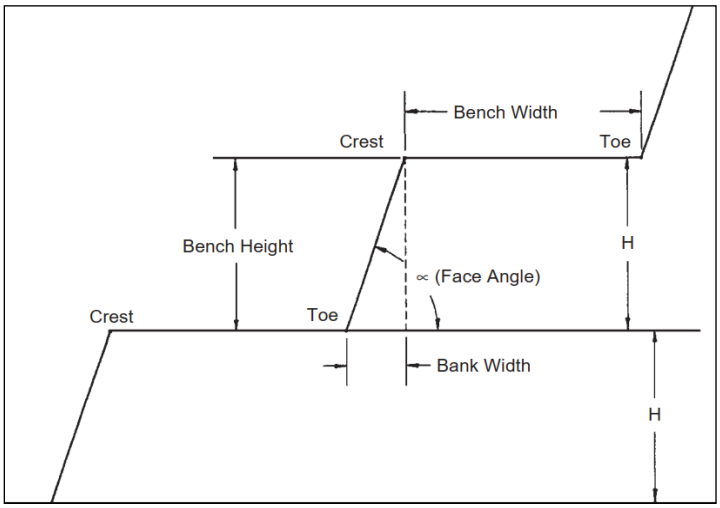

Figure 4.3 Typical bench configurations

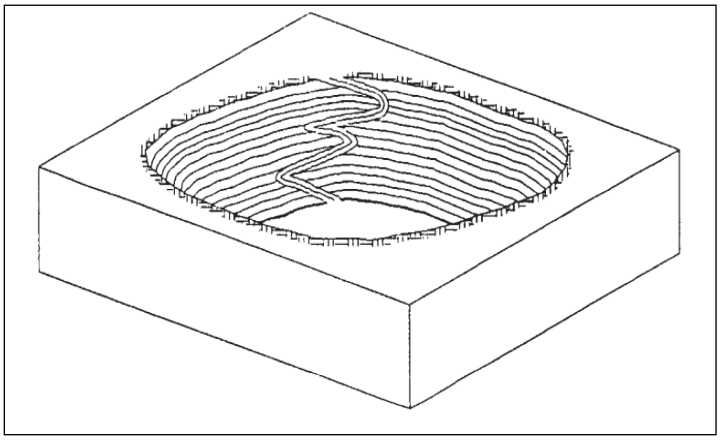

Figure 4.4 Pit geometry in OPM design (After Hustrulid et al., 2013)

At a conceptual stage of mine project development, data are limited and the geotechnical model is usually not yet fully developed, hence empirical charts can be extremely useful for establishing preliminary slope designs while recognizing their extreme conservative constraint. The design charts offer guidelines by merging the experience gained from the known performance of slopes at various mine sites with the information provided by a classification scheme. Many authors have attempted and published slope angle versus slope height charts. Notable examples include charts published by Hoek (1970) and Sjöberg (1999) as presented in Figure 4.5.

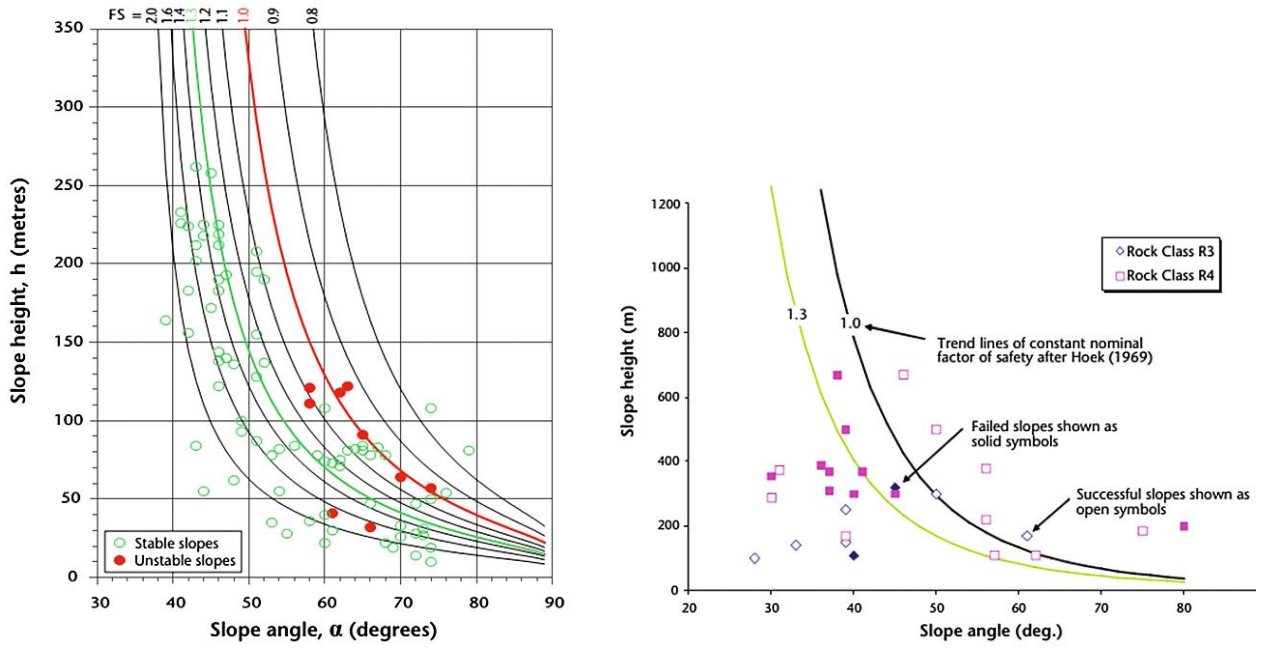

(a) (b)

Figure 4.5 Rock slope versus slope height, distinguishing between failures and non-failure: (a) developed by Hoek (1970) and (b) Sjöberg (1999) (Saadoun et al., 2018)

Stacey et al. (2003) added to the charts cases extending as deep as 850 m. The approach by Hoek compared slope angle with slope height from actual successful and failed slopes. In an updated direct application by Sjöberg, the classification of the slopes was correlated to the characteristic rock-hardness rating. In both cases, the correlation of slope angle versus slope height to an approximate FoS trend line indicates that with Hoek's findings, some slopes seem stable when a slope angle versus slope height classification predicted failure, while others failed where stability was anticipated, and Sjöberg's update of Hoek's work suggests a wider gamut range of uncertainty. Another renowned design chart that has been globally applied was published by Haines and Terbrugge (1991) based on the Laubscher MRMR rock mass rating scheme Figure 4.6. However, the major limitation of this approach is the presumption that slope angles and slope heights can be determined solely on the basis of the MRMR rating of the rock mass.

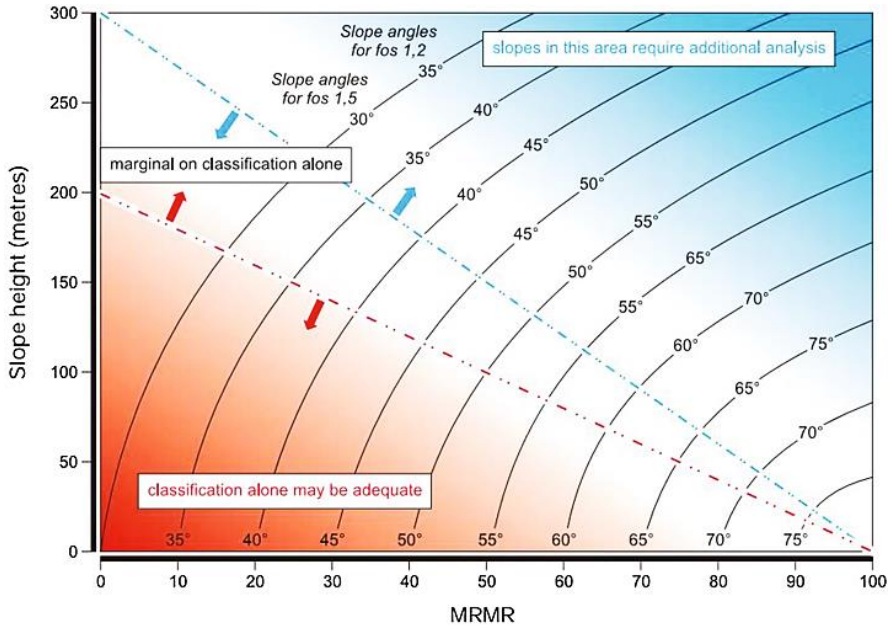

Figure 4.6 Haines & Terbrugge chart for determining slope angle and slope height (Saadoun et al., 2018)

It can be observed that the limitations of using design charts are their experiential and semi-quantitative nature. Thus, this phenomenon stresses the need for a detailed analysis of every project because mine sites are characterized by unique rock mass quality. In this work, a number of conceptual configurations for the Songwe Hill project were developed for evaluation in numerical modelling. The benching design adopted a 15 m bench height given the competence of the carbonatite rock mass as evaluated in the preceding chapter. This is a single benching strategy though in some cases double benching could be considered. The determination of the bench width was based on the formula;

$$W_B = 0.2H_B + 4.5 \qquad (4.1)$$

where W_B is the bench width and H_B is the bench height

Bench face angle was varied in a decreasing trend from 78º - 58º (65°-58° in SS and 78°-63° in NS). The changing of the BFA influenced a variation in the overall slope angle (OSA) from 45º to 40º in the southern slope section and 60° to 45° in the northern slope respectively.

The different OSAs in the respective sections is squarely due to the topography of the mine site. The global slope height (GSH), which is the height projected in the vertical axis between the lowest most toe and the uppermost crest, is anticipated to stretch to 300 m but currently, the pit height of 250 m is planned based on the geological confidence from the drilling project. The delineation of the resource is well quantified to the depth of the current plan because a limited number of holes were drilled to at least 300 m due to mostly extended sections of cavities that posed a technical challenge. Thus, the configurations were considered for a minimum pit height at 250 m and a maximum of 300 m. Meanwhile, we assume that all the blocks meet the costs of mining, processing, and marketing at the GSH of 300 m which shall constitute the ultimate referenced depth of the mine.

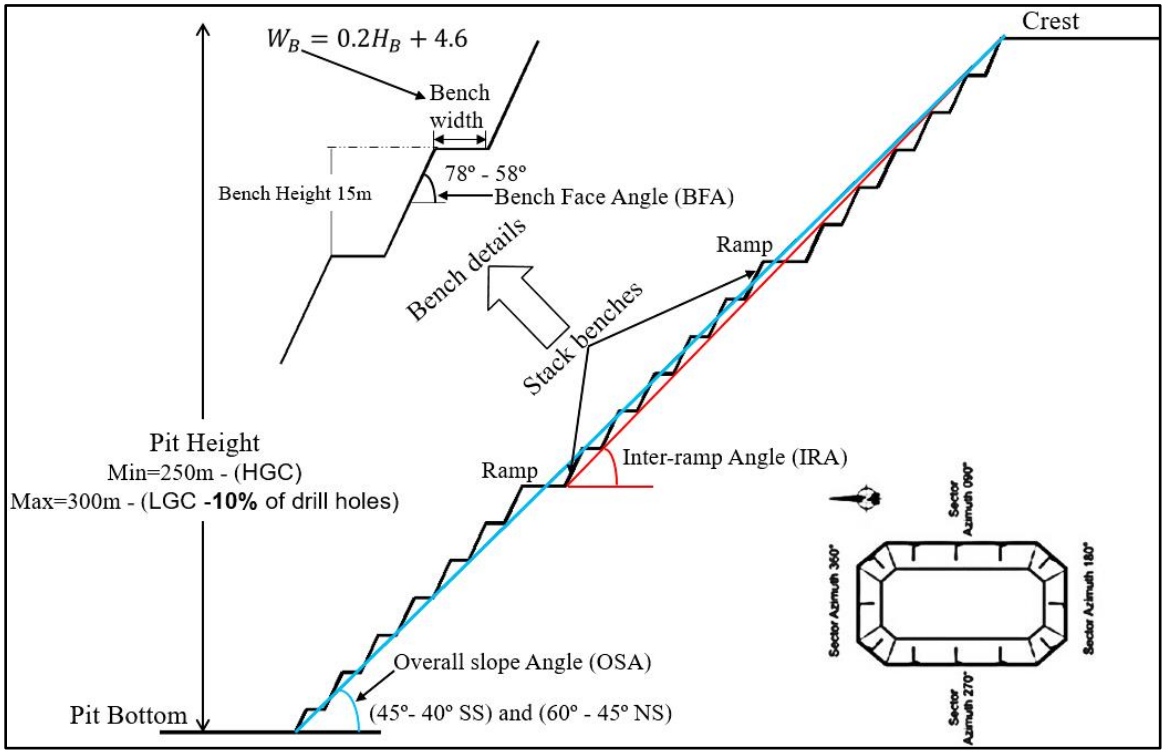

Figure 4.7 Conceptual pit configuration of the planned Songwe Mine: HGC – high geological confidence and LGC – low geological confidence

4.4 Numerical Model Development

The numerical model of the pit was guided by the hill dimensions. Songwe Hill has a north-south diameter of 800 m and measures about 450 m east to west. The planned open-pit mine at the site is anticipated to cover almost the whole stretch of the hill. The overall dimensions of the pit are planned to be approximately 650 m north to south and 400 m east to west. Regarding pit height, it is expected that the deepest level will be 300 m when measured from the highest reduced level (RL) of the pit on the southern side of the pit (see Figure 4.8). Thus, the simulation model stretches 1,000 m in length, 400 m in height, and the width measures 400 m. The 100 m addition in both sides of the x-axis is to make sure that the boundary conditions do not influence the solution when stepping. Monitoring points were added at the mid-section of the pit to observe displacements and stress regimes on the pit walls. The excavation of the stack benches (dimension 15 m height and 7.5 m width) was done in sequential stages as suggested by Moses et al. (2020). As aforementioned, two main conceptual cases were generated with respect to pit height. In the first scenario, shear strain behavior on the pit-slope was investigated at the current planned depth of 250 m and 280 m depth was included as a bonus analysis.

The current planned depth is within the bounds of proven ore reserve hence the geological confidence is high. The second scenario is for the GSH of 300 m. At this depth, the geological confidence is relatively low since less than 10% of the drilled holes reached 300 m. In both cases, the analysis was conducted at different overall slope angles (OSA) that could be practical in the design. Thus, OSA was varied from 45°to 40° in the south section (SS) and 60° to 45° in the north section (NS) of the hill. The models were governed by the following boundary conditions; roller boundaries were assigned in the *x*- and y-direction thereby fixing the boundary planes in the *x*- and y-direction respectively, pinned boundary (i.e., constrained in the *x*-, *y*- and *z*-directions) was applied at the bottom of the model and the top boundary of the model was left unconstrained. Mechanical properties applied in the study are presented in Table 4.1

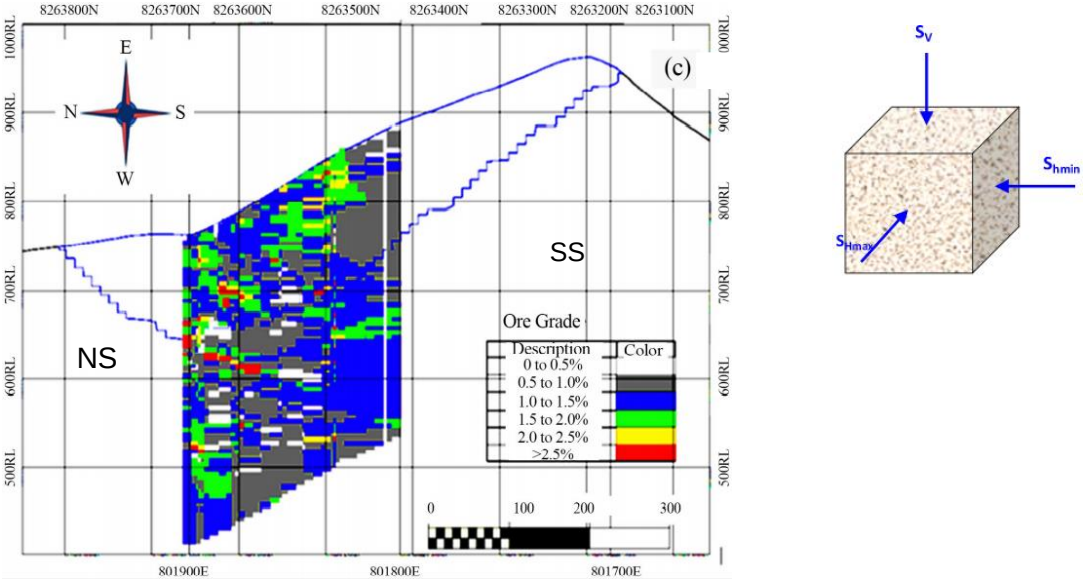

(a) cross section of Songwe open-pit Mine

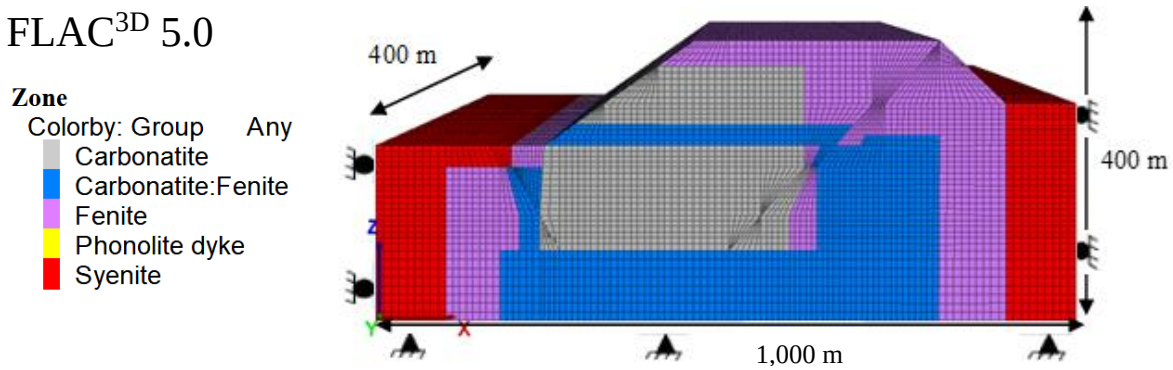

(b) Model extents

Figure 4.8 A cross section of Songwe open-pit Mine

Table 4.1 Mechanical Properties

Rock Type	Uniaxial Compressive Strength (MPa)	Density (g/cm^3)	Young's Modulus (GPa)	Tensile Strength (MPa)	Friction Angle (°)	Cohesion (MPa)	Poisson Ratio
Carbonatite	83.2	2.78	45.30	8.6	35	0.32	0.28
Fenite	118.6	2.70	44.40	10.4	36	0.30	0.29
Phonolite	150.4	2.88	64.30	11.5	37	0.45	0.29
Syenite*	70.0	2.55	53.40	3.37	30	0.28	0.25

*Based on empirical values (Croll et al., 2014; Katz et al., 2000)

4.5 Results and Discussion

The principal objectives of the open pit slope stability analyses are to investigate the pit slope stability conditions, probable failure mechanism, slope sensitivity or vulnerability and to design optimum pit slope angles in terms of safety, reliability and economic lucrativeness. Generally, stability of open pit slope depends on geometry of slope, rock mass characteristics and shear strength behavior of the joints (Soren , Budi, & Sen, 2014). In slope stability analysis, factor of safety (FoS) is used as an index to determine the stability conditions. The factor of safety is a ratio between shear strength and shear stress to determine the stability of excavated sections. The evaluation of the safety of slope in FDM, as adopted in this research, is based on the shear strength reduction (SSR) technique that entails a systematic iterative search for a value that stretches the slope to convergence (Itasca, 2012), presented as;

$$\frac{\tau}{F} = \frac{c}{F} + \sigma \frac{tan\,\varphi}{F} \qquad (4.2)$$

where: τ is shear stress; c is cohesion, φ is internal friction angle, σ is normal stress, and F is strength reduction factor or slope safety factor

The SSR technique as developed by Itasca (2012) has the following advantages:

a. No assumptions are suggested in advance regarding the shape or location of the failure surface. Thus, failure happens “naturally” through the zones within the soil or rock mass in which the shear strength is incapable to resist the shear stress leading to non-convergence

b. It accounts for different material stress-strain behaviors

c. It provides information on deformation at working levels and is able to monitor the propagation of failure up to and including overall shear failure.

d. It provides information on deformations, bending moments and, axial loads of support elements at failure

The basic minimum requirement for stability assurance when assessing the performance of excavated sections is that FoS should be equal to 1, which is a state of equilibrium. However, in mines, the minimum requirement is > 1. Generally, the benchmark value varies by region and mining guidelines enforced by different countries. After a compilation of data from numerous OPM, (Adams, 2015; Sullivan, 2013; Read & Stacey, 2009) established that the minimum criterion for safety assurance in OPM is for FoS to be ≥ 1.2 as shown in Figure 4.9. Thus, in this work, reference is made to the benchmark value of safety in the analysis.

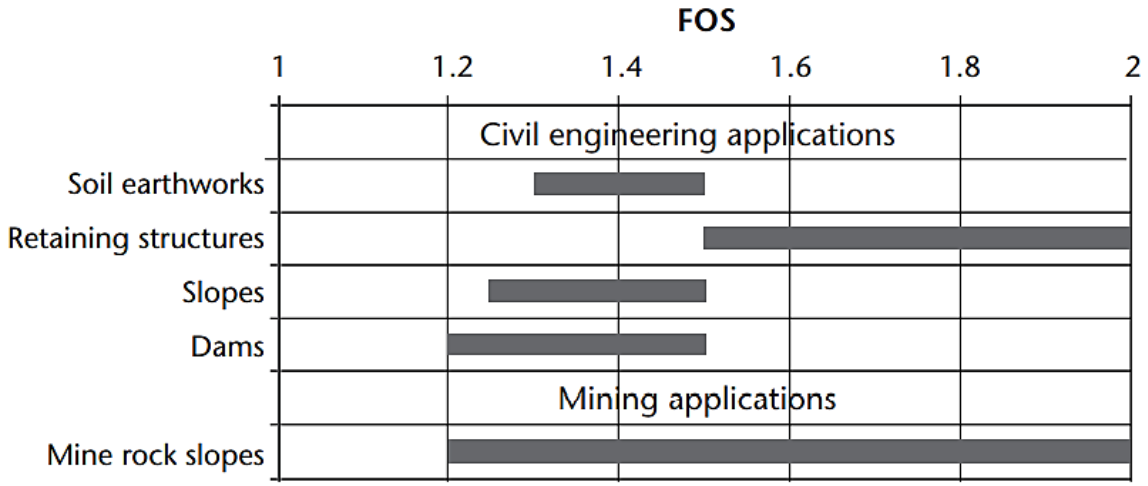

Figure 4.9 Empirical acceptable FoS values for various projects (Read & Stacey, 2009)

4.5.1 Pit Slope Stability Condition

In most mining engineering projects, analyses are performed considering a worst case scenario. As previously indicated, the OSA was varied across the scenarios from 45°, 43º, 41º to 40° in the south section slope and 60°, 55º, 50º, and 45º in the north section slope. Figure 4.10 presents the summary of stability conditions of the separate sections and the pit as a whole. The results at shallow excavation depth show that FoS is satisfactory across all the slope angles both in the north and south section when analysed separately. The values of FoS are well above the threshold of 1.2 applicable in rock slope mines. However, as anticipated, the reliability of the safety reduces as the slope angle increases.

For the north section, at the initial excavation (exc 1 = 100 m) depth corresponding to 250 m in the south section with an angle of 45°, the FoS is 1.76, and it reduces to 1.71, 1.57 and 1.55 at 50°, 55° and 60° respectively. On the other hand, at 250 m in the south section, the FoS is 1.38, 1.36, 1.31 and 1.25 at 40°, 41°, 43° nd 45° in that order. Evaluation as a whole pit, at 40º, the FoS is 1.41 which is very reliable for mining operations and at 45º FoS drops to almost the criterion benchmark at 1.23. On the other hand, extending the pit through 280 m to 300m shows that all slope angles in the north section would be stable at second excavation corresponding to 280 m and only 45° and 50° would be stable at last excavation (exc 3 = 150 m) corresponding to 300 m in the south section. Meanwhile in the south section and entire pit only slope angles of 40º and 41º give reliable safety factors. For the whole pit mine at 40º, FoS is 1.27 and 1.23 at 41º. The slope angles of 43° and 45º have undependable solutions with FoS values of 1.19 and 1.12 respectively.

To appreciate the pit wall stability conditions, Figure 4.11 presents qualitative results of the mine pit walls. As it would be anticipated, the shear strain is intense at the toe in all the models signifying a high concentration of stress towards the pit bottom. Furthermore, the potential slip surface represented by a red-yellow contour band becomes larger in the south section as the angle is steepened at 250 m pit height. However, as the mine extends to a deeper horizon the slip surface is drawn down to the toe, hence compromising the bearing capacity of the toe translating to unreliable performance of the pit walls. In general, the simulation outcome reveals that the south section of the pit facing north, due to the topography of the hill, is prone to instability especially at 45º as the pit extends to the GSH. On the other hand, the north section pit wall is very stable with no manifestation of potential slip surface when the pit is analyzed as a whole at 250 m but as excavation progresses, the north section begins to show instability due to steepened slope angle.

4.5.1.1 Slope Angle Optimization

It must be appreciated that in mining operations, exploitation of ore in OPM involves relating slope angle design to a pair of contradictions between resource recovery and safety. Thus, to achieve an optimum design, there must be a trade-off between a slope that is steep enough to be economically acceptable and one which is gentle enough to be safe.

The heightening and steepening of excavation bench slopes are largely preferred to ensure a small stripping ratio as the excavation targets the ore body. This proves exciting for mining operations to swing towards more profits. However, as observed, this process may affect the security of the overall slope thereby inducing instability. Thus, slope angle optimization aids in finding a poise between safety and mining economic benefits. Based on the current predictive analysis, if the pit is projected to extend to 300 m depth, it would be recommended that from inception bench angles should be designed to target the 40º OSA, which gives a much more reliable assurance of pit stability. The proposed optimization option at the initiation of the mining operation could assist in evading costs due to the onset of instabilities. It is feasible to adopt a 42° /53° OSA given that stability of the wall is just barely below the benchmark value at 43°/55°. However, as observed in kinematic analysis, such a decision must be cautiously related to the influence of discontinuities, which is not considered in continuum methods.

The slope optimization approach has proven crucial in balancing between safety and economics. For instance, a study by Bye and Bell (2001) demonstrated that the optimization of slope design at Sandsloot Platinum mine in South Africa protracted the life of mine permitting two additional benches after the 300m planned depth. The optimization process was attained by varying slope configurations that evolved when more geotechnical data became available that took into account the kinematic failure mechanism. The adjustment of a single degree saved the company $4 million in stripping costs, hence savings in the order of $28 million in stripping costs were realized and enabled the company to accrue $100 million in additional profits. Meilnikov et al. (2003) also acknowledge that there are considerable economic benefits of steepening the front-to-back to optimal slope angle which increases the ultimate value to tens of millions of dollars in medium-sized open-pits to hundred millions of dollars in large pits. However, they cited examples of over-optimizing the angle at the expense of safety, which experienced loss in stability in the zones of pit walls and greatly worsened the mining operations resulting in a huge losses (Melnikov et al,. 2003)

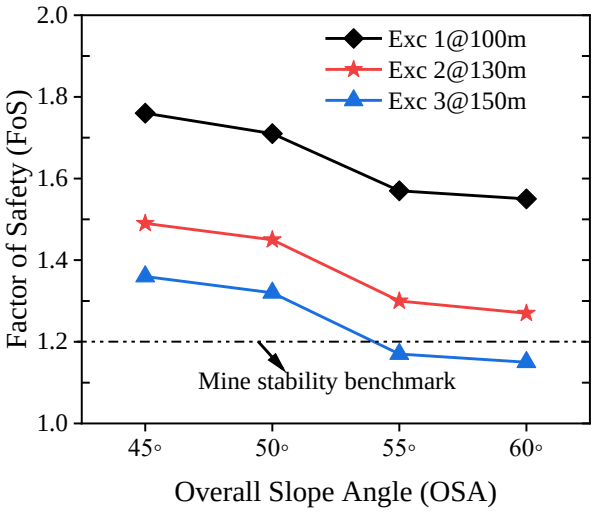

(a) Rock slope stability of the North section

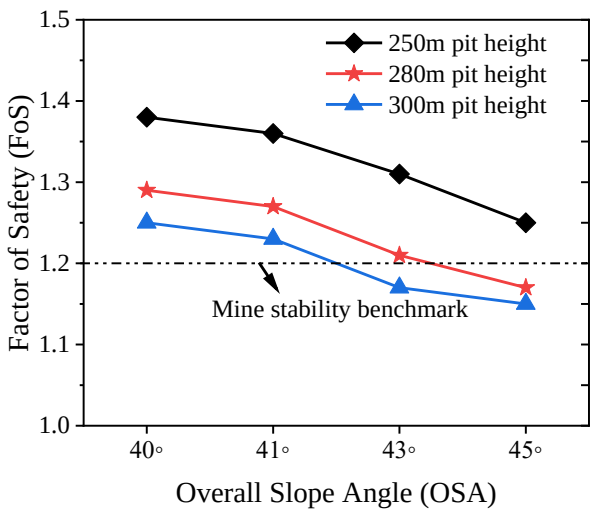

(b) Rock slope stability of the South section

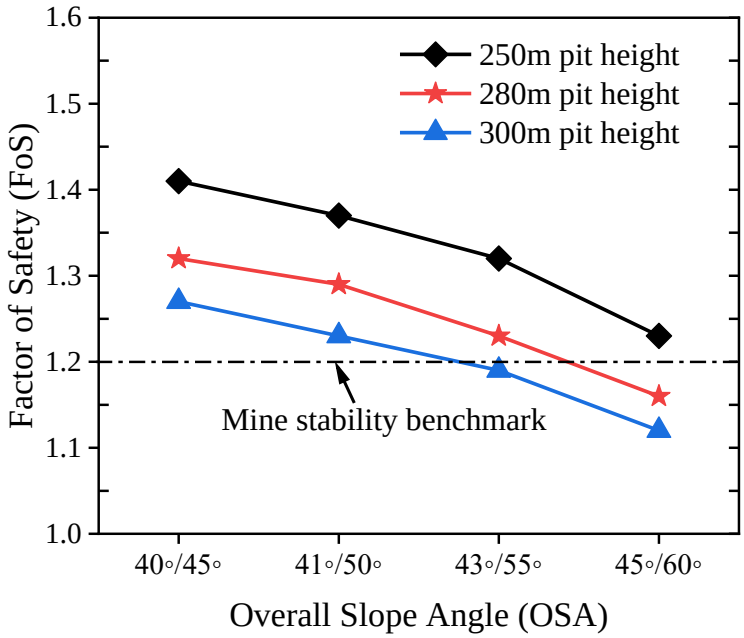

(c) Rock slope stability of the pit as a whole

Figure 4.10 Pit stability condition at different excavation depth

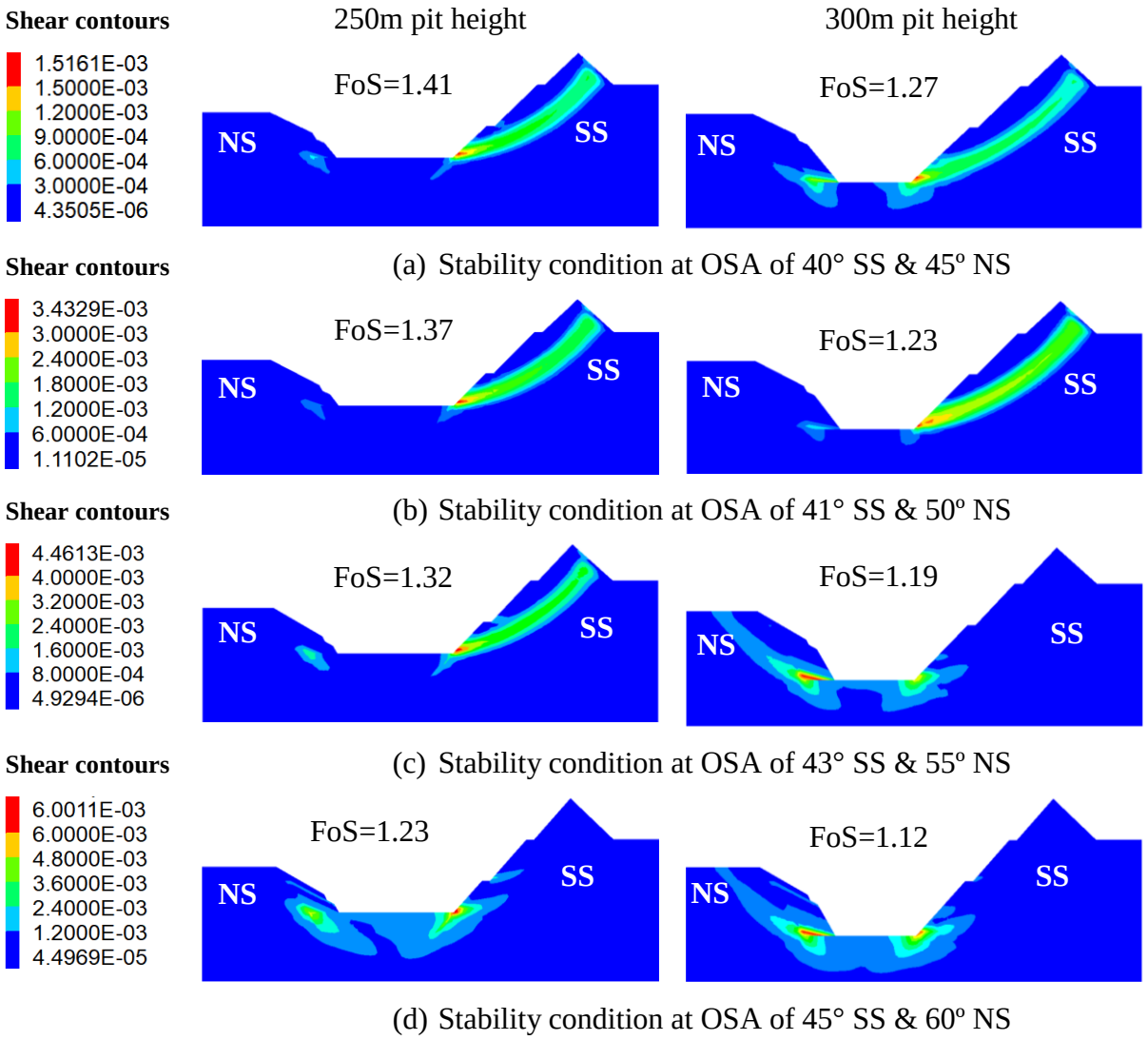

Figure 4.11 Pit stability condition at different pit heights

4.5.2 Displacement of Pit Slopes

Mining activities induce volumetric as well as stress-strain changes in the rock mass around a mine. To complement the shear strain analysis, it is crucial to investigate the potential extent of the movement that could be subjected to the rocks making up the slopes surrounding the OPM. Contrary to when mining operation is ongoing, in which case monitoring is conducted from time to time and sometimes robotically using reference points, at the simulation level, this was attained by pinning monitoring points on strategic points.

The horizontal movement of pit slopes is a crucial component of evaluating the volumetric changes in the walls. As discussed by Wessels (2009), the X-displacement can be categorized into four stages with a varying scale of displacement. The stages are graphically presented in Figure 4.12. The first stage takes an elastic displacement which occurs at a scale of millimeters in hard rocks at a shallow depth to meters in deep horizons for soil and/or soft rock. The second stage involves crack and dislocation at 0.2 to several meters scale. Preceding the last stage of material movement on the pit slope is creeping displacement that can take a rate of 10 to 100 millimeters per second. The last stage of displacement is a strained elastic movement which takes a scale of $\geq$ 0.5. At every stage, the displacement extents are governed by the type of rock mass that makes up the slope and the slope height.

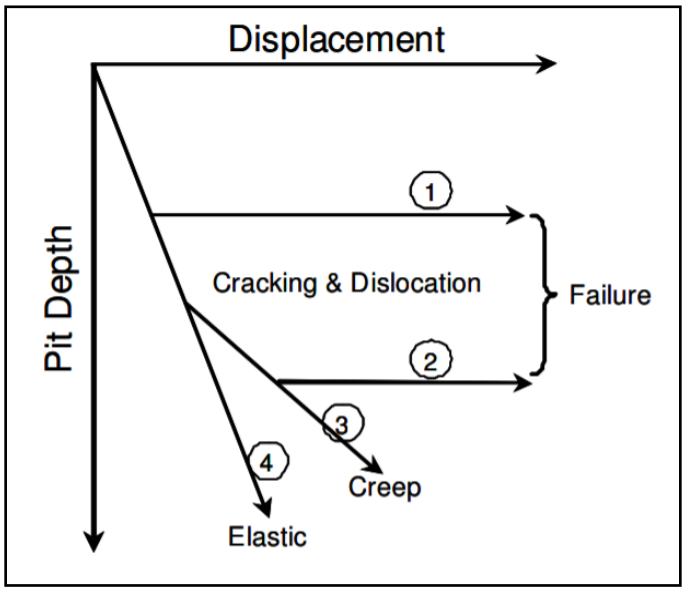

Figure 4.12 Ground reaction curves (Wessels, 2009)

Curve 1 in the model represents wedge or planar failure where the weak planes are exposed as the excavation progresses to a greater depth. The slope movement in curve 2 is characterized by complex failures triggered as the mine deepens. The displacement could culminate into the collapse of the slope. Studies have shown that displacement curves 3 and 4 that involve creep and pure elastic movements do not normally affect mining operations due to very low displacement rates (Wessels, 2009).

Apart from the type of material and pit height, displacement is time-dependent. Regarding time, deformation progressively undergoes three phases namely: Phase I initial response, phase II strain hardening, and phase III progressive failure (see Figure 4.13). The slope deformations recorded at the initial response are basically adjustments in response to the excavation of the material. Even though failure could not be anticipated at this level, displacements ranging from a few centimeters to more than a meter could be recorded. However, the displacement rate can change from several millimeters a day to almost no movement. This relationship is described by an exponential relationship involving rock mass quality, slope geometry mining rate, and failure mechanism as shown in Figure 4.13. The "locking up" of rock mass due to dilation tends to occur during the strain hardening phase and the available shear strength on discontinuities or within the rock mass gets mobilized resulting in increased stability (Wessels, 2009). Thus the strain hardening phase demonstrates a regressive behavior characterized by short periods of increased displacement rates.

On the other hand, strain-softening takes place as a result of the decrease in shear strength as displacement gradually increases. If there are no external forces, the displacement occurs at a constant rate but external events like blasting and rainfall may lead to an acceleration of movements and eventually slope collapse. To manage unprecedented pit instabilities, the displacement pattern on the pit walls was simulated and monitored. The data on the horizontal movement of pit slopes were collected from monitoring points pinned strategically in the rock mass. The displacement trend, based on k = 1 with the non-associated flow rule, is presented in Figure 4.14. The northern section, separated by pit bottom (PB), recorded small displacement values as compared to the south section. This is apparently due to the discrepancy in the slope heights owing to the site topography. The displacement values are positive with a bulging curve implying movements out of the pit slopes, which progressively increase as the excavation depth increases. This is indicative that the material is being pushed out away from the monitoring point.

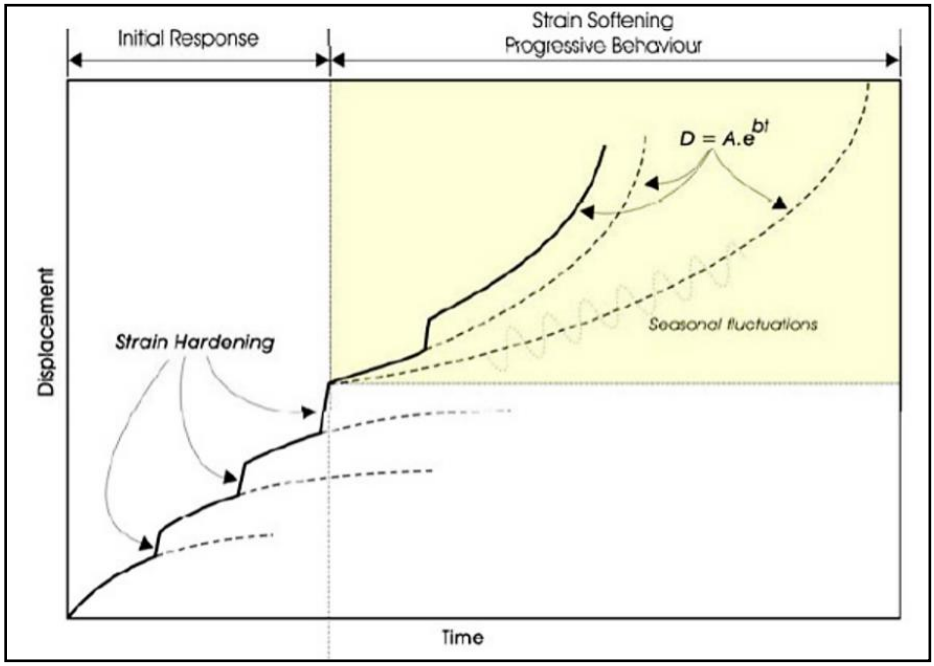

Figure 4.13 Time dependant deformation behavior model (Wessels, 2009)

At 250m height, the maximum horizontal displacements (positive) in the north section are 10 mm at 40º, 9 mm at 41º, 12 mm and 11 mm at 43º and 45º respectively. After excavating to 300 m depth, the displacement at 40° increased to 17 mm at 40° and averaged 19 mm at 41° 43° and 45°. This positive x-displacement response to induced mining stress could be described in terms of elastic rebound of the rock mass due to the relaxation and release of high-stress experienced in the high RL, south section of the pit. Regarding the extent of displacement, the displacement values in this section increase as the depth of the pit increases though slightly variant with respect to adjustments in overall angle. The horizontal displacements in the south section are negative moving into the pit indicating pit wall stress relaxation. From Figure 4.14, we can observe that displacement varies with depth and OSA. Generally, the highest displacement values are registered in the third phase of excavation at E. At a pit height of 250 m, the maximum displacements are 152 mm, 115 mm, 162 mm and 181 mm for 40°, 41°, 43° and 45° angles respectively. Further excavation to 300m pit height, the maximum x-displacements picked up except at 40°. The displacement values recorded were 141 mm at 40°, 145 mm at 41°, 184 mm at 43°, and 227 mm at 45°.

The phenomenon of a relatively large slope deformation recorded at shallow depth with gentle slopes may be reflective of the initial response of adjustments consequent to the excavation of the materials. But, even though displacements could be high at such shallow depth, Wessels (2009) and Sjoberg (1996) established that failure could hardly be anticipated at shallow levels but rather deeper levels. Additionally, it is crucial to appreciate that apart from material conditions, displacement is time-dependent. Thus, in this case, the displacement rate can change significantly over time. On another note, strain hardening can set in causing the available shear strength within the rock mass to get mobilized resulting in increased stability characterized by an extended phase of plasticity.

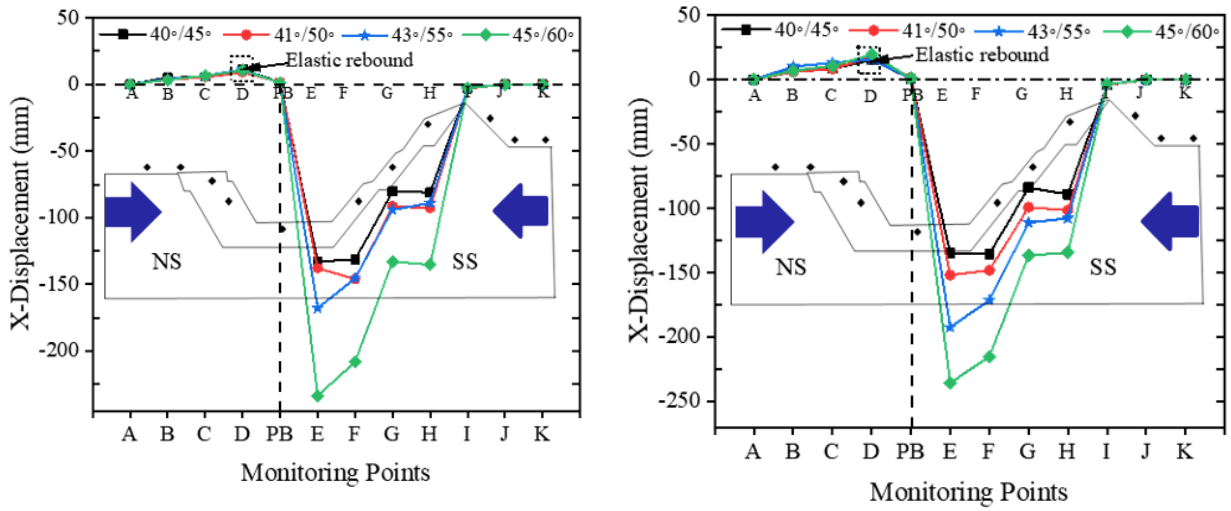

(a) 250m pit height (b) 300m pit height

Figure 4.14 Pit wall displacement at different pit heights

4.5.3 In situ Stress in Open-Pit Mine

The stress concept is fundamental to rock mechanics principles and applications (Hudson & Harrison, 1997). The understanding of stress is critical in mining because pre-existing stress state directly have an influence on the analysis and design and during rock excavation, the stress state can change dramatically since the load's stress gets redistributed. The pre-mining initial stress state is a critical aspect in numerical modelling for equilibrium stepping and determination of mining-induced stress.

In situ stress can be described as the stress prior to initiating excavation. Traditionally, the investigation of the influence of in situ stress has been confined to underground mining studies. In underground mining, the analyses focus on failures such as squeezing, spalling, and rock bursting which could impact mine safety and production. Despite being a fundamental concern in the design of underground excavations, in situ stresses for open-pit projects are simply not regarded as influential. This is because the stress conditions in OPM are regarded dilationary and that instabilities are accredited to be gravity-driven. However, Stacey (2003) and Sjoberg (1996) unanimously describe this sweeping statement as very dangerous since the impact could indeed be negligible only to the region close to the pit walls, and at the toe of small scale slopes and not in large scale slopes and high tectonic stresses regions. Hence, it is important to investigate the role of in situ stress in OPM on slope instability since excavation creates stress disequilibrium.

4.5.4 Determination of In situ Stress in Great Rift Valley Region

Rock masses are inherently inhomogeneous and geological features tend to change the stress field. This has been verified to be true near structures where stress magnitudes can increase or decrease sharply, and stress orientations can rotate as much as 90^{o} when the discontinuities are crossed (Martin & Kaizer, 1998; Martin & Chandler, 1993). For this reason, measurements taken contiguous to geological structures may not really represent the far-field stress situation. Brady & Brown (2005) add that the rock mass strength and stiffness can also impact the stress distribution within a rock mass. Thus, in tectonically stress areas, stronger rocks are likely to show major principal stress magnitudes significantly greater than both the vertical and the other horizontal components. In this research project, due to unavailability of site-specific data, which is technically complex and expensive to collect, the pre-mining stresses were approximated from African regional stress compilation in OPMs; Impala, Parabola, and Rusternberg mines grouped as A, B and C respectively, Calolusberg and Kersdorp mine all located in South Africa. The average in situ stress at unity from the data set is 10.5MPa. The average was drawn from the mines that have almost the depth of 400 m. Based on the regional data, it can be observed that the mean ratio between vertical stress and major horizontal stress can be tested up to K=2.5 in open-pit mines (see Figure 4.15).

It is crucial to highlight that the local stress at the study site could be substantially different compared to the regional one. The precaution is stated out because of a number of reasons as discussed in (Brady & Brown, 2005; McKinnon, 2001; Zoback & Zoback, 1989; Zoback & Zoback, 2003):

1. The state of stress in an element of rock depth depends on both the loading conditions in the rock mass and the stress path defined by its geological history
2. Mechanical processes such as brittle fracture growth and sliding along discontinuities can modify stress field,
3. Change of stress associated with temperature changes as well as chemical processes such as leaching, precipitation, and crystallization.
4. Site-specific local geology, discontinuities, rock mass properties, and topography

For reasons aforementioned, different stress ratios (σ_{Hmax}/σ_v) regimes were evaluated to appreciate the influence they could have on the stability of the pit walls, but the author considers that the horizontal stresses are high in the region based on world stress trajectory by (Heidbach, et al., 2018).

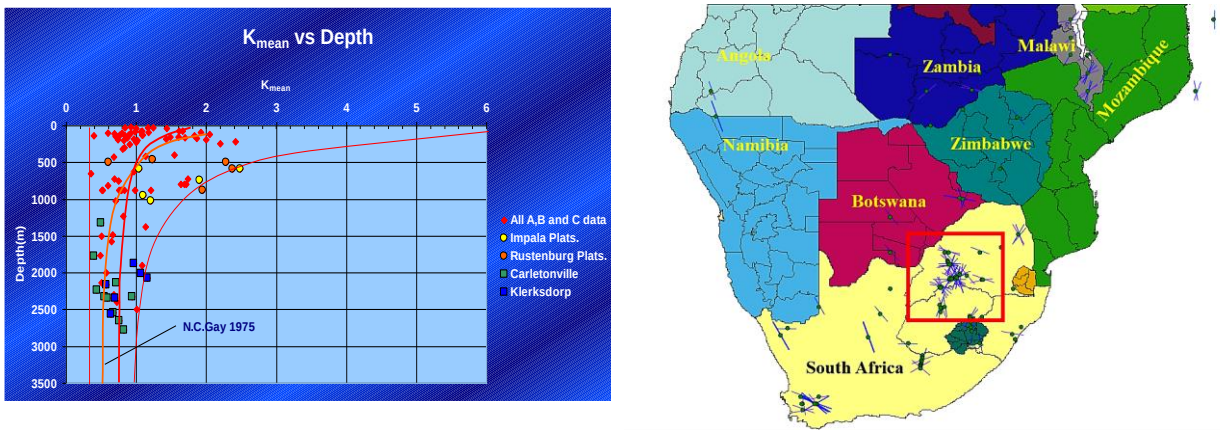

(a) Mean stress ratios for representative OPM (b) Location of data representative mines

Figure 4.15 The averaged ratio of vertical stress and maximum horizontal stress (Stacey & Wesseloo, 1998)

4.5.4.1 Influence of Stress Ratio on Pit Slope Stability

In situ stress at pre-excavation phase are presumably at equilibrium. However, the field conditions may be different depending on the tectonic setting and topography. The commencement of mining operations causes a considerable imbalance of the initial stress condition. The pre-existing horizontal stress is redistributed in response to the excavation causing the horizontal stresses to flow beneath the pit bottom. On the other hand, the vertical stresses are reduced through the removal of the overlying rock material. This implies that the rock lying between the pit outline is largely distressed. Thus, change of the stress regimes could have an impact on the stability of the pit walls over time. Using a case of 300 m GSH, the stress ratio ($^{\sigma_{Hmax}}/_{\sigma_v}$) was varied to qualitatively assess the shearing pattern around the pit wall and quantitatively evaluate the slope performance. The results of the analysis are presented in Figure 4.16 and Figure 4.17. The qualitative evaluation of the stability state through shearing contour reveals that large in situ stress field has a major influence on the stress distributions in slopes leading to varied pit wall strain conditions.

Generally, the pit wall shearing becomes intense and the straining impact area of the walls becomes large under high-stress ratio conditions. Since the failure of slopes is consequent to accrued effect of supply (shear strength) versus demand (shear stress), it should be appreciated that with the passage of time, the pit walls could potentially fatigue under such conditions. Furthermore, a critical observation of Figure 4.16 and Figure 4.17, it can be noted that the mechanism of failure appears to be significantly different along the failure surfaces. The failure pattern due to the stress state in a slope is presented in the conceptual proposition in Figure 4.18. At uniform stress, the potential failure surface (PFS) trajectory is conventionally from the crest through the interior of the slope to the toe at points 1, 4, and 3. Generally, at the toe, the normal stress is moderate while the shear stress is comparatively high. Failure at crest can be facilitated by the existence of tension cracks. On the other hand, non-uniformity of stress state leads to the development of a secondary PFS at point 2 in addition to the primary PFS although primary PFS is not well developed under high vertical stress where shearing is concentrated to the toe.

In the case of a high vertical stress state, the pit bottom sustains high straining than the pit walls along the trajectory of the primary PFS. Nevertheless, in both scenarios, high-stress acting non-uniformly tends to induce frontal failure in the direction perpendicular to the slope face. However, as adjudged quantitatively by a deterministic index, that is FoS, the outcome shows that in situ stress has a negligible impact even under high-stress ratio conditions. As observed from Figure 4.19, the FoSs remain the same at 250 m under different stress regimes except when the pit extended to 300 m pit height where a marginal decrease of 1% in FoS is recorded beyond k=1.

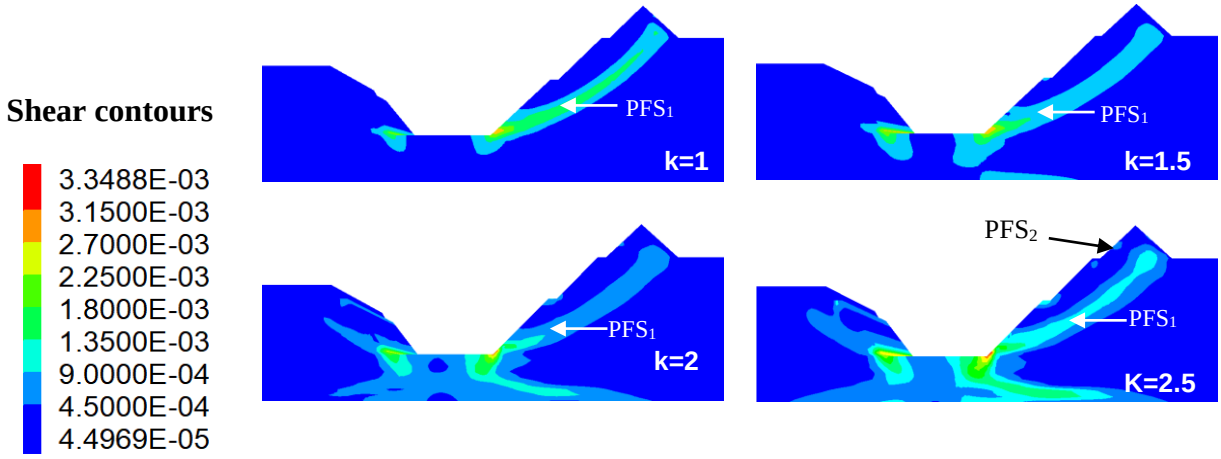

(a) Shearing pattern of pit walls for 40°/45° OSA

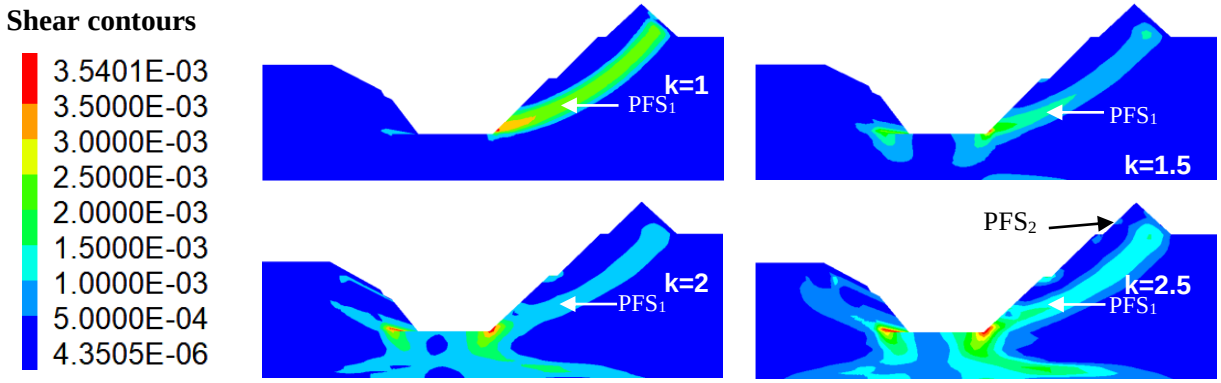

(b) Shearing pattern of pit walls for 41°/50° OSA

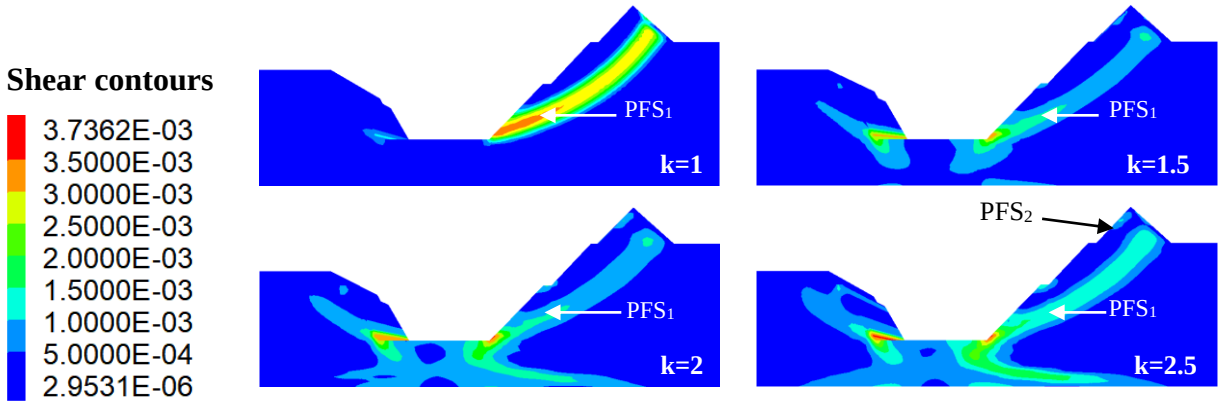

(c) Shearing pattern of pit walls for 43°/55° OSA

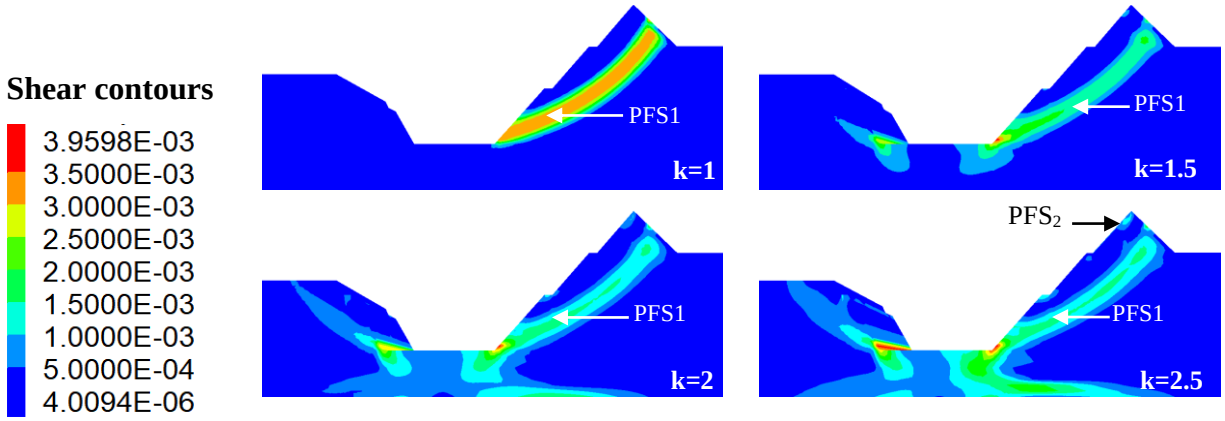

(d) Shearing pattern of pit walls for 45°/60° OSA

Figure 4.16 Shearing pattern under high horizontal stress conditions at 300 m pit height

Since the determination of stability is conventionally quantitative, this phenomenon explains why in situ stress is traditionally not considered in OPMs. However, with respect to the life of mine (LoM), it is important to understand that induced stresses respond to the initial stress conditions thereby influencing the stability of excavations. As a 'first check' in the assessment of the stability of a pit slope, we apply the strain-based approach to failure prediction and establish if further attention could be necessary to incorporate the trigger action response plan (TARP) for instability in different stress regimes.

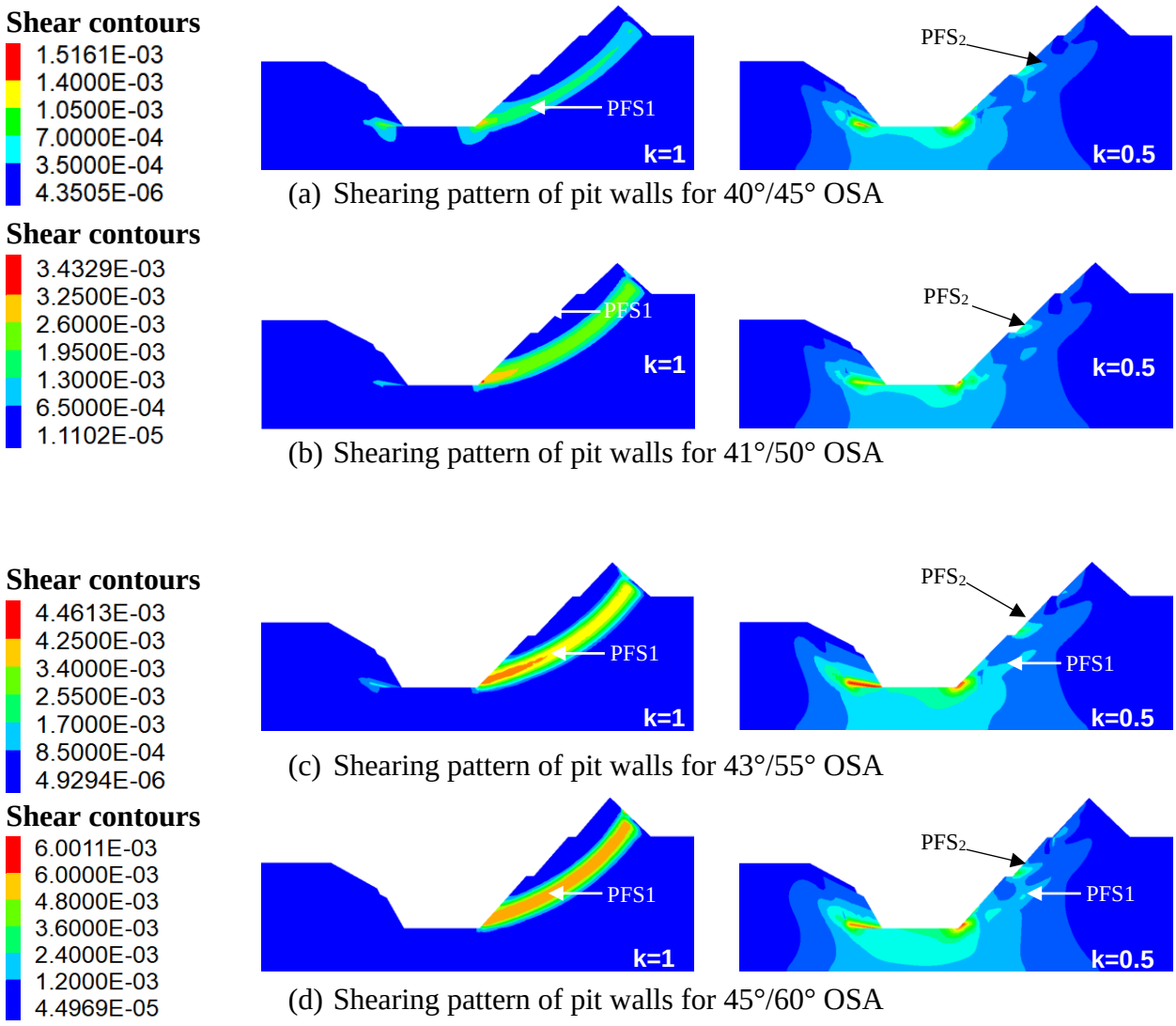

Figure 4.17 Shearing pattern under high vertical stress conditions at 300 m pit height

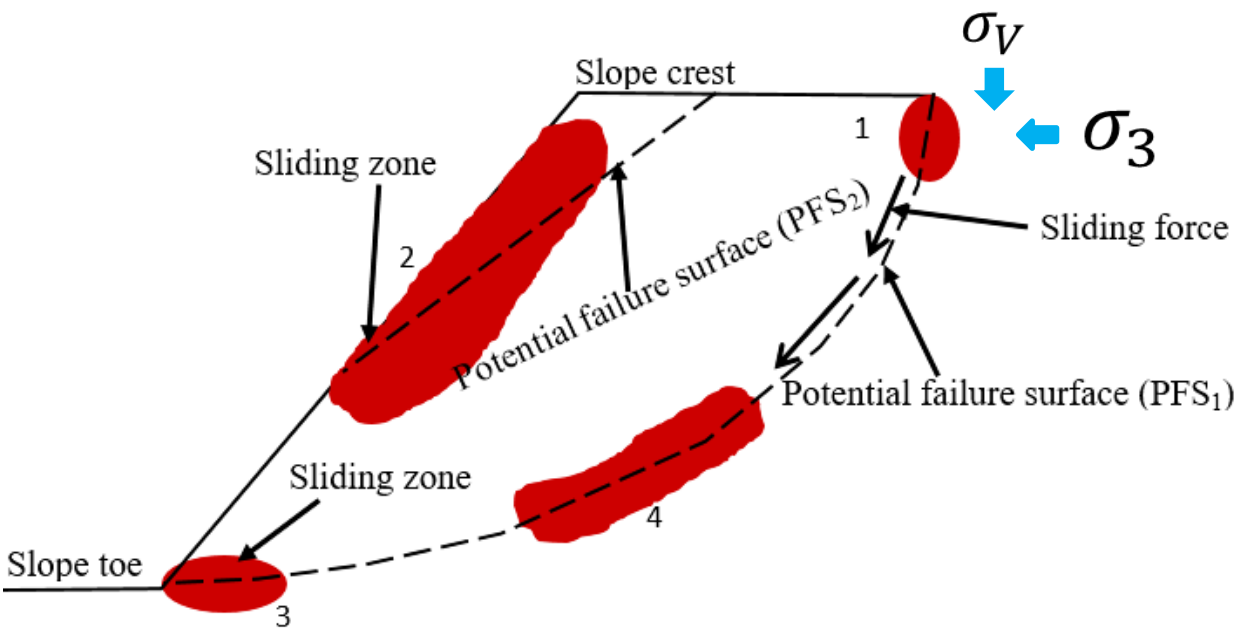

Figure 4.18 Conceptual illustration of failure pattern in different stress state

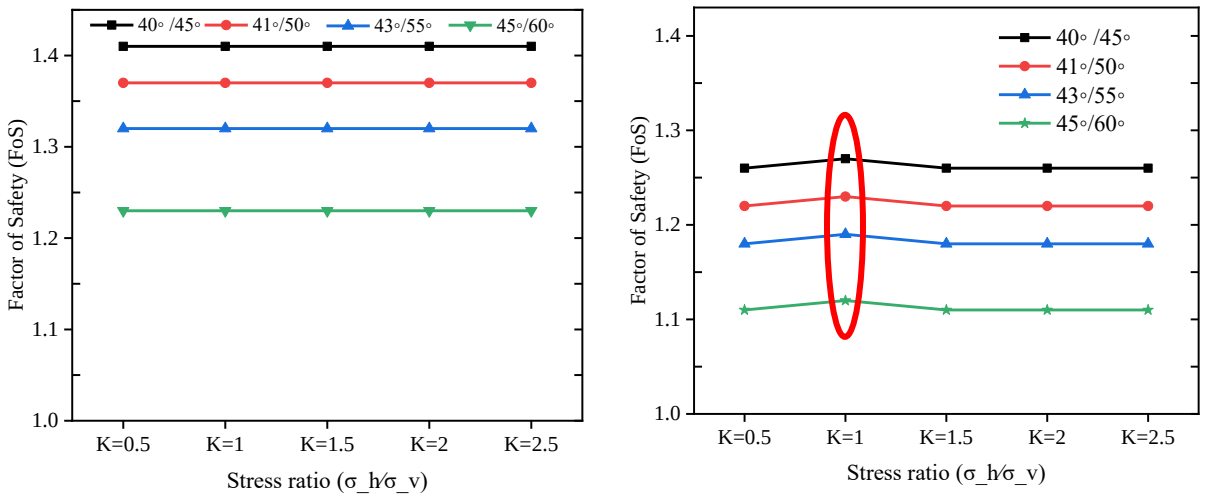

(a) 250 m pit height (b) 300 m pit height

Figure 4.19 Stability condition in different stress conditions

4.5.4.2 Total Displacement Pattern

To check the criticality of the stability state, extents of displacement were assessed under different stress conditions. The results of total displacement (interplay of vertical and horizontal displacements) with respect to k-ratio are presented in Figure 4.20 and Figure 4.21.

In the former figure, a qualitative representative case at 41° OSA is shown and the latter figure gives a quantitative summary of all the scenarios. It can be observed that the pattern of displacement is such that as the stress ratio is increased or decreased from equilibrium state, the extent of total displacement also increases. At the state of stress equilibrium (k=1), the displacement values are lower than at any other stress ratio (both at high horizontal and high vertical stress regimes). That is, at the state of stress equilibrium (k=1), the displacement values were found to be almost four times lower than at k=2.5 and two times lower when k=0.5. In terms of slope angles, steep angles of 43° and 45° recorded low values of total displacements at equal vertical and horizontal stresses than at gentle angles. This could be explained in terms of expansion of destressing region in steep slopes. This phenomenon allows the horizontal stress path to the slope and hence low deformation on the excavation face. As Call et al. (2001) argued, normally steeper slopes experience greater velocities and larger overall displacements but he noted and established that there is a maximum limit to the angle that can be excavated before a progressive accelerating slope failure occurs.

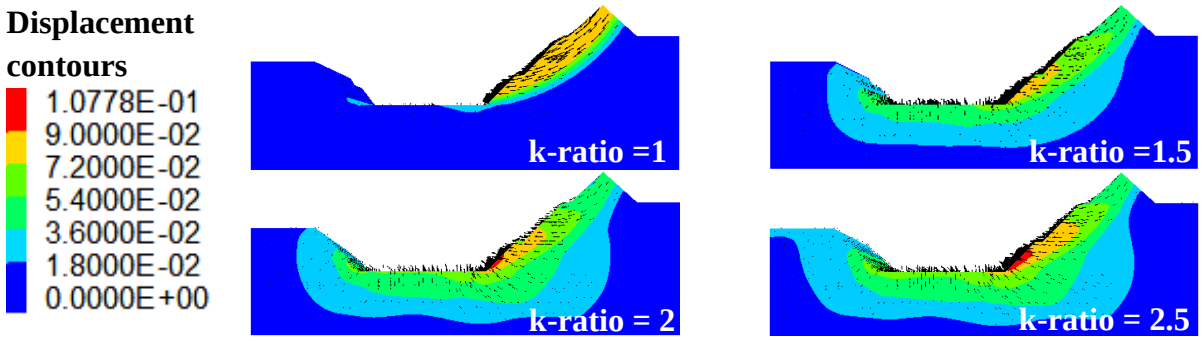

(a) Total displacement of pit walls for 41°/50° OSA at 250 m pit height

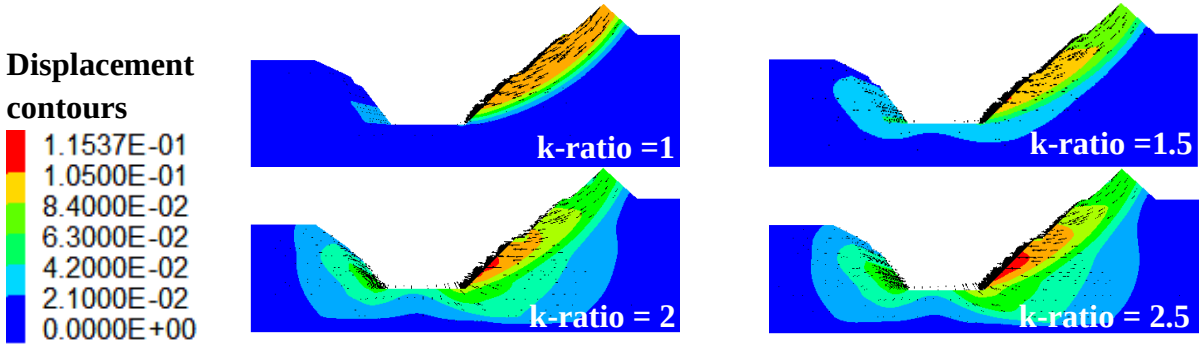

(b) Total displacement of pit walls for 41°/50° OSA at 300 m pit height

Figure 4.20 Qualitative contours of total displacement of pit walls for 41°/50° OSA

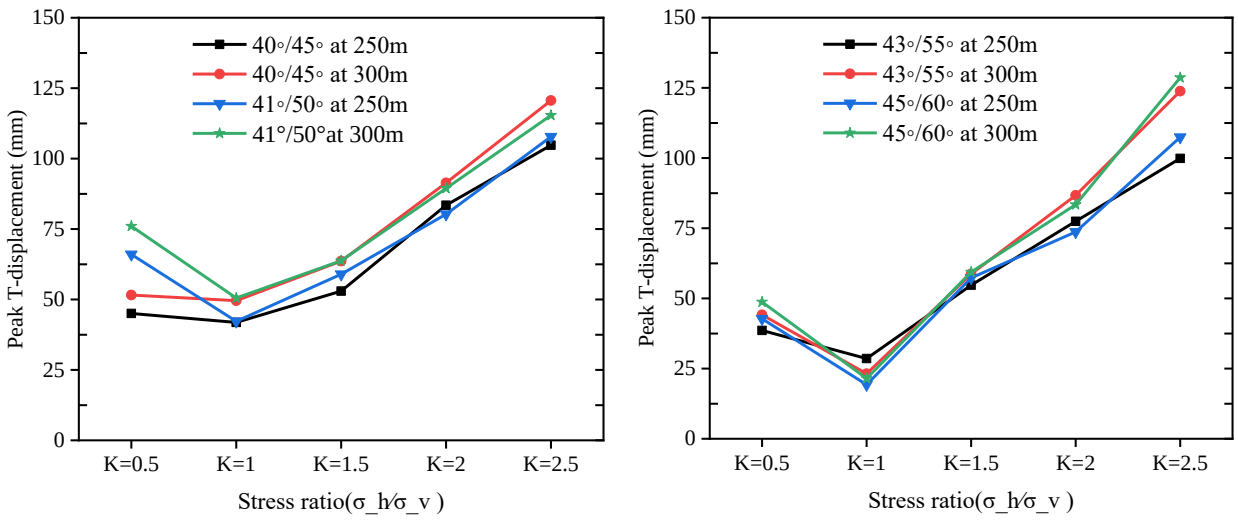

(a) 40°/45° and 41°/50° OSA at 250 m (b) 43°/55° and 45°/60° OSA at 300 m

Figure 4.21 Pit wall displacement under different stress conditions

4.5.4.3 The Strain Criteria Approach to Failure Prediction

The ability to differentiate between non-critical pit wall displacements due to rebound or relaxation of the excavated slopes and movements that may be indicative of slope failure is crucial for maintaining a safe working environment and maximizing production (Newcomen & Dick, 2016). Thus, the strain-based approach, as applied in this study, helps to provide guidance regarding strain thresholds for pit walls in diverse stress conditions. Strain is the ability of a stressed material, in the presence of a stress field, to deform. Generally, rock mass succumbs to the application of stress which is due to the rearrangement of the natural in situ stress field when the slope is excavated. The extent of straining is consequent to the slope geometry and slope construction and in situ stress conditions. The strain-based approach to assessing pit slope stability utilizes the fundamental principles of the strain formula after Brox & Newcomen (2003) given as.

$$\varepsilon = \frac{\Delta x}{H}$$

where: Δx = the maximum deformation of the pit wall, H = the total height of the wall and ε = the strain in percentage

Based on over 12 case studies, Newcomen & Dick (2016), Brox & Newcomen (2003), and Zavodni in Hastrulid (2001) developed the strain percentage criteria for the principal failure modes in various rock mass classes. In establishing the strain criteria, rock mass quality RMR by Bieniawski (1976) and inferred instability mechanism was utilized in order to compile an empirical high wall stability chart. The threshold strain levels for rock mass were established to have a lower bound strain at collapse of 0.1% and upper bound strain to collapse of 3% (Coetsee, et al., 2020; Newcomen & Dick, 2016). The results of the stability performance of pit wall, based on strain approach, against failure under different stress regimes is presented in Figure 4.22. It can be observed that the strain rate increases with higher stress regimes. That is, as the k-ratio increases, the straining correspondingly increases. Similarly, when the vertical stress is higher than the horizontal principal stress, the strain rate increases. This trend is in tandem with the qualitative shearing conditions of the pit wall previously presented in Figure 4.16 and Figure 4.17.

However, the percentage of strain demonstrates that the pit walls would be below the lower bound strain to collapse in all the simulated cases. The highest strain rate of almost 0.04% is recorded at 300m height (45° slope angle) with the highest possible in situ stress condition of k = 2.5. Thus, at this rate of straining the pit walls stability performance would still be guaranteed though the strain rate is relatively increased. Regarding slope geometry, steeper slope angles have relatively high strain rates compared to gentle slopes. For instance, at k = 2.5 with 300 m height, the straining value is 0.03% at 40° and 0.04% at 45°. Corollary, stress redistribution along with stress relaxation in areas where confinement has been lost tends to localize stress particularity at the toe of the slope thereby straining the rock mass into instability. The pit height is also an important determinant of straining on pit slopes as the calculation relies on it. The outcome shows that as the pit extends to a deeper horizon, the strain rate congruently increases. At the GSH of 300 m, the strain values are comparatively high against 250 m pit height. For example, at the high lateral stress condition of k = 2, the strain values are 0.02% at 250m and 0.03% at 300m pit height with respect to 45° slope angle representing a 50% change. Nevertheless, it must be noted that the strain criterion does not consider the influence of discontinuities in the strain bounds to collapse.

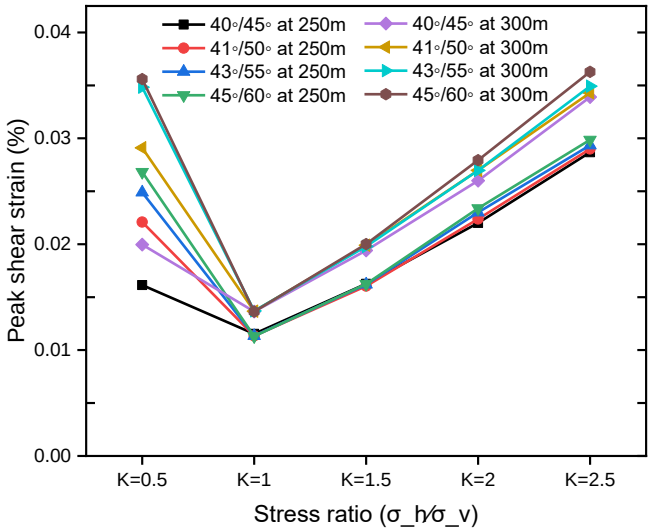

Figure 4.22 Strain state of pit walls under different stress regimes

4.6 Influence of In situ Rock Damage

Carbonatite intrusions, just like the Songwe carbonatite complex, are highly affected by the later stage hydrothermal and carbo-hydrothermal phase where expelled fluids in fissures lead to the formation of new weak features like Mn-Fe veins and/or damage of the rock mass. Hence, rock slope failure in these hard rocks is complex since structures within the rock mass form weak links that could potentially control slope stability. Stead & Wolter (2015) highlighted instances of the significant impacts of sheeting, exfoliation, and joints on slope stability. Generally, when considering structurally controlled stability in hard rocks emphasis is given on the role of discontinuity persistence, orientation, and intensity. But the complexity of failure mechanisms in rock slopes is when a combination of pre-existing geological weak planes and failure of intact rock induce instability. Intact rock can be subjected to physical damage of different forms. The concept of damage of intact rock and rock mass relates to the degradation of their strength properties. The physical damage usually takes place in planes of weakness ranging in scale from micro-cracks to faults. Table 4.2 provides a summary of different processes causing rock damage. The ultimate effect of the damage processes is the degradation of the intact rock properties towards damaged rock mass and the rupture in intact rock is regarded as the accumulation of the damage (Brideau, Yan, & Stead, 2009).

Table 4.2 Types of rock slopes damage (Brideau et al., 2009)

Type of damage	*Process*
Brittle	Initiation, comminution
Ductile	Rigid block overlying soft rocks
Creep	Sub-critical crack growth
Fatigue	Low/high frequency loading/ unloading cycles (glaciation, isostasy, pore water pressure fluctuation, freeze–thaw, wet/dry, seismicity)
Thermal	Heating and cooling cycles
Tectonic	Preconditioned damage due to faults, folds and in-situ stress
Anthropogenic	Excavation, blasting
Physio-chemical	Hydrothermal alteration, weathering, corrosion
Geomorphic	Stress induced damage associated with valley formation, cambering, erosion, thermal cycling

The determination of the rock damage condition has mostly been made possible through rock mass classification systems. Among sundry classification schemes, GSI has proven to be pivotal in the rock damage characterization process with respect to stability analysis. A number of studies have investigated the control of folds and faults, shearing and clay-infill in joints on the stability of rock slopes. A study by Bye & Bell (2001) revealed that steep dipping and persistency of the joints at Sandsloot open-pit in South Africa were principal causes of the slope instability at the mine triggering failure. Faults and fault damage have also been recognized to compromise the performance of the slopes by affecting the regional geology, rock mass, and stress conditions in large open pits. The impact of fault characteristics is directly linked to stress heterogeneities created by the interaction between the faults and the mining-induced stresses generated during excavation leading to localized high plastic shear strain and high extensional train around the fault (Severin, 2017; Stead & Wolter, 2015). Bachmann et al. (2004) also examined the influence on slope stability of both damage due to weathering and the presence of large-scale fractures using 3-dimensional scaled analogue physical models.

The experimental results demonstrated that the introduction of a weathered material on the surface of the rock mass controlled the ease, depth, and extent of the slope failure. However, the presence of large-scale fractures had little effect on slope stability. Based on the findings by Bachmann et al. (2004), the fractures controlled the lateral extent of the slope failures. Recently, Zheng et al. (2018) and Qian et al. (2017) investigated the influence of rock mass disturbance caused by blasting on rock slope stability. The numerical approach was used in the study by Zheng et al. (2018) and Qian et al. (2017) took a comparative approach of Limit Equilibrium (LE) method against the numerical method. Both studies found that the thickness of the blasting damage zone substantially lowers the rock slope stability. In this study, since carbonatite emplacement is often accompanied by widespread brecciation and fracturing (Elliott, et al., 2018), consideration is given to in situ rock damage in brittle form as a result of a unique phenomenon of brecciation associated with carbonatite complexes and its role in preconditioning instability on mine pit walls.

4.6.1 Brecciation Mechanism

Breccia (Bx) is a term commonly used for an enigmatic rock group that comprises of a variety of discrete broken fragments of rocks, every so often angular and bound together by a fine grain matrix and occasionally vitreous matrix which may or may not resemble the composition of rock fragments (Shukla & Sharma, 2018). These rock masses can be identified in different geological settings mostly associated with various ore types. In carbonatite complexes, breccia is a common structural feature. Shukla & Sharma (2018), Sibson (1986), and many other authors have discussed mechanisms of brecciation in different geological environments including the volcanic setting. Among many mechanisms of brecciation, two phenomena can be attributed to be the occurrence of the breccia at the study site namely: hydro-fracturing and tectonic forces along a pre-existing plane of weakness. The hydro-fracturing process for brecciation involves high-pressure fluids. This hydrothermal process readily affects carbonate-rich rocks. In this process, the pre-existing rock interacts with water-rich hydrothermal solutions that increase the fluid pressure within a fissure, and the effective pressure decreases leading to fracture propagation (Figure 4.23).

Elliott, et al. (2018) explain that the occurrence of breccias at several carbonatite complexes corroborates the explosive release of fluids and volatiles from an evolving magma underneath. For Songwe carbonatite, Broom-Fendley et al. (2021) stress that based on the angular nature of the clasts and the comminuted groundmass, the breccia formed by in situ rapid volume expansion, most likely as a result of subsurface explosive release of volatiles from the proposed underlying carbonatite bodies. Thus, the explosive hydrothermal brecciation and the metasomatic action of hydrothermal fluids can be considered responsible for the generation of the breccia in carbonatite complexes like the Songwe Hill. On the other hand, tectonic disturbances resulting from fault movements also can account for the brecciation as the area is located in rifting setting with potentially high-stress acting along the weak plane causing rock comminution. Accordingly, the brecciation associated with the fault system forms due to the grinding action of rock blocks along a plane of weakness as presented in Figure 4.23.

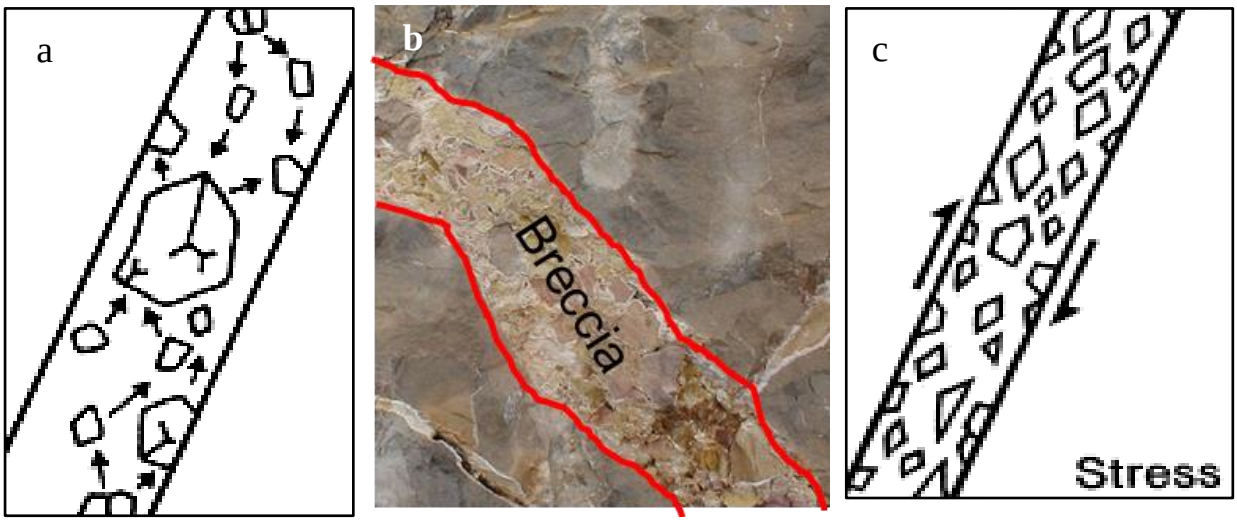

Figure 4.23 Brecciation mechanism in carbonatite-alkaline complexes; (a) hydro-fracturing, (b) illustration of a breccia, and (c) tectonic damage.

4.6.2 Model Construction

Since the brecciated rock section has apparent exposure in the south section of the planned pit, the modelling focused on the south pit wall. Therefore, the north section of the pit model was truncated from the simulation. The dimensions of the model measured 600 m in length and 400 m vertical extent from the highest RL (see Figure 4.24). The brecciated body section was incorporated in the models to understand its influence. Just as in the previous model, the excavation of the stack benches (dimension 15 m height and 7.5 m width) was done in three sequential stages. Three cases were generated with respect to the conceptual extents of the damaged rock section. In the first scenario, shear strain behavior on the pit slope was investigated without including the damage section. The second scenario incorporates the 10 m brecciated rock section and the last case having a 20 m thickness of brecciation. The 10m brecciation thickness is considered the closer representation of the damaged zone for the site. The emplacement of the breccia is estimated to be dipping at roughly ≥ 50° and as Broom-Fendley, et al. (2021) established, the breccia grades down into an underlying carbonatite body at great depth. To cater for uncertainties, the angle was varied from 30° to 70° at an equal interval of 10°. Similar to initial analyses, the case studies were conducted at the current planned 250 m pit height and the expected GSH of 300 m. In order to conceptualize an ideal mine design, analyses were performed at the pilot slope angles between 40° and 45°. The material properties used in this simulation are presented in Table 4.3 .

Table 4.3 Mechanical properties of the rock units

Rock Type	*Uniaxial Compressive Strength (MPa)*	Density (g/cm^3)	*Young's Modulus (GPa)*	*Tensile Strength (MPa)*	*Friction Angle (°)*	*Cohesion (MPa)*	*Poisson Ratio*
Carbonatite	83.2	2.78	45.3	8.6	35	0.32	0.28
Fenite	118.6	2.70	44.4	10.4	36	0.30	0.29
Breccia	**37.5**	**2.35**	**17.6**	**3.37**	**30**	**0.10**	**0.22**
Syenite*	70.0	2.55	53.4	3.37	30	0.28	0.25

*Based on empirical values (Katz et al., 2000; Croll, et al., 2014)

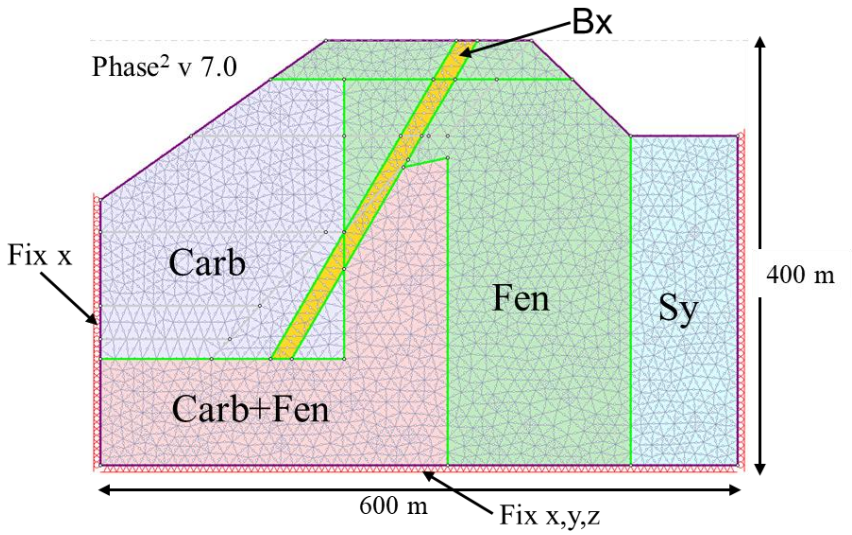

Figure 4.24 Conceptual model: Bx = Breccia, Sy = Syenite, Carb = Carbonatite, Fen = Fenite

4.6.3 Results

The qualitative analysis of the influence of brecciation is presented in Figure 4.25 and Figure 4.26, and a quantitative summary is presented in Figure 4.27. The research object of the qualitative analysis presented only covers the GSH of 300m at a slope angle of 45°. On the other hand, the quantitative analysis caters for all the simulated pit heights and slope angles. Since the results are based on a 2D numerical modelling in an out of the plane mode, the benchmark FoS tolerable is 1.3. From Figure 4.25 and Figure 4.26 we notice a significant change in the shear failure path prior to and after the inclusion of breccia in which case there is a rotational/circular and translational potential failure respectively. The circular failure path prior to the inclusion of brecciated rock manifests after the second excavation, and then the shearing strain concentrates at the slope toe. On the other hand, the translational failure path is well developed at a gentle angle of emplacement of the breccia especially at 40° and 30°. The performance of the slope at these angles is critically low since the overlying block is supplied with a slipping plane characterized by low cohesion and friction resistance along the in situ damage section. At a relatively steep emplacement angle of the brecciated rock, that is 50° and 60°, the failure path is characterized by compound shearing failure path featured by a combination of circular and translational shearing.

That is, the circular shearing failure path joins up the translational shearing failure path induced in the breccia. At a much steeper angle of 70°, the failure path is almost identical to the condition prior to inclusion of brecciated rock, implying a negligible influence which is reflected in the FoS being almost equal.

4.6.3.1 Orientation of Breccia

The emplacement of the breccia into the carbonatite complexes is of interest to understand how it would have a bearing on the stability of the pit wall. From the analysis results, regardless of the angle at which the breccia is orientated, its mere existence reduces the stability performance of the pit wall but as the dipping angle of the breccia gets gentler, the impact becomes enormous. At the dipping angles of 70°, 60° and, 50° the FoS slightly reduces at OSA of 40° and 41° with the 70° orientation having almost the same FoS value prior to the inclusion of the brecciated rock section (Figure 4.27). However, at steep slope angles viz. 43° and 45°, the stability performance of the pit-wall significantly reduces with the 50° orientation registering a sharper drop, and the FoS values fall further below the threshold at all simulated pit heights. If the breccia is emplaced at gentler angles i.e. 30° and 40°, the stability of the pit-wall falls below the benchmark value of mine stability at all slope angles (40° – 45°). Thus, to attain a good performance of the slope in this condition it would require safe guarding the slope toe against the breccia position by ensuring that there is an optimal buffer zone.

4.6.3.2 Thickness of the Brecciated Zone

The thickness of the brecciated rock appears to have an equivocal influence. On a steep slope angle (45°), at breccia dipping angle of 60°, 70° and 30°, the thickness has a fair influence because the index of slope stability reduces though not quite distinct. However, at dipping angles between 50° - 40°, the impact on the pit slope performance becomes significant. This can be ascribed to the increased weak surface area within the translational failure plane trajectory which adjoins the nascent circular shearing trajectory (see Figure 4.26). However, on gentle slope angle, viz. 40° and 41°, the impact of breccia is negligible all dipping angle of the breccia (refer to Figure 4.27).

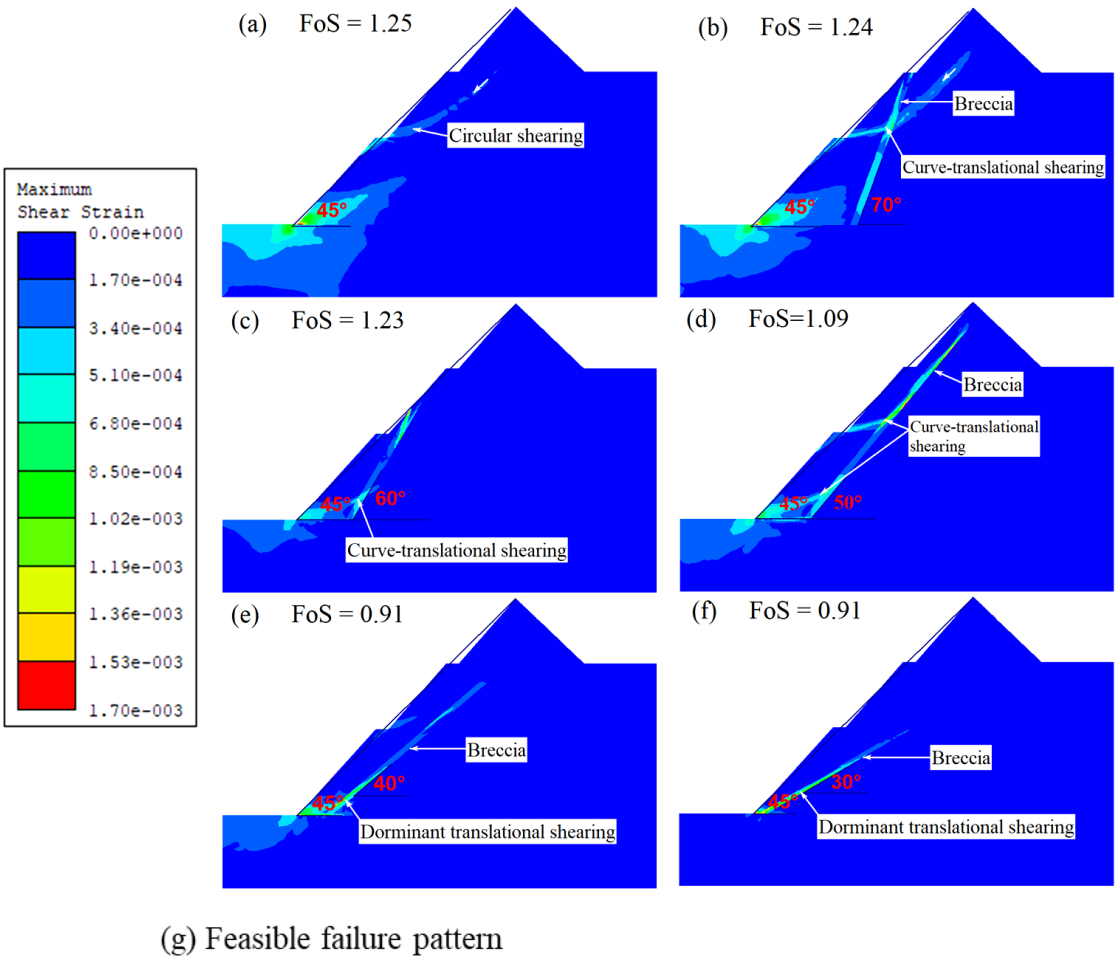

(g) Feasible failure pattern

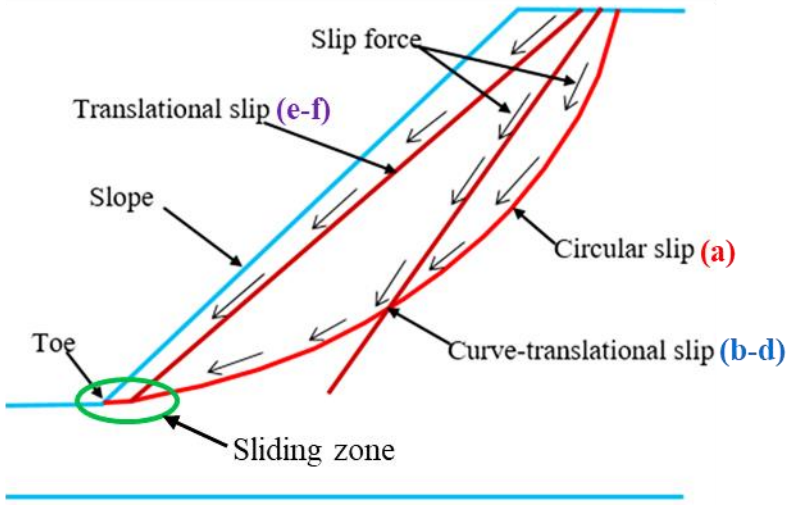

Figure 4.25 Pit wall stability conditions under 10 m brecciated stretch

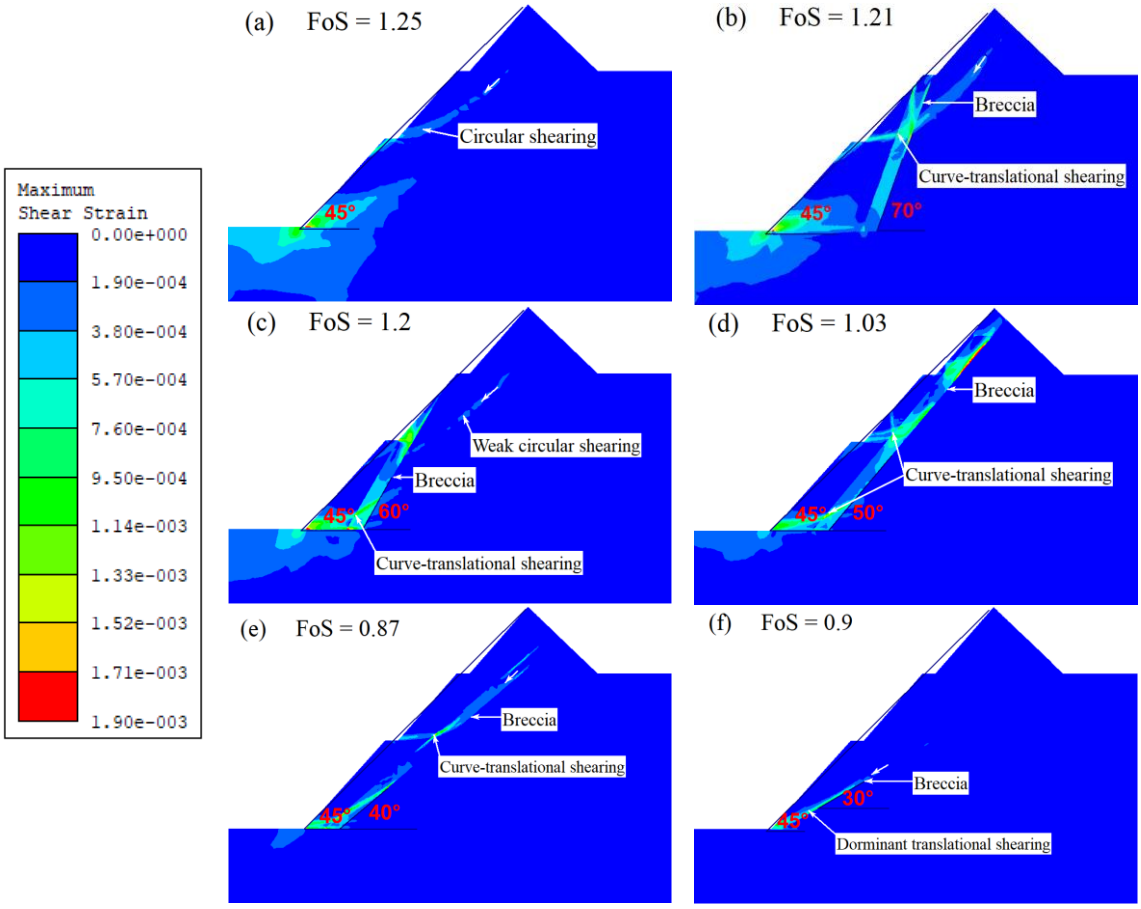

Figure 4.26 Pit wall stability conditions under 20 m brecciated stretch and feasible failure patterns

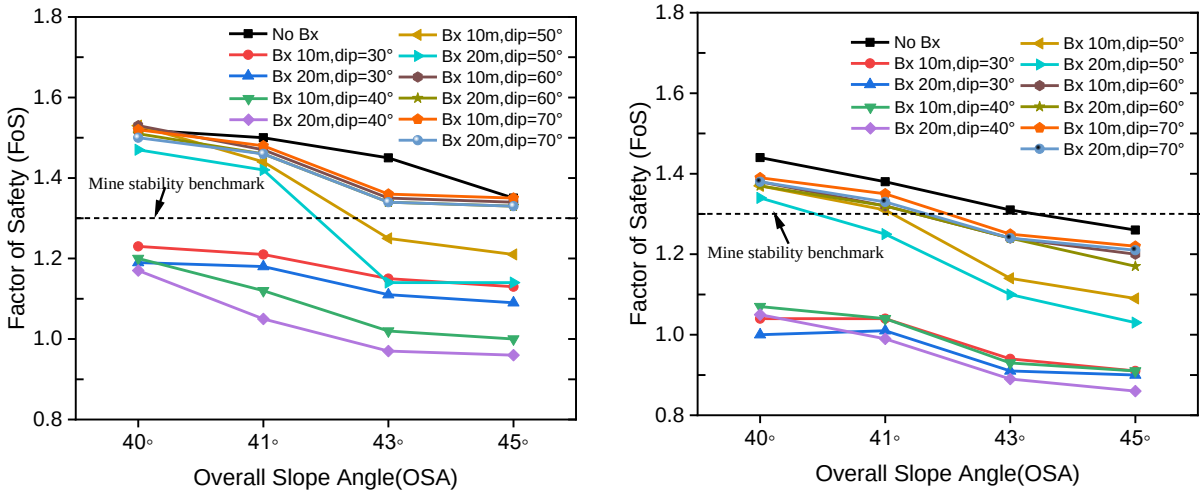

(a) Stability condition at 250m pit height (b) Stability condition at 300m pit height

Figure 4.27 Stability conditions with and without a brecciated zone

We can thus deduce that thickness of the brecciated rock has a considerable impact at moderately gentle angle of the emplaced breccia with steep angles, in this case study at 43° and 45°, otherwise it would not have a significant influence on the stability performance of the appropriately optimized slopes.

4.6.3.3 Displacement Pattern

The study also assessed the influence of brecciation on pit wall displacement. In this case, the 45° OSA at 300 m was used as the research object. The trend of total displacement is presented in Figure 4.28 and Figure 4.29. It can be seen from the figures that the orientation of the breccia has an apparent control on the movement of the geological materials on the slopes. Prior to the introduction of the breccia, the peak displacement is in the last excavation phase close to the toe of the slope where the shearing stress and strain is concentrated. When the breccia is introduced, the peak displacement at steep dipping angle of breccia locates in the upper section of the slope where the brecciated section is emplaced. This can be identified at 50°, and 70° but in the case of 60° the peak displacement is down to the slope toe due to minimal impact of the breccia at intersection with the slope face. At gentle dipping angle of the breccia where translational shearing strain is predominant, the peak displacement is at the slope toe with an evident trajectory provided on the brecciated zone. On another note, the change in the thickness of the breccia slightly changes the impact area but the section of the peak displacement remains the same. From the analysis, it can be deduced that the displacement trajectory of materials on the pit walls is influenced by the orientation of the brecciated section in the rock mass.

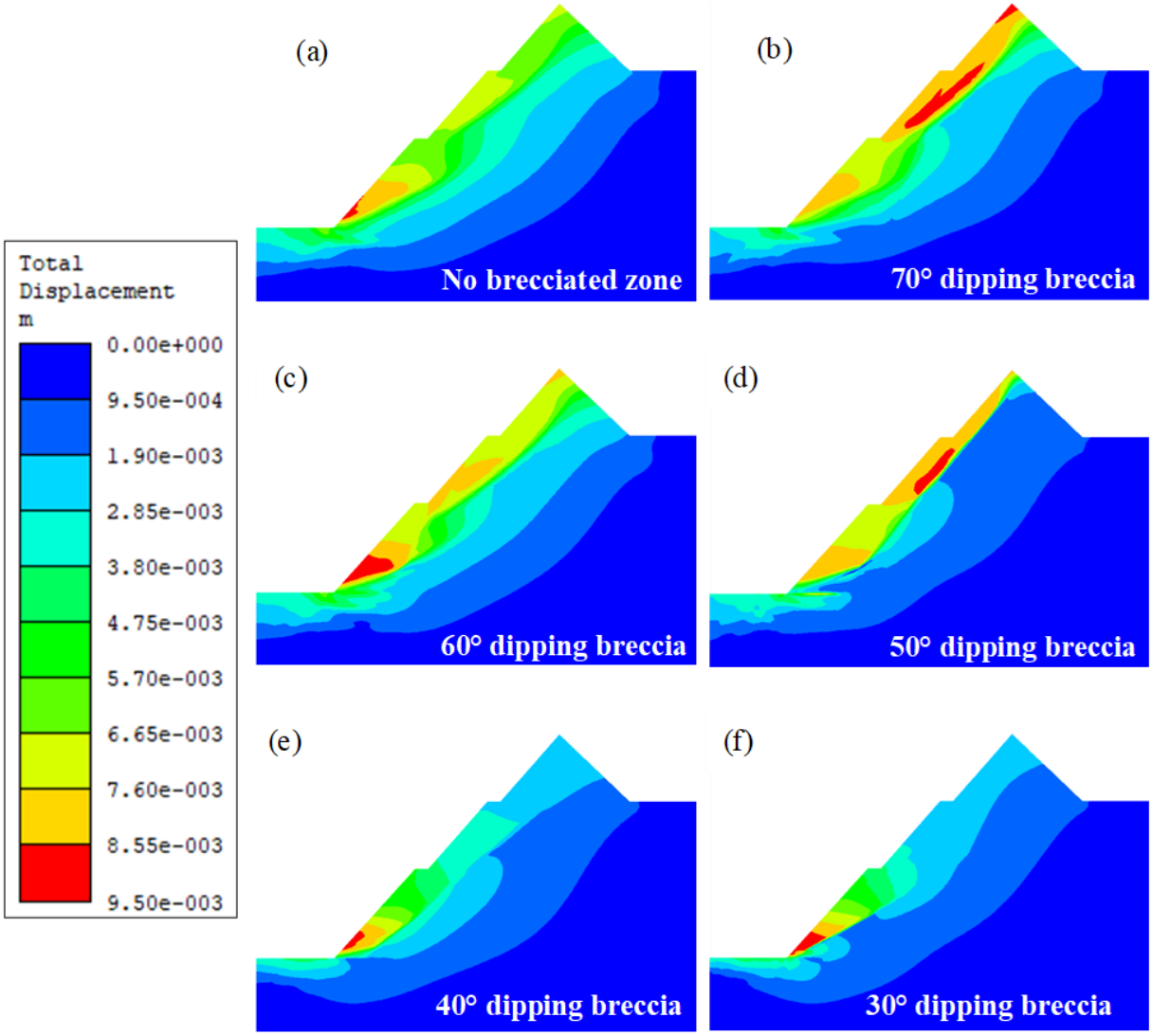

Figure 4.28 Pit wall displacement under 10m brecciated stretch

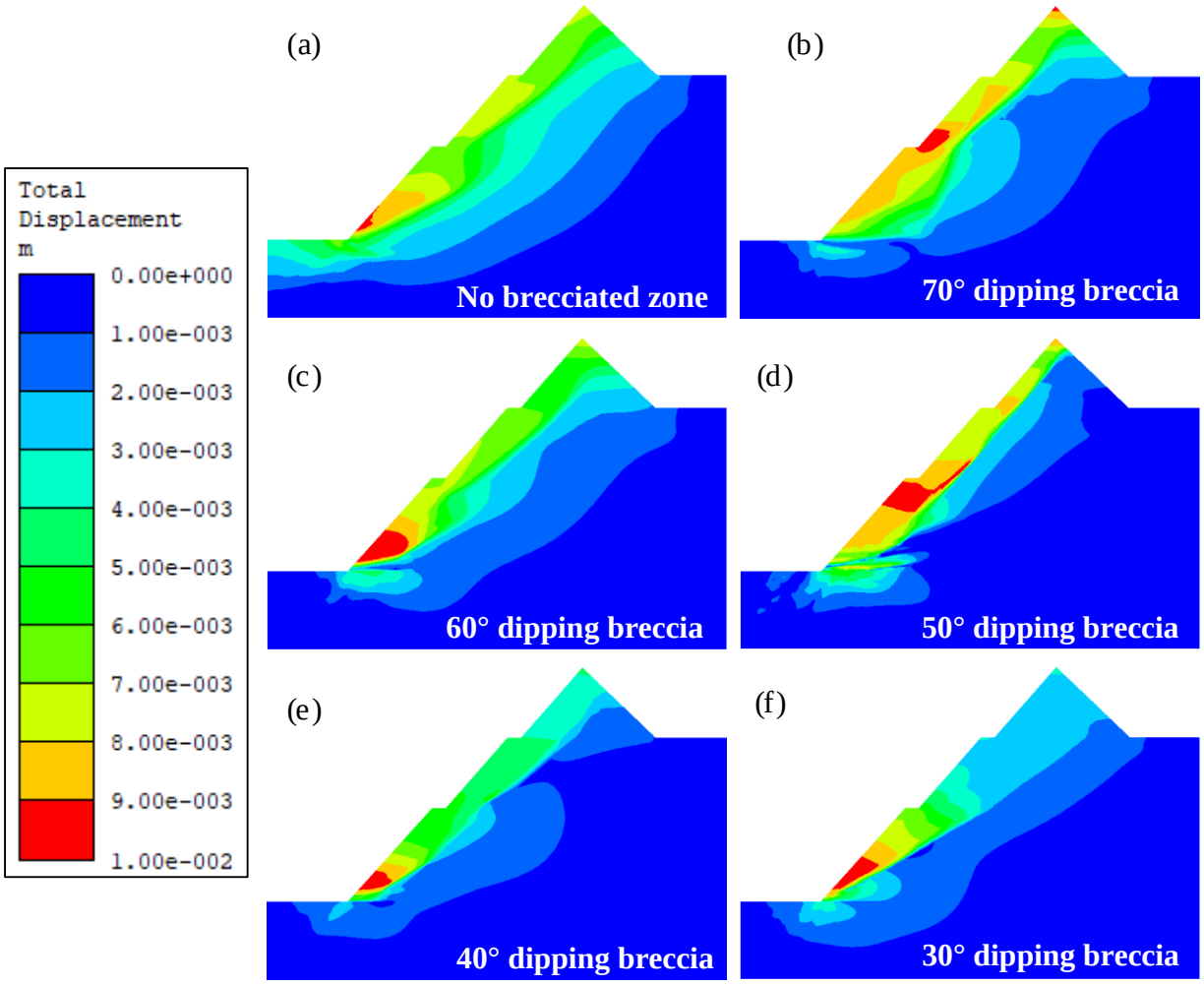

Figure 4.29 Pit wall displacement under 20m brecciated stretch

4.6.3.4 Impact of Breccia Position from the Slope Toe

As a parametric analysis, the study evaluated the impact of the position of the breccia and the pit wall with reference to the slope toe. In this regard, the position of the breccia was changed from the initial position by a factor of 10 from 10 m to 50 m. The initial positions of the breccia with respect to the angle of orientation were 10 m at the most gentle dipping angle, and 90 m at steeper dipping angle respectively. The qualitative results of the parametric analysis performed are given in Figure 4.30, Figure 4.31, Figure 4.32, Figure 4.33, and the summary is given in Figure 4.34.

Four scenarios were identified when the position of breccia was changed. The first scenario is when the dipping of the breccia is at the most gentle angle 30° as presented in Figure 4.30. As it would be anticipated, as the initial position of breccia is increased away from the pit wall, the stability performance of the slope increases. At an increase of 10 m, the FoS was observed to be 1.08 and at 50 m increase the FoS improved to 1.21 representing a 12% change in FoS. Basically, moving the gentle dipping brecciated section minimizes the effect of translational shearing strain within the breccia because the buffer zone between slope toe and breccia increases. This trend was similar to the 40° dipping angle of breccia. On the contrary, in the second case where the dipping angle of breccia is 50° the stability trend is dissimilar.

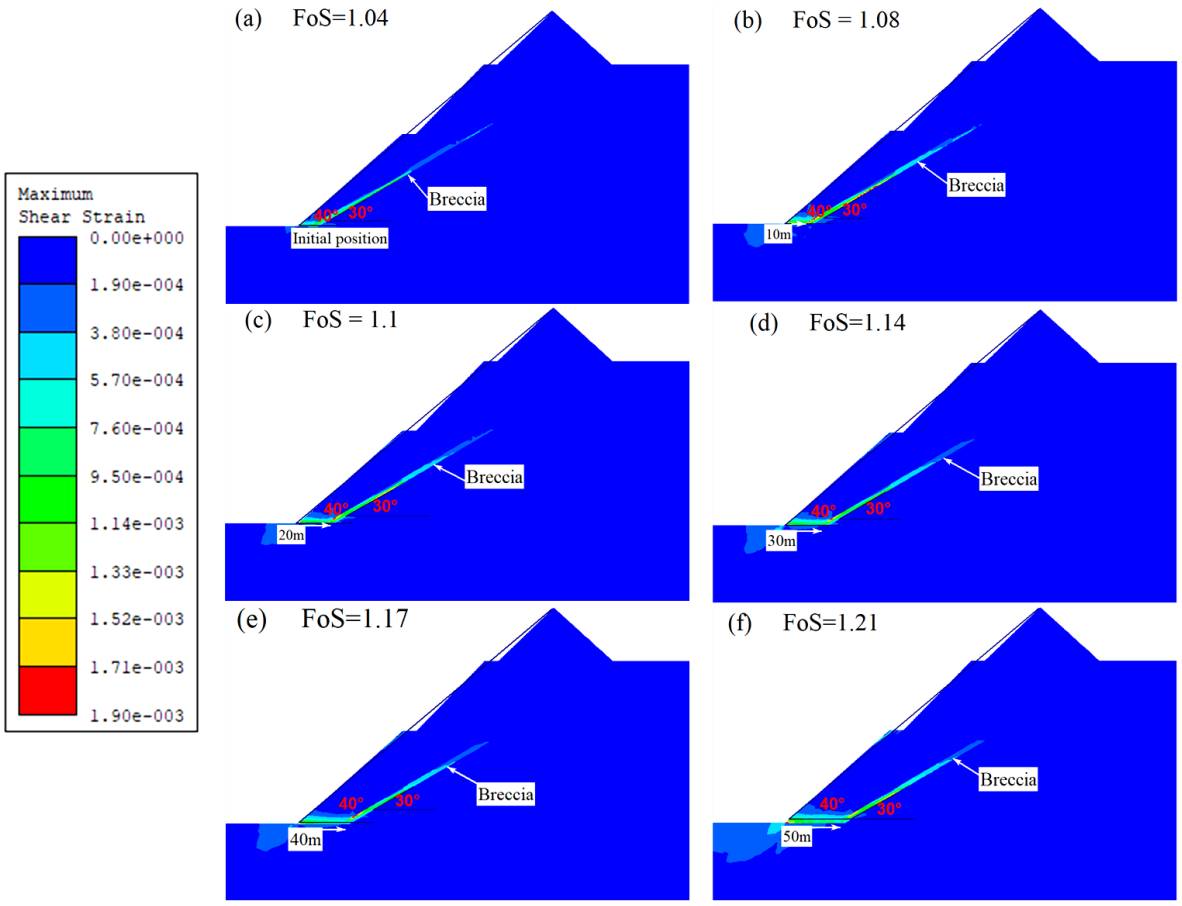

Figure 4.30 Pit wall stability with respect to the position of breccia at a dipping angle of 30°

As shown in Figure 4.31, when the position of breccia is moved 10 m away from the slope, the performance of the slope begins to decline and at 50 m increase the stability further declines. The FoS after a 10 m increase is 1.36 from the initial 1.39, and at 50 m the FoS reduced to 1.26. The reason for this trend is that the breccia wholly locates immediately behind the pit wall, thereby creating an extended plane of translational shear failure path which weakly combines with the circular shear failure path. This was observed only for gentle slope angles of 40° and 41°. However, at relatively steep slope angles i.e. 43° and 45°, the pit wall stability performance improved as the position of breccia increases away from the pit wall as presented in Figure 4.32.

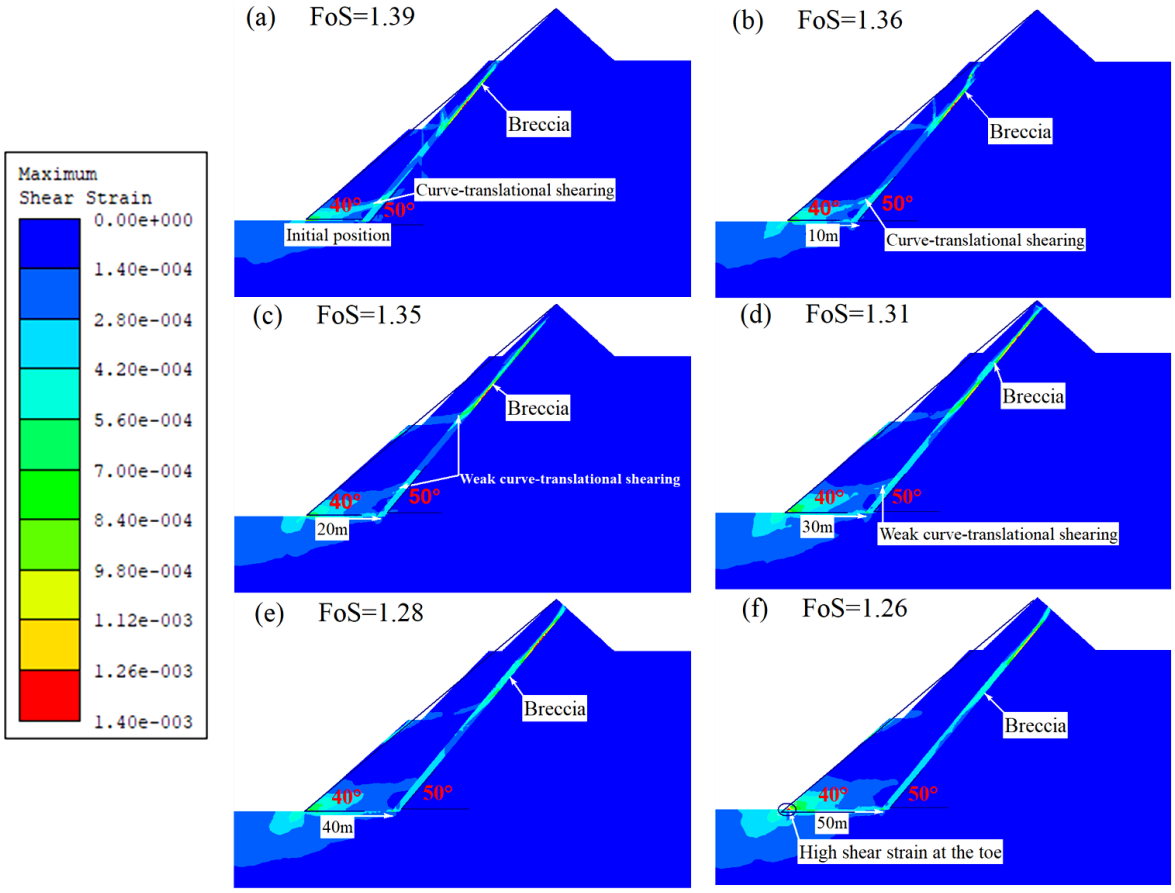

Figure 4.31 Pit wall stability with respect to the position of breccia at a dipping angle of 50° with gentle slope angle

In this third scenario, it can be observed that when the slope angle is steepened, the breccia locates closer to the pit wall. This provides the conditions for the curve-translational slip as the circular shearing failure path combines with the translational shearing failure path. When the breccia is moved further away from the initial position, especially at ≥ 30 m, the circular shearing failure path and the translational shearing failure path become disjointed. This situation reduces the combined circular and translational shearing impact in the pit wall, hence the disjoint implies a discrete influence of the shearing paths and the stability performance of the slope is enhanced.

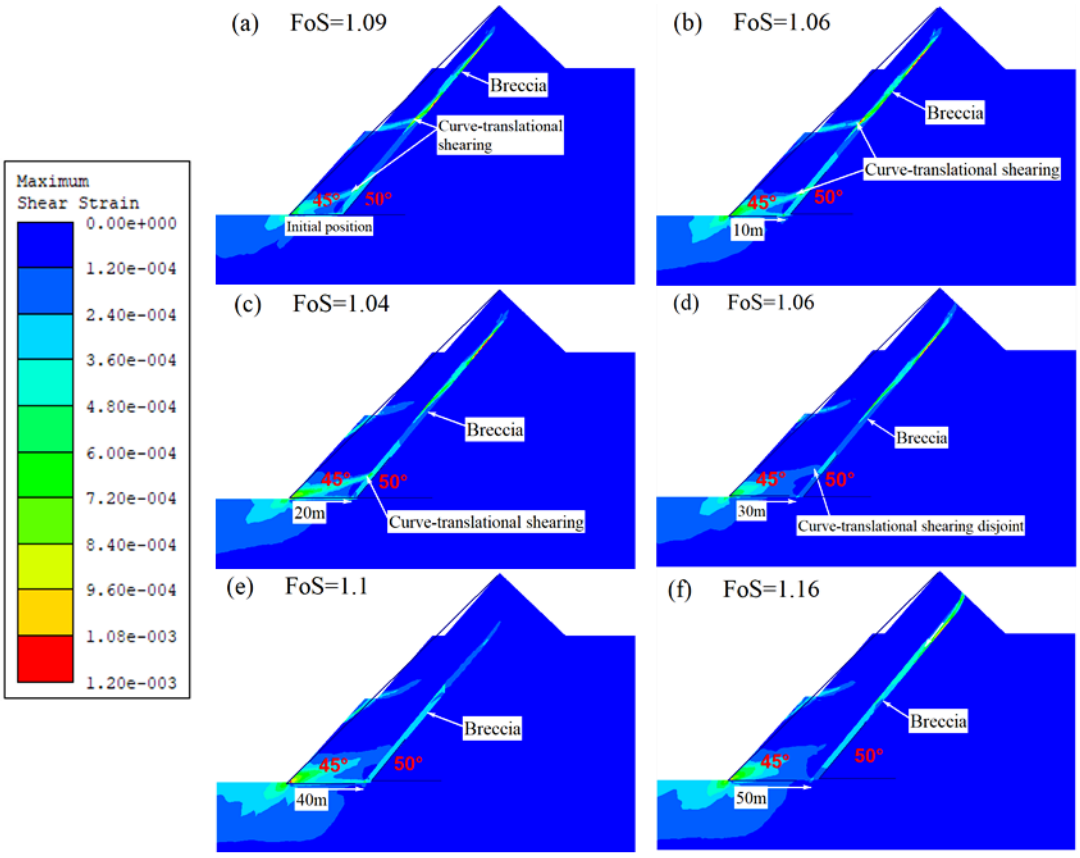

Figure 4.32 Pit wall stability with respect to the position of breccia at a dipping angle of 50° with steep slope angle

In the fourth scenario, which is shown in Figure 4.33, it can be noted that a steep dipping angle of the breccia at 70° barely has an effect on the stability of the pit wall when the position of the breccia is changed. A similar pattern was noticed at 60° dipping angle of breccia.

-In both cases, the safety factor remained almost the same. Thus, it can be concluded that in steeply dipping breccia, the translational shearing within the damaged rock section is minimal and also at the designed slope angle part of the breccia is truncated.

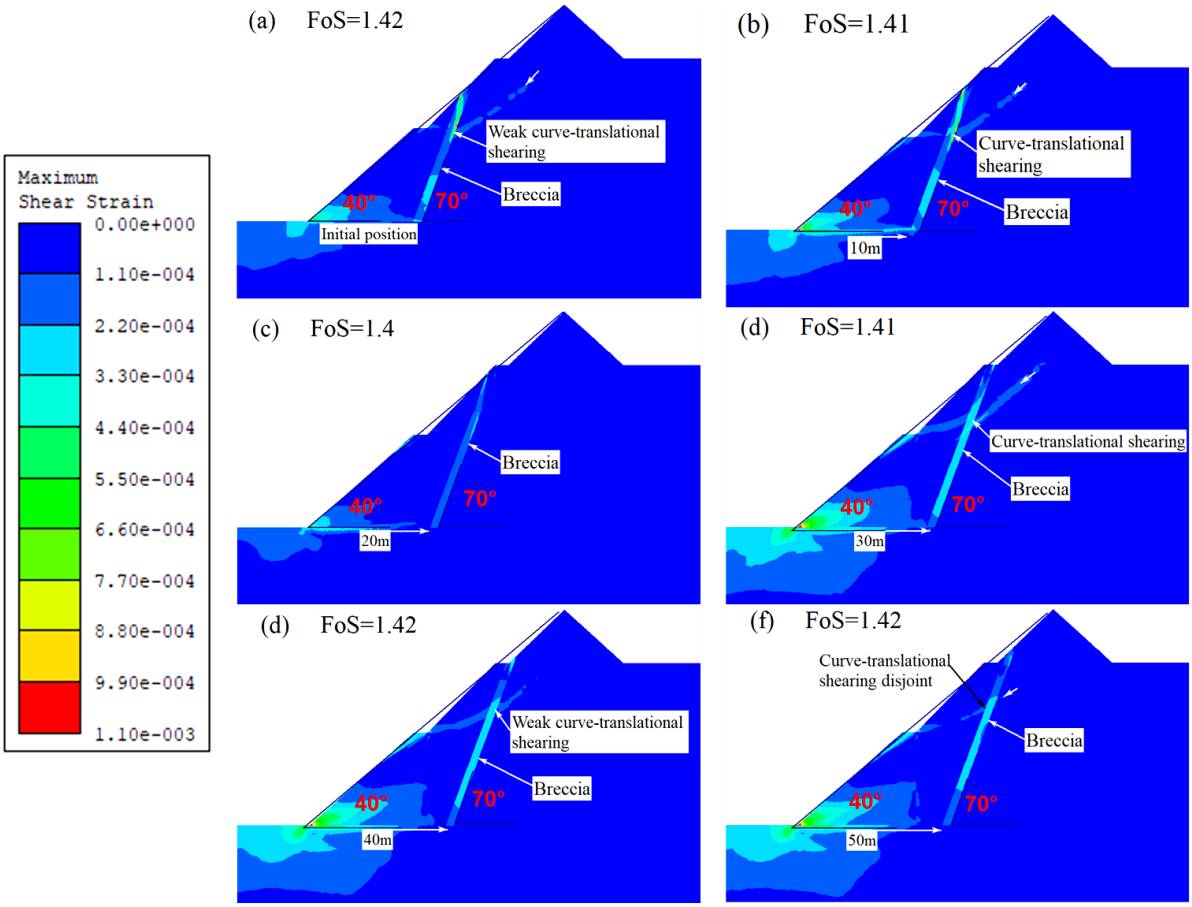

Figure 4.33 Pit wall stability with respect to the position of breccia at a dipping angle of 70°

In general, we note that the existence of the breccia poses a threat to the stability of the pit slope and an intervention has to be undertaken to counter its impact. From a series of analyses executed and presented in a summarized graph in Figure 4.34, an approach is suggested to deal with the breccia in slope design. The proposal is based on the relationship of FoS, excavation depth and the position of the in situ damaged rock. In this approach, we recommend that OPM design in brecciated rock masses, the ratio of 1:5 between the breccia distance from slope toe of the pit limit and pit depth should be adopted to counter the impact of breccia.

For instance, at the pit depth of 100, the distance of 20 m between the slope toe and breccia should be left, while at 250 m, the pit limit should be designed such that the slope toe is 50 m far from the breccia and at 300 m pit depth the slope toe should be at 60 m. If the breccia is within or close to the pit limit, a deliberate effort must be made to mine out or truncate the breccia because it has the capability to cause instability when there is a load above it.

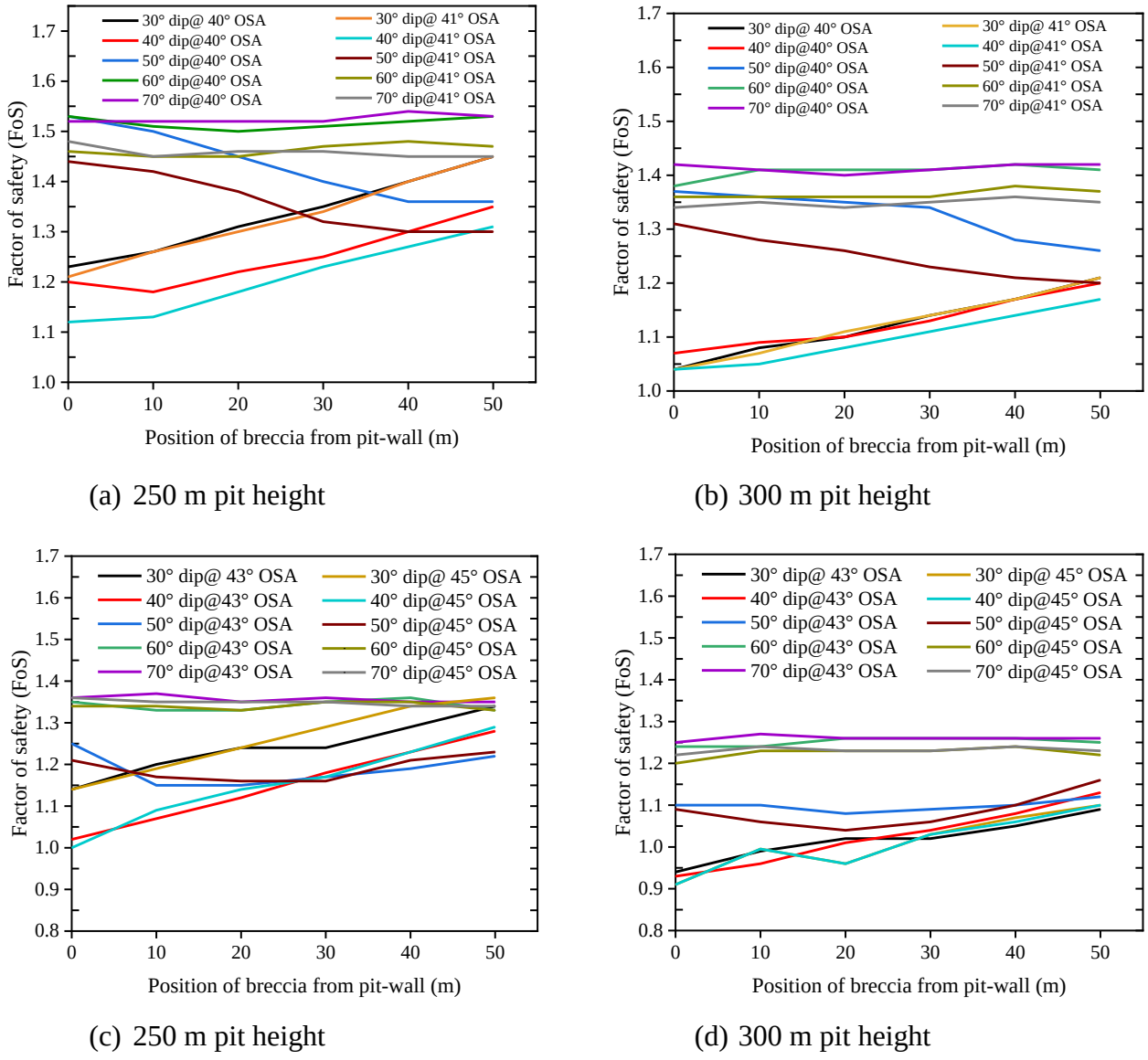

(a) 250 m pit height

(b) 300 m pit height

(c) 250 m pit height

(d) 300 m pit height

Figure 4.34 Stability conditions of pit wall with respect to the position of the in situ damaged rock

4.6.3.5 In situ Stress Regimes and Brecciation

As aforementioned, rock masses are inherently inhomogeneous and geological features such as breccias can change the stress field, which can have a bearing on the stability of excavation. To comprehend the impact of the interactions between the stress regimes and breccia, simulation was undertaken at different stress ratios. The analysis involved scenarios of high horizontal and vertical stress regimes. The research objects for analysis were selected at gentle slope angle of 40° and steep angle of 45° with the dip of breccia at 50° at a GSH of 300 m. The results of high horizontal stress ratio are presented in Figure 4.35 and Figure 4.36 whereas for high vertical stress regime the results are presented in Figure 4.37. It would be anticipated that high horizontal stress could lower the performance of the pit wall as the induced stress gets redistributed to the excavated section. However, the existence of the breccia close to the slope appears to increase the performance of the slope. As shown in Figure 4.35 and Figure 4.36, stress magnitudes tend to be dissipated greatly, and stress orientations rotate as much as dipping angle of breccia on crossing it.

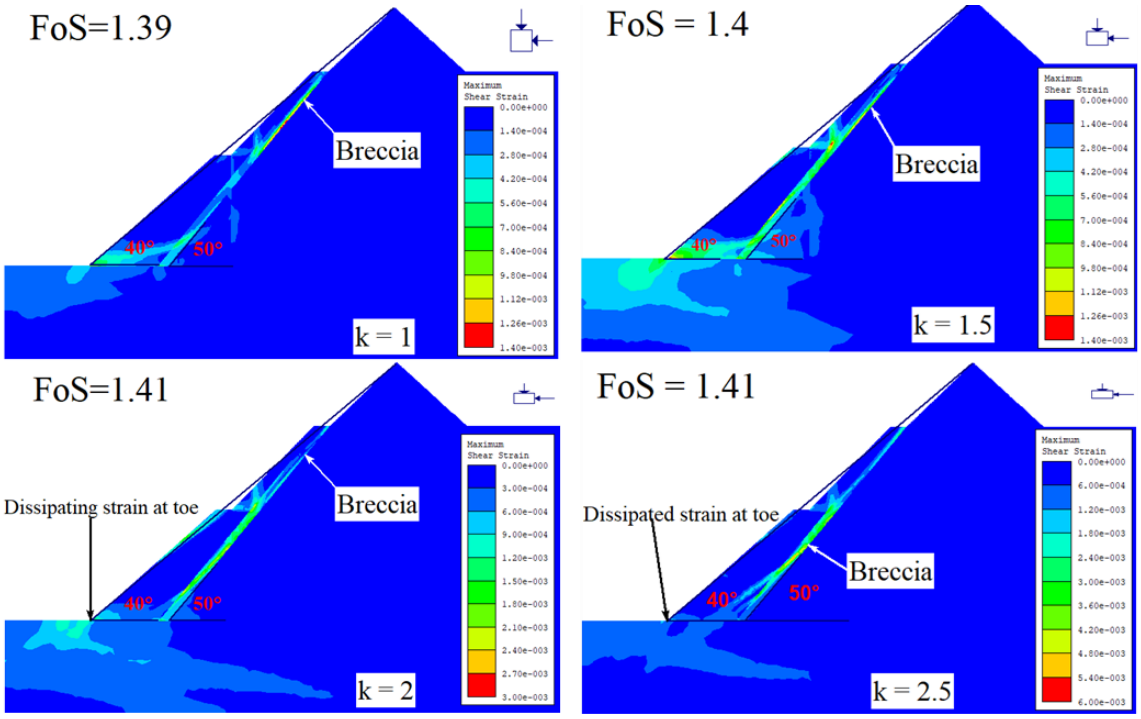

Figure 4.35 Shearing pattern under high horizontal stress conditions for 40° at 300 m pit height

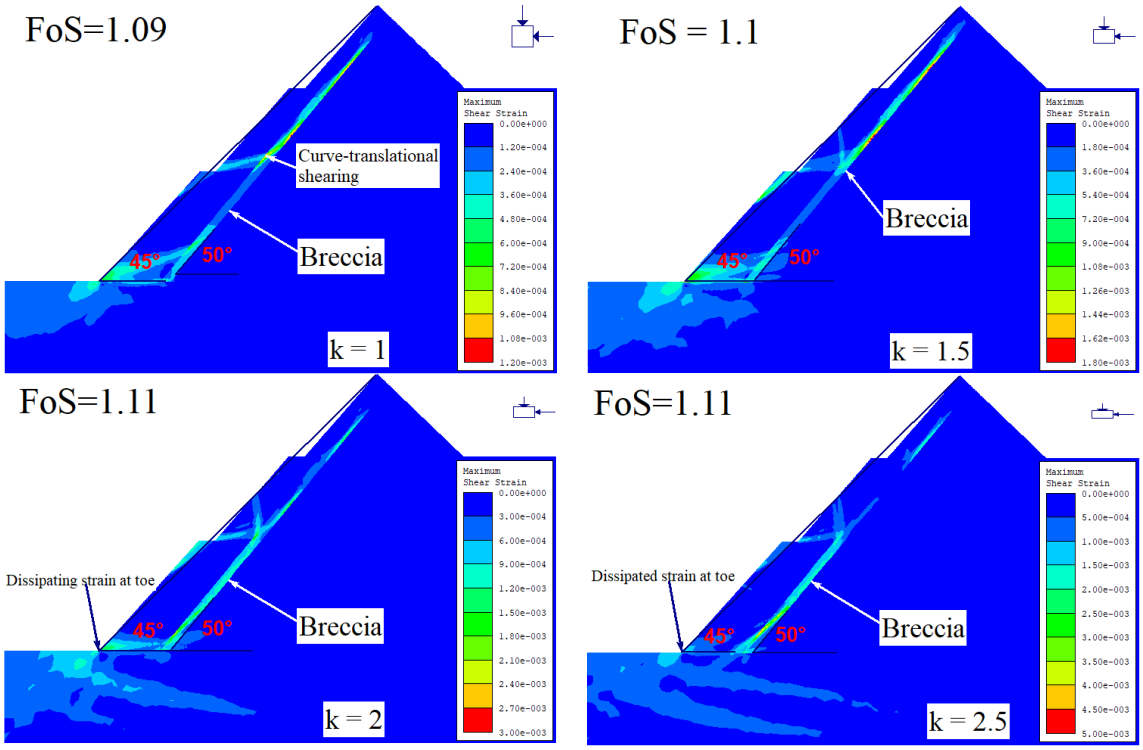

Figure 4.36 Shearing pattern under high horizontal stress conditions for 45° at 300 m pit height

The changing of the direction of stress is manifested in the shear strain failure path along the breccia. At stress ration of k=1, the shear strain is concentrated at the toe of the slope and there is a weak adjoining of circular and transformational shearing path. This combination evidently lowers the stability performance of the pit slope. However, when the vertical stress is reduced as horizontal stress increases, the horizontal stress gets redistributed and changes its orientation and align with the breccia dipping. Thus, the breccia acts as a buffer to the slope and the shear strain at the slope toe is dissipated making the slope performance enhanced.

On the contrary, high vertical stress regime reduces the slope stability performance as shown in Figure 4.37. The FoS at gentle slope angle reduced from 1.39 to 1.38 and at steep angle the FoS decreased from 1.09 to 1.03. However, it must be noted that the mechanisms leading to low stability performance of the pit slopes is different at gentle and steep angles. On gentle slopes, it can be observed that the mechanism involves adjoining of the circular and translational shear failure paths which causes potential curve-translational slippage.

On the other hand, at steep slope angle, the mechanism does not involve adjoining of circular and translational shearing failure path but rather distinct translational failure path and the intensification of shear strain at the toe of the pit slope. The concentration of the strain at the toe basically minimizes the bearing capacity of the toe to the overlying burden, hence reduced stability performance. Although, the Southern African average regional stress is determined to be at k = 1.5 as presented in the work of (Stacey & Wesseloo, 1998), the tectonically stresses vary depending on structural setting. Thus, the results of k = 0.5 are significant to anticipate this phenomenon in normal faulting predominated areas.

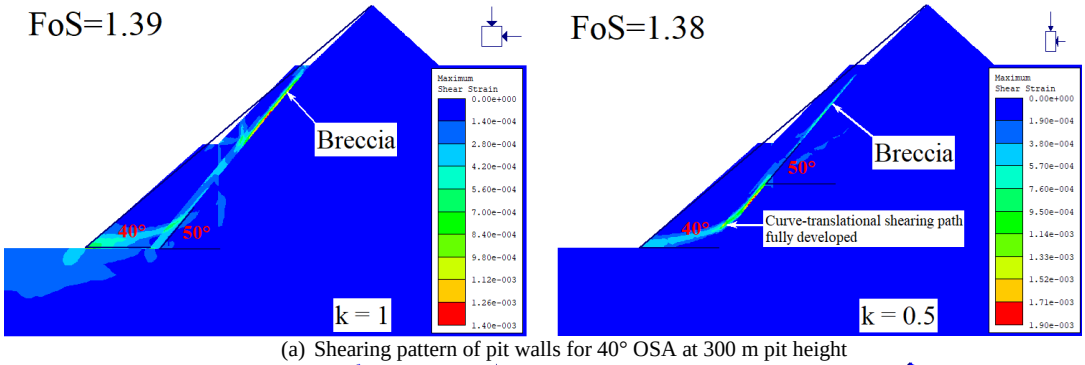

(a) Shearing pattern of pit walls for 40° OSA at 300 m pit height

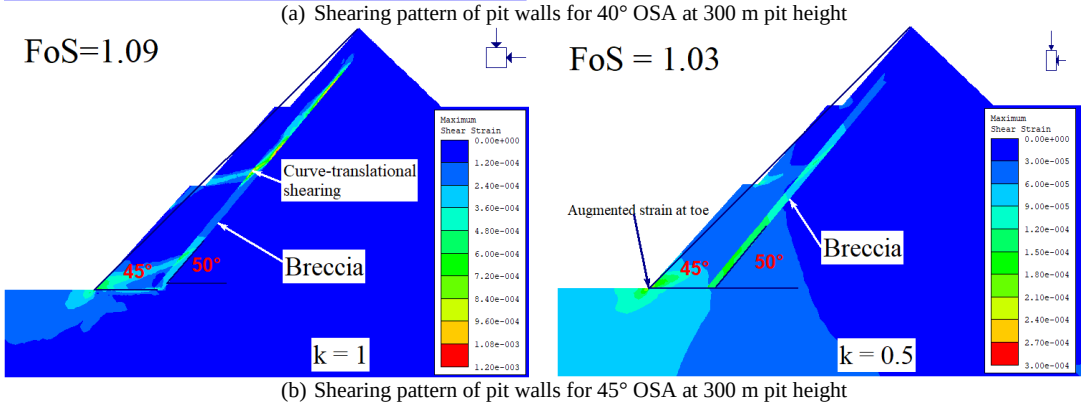

(b) Shearing pattern of pit walls for 45° OSA at 300 m pit height

Figure 4.37 Shearing pattern under high vertical stress conditions

4.6.4 Countermeasures

In general, we note that the existence of the breccia poses a threat to the stability of the pit slope and an intervention has to be undertaken to counter its impact. The stabilization of slopes in mining presents a distinct range of issues and challenges from those in civil engineering. Read & Stacey (2009) articulate that in mining, the economics and practicality of artificial support are

affected by the larger volumes of rock to be supported. Generally, the length and height of slopes in mining are often much greater, and the service life of artificial support is often short especially where a number of different cutbacks are to be undertaken. Experience from different projects has demonstrated that slopes approximately 100 m high were the maximum that could be artificially supported with 30 m long cable bolts. Beyond the 100 m height, failure occurs behind the supported volume, creating larger deeper-seated masses which are more difficult to control (Read & Stacey, 2009). On the contrary, artificial support like rock or cable bolts, earth and rock anchors applied to rock slopes is relatively common practice in civil engineering applications where excavations are of moderate dimensions and the costs of structures (roads, bridges, high-rise buildings) are high compared to the excavation and support costs.

From this background, in large open pits, global wall reinforcement to attain stable slopes with aggressive wall angles could be challenging if not unachievable. Thus, from a series of analyses executed and presented in a summarized graph in Figure 4.34, we observed the pattern of failure with respect to the slope toe and an approach is suggested to deal with the breccia in slope design. The proposal is based on the relationship of FoS, excavation depth and the position of the in situ damaged rock. In this proposition, we recommend that OPM design in brecciated rock masses, the ratio of at least 1:5 between the breccia distance from slope toe of the pit limit and pit depth should be adopted to counter the impact of breccia. For instance, at the pit depth of 100, the distance of 20 m between the slope toe and breccia should be left as a buffer, while at 250 m, the pit limit should be designed such that the slope toe is 50 m far from the breccia and at 300 m pit depth the slope toe should be at 60 m. If the breccia is within or close to the pit limit, a deliberate effort must be made to mine out or truncate the breccia because it has the capability to cause instability when there is a load above it. The ultimate intention is to increase the resisting forces along the translational shearing plane generated within the damaged rock section.

Furthermore, the traditional approach of making the slope gentler could be a more pragmatic remediation that could be applied in the event of the shallow angle emplaced breccia in the rock mass. Based on this case study, the stable performance of the pit slopes at the GSH of 300 m would be assured at 38° OSA for a breccia emplaced at gentler angle.

The intervention obviously implies an enormous increase in the stripping ratio for the mine, but it may prove a necessary step if undesirable risks were to be sidestepped.

4.7 Summary

In this chapter, the stability conditions and deformation behavior of the geological materials on the pit slopes were evaluated. This was achieved by numerical methods carried out with finite difference and finite element codes using $FLAC^{3D}$ V 5.0 and $Phase^2$ V 7.0 software respectively. The analyses were performed in elasto-plastic state with Mohr-Coulomb constitutive model and failure criterion. Due to the competency of the rock mass, analysis shows that overall slopes can be developed at steep angles 45-50° at shallow depth $\leq$ 250 m, but caution has to be taken at greater depth and when discontinuities are predominant. With regards to in situ stress, a qualitative evaluation of the stability state through shear strain analysis reveals that the pit wall stability conditions could be compromised under high-stress regimes such that non-uniformity of stress state leads to the development of a secondary potential failure surface (PFS) in addition to the primary circular PFS which has been the sole engineering concern in slope stability analyses. Furthermore, the displacement values, at the state of stress equilibrium (k=1), were found to be almost four times lower than at k=2.5 and two times lower when k=0.5. This demonstrates that non-uniform high-stresses could indeed adversely affect pit wall performance. To test the criticality of the risk to failure, the strain criterion to failure, which is a ratio of the maximum deformation and the height of excavation, was applied and the shear strain rate indicates that the rock mass slopes may not be significantly endangered, a phenomenon accredited to its competence. For instance, the maximum possible strain rate of 0.04%, which is below the lower bound strain at collapse of 0.1% was recorded in the study case. Complementarily, quantitative evaluation indicate that its influence is negligible as the FoS experiences minimal 1% reduction. This phenomenon explains why in situ stress is conventionally only considered in underground mines. In spite of the countering outcome of the quantitative evaluation, it would be prudent to undertake "in situ stress-stability analysis" particularly in deep mines and in tectonically active settings since failure is a function of accrued stresses effect other than a sudden singular occurrence of the phenomenon.

In terms of in situ rock damage, the existence of breccia in the competent rock mass has the capability to reduce the stability performance of the pit wall and the enormity of the impact increases at gentle dipping angle in close range to the slope toe. However, as the initial position of breccia increases away from the pit wall, the stability performance increases at gentle dipping angle namely 30° and 40°. On the contrary, at the dipping angle of 50° the performance of slope reduces, and at steeper angle >50° the impact gets negligible. Thus, for OPM design in brecciated rock masses, the ratio of 1:5 between the breccia distance from slope toe and pit depth should be implemented to counter its impact. If breccia is within or close to the pit limit, a deliberate effort must be made to mine out or truncate it. Additionally, the traditional approach of making the slope gentler could be a more pragmatic remediation that could be applied in the event of the shallow angle emplaced breccia in the rock mass

4.8 References

Adams, B. M. (2015). *Slope Stability Acceptance Criteria for Opencast Mine Design*. New Zealand: Golder Associates (NZ) Limited.

Alejano, L. R., & Alonso, E. (2005). Considerations of the Dilatancy Angle in Rocks and Rock Masses. *International Journal of Rock Mechanics & Mining Sciences*, 42, 481–507.

Brady, B. H., & Brown, E. T. (2005). *Rock Mechanics for Underground Mining*. USA: Springer Science and Buisness Media.

Brideau, M.-A., Yan, M., & Stead, D. (2009). The Role of Tectonic Damage and Brittle Rock Fracture in the Development of Large Rock Slope Failures. *Geomorphology* (103), 30–49. doi:10.1016/j.geomorph.2008.04.010

Broom-Fendley, S., Elliott, H. A., Beard, C. D., Wall, F., Armitage, P. E., Brady, A. E., Dawes, W. (2021). Enrichment of Heavy REE and Th in Carbonatite-derived Fenite Breccia. *Geological Magazine*, 1-17. doi:https://doi.org/10.1017/S0016756821000601

Brox, D., & Newcomen, W. (2003). Utilizing Strain Criteria to Predict Highwall Stability Performance. *Technology roadmap for rock mechanics*, 1-5.

Chen, Y., & Lin, H. (2019). Consistency Analysis Of Hoek–Brown and Equivalent Mohr–Coulomb Parameters in Calculating Slope Safety Factor. *Bulletin of Engineering Geology and the Environment*, 78, 4349–4361. doi:https://doi.org/10.1007/s10064-018-1418-z

Coetsee, S., Armstrong, R., & Terbrugge, P. (2020). The Use of Strain Threshold in Slope Stability Trigger Action Response Plans. *Australian Centre for Geomechanics*, 339-352.

Croll, R., Swinden, S., Hall, M., Brown, C., Beer, G., Scheerpers, J., & Trusler, G. E. (2014). NI 43-101 *Pre-feasibility Report*. Johannesburg, South Africa: MSA Group (Pty) Ltd.

Guo, M., Ge, X., & Wang, S. (2011). Slope Stability Analysis under Seismic Load by Vector Sum Analysis Method. *Journal of Rock Mechanics and Geotechnical Engineering*, 3(3), 282–288.

Hack, R., Alkema, D., Gerard, K. A., Leenders, N., & Luzi, L. (2007). Influence of Earthquakes on the Stability of Slopes. *Engineering Geology*, 91, 4–15.

Hart, R. (2003). Enhancing Rock Stress Understanding through Numerical Analysis. *International Journal of Rock Mechanics & Mining Sciences* (40), 1089–1097. Doi: 10.1016/S1365-1609(03)00116-3

Hudson, J. A., & Harrison, J. P. (2005). *Engineering Rock Mechanics: An Introduction to the Principles*. Oxford OX5 IGB, UK: Pergamon.

Hustrulid, W., Kuchta, M., & Martin, R. (2013). *Open Pit Mine Planning and Design; Fundamentals*. New York: Taylor & Francis Group.

Itasca. (2012). *Fast Lagrangian Analysis of Continua in 3Dimensions User's Guide*. Minneapolis, Minnesota: Itasca Consulting Group Inc.

Jing, L. (2003). A review of Techniques, Advances and Outstanding Issues in Numerical Modelling for Rock Mechanics and Rock Engineering. *International Journal of Rock Mechanics & Mining Sciences* (40), 283–353. Doi: 10.1016/S1365-1609(03)00013-3

Jing, L., & Hudson, J. A. (2002). Numerical Methods in Rock Mechanics. *International Journal of Rock Mechanics & Mining Sciences*, 39(4), 409–427. Doi:https://doi.org/10.1016/S1365-1609 (02)00065-5

Li, A. J., Lyamin, A. V., & Merifield, R. S. (2009). Seismic rock slope stability charts based on limit analysis methods. *Computers and Geotechnics*, 36, 135–148.

Lin, H.-D., Wang, W.-C., & Li, A.-J. (2019). Investigation of Dilatancy Angle Effects on Slope Stability Using the 3D Finite Element Method Strength Reduction Technique. *Computers and Geotechnics*, 118, 1-13.

Logani, L. K. (1973). *Dilatancy model for the failure of rocks*. Michigan: Lowa State University.

McKinnon, S. D. (2001). Analysis of Stress Measurements Using a Numerical Model Methodology. *International Journal of Rock Mechanics & Mining Sciences*, 38, 699–709. Doi: 10.1016/S1365-1609(01)00037-5

Moses, D., Shimada, H., Sasaoka, T., Hamanaka, A., Dintwe, T. K., & Wahyudi, S. (2020). Rock Slope Stability Analysis by Using Integrated Approach. *World Journal of Engineering and Technology*, 8, 405-428. doi:10.4236/wjet.2020.83031

Newcomen, W., & Dick, G. (2016). An update to the Strain-Based Approach to Pit Wall Failure Prediction. *The Southern African Institute of Mining and Metallurgy*, 116, 379-385.

Read, J., & Stacey, P. (2009). *Guidelines for open pit slope design. Australia*: SCIRO Publishing.

Saadoun, A., Hafsaoui, A., & Fredj, M. (2018). Landslide Study of Lands in Quarrys: Case Chouf Amar - M'sila, Algeria. D. N. Singh, & A. Galaa içinde, *Contemporary Issues in Geoenvironmental Engineering, Sustainable Civil Infrastructures* (s. 15-28). Netherlands: Springer International Publishing. doi:10.1007/978-3-319-61612-4_3

Severin, J. M. (2017*). Impact of Faults and Fault Damage in Large Open Pit Slopes*. University of British Columbia: Doctor Thesis, 1-168.

Shen, J., Priest, S. D., & Karakus, M. (2012). Determination of Mohr–Coulomb Shear Strength Parameters from Generalized Hoek–Brown Criterion for Slope Stability Analysis. *Rock Mech Rock Eng*, 123–129. doi:https://doi.org/10.1007/s00603-011-0184-z

Shukla, M. K., & Sharma, A. (2018). A brief review on breccia: it's contrasting origin and diagnostic signatures. *Solid Earth Sciences*, 3, 50-59. doi:10.1016/j.sesci.2018.03.001

Sjoberg, J. (1996). *Large Scale Slope Stability in Open Pit Mining*. Sweden: Division of Rock Mechanics; Lulea University of Technology.

Sjorberg, J. (1999). *Analysis of Large Scale Rock Slopes (Ph.D. Thesis)*. Lulea: Lulea University of Technology.

Sonmez, H., & Ulusay, R. (1999). Modifications to the Geological Strength Index (GSI) and their Applicability to Stability of Slopes. *International Journal of Rock Mechanics and Mining Sciences*, 743-760.

Sonmez, H., Gokceoglu, C., & Ulusay, R. (2003). An Application of Fuzzy Sets to the Geological Strength Index (GSI) System Used in Rock Engineering. *Engineering Applications of Artificial Intelligence*, 16, 251–269.

Soren , K., Budi, G., & Sen, P. (2014). Stability Analysis of Open Pit Slope by Finite Difference. *International Journal of Research in Engineering and Technology*, 326-334.

Stacey, T. R., & Wesseloo, J. (1998). In situ stresses in mining areas in South Africa. *The South African Institute of Mining and Metallurgy*, 365-368.

Stacey, T. R., Xianbin, Y., Armstrong, R., & Keyter, G. J. (2003). New Slope Stability Considerations for Deep Open it Mines. *The South African Institute of Mining and Metallurgy*, 373-390.

Stead, D., & Wolter, A. (2015). A critical review of rock slope failure mechanisms: The importance of structural geology. Journal of Structural Geology, 74, 1-23. doi:10.1016/j.jsg.2015.02.002

Sullivan, T. D. (2013). Pit Slope Design and Risk – A View of the Current State of the Art. *The South African Institute of Mining and Metallurgy*, 51-80.

Wessels, S. D. (2009). *Monitoring and Management of a Large Open Pit Failures*. Johannesburg: University of Witwatersrand (Thesis).

Witley, J. C., Swinden, S., Trusler, G., & Dempers, N. (2019). *Songwe Hill Rare Earth Elements (REE) Project, Phalombe District, Malawi*. South Africa: MSA Group.

Zavodni, Z. M. (2001). Time-Dependent Movements of Open-Pit Slopes. In W. A. Hastrulid, M. K. McCarter, & D. J. Van Zayl, *Stability in Open Pit Mining* (s. 81-88). Littleton: Society for Mining, Metallurgy, and Exploration.

Zhao, L.-H., Cheng, X., Zhang, Y., Li, L., & Li, D.-j. (2016). Stability Analysis of Seismic Slopes with Cracks. *Computers and Geotechnics*, 77, 77-90.

Zoback, M. D., & Zoback, M. L. (2003). Stress in the Earth's Lithosphere. D. M. Zoback, & M. L. Zoback içinde, *Encyclopedia of Physical Science and Technology* (s. 143-154). USA: Stanford University.

Zoback, M. L., & Zoback, M. D. (1989). Tectonic Stress Field of the Continental United States. In L. C. Pakiser, & W. D. Mooney, *Geophysical framework of the continental United States* (s. 523-539). Colorado: Geological Society of America.

5 PROJECT ECONOMIC EVALUATION

5.1 Introduction

Mining has proven to be a crucial aspect in the expanding economies of various countries. However, the venture is complex and attracts criticism due to operational impacts, high risks, and uncertainties. Mining operating companies always strive to make a trade-off between exploitation and economic benefits of the project. Hence, the country where the resource is being developed experiences both positive and negative impacts. Hosoi (2009) notes that positive or negative implications of mining are distinguished according to individual judgment and different minerals, otherwise there is no entirety in the two aspects. Prior to determining whether the mining operation will be successful or not with respect to the national and local community, it is necessary to understand the dimensions of the mine development for successful development. In this section, the aspects of mining: production capacity, mineral commodity price in the world market, and revenue inflow generated from the sales proceeds are evaluated and related to prevailing Malawi mining taxes and the potential impacts on the country's development path.

5.2 Mine Development and Benefits

The benefits of mining to the nation are evaluated mainly in terms of direct and indirect benefits. Although indirect benefits are difficult to quantify, it is very important to consider and discuss them with regard to mine sector development. Usually, the indirect benefits are measured based on the multiplier effect on economic output and capital expenditure related to mine development. For instance, employment in the mining industry may cause a multiplier effect as the employees tend to employ members of the communities to cultivate their farms. The direct contributions of mining to the micro and macro economy include the following:

a) Increased public revenue from taxes, duties, and royalties

Income of the mining company through mineral product sales and personal incomes of the mining company's employees generate growth in public tax revenue.

Furthermore, companies and persons in related businesses tend to receive increased incomes from their service contracts to the mining companies, thereby increasing taxes and loyalty receipts of the government. The lined up potential mining projects in Malawi may in essence boost the national revenues.

b) Foreign exchange earnings

The international trading currency of the mineral products is by standards in United States Dollar (USD). The mineral products from developed mines that are exported overseas markets attract foreign currency to the mineral resource developing country. Currently, Malawi's foreign currency earner is Tobacco, but there are sanctions being imposed on Tobacco production as part of the global efforts to promote healthy living. Thus, mining could be a big advantage to the economy.

c) Economic diversification

Malawi has for decades depended on agriculture as the backbone of her economy. After witnessing dwindling proceeds from the agricultural industry and other small supporting sectors, the Malawi government has embarked on a strategy geared to promote mining as a strong sector for diversification to drive the fragile country's economy. Additionally, since mine development and mining activity would require consumer goods, machines, tools, fuels, constructions, transportation, and other businesses related to mining would also oversee a growth in other sectors.

d) Infrastructure development

Improvement and development of new infrastructure may also result from mine development. Mining activities lead to the construction of roads, ports, harbors, power lines, electric generating plants, supply of water, and related needs required at the community and regional level.

e) Employment

Operations at the mine require persons with various skills. Workers ranging from managers, engineers, geologists to laborers are employed at the mine to make the mining activities run. Employment in related to industries and business companies, such as factories that make tools and machines, repairing workshops, transportation companies, retail sale business, trade business would as well increase thereby raising total employment opportunities.

Factories making tools and machines and repairing workshops increase public funds. On the other hand, transportation companies, retail sales businesses and trade businesses are bound to attract foreign exchange earnings. However, the magnitude of benefits derived from mining on the macroeconomy varies from nation to nation as well as the level of the country's economy in terms of developed and developing economies.

f) Improved health, education and welfare

In the best-case situation, like Mkango Resources' efforts, corporate social responsibility (CSR) of the mining company can lead to communities surrounding the mine benefit from the increased revenues for public infrastructure and facilities, opportunities for small business, new jobs for skilled and unskilled laborers, and increased need for professionals such as doctors and teachers. Regional prosperity also becomes possible as rural areas are developed through local social facilities such as hospitals, schools, and churches are built for workers, their families, and the communities. On a national scale, the total increase of national revenue from the mine development can improve the health, education, and welfare of the people.

g) Contributions of the mining industry to growth domestic product (GDP)

Large scale mining operations contributions to the country have been examined in different countries and it has been found that the GDP contribution ranges from 10.3 percent to 67 percent (Hosoi, 2009). In the case of Malawi, merely one large mine significantly transformed the economic landscape of the country between 2009 and 2014 with a contribution of 10% towards the country's GDP from a negligible 1% prior to mining operations and post-mining mine closure. It is self-evident that such a contribution to the economy brings stability and sustainability, hence minimizing the government's tendency to borrrow or depend on donor aid.

5.3 Mine Development and Negative Impacts

Although the mining industry forms an important pillar of economies across the globe, it is associated with a number of harmful impacts both to the community and the environment. The impacts vary depending on the mineral product being extracted. In spite of that, there are issues that cut across all kinds of mining ventures as listed;

a) Threat to human health

The community and people working in a mine are exposed to various potential diseases that come from the pollutants released into the air and water during the mining process. For instance, during smelting operations, some pollutants such as the suspended particulate matter (arsenic particles and cadmium) could be emitted. Miners also face occupational health hazards as mining activities progress. Some may suffer from respiratory diseases like silicosis or black lung disease due to excessive inhalation of dust. Thus, it should be the priority of mining companies to keep any risks to the utmost lowest, and if possible extirpate them.

b) Pressure on infrastructure, housing and services

Mining tends to attract people from around the communities and beyond as they seek opportunities. As a result of the drive-in, mining communities experience critical shortages on essential human needs. The mining workforce and residents often outnumber the available housing in a mining town as such the high demand of houses and limited supply of it may trigger increased housing and rental prices (Sincovich et al., 2018).

c) The Dutch disease

Mining is a lucrative venture once proven that the deposit can be exploited at a profit. Mine development has the capability to swing the economic landscape of the country. The apparent development of the mining sector may lead to the decline in other sectors like agriculture. The putative mechanism of the phenomenon is the increased revenues realised from the booming sector which makes the national currency to appreciate against currencies from other nations. The development may result into other country's exports becoming exorbitant for other countries to purchase. Hosoi (2009) highlights that the most anticipated Dutch disease effect is that of open unemployment resulting from sharp rises in general wages due to the introduction of high wages in the booming mineral resource projects, which was reportedly experienced when the first large mine at Kayerekera in Karonga, Malawi was commissioned. To avoid such situation, government policies that regulate the wage scale need to be adhered to, however it is hard and probably unfair to mine workers given the nature of hardship of the mining works.

d) Environmental impacts

It is impossible to undertake mining operations without causing significant perturbations to the environment. Nature is at the mercy of the mining companies on how they intend to minimize the negative effects to the environment. The drastic modification of the original site and the release of chemical substances can have a tremendous impact on biodiversity in the surrounding. Destruction of the habitat is a key aspect of biodiversity losses. Furthermore, direct poisoning caused by mine-extracted materials and indirect poisoning through food and water can also affect animals, humans, vegetation and microorganisims. However, it is important to note that the adverse mining impacts on biodiversity rely to a larger extent on the nature of the contamination, the level of concentration at which the substance can be found in the environment and the nature of the ecosystem. The Songwe carbonatite complex has revealed the occurence of sulfides, namely pyrites, as disseminations in some of the drilled core samples but the extent of the concentration of the pyrites is not quantitatively known. In this regard, caution shall have to be exercise to avoid potential acid mine drainage (AMD) during operations, which occurs when sulfides interact and react with oxygen.

e) Water pollution

Mining activities can have harmful effects on the surrounding surface and groundwater. In a case where necessary precautions are not adhered to, unnaturally high concentrations of chemicals such as arsenic and sulfuric acid interact with surface or subsurface water. With a lot of water used for various purposes like mine drainage, mine cooling, and other mining processes, it increases the possibility for the aforementioned chemicals to contaminate water. Contamination of watersheds as a result of leakage of chemicals also has adverse impacts on the health of the local population. For instance, at the Kayerekera Uranium mine a ‘zero-discharge operation’ was undertaken by the mining company. However, results by an independent radiation laboratory CRIIRAD, which collected samples and performed radiation measurements in the surroundings of the mine indicated an elevated uranium concentrations in the water of the Champhanji creek which flows from the open pit mine to the nearby Sere River (Chareyron, 2015). Hence, it is the responsibility of both the operating companies and government, through clear policy tools, to be accountable and protect the communities when mineral resources are being extracted.

5.4 Mining Economics

The evaluation of the profitability of a mine project is crucial to know the worthiness of investing in the mining venture and progression to operationalization. There are numerous profitability criteria applied in the mining industry, financial institutions and government agencies when evaluating individual projects. Kennedy (2009), divided the profitability criteria into two general categories: 1) Non-discounted cash flow; payback period and average internal rate of return (IRR) and 2) Discounted cash flow; Hoskold formula, Net Present Value (NPV), IRR, Profitability Index (PI), payback period.

Meanwhile, the discounted cash flows are the only profitability criteria used for evaluation purposes since the time value of money is the paramount principle (Hustrulid et al., 2013; Kennedy, 2009). The choice of the criterion to be used to evaluate the mining property usually relies on the suitability for the investment objective. Nevertheless, the application of NPV and IRR techniques have proven to be satisfactory because they are capable of simulating the impact of the uncertainty on the profitability measurement; either present value (PV) or rate of return. To consolidate the outcome of the project viability, three indicators are applied in the study namely NPV, IRR, and PI.

5.4.1 Net Present Value

The NPV provides an indicator of profitability for the project by giving the difference between the present value of cash inflows and present value cash outflows over a given period of time. When NPV is positive, it implies that the project earnings generated exceed the anticipated cost making the project viable for investment and development. On the other hand, a negative NPV indicates a net loss making it impossible for investments. This profitability criterion, which has been widely used since the 1960s (Kennedy, 2009), is computed as presented in Equation 5.1.

$$NPV = \sum_{n=0}^{N} -CF_0 + \frac{CF_1}{(1+DR)} + \frac{CF_2}{(1+DR)^2} + \cdots + \frac{CF_N}{(1+DR)^N} \quad (5.1)$$

Where CF_0 is the initial investment, CF is the cash flow, DR is dicounted rate and *N* is the number of years

5.4.2 Internal Rate of Return

The IRR is a metric applied in financial evaluation to approximate the profitability of potential project investment. IRR makes the NPV of all the cash flows equal to zero in a discounted cash flow analysis. Thus, its computation depends on the same formula as NPV as presented in the Equation 5.2.

$$IRR = \sum_{n=0}^{N} -CF_0 + \frac{CF_1}{(1+IRR)} + \frac{CF_2}{(1+IRR)^2} + \cdots + \frac{CF_N}{(1+IRR)^N} = 0 \qquad (5.2)$$

Or

$$0 = NPV = \sum_{n=0}^{N} \frac{CF_N}{(1+IRR)^N}$$

5.4.3 Profitability Index

The PI is the present value of future cash flow divided by the initial investment. This criterion is used in capital rationing scenarios and is mostly referred to as the "cost-benefit ratio". Just as IRR, PI applies the NPV In its computations as shown in Equation 5.3.

$$PI = \frac{\sum_{t=1}^{N} \frac{CF_N}{(1+DR)^N}}{OI} \qquad (5.3)$$

Where *OI* is the original investment

5.5 Mining Project Evaluation

5.5.1 In Put Parameters

Every open-pit mining undertaking is unique and cost estimation as an input parameter for economic evaluation may be a complex task. Meanwhile, a standardized method that suits every mine would be difficult to develop since costs can vary widely between similar operations depending on the physical characteristics of the deposit, site, and operational parameters. Nevertheless, all kinds of operations have something in common. Ore reserves are the fundamental aspect to determine the mine size and optimum production capacity. Once the production rate is found, approximated costs can be determined. Similar to other industries, an increase in production rate leads to a decrease in cost based on economies of scale. For this economic analysis, the ore reserve is estimated at 8,482,603 tonnes and the production capacity is pegged at 500,000 tonnes per annum (tpa). The price of REE is given as an averaged value of the elements at US$555.3 per kg as of 2019 (Gambogi, 2020).

The capital costs are presumed to be expent at the commencement of the project and the mining and milling capacities are held constant during the entire life of mine (LoM). The fixed costs, mining costs and processing costs are assumed to be constant over the years of operations. Table 5.1 presents the summarized capital cost, Table 5.2 gives the summarized operating costs, and Table 5.3 provides the mining and preprocessing input parameters for the project. The capital expenses (CAPEX), which refers to the investments incurred by the mining company in their fixed assets to produce REE, and the operational expenses (OPEX), which refers to the operational expenditures both direct and indirect incurred in the processing and marketing of ore to produce REE, are paramount measurements commonly applied in the forecasting and management of the cash flow (CF). Furthermore, the measurements provide more information regarding the accounting and budgeting of the project. For the mining and processing input parameters, the LoM is projected to extend to 18 years and all operations are spread across this life span.

Table 5.1 Project capital cost

Summary of initial capital expenditure	
Description	Amount (US$)
Site Facilities, Infrastructure and Power Supply	36,155,786
Mining	1,657,000
Plant Construction	135,018,786
Tailings Storage Facility	12,650,000
Equipment, Mobilization and Other	23,400,000
Sustaining Capital	23,000,000
Contingency @ 10%	20,900,000
Total Initial Capital Expenditure including Contingency	**253,000,000**

Table 5.2 Summarized-operating costs

Summary of Operating Expenditure (OPEX)	
Component	Amount (US$)
Mining Operating Costs	209,722,527
Processing Plant Operating Cost	886,138,721
Summary of closure costs	7,208,000
Total	**1,103,069,248**

Table 5.3 Production input parameters

Summary of production inputs		
Item	Unit	Value
Life of mine (LoM)	Years	18
Total life-of-mine ore production	000’t	8,483
Average yearly plant feed	000’t	500

5.6 Results and Discussion

The results provided in this analysis must be regarded as estimates based on input data from a pre-feasibility technical report for Mkango Resources Company.

Therefore, their precision are partially guaranteed since the updated final report is yet to be released. Furthermore, as the operation develops certain technical parameters will change that may affect the initial estimates made in this work. The results of the cash flow for the 18 year period are presented in Figure 5.1 . At the project development phase where construction of the plants and mobilization will be undertaken, the cash flow is at the lowest since production will not have commenced. In this phase, the cash flow is negative reflecting capital investment. After the commencement of production in the subsequent years, the cash flow begins to increase after which it drops with respect to the LoM. Connected to cash flow, the results of NPV, IRR, and PI are presented in Table 5.4. Based on the analysis, the NPV value at a discounted rate (DR) of 10% is U$$658.54 million.

The applied DR is based on the premize that the company is financially stable and self-sustaining for investment. Given that the final NPV is positive, it implies that the project earnings generated could exceed the anticipated cost making the project developable. For IRR, the project is extrapolated at 33% for the projected 18 years of operations. As per guidelines, the IRR of a project is expected to be greater than the minimum required IRR of 1 percent. Generally, the higher the IRR the more promising the project is. At the computed rate of IRR, the Songwe project can be described as attractive for development. As pointed out by Juhász (2011) on the complementarity, NPV is indicative of the the wealth growth that would be accumulated by the investment during the project operation, but it does not give information regarding the real profitability of the investment. However, IRR provides information on the real yield of the long investment for decision-making. Thus, based on the complementing results, the project can be rated as viable. Further to the aforementioned indicators, PI was computed to evaluate the return on investment. The results of the valuation are presented in Table 5.4. The calculations greater than 1.0 imply that the future anticipated discounted cash inflows of the project are greater than the discounted cash outflows. Thus, a project with a PI index of 1.0 is considered to break even, if < 1, the costs outweigh the benefits and if it is > 1, the venture is potentially profitable. For this project, the PI index at 10% DR is 2.6, which implies that the mining venture would return US$2.6 for every US$1 invested making it a potentially profitable project.

Table 5.4 Project performance indicators

Results		
Item	**Unit**	**VALUE**
NPV	(US$M)	658.5
IRR	%	33
PI		2.6

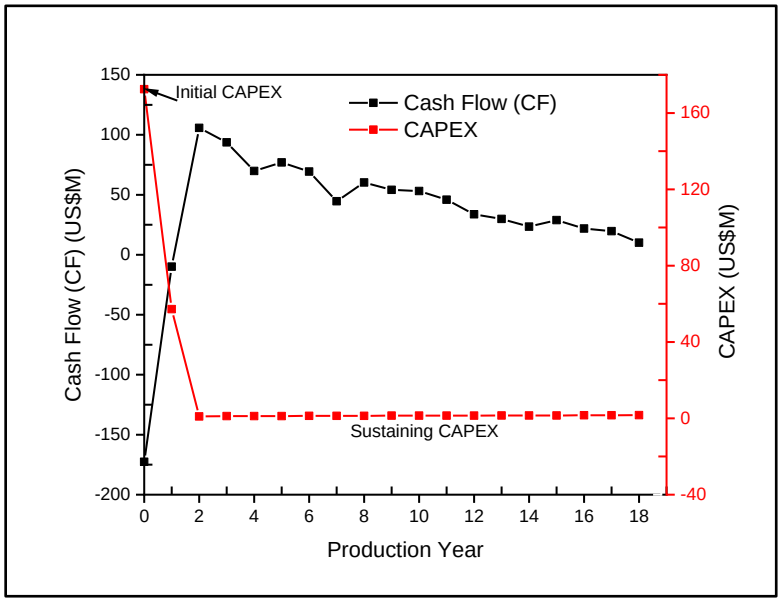

Figure 5.1 Project cash flow over the mining period

5.6.1 Sensitivity Analysis

Mining projects are generally long-term investments. In the course of the operation period, numerous technical and economic uncertainties can occur. The uncertainties, which affect the technical and economic aspects, can cause unexpected unmanageable values that would require new decision path. Among the key components are the production rate, design, discounted rate, ore market price, and dilution.

For instance, in 2014 Paladin Africa announced the temporary closure of the Kayelekera Mine in Karonga, Malawi due to extremely unmanageable low price of Uranium. Cases similar to Kayerekera Mine are many around the globe. Thus, this section provides the economic implications related to different parametric scenarios.

5.6.1.1 Discounted Rate Sensitivity Analysis

Discounted rate, which helps in determining the future success of the project, entails comprehending the future value of the cash flow and ensuring that the development is managed within budget. The DR is primarily utilized between companies and investors concerning project profitability. Since the value of DR varies with the nature of the entity; private or public, a number of scenarios were evaluated to understand the economic implications. The results of the sensitivity of DR are presented in Figure 5.2. It can be observed that DR is inversely proportional to NPV, IRR, and PI. As the value of DR increases, the values of NPV and IRR decrease. Thus, investment with entities that are not financially self-sustaining may attract higher DR than financially stable and self-sustaining entities.

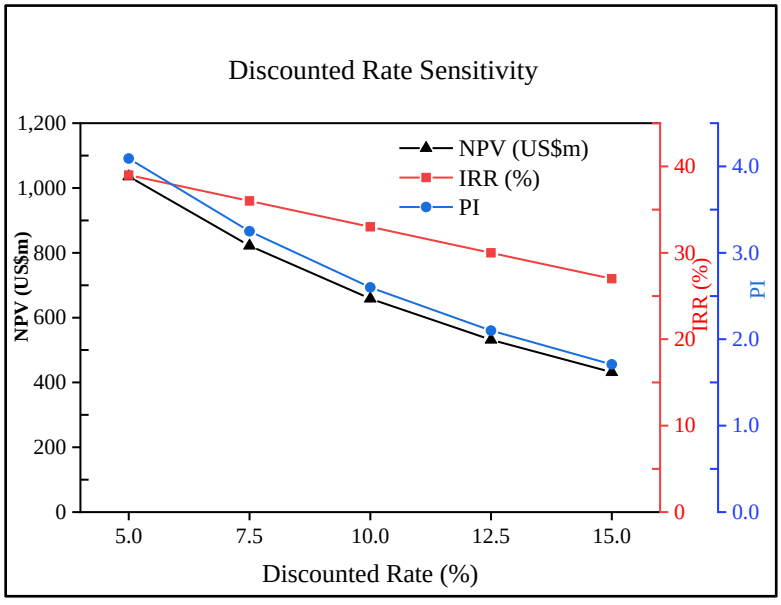

Figure 5.2 Influence of DR on project success

5.6.1.2 Price Sensitivity Analysis

Mineral price volatility is inarguably at the core of decision making in mine development. Although it is possible to recognize certain rules concerning future mineral supply and demand and extrapolate them into the future, it must be admitted that forecasting is a complex undertaking. The key aspects that determine long-term and short-term prediction of mineral price include; (i) the lifetime of reserves, (ii) development of the relative importance of production centers, (iii) forecasting of the depletion of a resource base, (iv) intensity-of-use factors, (v) growth rates of commodity consumption, and (vi) lead-time to production (Wellmer & Berner, 1997). The first three aspects are related to supply, whereas the intensity of use factors and the growth rates refer to the demand, and the lead-time to production is a technical constraint for the availability of mineral supply.

For REE, when China, who controlled more than 95% of global REE production in 2010 imposed a reduction in export quotas by 40%, the dysprosium price was a hundred times higher in 2011 than the plateau price phase in 2002/2003 (Renner & Wellmer, 2020). Currently, technological advances and the geological scarcity of REE are highlighted to be key components in REE's expected rising price trend. However, Henckens et al. (2016) found that there is no certainty that the price mechanism of the free market system will lead to timely, automatic, and sufficient conservation of geologically scarce non-renewable mineral resources for the future. Therefore, to understand the implications of mineral price volatility on project development, the price of REE was varied to assess the economic performance of the Songwe project. The applied REE price was changed by -30% and 30% at a 5% interval. The results of the analysis are presented in Figure 5.3.

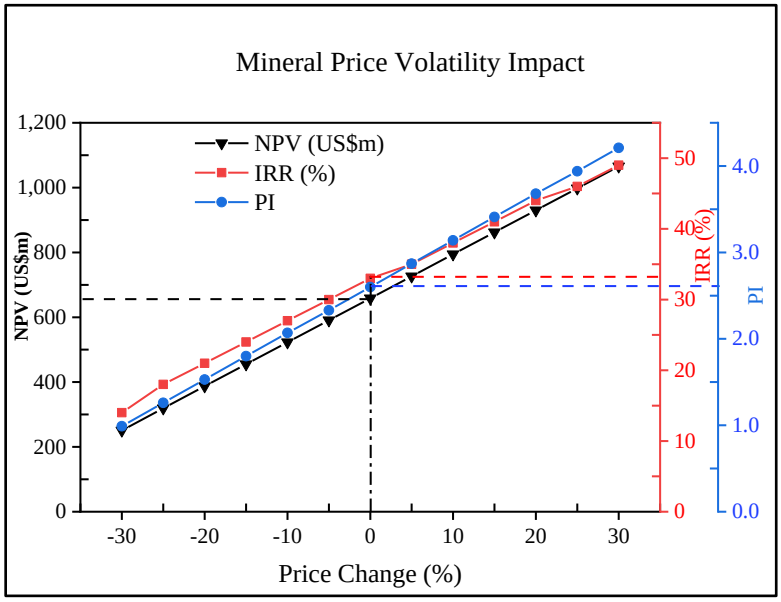

Figure 5.3 Influence of mineral price volatility on project performance

It can be observed that the extrapolated values indicate that the project could be developable with a reduction in the current price by less than 30%. At a 25% price reduction, the NPV, IRR, and PI indicate a relatively promising performance at US$319.32 million, 18%, and 1.26 respectively. However, if the price reduction increased to 30%, the project would just be barely below break-even. Price reduction further than 30%, the project would be undevelopable with benefits outweighed. On the other hand, any increase in price would put the project in the pore position of profitability. The outcome shows that an increase in REE mineral price by up to 30% would oversee the project profitability increase to 4.21. Thus, the venture would return US$4.21 for every US$1.00 invested in the project.

5.6.1.3 Processing Capacity Sensitivity Analysis

In mining operations, the process design, equipment selection and scheduling constitute the main steps in designing a good mineral processing plant. The ultimate aim is to meet production rates, operate at a competitive cost and conform to the environmental and safety regulations. Thus, the plant processing capacity is a key variable factored in before designing the mining operation.

However, mineral reserves cannot be exploited at presumed constant rhythms as expected. To be able to appreciate how economic variables would change, a sensitivity analysis was performed in order to calculate the different economic outcomes when the processing capacity varies. In this case, the annual production rate was increased and decreased from the planned annual production capacity of 500,000 tonnes by up to 15% with 5% as a minimum percentage change. The results of the analysis are presented in Figure 5.4. The change in production capacity due to supply and demand trade-offs or unforeseen circumstances indicates a direct proportionality in all parameters. Reduction in plant production capacity could lead to a reduced profitability of the project as the operations would have a protracted life span. On the contrary, an increase in production capacity could shorten the LoM, thereby giving the company the edge to maximize the project profitability. Nevertheless, in both cases, the project could be viable in terms of profitability. At negative 15% production capacity from the planned 500,000 tonnes, the NPV is 553.69US$m, IRR 28% and PI of 2.19 while at 15% production capacity, the NPV increases to 710.46US$m, IRR 36%, and PI at 2.81.

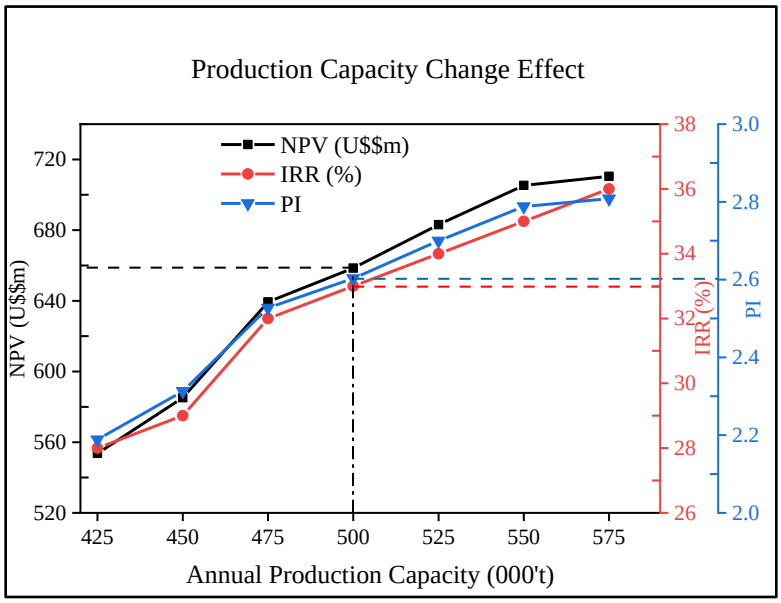

Figure 5.4 Influence of change in production capacity on project performance

5.6.1.4 Excavation Angle Sensitivity Analysis

The Mineral Reserve Estimate (MRE), which took into account all modifying factors, valuated the Songwe deposit to be 8.5 million tonnes (Mt). Accordingly, the Mineral Resources that are not Mineral Reserves have no demonstrable economic viability. This implies that such resources were assumed to carry no grade. Since the orebody is massive in nature, it was considered that mining dilution is ≤ 5 % and the overall stripping ratio at ultimate pit limit is 3.15. Dilution occurs when a portion of waste material is incorporated into the ore during its extraction, thus reducing the grades of ore previously estimated. The dilution can be due to geologic contacts or low grade pockets of ore that cannot be separated and are inevitably mined with the mining block. On the other hand, stripping ratio refers to the amount of waste removed to access a given ore quantity. Generally, as open-pit mines deepen, they often become burdened with excessive waste stripping requirements in order to access and extract the target ore, which is a direct function of slope angle. To understand the economic implications, a range of slope angles was tested for mining project sensitivity. The approach involved introducing modifying factors namely dilution and strip ratio to the initial valuated deposit.

The sensitivity assessment of excavation and economic returns is presented in Figure 5.5. It can be observed that the project performance indicators are more favorable at steep slope angle design than gentle designs. The steep mine design has exciting economic results due to the low strip ratio with no pre-stripping required as the initial mining phase is in ore. Hence, the mining operation drifts towards high profits. However, the extraction of ore in open-pit mines involves striking a balance between economic profits and safety. As a rule of thumb, safety is prioritized over profits because the collapse of mines can be costly leading to a huge loss. The deterministic results obtained from numerical analyses in this work indicate that steep angles do not have a reliable geotechnical safety. From the analysis, a steeper OSA of 50° from the high RL of Songwe mine, the geotechnical safety is low with FoS below equilibrium but the economic parameters recorded prospect of high returns. On the other hand, a gentler angle of 40° has a high assurance of stability but the prospect of profits is relatively low (see Figure 5.5).

Since mining involves trade off between resource recovery and safety, it is imperative to find a favorable equilibrium between the two aspects. In that regard, an attempt was made to establish the favorable situation. The outcome shows that an OSA of 42° in the high RL at 300 m GSH guarantees safety and the economic performance indicators are quite attractive. The fulcrum of safety and profit prospects is such that FoS is barely at 1.2 and the economic indicators at a discounted rate of 10% indicate that the deposit can be developed at a profit with NPV at around U$$580 million, IRR of 32%, and PI at 2.3.

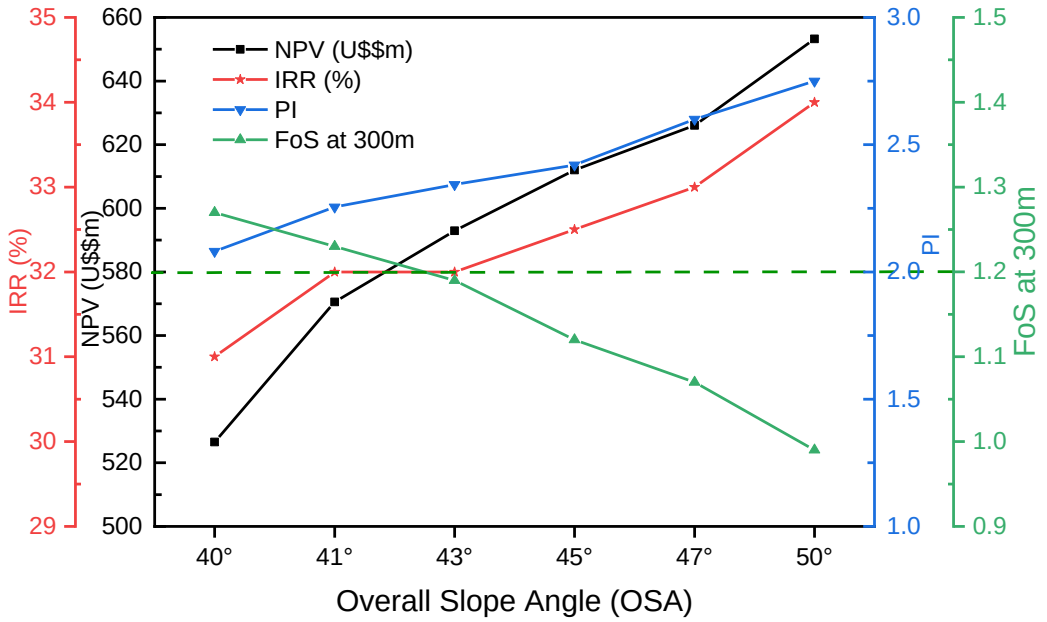

Figure 5.5 Influence of slope design on economic project performance

5.7 Summary

Despite the fact that it is almost impossible to make a precise estimate of the mining project performance due to numerous technical and economic uncertainties that can occur in the course of operation, it is important to forecast the project performance in order to know the value of investing into the mining venture. Generally, the assessment is based on economic performance indicators namely; Net Present Value (NPV), Internal Rate of Return (IRR), and profitability index (PI). The results show that steeper slope angles have higher prospects of profit due to low stripping ratio than gentle angles but their safety is unreliable.

This requires the mining trade off between resource recovery and safety. For the case study project, the indicators at a discounted rate of 10% indicate that the deposit can be developed at a profit with NPV, IRR and PI at US$658.54 million, 33%, and 2.6 respectively, however, at the slope angle that gives a fair equilibrium on recovery and safety, NPV is around U$$580 million, IRR at 32%, and PI at 2.3. Regarding sensitivity analysis of the mining parameters, it has been shown that mineral price volatility is very sensitive on project performance, hence at the core of the decision to mine the REE or not.

5.8 References

Chareyron, B. (2015). Impact of the Kayelekera uranium mine. Lilongwe, Malawi: EJOLT.

Gambogi, J. (2020). *Rare Earths Statistics and Information*. Washington DC: USGS.

Henckens, M. L., van Ierland, E. C., Driessen, P. P., & Worrell, E. (2016). Mineral resources: Geological scarcity, market price trends, and future generations. *Resources Policy*, 49, 102–111.

Hosoi, Y. (2009). *Mining and Development: A Case Study Assessing National Economic and Environmental Issues*. Saarbrucken: Lambert Academic Publishing AG & Co. KG.

Hustrulid, W., Kuchta, M., & Martin, R. (2013). *Open Pit Mine Planning and Design; Fundamentals*. New York: Taylor & Francis Group.

Juhász, L. (2011). Net Present Value versus Internal Rate of Return. *Economics & Sociology*, 4(1), 46-53.

Kennedy, B. A. (2009). *Surface Mining* (2nd Ed.). Colorado, USA: Society for Mining, Metallurgy, and Exploration, Inc. (SME). www.smenet.org

Renner, S., & Wellmer, F. W. (2020). Volatility drivers on the metal market and exposure of producing countries. Mineral Economics, 33, 311–340.

Sincovich, A., Gregory, T., Wilson, A., & Brinkman, S. (2018). The social impacts of mining on local communities in Australia. Rural Society, 1-17. doi:10.1080/10371656.2018.1443725

Wellmer, F. W., & Berner, U. (1997). Factors useful for predicting future mineral-commodity supply trends. Geol Rundsch, 86, 311—321.

6 MINE DESIGN AND IMPLEMENTATION

6.1 Introduction

The mine design process has proven that there are no standard recipes that can be adopted as a panacea with certitude because mine sites are characterized by unique rock mass quality, geology, structural features or network, seismic events, and different prevailing stress regimes. In addition to the aforementioned, the geometry of the mine and slope angles contribute to the stability of the mine. In order to develop an accurate mine design, a comprehensive site investigation that take account of geological and discontinuity mapping should precede stability studies to supply necessary and accurate input data for the stability analysis (Fleurisson, 2012). This is because the occurrence of slope failures in unstable mine slopes may affect the mining operations due to fatality, machinery damage and render the recovery of ore uneconomical if the mine was being actively mined (Read & Stacey, 2009; Sjoberg, 1996). Thus, an all-encompassing methodology was adopted in order to achieve the right solution with certitude. The process entailed a phased approach involving: 1) characterization of rock mass by acquiring and analyzing geological and geotechnical data, 2) identification of potential structural controlled failure, 3) evaluation of potential mechanisms of deformation and failure through numerical modelling.

The philosophy adopted in the design process and implementation proposal in this work is centered on ‘slope stability assurance’ and not ‘slope management’ because of the details gaps as the site is currently virgin. The manageable slope instabilities at an acceptable level of risk could be permitted other than stick to a rigid design that focuses on attaining stable pit walls reflecting aggressive slope design. This can be achieved by a ground control management plan (GCMP) with approval from certified mining engineers as the cut faces of the mine get exposed from interim pit phases, nested pits to the ultimate pit limit. Thus, it is prudent that the slope management approach be adopted and the slope stability assurance strategy be applied as a referencing tool since if slopes were to be designed for geotechnical complete stability, the mineral deposits could be deemed uneconomic and the subsequent gloomy decision not to develop the resource.

6.2 Mine Design

The design of rock slope presents the most challenging issues in geotechnical engineering because it has both economic and safety implications, especially for OPMs. Thus, its analysis and design is a key aspect of OPM as engineers seek to optimize the OSA in order to maximize the extraction of ore while maintaining the stability of the slopes. In this regard, the knowledge of the rock shear strength and the determination of the required FoS become the fulcrum for the ultimate design. To achieve an optimal design, the analysis of the slope excavations in rock mass calls for reliable geomechanical input parameters such as rock mass strength, friction angle, and cohesion. However, parameters are naturally uncertain and their exact values cannot be known, therefore, their variability must be properly accounted for in the stability analyses (Abdulai & Sharifzadeh, 2018). Therefore, the design confidence for open-pit at the conceptual stage prior to the operational stage was treated with caution due to uncertainties that can evolve as the comprehension and knowledge of the geotechnical conditions increase. Macciotta et al. (2020) described the uncertainties in slope stability analysis to comprise both aleatory (spatial variability, material randomness, random sampling, and testing errors) and epistemic (lack of information, systematic errors) factors. Hence, to attain the certitude of the design we adopted an integrated approach involving deterministic and stochastic methods.

In the deterministic approach, the design acceptance of the pit slope is typically determined by the design acceptance criteria (DAC) expressed in terms of FoS. The acceptability criteria with respect to FoS ≥ 1 is a deliberate attempt to ensure the reliability of slope performance and in this study a tolerable FoS of ≥ 1.2 was adopted. Prior to undertaking numerical analysis, from which FoSs are computed, the probability of failure due to the structural network was performed via kinematic analysis. The outcome from the kinematic analysis revealed that OSA of 40° would have an acceptable PoF of 7%, which is above the minimum tolerable PoF in mines. The potential of failure was found to be only planar instability along discontinuity planes. When compared to a steep possible OSA of 45°, the optimized angle could reduce the risk of potential planar failure to safety by over 44%. However, the current kinematic analysis has a limitation in that the assessment of failure modes was largely based on the drill core structural logging data.

So, the continuity of the discontinuities across the sections could not be ascertained since there are no excavated faces yet. Certitude in this regard shall be attained from finer details of the major discontinuities when pit walls get exposed using data from scan line surface mapping. Since, kinematic analysis does not provide a stability index, a complementary deterministic analysis using numerical methods was undertaken. To account for uncertainties, the PoF of the slopes was assessed using a methodology that utilizes available data on slope properties and considerations of force majeure. The principal uncertainties considered in the study include:

1) *Geological and structural feature deviation* represented by the variable orientation and size of weak lithological section which forms a contact plane with competent geotechnical units and potential fractures at contacts suggested to be sub-vertical to vertical.
2) *Stress regime deviations* represented by the variable in situ stress conditions which could change with respect to the faulting system within the tectonically active regions
3) *Model reliability* defined in terms of the FoS corresponding to failure condition of the slope in static and dynamic loading.

Taking into account the aforementioned aspects of uncertainties and economic evaluations, a number of possible designs of the final pit slope can be considered. Figure 6.1 presents the combinations of design parameters interplay. It can be observed that slope steepening has an advantage of increasing the NPV which is an economic performance indicator. Nevertheless, the reliability of slope performance continuously decline and the likelihood of failure measured by PoF increases. On the other hand, adopting a gentler angle increases the stripping ratio as well as potential dilution at contact zones. In this study case, the geotechnical details at this current mine development stage are scanty. In this regard, safety must be highly considered over high economic profit prospects, and we opted for a conservative excavating slope to evade taking avoidable risk. Thus, although OSA of 41° in the south section and 50° in the north section is implementable the author proposes an OSA of 40° despite the fact that there would be a fairly considerable stripping ratio and potential dilution. The suggested conservative design is aimed at slope stability assurance and not slope management because of the inadequate geotechnical details prior to commencement of the mining operations.

At the planned final depth of the mine, the design guarantees a reliable stability performance of the pit slopes, and the prospect of economic returns would be fairly good as evaluated in numerical analysis and economic evaluation respectively. The details of the design parameters are presented in Table 6.1.

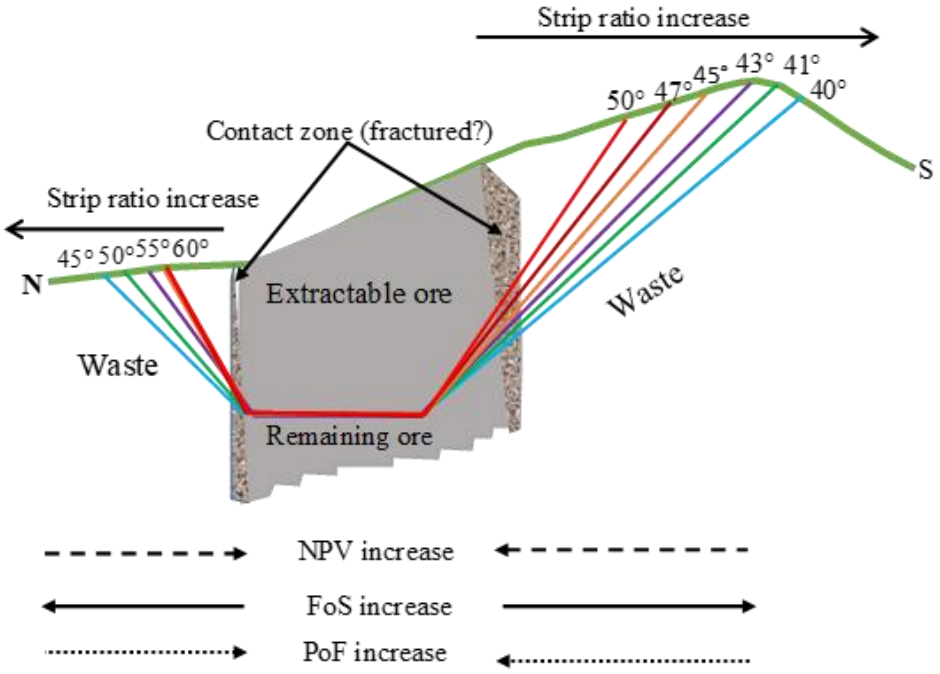

Figure 6.1 Mine design considerations

Table 6.1 Recommended pit design parameters for Songwe Hill mine

Design Parameter	**Units**	**Pit section**	
		South Section	North Section
Bench Height	m	15	15
Bench Width	m	7.5	7.5
Bench Face Angle (BFA)	(°)	58	71
Inter Ramp Angle (IRA)	(°)	42	50
Overall Slope Angle (OSA)	(°)	40	50
Ramp Width (Truck width + bench width + safety berm)	m	32.5	32.5
Pit Height from Crest	m	300	150

The fact that the deterministic approach does not cater for uncertainties in input parameters, the uncertainty in the final value of FoS is unknown. Thus, the single value of FoS may be misleading without verification. Abdulai & Sharifzadeh (2018) highlighted that there have been cases where rock slopes failed even though the failed slope had been considered stable with FoS > 1. In this regard, for a reliable design and analysis of rock slope, we incorporated methods that take into account variability in input parameters, like probabilistic methods. One measure of uncertainty is the coefficient of variation (COV). Coefficient of variation is a dimensionless value calculated as the standard deviation divided by the mean of a distribution (Read & Stacey, 2009; Macciotta et al., 2020). The COV is generally applied in geotechnical engineering to define uncertainty in geotechnical parameters, which is expressed by the relationship between the mean value of the FoS and the PoF. As a rule of thumb, coefficients of variation below 10% are low enough and are considered the best practices, between 15% and 30% are moderate implying good or recommendable practices, while greater than 30% are high and fall in the poor engineering category (Read & Stacey, 2009). The recommended slope design in this study was plotted to determine the confidence level as shown in Figure 6.2. The FoS and the associated PoF for the project fall between 15% and 20% confidence levels. At this COV, the engineering confidence of the design is within the acceptable bracket with potentially low risk.

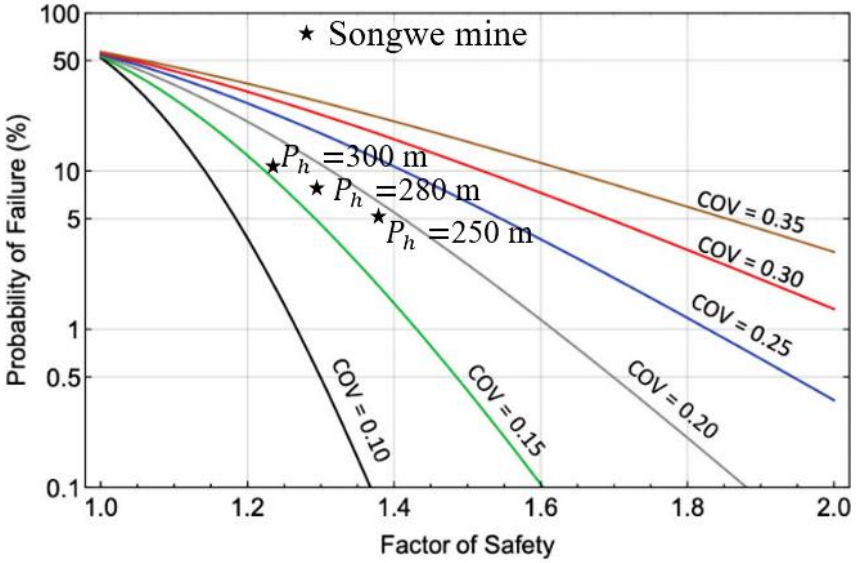

Figure 6.2 Data fitting for design confidence level determination after (Macciotta et al, 2020)

Since the study is conducted on a greenfield site (where no pit excavation is available) based on a limited amount of geotechnical information, we compared our engineering judgment to real world projects used in well-established empirical DCA for risk assessment as a decision management tool (see Figure 6.3). In terms of acceptability, we can observe that the Songwe Mine simulation results based on a 3D analysis plot closer to the curve related to pit slopes. The plots closer to the curve of mining projects imply a reliable fit with minimal uncertainty. From the fitting results, we can observe that the Songwe data demonstrates a good fit implying reliable performance of the mine design

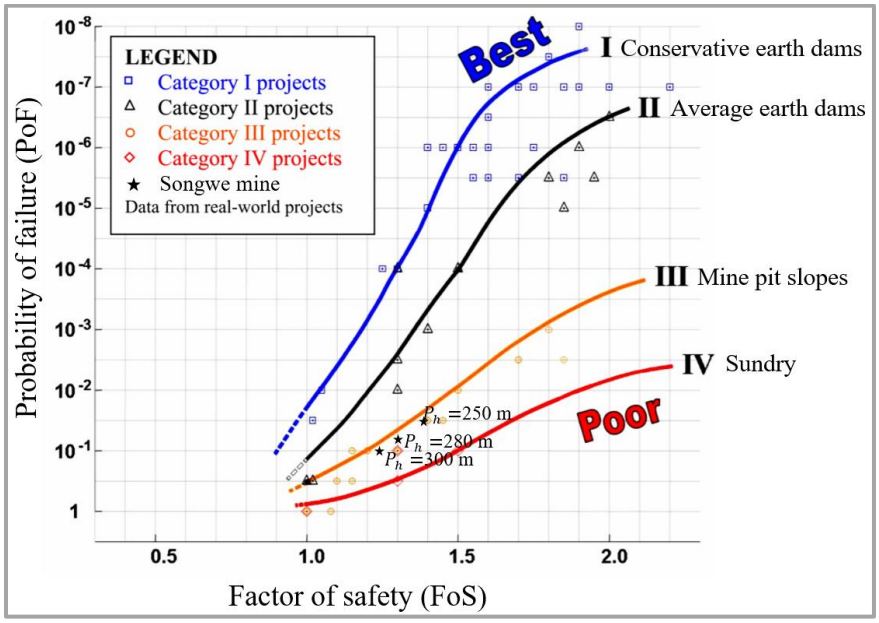

Figure 6.3 Data fitting of Songwe Mine design in empirical curve after (Silva, et al., 2008), and P_h means pit height.

6.3 Extraction Sequencing

Pit sequencing targets attaining the required heap feed production rate, mining of higher value material early in the life of mine, while ensuring a balance in grade and strip ratios. In this respect, OPM operation can be envisioned as the removal of blocks starting from the top of the ore body and proceeding to the bottom of the ore body until no block can be removed economically. The blocks are modeled as mineralized body and country-rock divided into a three-dimensional array of regular size blocks.

The ore body block is considered to be irremovable if the cost of extracting outweighs the benefits after marketing. This operation is dynamic leading to the evolution of the OPM. Khan & Niemann-Delius (2014), Meagher et al. (2014) discussed the mathematical formulation of the ultimate pit limit (UPL) problem, that is, the final contour to which it is economically feasible to mine. The UPL problem can be defined as follows:

$$UPL = \sum_{i=1}^{N} v_i x_i \qquad (6.1)$$

Subject to: $x_i \leq x_j$, I = 1, 2,……., N; j ∈ P_i, $x_i \in [0,1]$

where v_i represents the economic value of block i, N represents the total number of blocks in the block model, x_i represents a binary variable corresponding to block i which takes the value 1 if block i is inside the ultimate pit limits and 0 otherwise, and P_i represents the predecessor group of block i.

The verdict as to what should be mined within the UPL is time depended and the solutions like the "cone mining" method or the Lerchs and Grossmann (LG) algorithm, that take into account the knowledge of when a particular block will be mined and how long one needs to be stripping the waste, are generally applied. Since the ultimate pit limits cannot be determined without knowing when the individual blocks will be mined (Dagdelen, 2001), in the meantime we assume that all the blocks within the pit limits are extractable (see Figure 6.4) and in the first year of production 200,000t will be extracted, and in the subsequent years of operation before the projected 18 years, 500,000t will be mined out. Generally, the geometric shape of the surface, morphology and, mineralization style of the ore determine the evolution of the mine mostly represented by state equations of dynamic programming (Elevli, 1995). Based on the topography, the mineralization extent, and the discontinuity distribution of study area, the extraction sequencing is proposed to commence on the sloping face of the hill where ore hosting rock is exposed to the surface to shorten payback period and then create subsequent push backs in which case stripping will be required.

The suggested sequencing could critical in the exposition of the discontinuities which are principally dominant in the high RL south section, which would help in redesigning of bench slopes to ensure reliable slope performance. The approach could also permit the gradual release of the built up stress in the hill side as excavation progresses. Thus, the geometric shape (Figure 6.4) of the surface at time t is referred to as its state defined by the variables:

$$a_{ij}^{t} = k$$

$$e^{t} = (p, q)$$

where:

k is the depth of block (ij) at time t

(p,q) are the current (ij) indexes of equipment location

ij,k are the block indexes in the X.Y and Z direction

then, the surface geometry of the mine at time t can be denoted by the state vector s_t as follows;

$$s_t = (A_t, e^{t})$$

Where;

A_t is a collection of a_{ij} for every i and j

The transition from one state to another, is then based on the decision to remove or not to remove a block, which can be defined as;

$$u_t = (i, j)$$

And

$$u_t = 1 \; if \; block \; is \; mined \; and$$

$$u_t = 0 \; if \; not \; minable$$

then the new state will be represented by;

$$s_{t+1} = f(s_t, u_t)$$

$$u_t, s_t \; are \; set \; of \; all \; admissible \; decisions$$

Thus, the state transformation will be made on the basis of the following equation;

$$a_{ij}^{t+1} = a_{ij}^{t} + u_t \quad (6.2)$$

The new equation means, by the removal of a block, the depth at (*ij*) is increased by one as shown in Figure 6.5 and the subsequent cuts are undertaken obeying the principle presented above.

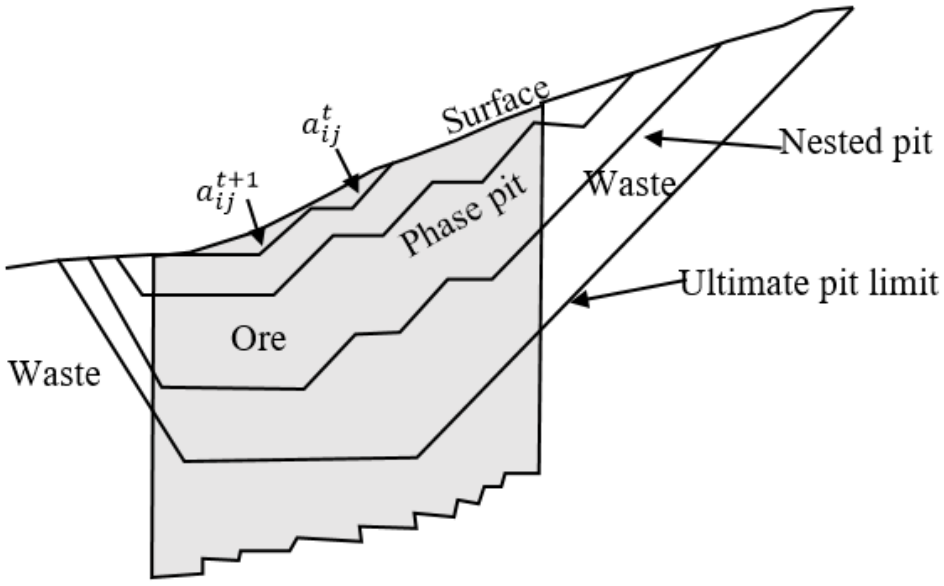

Figure 6.4 Proposed mining sequencing

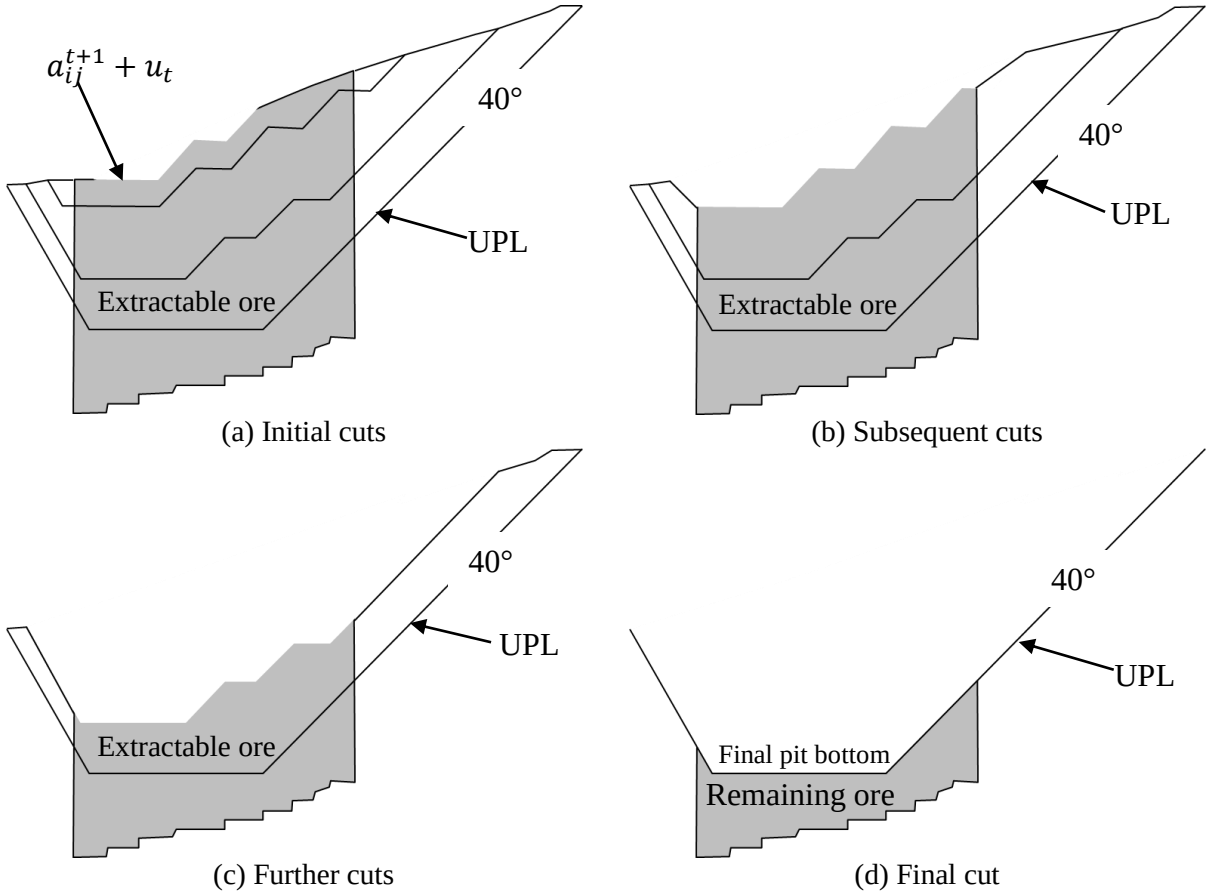

Figure 6.5 Proposed sequencing phases

6.4 Summary

In developing an optimal mine design, using a case of Songwe Mine for carbonatite complexes, an all-encompassing approach was adopted in order to achieve the right solution with certitude. The integrated approach applied involved rock mass characterization, kinematic and numerical methods complemented by non-deterministic methods. Basically, final slope design has to consider the balance between mining profits and safety. In carbonatite deposits it has shown that overall slopes can be developed at steep angles at shallow depth in order to yield high returns. But, since the contact zones of carbonatites and fenite may be fractured and also the existence of brecciation coupled with high tectonic stresses, the ultimate slope design at greater depth ought to be at the optimal gentle angle.

In the case of Songwe Mine, considering the topography and the mineralization extent, the extraction sequencing is suggested to commence from the sloping face of the hill where ore hosting rock is exposed to the surface to shorten payback period and then create subsequent push backs in a top-down approach targeting an OSA of 40° in high RL section, which guarantees a balance of safety assurance and good returns though requirement for stripping is fairly high. Since the site is virgin, the forward analyzed design was fitted in the data of standard design acceptance criteria (DAC) graphs to verify its stability performance. The graph fitting of the mine design demonstrated a good fit to empirical curve of real world projects implying reliable performance of the design. Nevertheless, the current proposed design at 300 m GSH is conservative aimed at stability assurance and not management because of the incomplete geotechnical details at the current stage. The pre-mining operation rigid design could be adjusted to a flexible design in the course of operation as more geotechnical data is collected.

6.5 References

Abdulai, M., & Sharifzadeh, M. (2018). Uncertainty and Reliability Analysis of Open Pit Rock Slopes: A Critical Review of Methods of Analysis. *Geotech Geol Eng*, 1-22. doi:https://doi.org/10.1007/s10706-018-0680-y

Dagdelen, K. (2001). *Open Pit Optimization - Strategies for Improving Economics of Mining Projects Through Mine Planning*. International Mining Congress and Exhibition of Turkey (pp. 117-121). Turkey: IMCET.

Elevli, B. (1995). Open Pit Mine Design and Extraction Sequencing by Use of OR and AI Concepts. *International Journal of Surface Mining, Reclamation and Environment*, 149-153.

Fleurisson, J.-A. (2012). Slope Design and Implementation in Open Pit Mines: Geological and Geomechanical Approach. *Procedia Engineering, 46*, 27 – 38.

Khan, A., & Niemann-Delius, C. (2014). Production Scheduling of Open Pit Mines Using Particle Swarm Optimization Algorithm. *Advances in Operations Research*, 1-9. doi:10.1155/2014/208502

Macciotta, R., Creighton, A., & Martin, C. D. (2020). Design Acceptance Criteria for Operating Open-Pit Slopes: An update. *CIM Journal*, 11(4), 248-265. doi:https://doi.org/10.1080/19236026.2020.1826830

Meagher, C., Dimitrakopoulos, R., & Avis, D. (2014). Optimized Open Pit Mine Design, Pushbacks and the Gap Problem—A Review. *Journal of Mining Science*, 3, 96–117.

Read, J., & Stacey, P. (2009). *Guidelines for Open Pit Slope Design*. Australia: SCIRO Publishing.

Silva, F., Lambe, W. T., & Marr, A. W. (2008). Probability and Risk of Slope Failure. *Journal of Geotechnical and Geoenvironmental Engineering*, 134(12), 1691-1699.

Sjoberg, J. (1996). *Large Scale Slope Stability in Open Pit Mining*. Sweden: Division of Rock Mechanics; Lulea University of Technology.

Wellmer, F. W., & Berner, U. (1997). Factors useful for predicting future mineral-commodity supply trends. *Geol Rundsch*, 86, 311—321.

7 CONCLUSIONS AND RECOMMENDATIONS

The exploration and extraction of rare earth elements has intensified in the recent decade following their explosive demand due to their application in high technological devices such as computer memory, rechargeable batteries, autocalytic converters, super magnets, and mobile phones. However, the economically exploitable REEs tend to occur in limited geological environments and carbonatites are highly potential hosts of REE, hence they are special target rock mass. Malawi, Africa is among the few countries endowed with the exceptional carbonatite intrusions and among the intrusions existent, Songwe Hill has proven economical for mine development. Since the deposit at the site is near the surface, open-pit mining has been proposed for the development of the deposit. Open pit mining is advantageous when exploiting shallow lying and even low-grade deposits. Nevertheless, the mining method is beleaguered by stability challenges resulting in failure of slopes due to partly poor designs that overlook some integral components. One overly disregarded aspect as a mining bottleneck is in situ stress, which has only been considered in underground mining based on the premises that the stress environment in OPM is dilationary other than confining and that failures are gravity-driven. Nevertheless, stress regimes, particularly in tectonically active regions like the East African Rift Valley system, can inevitably play a key role in the failure process on excavations. On the other hand, despite carbonatites being competent rock mass, they are characterized by in situ damage due to brecciation and have multi-faceted angular blocks generated by fractures and discontinuity sets. The failure mechanisms in such hard rocks entail initiation and progression of failure along the existing weakness planes, and even in intact state. In order to develop an optimal mine design guidlines in such carbonatite deposit under high-stress conditions in Great Rift Valley area, an integrated approach entailing rock mass characterization, kinematic and numerical methods was applied for design guideline. The main findings of the research can be summarized as follows:

Chapter 1: Introduces the significance of REE, their production and consumption disequilibrium, and the geological environments of occurrence. The emplacement of the carbonatite complex, which is a host of REE, is also discussed.

The carbonatite complexes are basically intruded into the country rock through an exceptional magmatic activity with an alkaline rich magma. The later stages of the Songwe carbonatite emplacement is uniquely featured with carbonatite transition from a magmatic to a hydrothermal regime where expelled fluids lead to fenitization, fluorite and Mn-Fe veining disseminated throughout the rock mass. The chapter also gives the background of the research, research objectives and methods.

Chapter 2: The chapter is dedicated to evaluating the geological and geotechnical conditions of the carbonatite rock mass. A field survey revealed distinctive features that the carbonatite complex is characterized by in situ rock damage due to brecciation, which is a result of hydro-fracturing involving high-pressure fluids due to high tectonic forces trending along pre-existing plane of weakness, and has high discontinuity frequency per unit area occurring parallel to the horizontal stress direction. To understand the rock quality in relation to mining, qualitative and quantitative rock mass classification systems, namely Geological Strength Index (GSI) and Rock Mass Rating (RMR) respectively, were applied to describe the rock mass. Based on the evaluation, carbonatites can be described as competent with RMR class II rating 60-74, and GSI value range of 55-69. In spite of the competency, they tend to have multi-faceted angular blocks generated by discontinuity sets, which pose a potential for structural controlled instabilities.

Chapter 3: Gives a discourse on the potential modes of slope failure in the discontinuity dominated carbonatite rock mass as revealed in chapter 2, performed using the kinematic approach. The kinematic checks were executed using Dips V 6.0 software designed to analyze features related to engineering analysis of rock structures. The outcome of the analysis indicate that the carbonatite rock masses have high potential of planar slope instability at steeper angles, for the case of Songwe at 45°. Since carbonatites occur in tectonically active regions, the high horizontal stresses acting parallel to discontinuity planes intersecting the orientation of the slope faces could act as a catalyst to failures. In order to minimize the risk of failure, slope angle optimization to a gentler angle can be adopted as a counter-measure. For the case study area, the risk of failure was observed to be high in the south and east sections of the pit, hence slope angle optimization to 40° was suggested, which could reduce the risk of failure to high safety.

Meanwhile, relatively steep angles in the opposite sections are implementable at safety viz. 43° in the north and 42° in the west sections.

Chapter 4: Presents analyses of stability conditions and deformation behavior of pit slopes under structurally complex and prevailing high-stress conditions in Great Rift Valley area in order to come up with ultimate optimal design guidelines for rare carbonatite deposits. This was achieved by numerical methods carried out with finite difference method and finite element method codes using FLAC^{3D} V 5.0 and Phase^{2} V 7.0 software respectively. The analyses were performed in elasto-plastic state with Mohr-Coulomb constitutive model and failure criterion. Due to the competency of the rock mass, analysis shows that overall slopes can be developed at steep angles of 45-50° at a shallow depth of ≤ 250 m, but caution has to be taken at greater depth and when discontinuities are predominant. With regards to in situ stress, a qualitative evaluation of the stability state through shear strain analysis reveals that the pit wall stability conditions could be compromized under high-stress regimes such that non-uniformity of stress state leads to the development of a secondary potential failure surface (PFS) in addition to the primary circular PFS which has been the sole engineering concern in slope stability analyses. Furthermore, the displacement values, at the state of stress equilibrium (k=1), were found to be almost four times lower than at k=2.5 and two times lower when k=0.5. This demonstrates that non-uniform high-stresses could indeed adversely affect pit wall performance. To test the criticality of the risk to failure, the strain criterion to failure, which is a ratio of the maximum deformation and the height of excavation, was applied and the shear strain rate indicates that the rock mass slopes may not be significantly endangered, a phenomenon accredited to its competence. For instance, the maximum possible strain rate of 0.04%, which is below the lower bound strain at collapse of 0.1% was recorded in the study case. In terms of in situ rock damage, the existence of breccia in the competent rock mass has the capability to reduce the stability performance of the pit wall and the enormity of the impact increases at gentle dipping angle in close range to the slope toe. However, as the initial position of breccia moves away from the pit wall, the stability performance increases at gentle dipping angle namely 30° and 40°. On the contrary, at the dipping angle of 50° the performance of slope reduces, and at steeper angle >50°, the impact becomes negligible.

Thus, for OPM design in brecciated rock masses, the ratio of at least 1:5 between the breccia distance from slope toe and pit depth is proposed to counter its impact. If breccia is close to the pit limit, a deliberate effort must be made to mine out or truncate it.

Chapter 5: Covers the aspect of mining economics. The objective is to give a forecast of the project performance in order to know the value of investing in the REE mining venture. The assessment is based on economic performance indicators namely; Net Present Value (NPV), Internal Rate of Return (IRR), and profitability index (PI). The results show that steeper slope angles have higher prospects of profit due to low stripping ratio than gentle angles but their safety is unreliable. This requires the mining trade off between resource recovery and safety. For the case study project, the indicators at a discounted rate of 10% indicated that the deposit can be developed at a profit with NPV, IRR and PI at US$658.54 million, 33%, and 2.6 respectively but at the slope angle that gives a fair equilibrium on recovery and safety, NPV is around U$$580 million, IRR at 32%, and PI at 2.3. On a different note, sensitivity analysis of the mining parameters showed that mineral price volatility is very sensitive on project performance, hence at the core of the decision to mine the REE or not. Thus, *ceteris paribus*, the project can be rated as economically viable.

Chapter 6: Gives the mine excavation plan and design. Basically, final slope design has to seriously consider equilibrating the fulcrum of mining profits and safety. In carbonatite deposits it has shown that overall slopes can be developed at steep angles at shallow depth in order to yield high returns. But, since the contact zones of carbonatites and fenite may be fractured and also the existence of dicontinuities and brecciation coupled with high tectonic stresses, the ultimate slope design at greater depth ought to be at the optimal gentle angle. In the case of Songwe Mine, considering the topography and the mineralization extent, the extraction sequencing is suggested to commence from the sloping face of the hill where ore hosting rock is exposed to the surface to shorten payback period and then create subsequent push backs in a top-down approach targeting an OSA of 40° in high RL section, which at preliminary stage guarantees a high geotechnical safety assurance and good returns though requirement for stripping is fairly high.

7.1 Recommendations

1. Follow up kinematic analysis studies are recommended when pit walls get exposed using data from scan line surface mapping to acquire the finer details of the major critical discontinuities and update the current findings. This is because the current kinematic analysis was largely based on the drill core structural logging data. So, the continuity of the discontinuities across the sections could not be ascertained since there are no excavated faces yet.
2. Numerical analysis based on discontinuum approach utilizing discrete element method (DEM) to incorporate discontinuities in the numerical model is suggested for further analysis. In this study we adopted a continuum approach in which the rock mass was treated as isotropic rock mass which may not be a realistic representation of the field conditions.
3. The author recommends that the slope management approach be adopted with the study's slope stability assurance strategy considered as a reference. This is owing to the fact that the analyses leading to OPM design and implementation in this work centered on the philosophy of 'slope stability assurance' and not 'slope management' because of the details gaps as the site is currently virgin. The author recognizes the fact that if slopes were designed for geotechnical complete stability, the majority of mineral deposits would be uneconomic and would remain undeveloped. The slope management approach can be achieved by a ground control management plan (GCMP) with approval from certified mining engineers as the cut faces of the mine get exposed from, interim pit phases, nested pits to the ultimate pit limit. The manageable slope instabilities at bench level in an aggressive slope design, at an acceptable low level of risk could be permitted.